



# **Flexible Forming of 3-D Metal Panels**

by

**Ali Mohamed Elghawail**

*A thesis submitted to The University of Birmingham  
for the degree of*

**DOCTOR OF PHILOSOPHY**

Department of Mechanical Engineering  
School of Engineering  
College of Engineering and Physical Sciences  
January 2018

UNIVERSITY OF  
BIRMINGHAM

**University of Birmingham Research Archive**

**e-theses repository**

This unpublished thesis/dissertation is copyright of the author and/or third parties. The intellectual property rights of the author or third parties in respect of this work are as defined by The Copyright Designs and Patents Act 1988 or as modified by any successor legislation.

Any use made of information contained in this thesis/dissertation must be in accordance with that legislation and must be properly acknowledged. Further distribution or reproduction in any format is prohibited without the permission of the copyright holder.

## ABSTRACT

The process of sheet metal forming is commonly used to create 3-D surfaces in, e.g., aircrafts and automobiles. Stamping is one of most common sheet metal forming processes but traditional forming processes which have been developed for mass production are inflexible and expensive, and economically unsuitable for small-scale production. More appropriate for small-batch and prototype production are flexible forming methods such as multi-point forming (MPF) which have been developed in recent years. A pair of opposed reconfigurable tools containing pin matrices could replace traditional solid stamping tools. Based on this technique, the construction of sheet metal forming tools becomes flexible and fast.

Springback, caused by elastic recovery and release of residual stress, is an unavoidable issue in all sheet metal forming and significantly affects the geometrical precision of the products. Springback is a defect, and if it is beyond permissible tolerance it will adversely affect the assembly process such as distortion of sub-assemblies and poor fit-up during welding. Estimation of springback remains an important and challenging issue for the sheet metal industry.

Based on the ABAQUS software, 3-D finite element models were generated, with the required constraints and boundary conditions described and applied in the simulation. The process of multi-point forming and springback were simulated by combining explicit and implicit algorithms. The influence of some significant working parameters, such as radius of forming curvature, blank holder force and elastic cushion thickness on final product quality (springback, thickness variation and wrinkling) has been investigated. The results show that springback was reduced for small radii of forming curvature and increased blank holder force, with the springback decreasing gradually. The elastic cushion thickness had no significant effect on springback but it did affect dimpling.

The Design of Experiments procedure was applied to produce an experimental strategy based on all the related working parameters, followed by an analysis of variance approach which was then used to define the most critical parameters. The use of statistical and optimisation methods led to improved final product quality and the derivation of an empirical model to predict the final part quality.

A new measurement technique for measuring the forming force on individual pins was developed. Fibre Brag Grating (FBG) sensors, as “smart” sensors were used to monitor the change in elastic strain of selected pins due to applied force, throughout the forming process.

An elastic block was used as a punch rather than a MPF punch to reduce adjustment time and tool cost. A comparison between the final products produced by this approach and the full MPF process showed a 50% reduction in tool cost or more and adjustment time by replacing upper matrix of pins with an elastic punch, also a reduction in part defects such as springback and wrinkling.

A series of experiments were carried out to compare the simulations with experimental results, it was observed the results were well matched in measurements of final parts defects.

## **DEDICATION**

To my parents, family, wife and children

## **ACKNOWLEDGEMENT**

The research was carried out at the University of Birmingham, School of Engineering during the period of October 2014 and January 2018.

My sincere thanks are due to my supervisor, Prof. Duc Pham, for the patient guidance, encouragement and advice he has provided throughout my research. It is the greatest honour to work under his supervision. I would also like to thank all the members of multi-point forming group research who supported me to finish this research.

Thanks to all staff members of the School of Mechanical Engineering, the University of Birmingham who has supported me throughout my scientific journey.

Finally, I am grateful to my wife and children for their understanding, support and encouragement throughout the period of my studies.

## **PUBLICATIONS**

- 1- Elghawail, A., Essa, K., Abosaf, M., Tolipov, A., Su, S. and Pham, D., 2017. Prediction of springback in multi-point forming. *Cogent Engineering*, vol. 4, 1400507. DOI: 10.1080/23311916.2017.1400507. (chapter 5)

## **Posters**

- 1- Elghawail, A. and Pham, D., 2017, Numerical simulation and experimental verification of flexible multi-point forming using an elastic punch. School of Engineering, University of Birmingham

## TABLE OF CONTENTS

<b>ABSTRACT.....</b>	<b>I</b>
<b>LIST OF FIGURES.....</b>	<b>XI</b>
<b>LIST OF TABLES.....</b>	<b>XVII</b>
<b>LIST OF ABBREVIATIONS .....</b>	<b>XVIII</b>
<b>NOMENCLATURE.....</b>	<b>XIX</b>
<b>CHAPTER 1: INTRODUCTION.....</b>	<b>1</b>
1.1 Background .....	1
2.1 Aims and objectives.....	2
2.1.1 Overall aims.....	2
1.2.2 Objectives.....	2
1.3 Research hypothesis and methodology.....	3
1.4 Structure of the thesis.....	3
<b>CHAPTER 2: LITERATURE REVIEW.....</b>	<b>5</b>
2.1 An overview of Metal Forming technology.....	5
2.2 Flexible sheet metal forming processes.....	7
2.3 Plasticity in sheet metal forming.....	12
2.3.1 Isotropic hardening.....	13
2.3.2 Kinematic hardening.....	14
2.4 Springback phenomenon in sheet metal forming.....	16
2.4.1 Analytical approach to predict springback in metal forming.....	17
2.4.1.1 Loading stage.....	21
2.4.1.2 Unloading stage.....	24
2.4.2 Numerical approach to predict springback in metal forming.....	25
2.4.3 Experimental approach to predict springback in metal forming.....	28

2.5	Design of Experiments and optimisation technique in sheet metal forming.....	31
2.6	Review of research into spring back errors.....	32
2.7	Summary.....	33
<b>CHAPTER 3: MPF TOOLS AND MEASUREMENT APPARATUS.....</b>		<b>35</b>
3.1	Mechanical tests for material properties.....	35
3.1.1	Uniaxial tensile test to failure.....	35
3.1.2	Anisotropy test.....	39
3.1.3	Uniaxial compression test of Polyurethane.....	41
3.2	Conventional MPF experiment set up.....	43
3.2.1	MPF punch and die specification.....	45
3.2.2	Blank holder.....	46
3.2.3	Load cell.....	47
3.2.4	Distance sensor.....	48
3.2.5	3D Faro arm scanner.....	48
3.3	Measurement tools of individual pin force.....	49
3.3.1	Fibre Bragg grating sensors (FBGs).....	50
3.3.2	Working principle of FBG sensors.....	50
3.3.3	A FBG sensing system.....	50
3.4	Summary.....	52
<b>CHAPTER 4: DEVELOPMENT OF FINITE ELEMENT MODELS FOR MPF.....</b>		<b>54</b>
4.1	FE Modelling of MPF Process.....	54
4.1.1	Model development.....	57
4.1.2	Boundary condition and material properties.....	59
4.2	Model validation.....	62
4.2.1	Mesh sensitivity analysis.....	63

4.2.2	Energy balance in quasi-static analysis.....	65
4.2.3	Experimental validation.....	65
4.3	Effect of process parameters on springback.....	67
4.3.1	Effect of friction coefficient on springback.....	67
4.3.2	The effect of radius of curvature on springback.....	69
4.3.3	Effect of blank holder force on springback.....	71
4.3.4	Effect of elastic cushion thickness on springback (type, thickness).....	73
4.4	Summary.....	76
<b>CHAPTER 5: FINITE ELEMENT MODEL AND OPTIMISATION OF SPRINGBACK IN MPF.....</b>		<b>77</b>
5.1	Design of Experiments (DOE).....	78
5.1.1	Process parameters.....	80
5.1.2	Response parameters.....	80
5.1.3	Results analysis and discussion.....	81
5.1.3.1	Springback.....	83
5.1.3.2	Sheet thickness variation.....	84
5.1.4	Prediction of response factors.....	86
5.1.5	Optimisation of process parameters.....	87
5.2	Thickness distribution and local strain on formed part.....	88
5.3	Summary.....	98
<b>CHAPTER 6: EXPERIMENTAL STUDY OF SPRINGBACK IN MPF.....</b>		<b>100</b>
6.1	Sensing principle of fibre Bragg Grating.....	100
6.1.1	Strain sensitivity of FBG.....	101
6.1.2	Operation principle of force measurement.....	103
6.2	Numerical simulation of the FBG system .....	108

6.3	Experimental validation setup and discussion .....	111
6.4	Summary.....	117
<b>CHAPTER 7: PROCESS DEVELOPMENT TO REDUCE GEOMETRICAL DEFECTS IN MPF.....</b>		<b>118</b>
7.1	Elastic punch with flexible MPF dies for metal forming (EP-MPF).....	118
7.2	Concept of elastic-punch multi-point forming (EP-MPF).....	120
7.3	FE Modelling of EP-MPF.....	121
7.4	Experimental results and discussion.....	123
7.5	Simulation results and discussion.....	128
7.5.1	Comparison of simulated forming forces for EP-MPF and MPF.....	128
7.5.2	Stress distribution on top and bottom surfaces of the formed sheet.....	130
7.5.3	Wrinkling.....	132
7.5.4	Springback.....	133
7.6	Optimisation of EP-MPF process parameters.....	135
7.7	Results and discussion.....	136
7.7.1	Wrinkling.....	138
7.7.2	Forming force.....	138
7.7.3	Springback.....	140
7.8	Prediction of response factors.....	142
7.9	Optimal parameters for working process.....	143
7.10	Summary.....	147
<b>CHAPTER 8: CONCLUSION .....</b>		<b>149</b>
8.1	Conclusions.....	149
8.2	Contributions.....	151
8.3	Future Work.....	151

REFERENCES.....	153
Appendix 1.....	166
Appendix 2.....	167
Appendix 3.....	168

## LIST OF FIGURES

Figure 2-1 Categories of metal forming processes [3].....	5
Figure 2-2 Temperature ranges for different metal forming operations .....	6
Figure 2-3 Schematic of the drawing process.....	6
Figure 2-4 V Bending .....	7
Figure 2-5 Schematic diagram of a flexible forming tool.....	8
Figure 2-6 Different parts formed by MPF [7] .....	9
Figure 2-7 Schematic diagram of MPF process using blank holder [17] .....	10
Figure 2-8 Springback modification of the working surface of a digitised tool [20] .....	11
Figure 2-9 Elastic recoveries during unloading [22] .....	12
Figure 2-10 The yield surface expands under the isotropic hardening assumption [24] .....	14
Figure 2-11 Reverse loading with isotropic hardening [24] .....	15
Figure 2-12 Shows (a) the transformation of yield surface under kinematic hardening, and (b) stress-strain curve with shifted yield stress in compression [24].....	16
Figure 2-13 Sheet bending along a line [29].....	18
Figure 2-14 Plane strain bending: (a) parameter explanation; (b) Equilibrium diagram of stress distribution [29].....	18
Figure 2-15 Three parts a,b and c known as sensitive to springback [28].....	27
Figure 2-16 Springback ( $\Delta\theta$ ) for V-bending (a) loading (b) unloading step .....	29
Figure 2-17 Springback ( $\Delta\theta$ ) for U-bending (a) loading (b) unloading step .....	29
Figure 2-18 Springback ( $\Delta\theta$ ) of straight flanging part (a) loading (b) unloading step .....	29
Figure 2-19 Definition of springback in the stretch bending [41] .....	30
Figure 2-20 Schematic of draw-bend test [42] .....	31
Figure 3-1 Uniaxial tensile machine .....	36
Figure 3-2 Standard specimen for mechanical tests .....	36

Figure 3-3 Tensile test specimens (different angles to the rolling direction) .....	37
Figure 3-4 Stress-strain curve for Aluminium alloy 5251-O .....	38
Figure 3-5 Yield and ultimate stress for Al 5251-O .....	39
Figure 3-6 Compression test for A90 Polyurethane specimen .....	42
Figure 3-7 Load-displacement relations obtained for 90 Shore A Polyurethane.....	42
Figure 3-8 MPF test rig.....	43
Figure 3-9 Pin dimensions .....	44
Figure 3-10 Press machine.....	44
Figure 3-11 MPF punch.....	45
Figure 3-12 Blank holder with springs .....	46
Figure 3-13 Richmond Industries 100 Series low profile load cell .....	47
Figure 3-14 Microsonic M30 distance sensor connected to data logger .....	48
Figure 3-15 Geomagic software connected to Faro arm scanner .....	49
Figure 3-16 Concept and working principle of FBG sensor [71] .....	51
Figure 3-17 Block diagram of strain measurement system .....	51
Figure 3-18 Tools to sense, measure and analyse local forming force .....	52
Figure 4-1 The procedure of ABAQUS simulation [76] .....	55
Figure 4-2 Finite element model and model dimensions [80] .....	58
Figure 4-3 Boundary conditions and mesh types of FE model [80] .....	59
Figure 4-4 Stress-strain curve for aluminium alloy 5251-O [80] .....	60
Figure 4-5 Hyperelasticity evaluation for A90 Polyurethane by ABAQUS [80].....	61
Figure 4-6 Quarter of FEM without blank holder.....	62
Figure 4-7 Mesh density vs springback .....	64
Figure 4-8 Springback for sheet, element size 0.4×0.4×0.4 mm .....	64
Figure 4-9 Energy balance in quasi-static analyses .....	65

Figure 4-10 Model validation: Forming force [80].....	66
Figure 4-11 Model validation: final profile [80].....	66
Figure 4-12 The effect of coefficient of friction on simulated springback.....	67
Figure 4-13 Simulated part for coefficients of friction 0.2.....	68
Figure 4-14 3D (a) diagram of formed part, (b) part profile showing how spring back was measured [80].....	69
Figure 4-15 The effect of radius of forming curvature on springback .....	70
Figure 4-16 Equivalent plastic strain distributions for different radii of forming curvature ...	71
Figure 4-17 Simulated result for springback for blank holder force of 15 kN and radius of forming curvature 800 mm .....	72
Figure 4-18 The effect of blank holder force on springback, for radius of curvature 800 mm	73
Figure 4-19 Simulated effect of elastic cushion hardness on springback, (a) A50, (b) A65 and (c) A90 .....	74
Figure 4-20 The simulated effect of 3 mm thick elastic cushion of different hardness values on springback.....	74
Figure 4-21 Simulation results of effect of Shore A90, elastic cushion thickness on springback, (a) 3 mm, (b) 5 mm and (c) 7 mm. (Radius of curvature 700 mm).....	75
Figure 4-22 The simulated effect of elastic cushion thickness on springback .....	76
Figure 5-1 Sequences for optimisation and DOE procedures.....	79
Figure 5-2 Springback as a function of blank holder force and radius of curvature for constant elastic cushion thickness[80] .....	83
Figure 5-3 Variation in sheet thickness as a function of blank holder force and radius of curvature for constant elastic cushion thickness [80] .....	84
Figure 5-4 Variation in sheet thickness as a function of blank holder force and elastic cushion thickness [80].....	85

Figure 5-5 Measured springback for final formed surface [80].....	88
Figure 5-6 Simulated distribution of sheet thickness for BHF = 5 kN and R=800 mm .....	90
Figure 5-7 Simulated thickness distribution along O-X (Exp #17) (The vertical axis is sheet thickness and the O-X direction is as shown in the panel.) [80].....	90
Figure 5-8 Simulated thickness distribution along O-Z (Exp #17) (The vertical axis is sheet thickness and the O-Z direction is as shown in the panel.) [80] .....	90
Figure 5-9 Simulated distribution of sheet thickness for BHF = 15 kN and R=400 mm .....	91
Figure 5-10 Simulated thickness distribution along O-X (Exp #2) (The vertical axis is sheet thickness and the O-X direction is as shown in the panel.) [80].....	92
Figure 5-11 Simulated thickness distribution along O-Z (Exp #2) (The vertical axis is sheet thickness and the O-Z direction is as shown in the panel.) [80] .....	92
Figure 5-12 Local and global coordinate: ABAQUS .....	93
Figure 5-13 Inter-relation of local and global coordinate systems .....	94
Figure 5-14 Local deformation along path O-X for 800 mm radius of forming curvature and blank holder force 5 kN .....	95
Figure 5-15 Local deformation along path O-Z for 800 mm radius of forming curvature and blank holder force 5 kN .....	96
Figure 5-16 Local deformation along path O-X for 400 mm radius of forming curvature and blank holder force 15 kN .....	97
Figure 5-17 Local deformation along path O-Z for 400 mm radius of forming curvature and blank holder force 15 kN .....	98
Figure 6-1 Working principle of a Fibre Bragg grating [110] .....	101
Figure 6-2 Principle of Strain sensitivity using FBGs [110] .....	102
Figure 6-3 Measurement system for forming force on individual pins (quarter MPF tool) ..	104
Figure 6-4 different pins shape different force distributions [119].....	106

Figure 6-5 Force distributions on different pins (R=800mm) .....	106
Figure 6-6 Forming force on pin at centre of the punch for different forming radii .....	107
Figure 6-7 Forces on individual pins for different radii of forming curvature .....	108
Figure 6-8 (a) Positions of selected pins and (b) simulated springback value after unloading for 40% compression ratio of elastic cushion .....	109
Figure 6-9 simulation results of different elastic cushion compression ratios.....	110
Figure 6-10 Forming force on individual pins .....	110
Figure 6-11 Springback vs force on different pins for different compression ratios.....	111
Figure 6-12 Experimental setup.....	113
Figure 6-13 Locations of selected pins on MPF tool.....	114
Figure 6-14 Wavelength shift versus forming time for the single pin at the centre of the MPF punch.....	115
Figure 6-15 Validation of simulated forming force for radius of forming curvature 800 mm .....	117
Figure 7-1 Schematic diagram of EP-MPF tool .....	120
Figure 7-2 Experimental setup of EP-MPF .....	121
Figure 7-3 FE models of EP-MPF techniques .....	122
Figure 7-4 Mesh elements and boundary conditions in FE model .....	123
Figure 7-5 Samples of parts fabricated by each technique .....	124
Figure 7-6 Wrinkling measured method [83] .....	124
Figure 7-7 Scan steps to capture formed part .....	126
Figure 7-8 Wrinkling at edge of formed part (R = 400 mm).....	127
Figure 7-9 Springback of formed part along path O-B (R = 800 mm).....	127
Figure 7-10 Forming force-versus time curve for 800 mm radius of forming curvature .....	128
Figure 7-11 Forming force-versus time curve for 400 mm radius of forming curvature .....	129

Figure 7-12 Pressure distributions on top and bottom surface of formed part pre-springback (R=400 mm).....	131
Figure 7-13 Pressure distribution on top and bottom surface of formed part pre-springback (R=800 mm).....	132
Figure 7-14 Wrinkling simulation at formed part using two different techniques (R = 400 mm).....	133
Figure 7-15 Springback simulation results for workpiece formed by MPF and EP-MPF.....	134
Figure 7-16 Springback of part formed by MPF (R = 800 mm).....	135
Figure 7-17 Springback of part formed by EP-MPF (R = 800 mm).....	135
Figure 7-18 Effect of radius of curvature on wrinkling.....	138
Figure 7-19 Effect of radius of forming curvature on forming force .....	139
Figure 7-20 Effect of punch compression ratio on springback.....	140
Figure 7-21 Effect of radius of forming curvature and punch thickness on springback.....	141
Figure 7-22 Effect of radius of curvature and compression ratio on springback.....	141
Figure 7-23 Effect of punch thickness and punch compression ratio on springback .....	142
Figure 7-24 Simulation result of wrinkling for optimum values of process parameters .....	144
Figure 7-25 scanned formed part (optimum process parameters) .....	145
Figure 7-26 Comparison between simulation, experimental results and target shape for optimum values of process parameters .....	145
Figure 7-27 Simulation result of springback for optimum values of process parameters .....	146
Figure 7-28 Springback along diagonal of formed part O-B (mm) for optimum values of process parameters .....	146

## LIST OF TABLES

Table 3-1 Ra for aluminium alloy 5251-O .....	40
Table 4-1 Measured mechanical properties of tested material .....	60
Table 4-2 Process parameters investigated [80] .....	69
Table 5-1 Value and level of the selected DOE parameters [80] .....	80
Table 5-2 Experimental plan and simulation results [80] .....	82
Table 5-3 Factor-response interactions with P-values [80] .....	82
Table 5-4 Coefficient values for objective function [80].....	86
Table 5-5 Comparison of numerical simulation results and experimental validation [80].....	87
Table 6-1 Wavelength changes under forming force for the selected pins.....	115
Table 7-1 Level and value of the DOE parameters.....	136
Table 7-2 Experimental plan and simulation results.....	137
Table 7-3 Process parameters and corresponding P-values.....	137
Table 7-4 Coefficients of objective function .....	143
Table 7-5 Optimum values of process parameters to jointly minimise wrinkling, springback and forming force.....	144
Table 7-6 Predicted and experimental results at optimum process parameters .....	147

## ABBREVIATIONS

ANOVA	Analysis of Variance
BHF	Blank Holder Force
CAD	Computer Aided Design
CCD	Central Composite Design
DA	Displacement Adjustment
DOE	Design of Experiments
EP-MPF	Elastic-Punch Multi-point Forming
FBG	Fibre Bragg Grating
FEA	Finite Element Analysis
LE	Logarithmic Strain
MPDD	Multi-point Deep Drawing
MPF	Multi-point forming
PLC	Portevin–Le Chatelier
RSM	Response Surface Method
SB	Springback
SF	Spring Forward

## NOMENCLATURE

$P^{(k)}$	The form of the working surface and ( $k$ ) number of correction iteration
$\Delta S$	Shape error of the formed part
$\bar{\sigma}$	Effective Von Mises stress
$\sigma_y$	The yield stress
$\alpha$	Back stress tensor
$l_0$	Original length of a line segment
$l_m$	Length of a line segment at the mid-surface
$\varepsilon_\theta$	Circumferential true strain
$\varepsilon_a$	True strain in the mid-plane
$\varepsilon_b$	Bending true strain
$\varepsilon_m$	Membrane engineering strain
$\varepsilon_\theta^p$	Plastic strain
$\sigma_\theta^p$	Circumferential stress
$T^e$	Force produced by the elastic stresses
$T_T^p$	Tensile force produced by the plastic stresses
$T_C^p$	The compressive forces produced by the plastic stresses
$M^e$	Elastic bending moment
$M_T^p$	Plastic part of the total bending moment in the tension area
$M_C^p$	Plastic part of the total bending moment in the compression
$A_0$	original area of the specimen
$r_a$	Plastic anisotropy
$\varepsilon_2 + \varepsilon_3$	Width and thickness strain of the specimen
$\lambda_B$	The Bragg wavelength

$n_{eff}$	Effective refractive index
$\alpha_t$	Thermal expansion
$\alpha_n$	Thermo-optic coefficient
$p_e$	Photo-elasticity coefficient,

# CHAPTER 1: INTRODUCTION

## 1.1 Background

Sheet metal forming is a manufacturing process used widely across the industrial production sector, including domestic appliance (e.g. cooker, sinks, and freezers), the food sector (e.g. cans, pots), the aeroplane industry (e.g. wings, fuselage) and the automobile industry (e.g. hoods, doors, body panels) [1]. In this process, the final shape of a part is achieved through plastic deformation of a flat metal sheet into the required die. In most cases, a certain amount of the elastic deformation is recovered, as happens with, especially, bending, bending-unbending, and reverse bending. This leads to a difference between the desired shape of the part and the unloaded formed part, due to the phenomenon known as springback.

Springback is considered the most common of sheet metal forming defects: a change in the geometry of a final formed part at the completion of the forming process when the product is released from the forming forces. As a result, two factors must be considered in order to achieve the desired final geometry: the springback must be predicted and the part design must allow for this, and appropriate tools and techniques must be used which minimise springback. The quality of the springback prediction depends on accurately modelling the material behaviour of the sheet through the forming process, of correctly specifying the process boundary conditions used for the modelling and, for the FE analysis, determining an appropriate mesh size and element type, and so on.

An additional problem associated with springback occurs when using convention stamping tools or solid tools for producing a designed shape with a specific material. If the material of

the metal sheet is changed, the same tool will produce a noticeably different shaped final product. This means that there would need to be a change in the dimensions of the solid tool (or even a new tool) to compensate for the change in springback effect. This means additional costs, especially in the case of prototype and small batch production. Flexible metal forming processes such as the multi-point forming (MPF) processes and rubber-metal forming is an ideal choice to overcome these problems at least for certain common shapes such as spherical and saddle-shaped parts. In addition to the springback, wrinkling is another defect in sheet metal forming process, especially if the forming process is applied without using a blank holder force to clamp the sheet. This defect will be considered when comparing the quality of the final formed sheet under different working conditions.

## **1.2 Aims and objectives**

### **1.2.1 Overall aim**

The aim of this research was to improve MP sheet forming as a flexible process by (a) improving existing sheet material characterisation techniques, (b) understanding the influence of process parameters in MP sheet forming, (c) minimising MPF process defects in the final formed part by using unique forming techniques, (d) measuring the forming forces on individual pins of MPF tools by using FBG sensors to monitor the elastic strain of the pins.

### **1.2.2 Objectives**

- Revise the literature on springback in sheet forming in general, and on MPF in particular, to understand the phenomenon.
- Develop numerical models of spherical shapes with different radii of curvature to predict springback and study the effect of process parameters on springback.

- Use the test rig designed by Abosaf [2] to conduct experiments on forming spherical shapes in order to measure the magnitude of the springback under various process parameters and validate the numerical models.
- Optimise the most important of the process parameters to minimise springback and thickness variation in the final formed part.
- Measure the forming forces on the individual pins of MPF tools by using Fibre Bragg Grating (FBG) sensors and relate these forces to springback of the final formed part.
- Apply a forming approach (elastic-punch multi-point forming – EP-MPF) to improve the formed part quality in terms of wrinkling and springback.

### **1.3 Research hypothesis and methodology**

The hypothesis of this research is that flexible forming tools such as rubber tools can be combined with MPF to improve the quality of the shape of the formed part.

This research used the ABAQUS finite element modelling (FEM) software as a simulation tool with statistical analysis, to investigate the effect of simulation and process parameters on the quality of the formed part. Subsequently, flexible MPF tools were used to validate the simulation findings.

### **1.4 Structure of the thesis**

This thesis contents eight chapters structured as follows:

Chapter 1 presents a brief explanation of the research field and outlines the scope and aim of the research with research hypothesis and methodology. Chapter 2 provides a comprehensive overview of sheet metal forming by traditional and flexible methods, offering an understanding of the springback phenomenon in metal forming processes analytically,

numerically and experimentally. Finally, a description is given of how to use optimisation techniques in the field of metal forming. The mechanical properties of materials used are presented in chapter 3 which explains how they were obtained experimentally. The forming tools and measurement apparatus required in this research are described in detail. Chapter 4 gives details of the process models for MPF, providing an overview of modelling processes using ABAQUS software, development of FEM for MPF is presented and following that, model validation by experiment. Finally, the effect of process parameters on springback is discussed. Chapter 5 contains results and discussion of the optimisation of the main process parameters; radius of curvature of the form, value of blank holder force, elastic cushion thickness and their effect on quality of doubly curved parts in MPF. The influence of these parameters on springback and thickness variation across the formed panel are investigated, also the subsequent effect of those variations on springback is explored. Chapter 6 explains the procedure of modelling the forming force on individual pins, and then validation of the simulated results experimentally, followed by establishing a relationship between these forces and springback in the final formed part. Chapter 7 introduces a forming technique to form doubly curved panels. The comparison between products produced by conventional MPF tools and the proposal technique are presented in term of wrinkling and springback. The contribution of this work to, and its expected benefits for, sheet metal forming are summarised in Chapter 8.

## CHAPTER 2: LITERATURE REVIEW

### 2.1 An overview of metal forming technology

Materials are converted into final products via different manufacturing processes of which metal forming is a very important one, due to its advantages which include the flexibility of the process, material saving and possible enhancement of the material's properties.

Metal forming is divided into two basic groups, bulk deformation and sheet metal deformation, determined by the size and shape of metal workpiece. These are sub-divided depending on the forming process used to shape (form) the metal, as shown in Figure 2.1. It is also possible to divide the processes according to the temperature of the material during the forming process. Based on temperature, there are three categories: cold, warm and hot forming as shown in Figure 2.2, where  $T_A$  is the ambient temperature and  $T_m$  is the melting temperature of the work metal. In term of operation, processes can be classified as a primary process where raw material at high temperatures is cast into convenient shapes such slabs, plates and billets, and a secondary process where the output of the primary process is used to produce, e.g. sheets and wire.

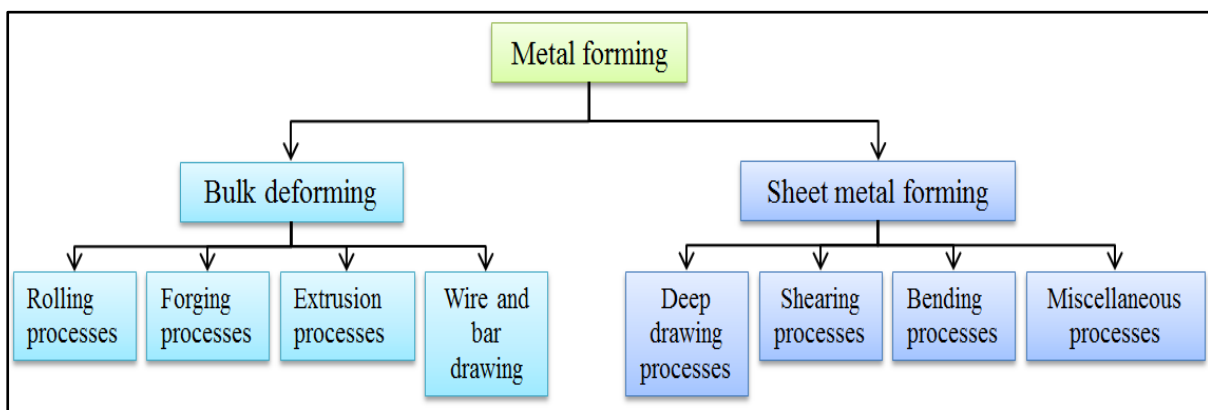


Figure 2-1 Categories of metal forming processes [3]

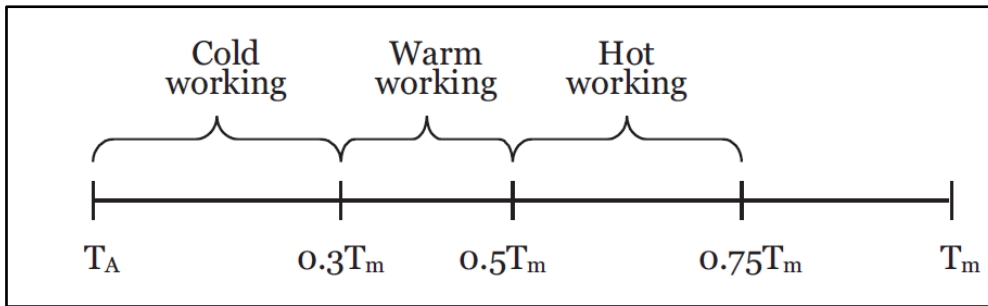


Figure 2-2 Temperature ranges for different metal forming operations

A metal sheet (metal blank) is formed into a required shape in a method called metal forming. Usually, in metal forming processes, the forming tools consist of rigid parts, which typically include a die that contains the design shape, a punch to drive the metal sheet into the die and a blank holder to fix the sheet throughout the forming process, as shown in Figure 2.3.

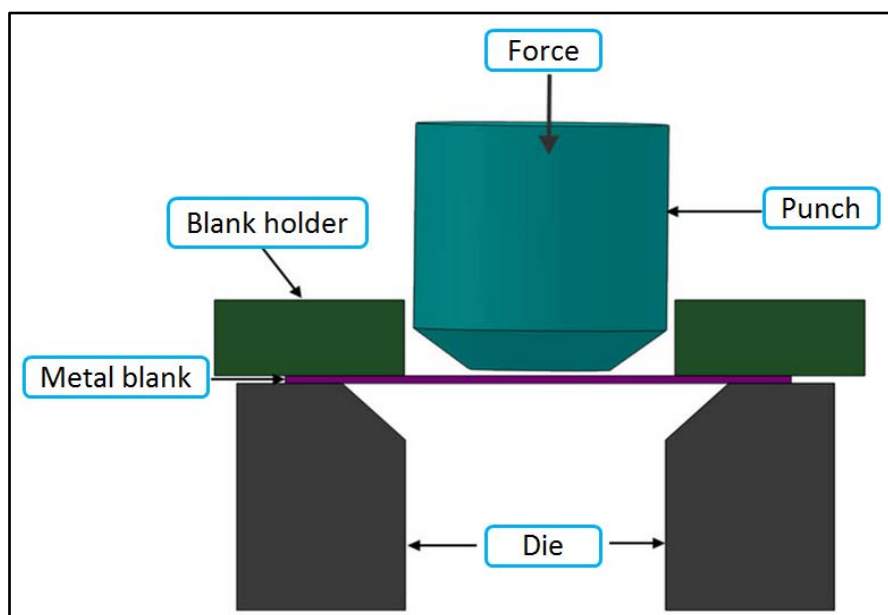


Figure 2-3 Schematic of the drawing process

However, in some methods used to form metal sheet, there is no requirement to hold the sheet and this is known as air bending, see the V-bending shown in Figure 2.4.

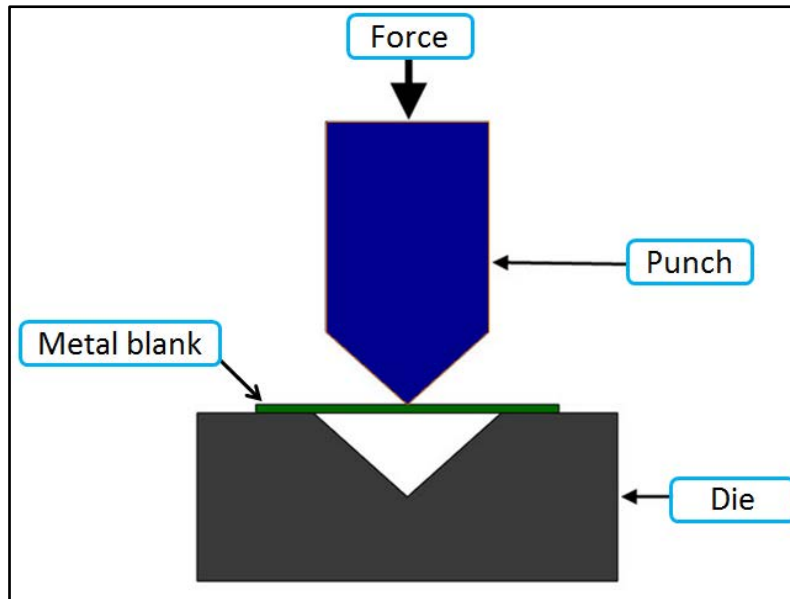


Figure 2-4 V Bending

The most widely used conventional technique to obtain a three-dimensional formed shape is stamping. For mass production, tools are designed specifically for each target shape, but these tools are both very large and very expensive, so this technique is unsuitable for producing low numbers of products [4]. As a result, a new forming technology was developed [5], using changeable discrete dies to produce three-dimensional surfaces.

The type of tool used to deform the metal sheet is considered to be the main difference between the conventional and unconventional forming processes. Usually, in conventional forming, a rigid punch drives the sheet into the die using tensile and compressive forces. In the so-called unconventional forming processes, a flexible tool using discrete pins, fluids or an elastic block is used to force the sheet into the die [6].

## 2.2 Flexible tooling in metal sheet forming

Flexible tool techniques for metal sheet forming, such as multi-point forming (MPF) and rubber-pad forming are used in manufacturing field to decrease the time and cost of

production. The MPF process is a technique developed initially for metal sheet forming using a geometrically reconfigurable die as shown in Figure 2.5. The MPF tool is fabricated of two matrices of pins whose lengths can be varied independently to allow an approximation of a three-dimensional surface to be constructed. The application of flexible tools in metal forming procedures has become common-place in many industrial applications, including, aerospace, architecture and automobiles.

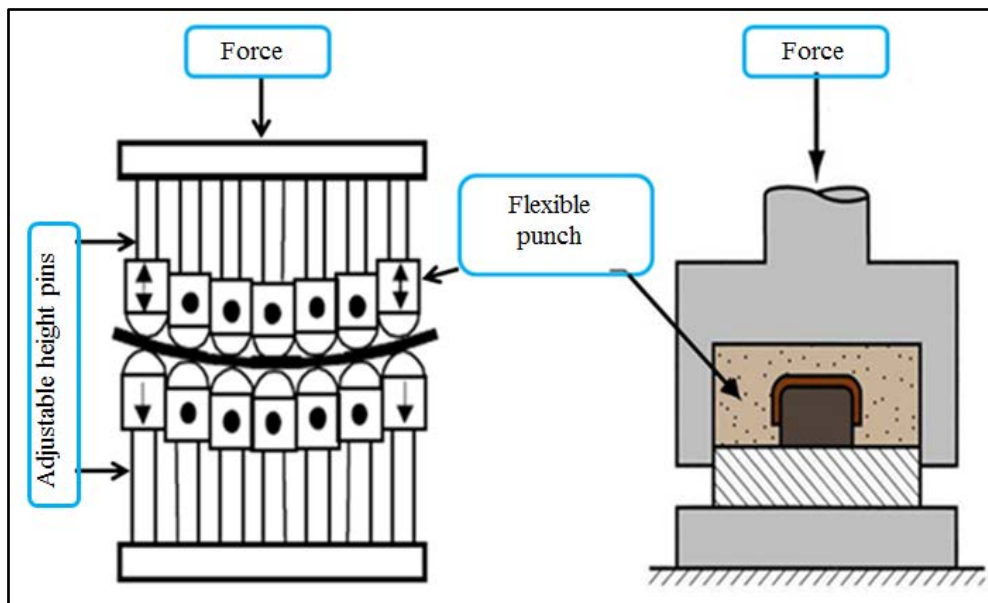


Figure 2-5 Schematic diagram of a flexible forming tool

Adopting this technology provides several advantages, such as different forms can be produced using the same or similar tools as shown in Figure 2.6 [7]; springback can be compensated for after starting production by re-adjusting pin height. Such a flexible approach supports low batch and prototype production. On the other hand, the limitation in the ability of these tools to produce complex shapes or sharp sides is considered as a disadvantage.

Wrinkling [8], thinning [9], cracking and necking [10] are defects associated with traditional metal forming processes as well as MPF, which also exhibits dimpling as a consequence of

discontinuous contact between pins and the metal sheet [11]. In addition, there is always the deviation between target shape and formed part due to springback [12].

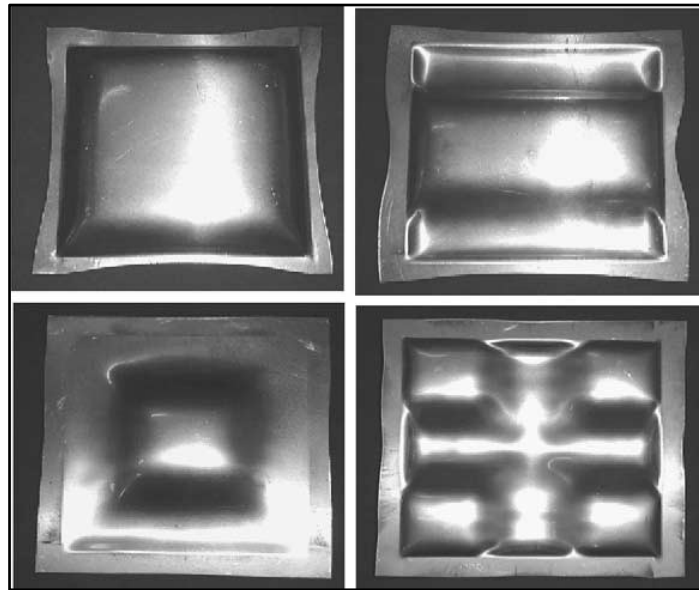


Figure 2-6 Different parts formed by MPF [7]

As explained in Chapter 1, springback is a common defect in sheet metal processes and needs to be minimised or compensated for, depending on part usage [13]. Using an elastic cushion, a layer of material with an appropriate hardness and thickness between the pins and the metal sheet, is an effective technique to eliminate the dimples in MPF processes by distributing the concentrated stresses over the entire sheet [14]. Similarly, as in conventional stamping, forming sheet metal using a blank holder (as shown in Figure 2.7) can suppress wrinkling and control the springback. Sun *et al.*, [15] reported that using a flexible blank holder enhanced the forming limit and removed wrinkling in thin metal sheets.

Cycle production time is reduced using this technique because a range of three-dimensional surface shapes can be constructed without replacing the entire tool; instead, the positions of

the pins are changed according to the new shape geometry. Furthermore, additional costs are avoided because the construction of very costly rigid dies is eliminated [16].

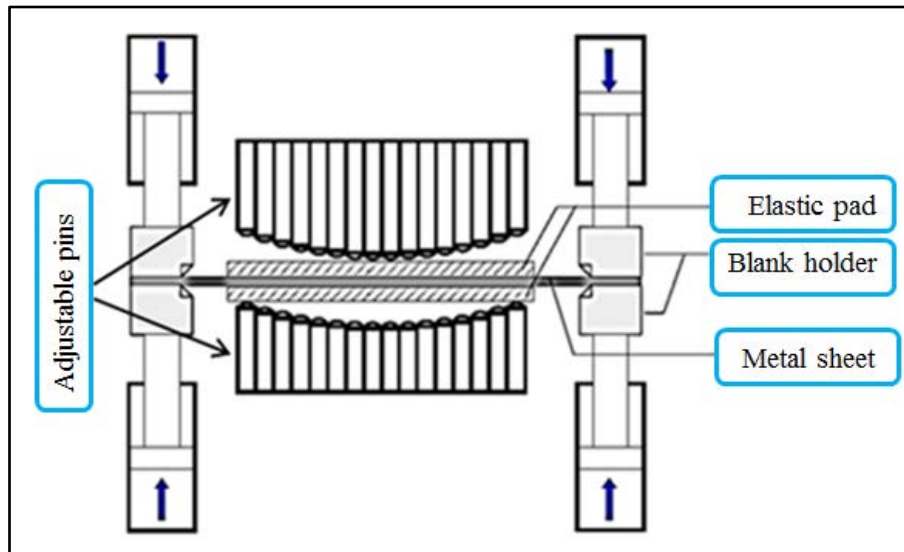


Figure 2-7 Schematic diagram of MPF process using blank holder [17]

When the punch is removed at the end of forming stage, the elastic element of strain is recovered, particularly where bending, bending-unbending, and reverse bending are concerned. The associated springback due to this strain causes errors in the dimensions of the final object compared to the desired object. However, pin height modification can be used to compensate for springback [18]. The shape of the formed part at the end of the forming step is compared to the target shape, then the pins are reconfigured, in an iterative process, according to the difference between the two shapes, systematically reducing the difference [19-21].

The procedure, in general, is expressed as [20]:

$$\mathbf{P}^{(k+1)} = \mathbf{P}^{(k)} + \nabla^{-1} \mathbf{F}^{(k)} \Delta \mathbf{S}^{(k)} \quad (2.1)$$

Where  $k$  presents the total number of correction iterations, see Figure 2.8;  $P^{(k)}$  is the form of the working surface and  $\Delta S^{(k)}$  is the shape error of the formed part after  $k$  correction iterations;  $P^{(k+1)}$  is the working surface for the following iteration as seen in Figure 2.8(b) and  $\nabla^{-1} F^{(k)}$  is an improvement matrix. For a digitized tool contained  $m \times n$  pins on each part, the entire profile error of a formed part is estimated by [20]:

$$E_s^{(k)} = \frac{1}{mn} \sum_{i=1}^{m \times n} |\Delta S_i^{(k)}| \quad (2.2)$$

Springback can be explained by reference to the stress-strain curve as presented in Figure 2.9. By releasing all applied forces and moments the point B would follow the line BC, and AC would represent the permanent (plastic) deformation. CD is the recovered (elastic) deformation, the springback. It can be seen that the elastic recovery is bigger for materials with greater strength. Elastic recovery is the most important parameter obstructing the attainment of the required dimensional accuracy of formed shapes [22].

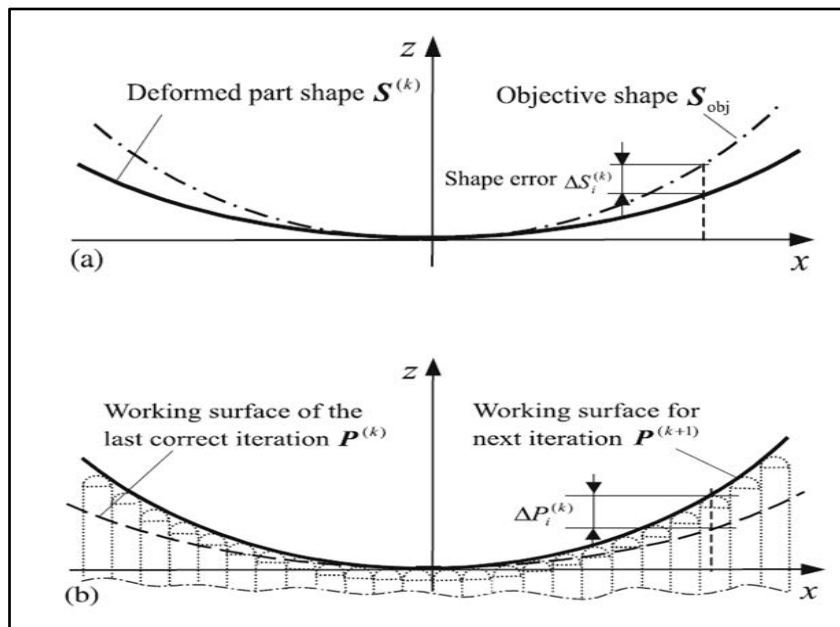


Figure 2-8 Springback modification of the working surface of a digitised tool [20]

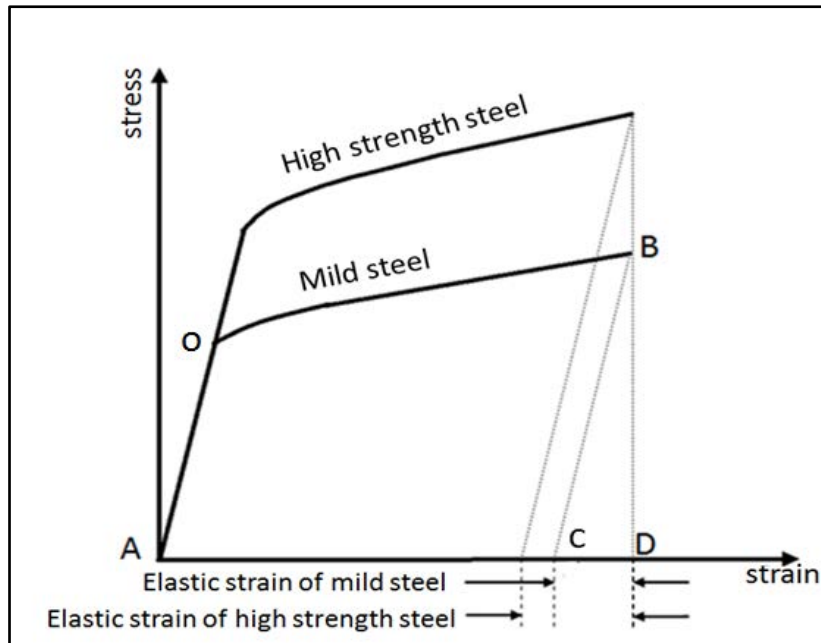


Figure 2-9 Elastic recoveries during unloading [22]

### 2.3 Plasticity in metal sheet forming

Throughout the deformation stage of metal sheet, if the strain value is low (elastic region) most metals exhibit an approximately linear elastic behaviour and the slope of the line (AO) known as the modulus of elasticity or Young's modulus is constant [10]. If the applied load reaches some critical value, called the yield stress, which is a property of the material, the relationship between stress and strain becomes nonlinear, and the material exhibits inelastic behaviour, which is referred to plasticity (plastic deformation region).

Elastic deformations are reversible; the energy consumed in the deformation is stored as elastic strain energy and is fully recovered upon load removal. Permanent deformations are irreversible and the original form can be achieved only by applying more energy. Finite element analysis (FEA) can be used to simulate and predict metal sheet forming processes and determine defects in a formed part due to such factors as springback. The accuracy of simulation results depends on the accuracy to which the process factors (friction, tool

geometry, forming speed, etc.) and simulation input parameters (element size, material constitutive model, contact control, etc.) are known. Among these factors, the material's constitutive equations play an important role in describing the stress distribution in the formed part. A number of constitutive models are available to define early yielding and its development throughout the plastic deformation stages, for instance, isotropic hardening and kinematic hardening models [23].

### 2.3.1 Isotropic hardening

When a material is subject to plastic deformation it can, beyond a certain level of deformation undergo work hardening (also known as strain hardening). This apparent increase in strength is the additional stress necessary to produce further plastic deformation and is often a function of aggregated plastic strain. Figure 2.10 shows a uniaxial stress-strain curve with nonlinear hardening together with chart illustrations of primary and following yield surfaces. In case of uniform expansion in stress space, the hardening is referred to as isotropic. In Figure 2.10, as the load changes in vertical direction, hence the load starts from zero till it comes across the yield surface at  $\sigma_2 = \sigma_y$ , where yield take place at this point. For hardening to occurs, as the load ( $\sigma_2$ ) increases the yield surface also expand as shown in Figure 2.10. The degree of expansion is often taken to be a function of total plastic strain. So for the isotropic hardening, the yield function equation is expressed as [23]:

$$f(\sigma) = \bar{\sigma} - \sigma_y = 0 \quad (2.3)$$

where  $\bar{\sigma}$  represents the effective Von Mises stress and  $\sigma_y$  is the yield stress

The yield surface increases uniformly as indicates in Figure 2.9. The yield stress with the opposite loading is equivalent to that in forward loading. Therefore, isotropic hardening is not

often sufficiently accurate to define the Bauschinger effect and kinematic laws need to be introduced.

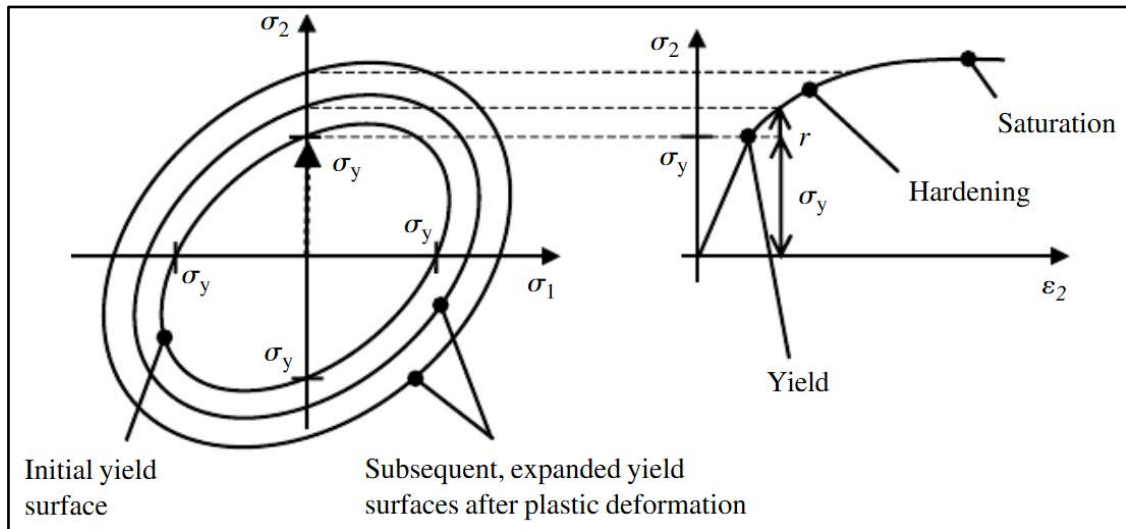


Figure 2-10 The yield surface expands under the isotropic hardening assumption [24]

### 2.3.2 Kinematic hardening

Figure 2.10 illustrates isotropic hardening and shows how this leads to a large elastic area throughout reverse loading but this is often not what would be observed in experimental data. A much smaller elastic area is estimated and this is a consequence of what is named the Bauschinger effect, and kinematic hardening. The yield surface translates in stress space as kinematic hardening rather than growth due to this effect as shown in Figure 2.10.

In Figure 2.11, the load increases till yield stress  $\sigma_y$ . By increasing the load to point (1), the plastic behavior describes the material deformation flow, and then the load is reversed therefore the material deforms elastically and the load reaches point (2). As a consequence to this action, the initial yield surface expanded.

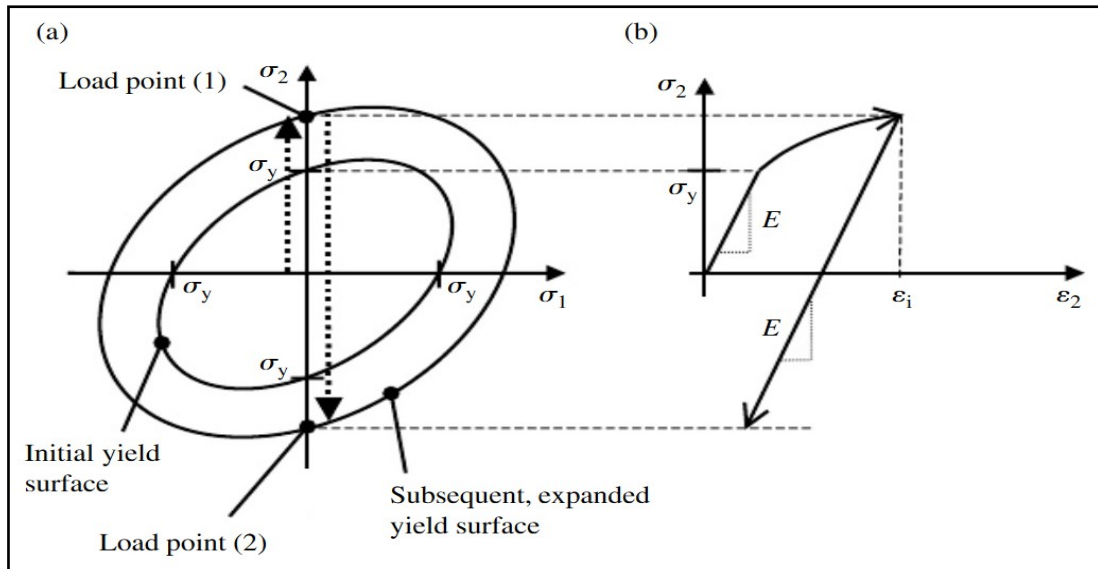


Figure 2-11 Reverse loading with isotropic hardening [24]

The early yield surface is shown in Figure 2.12. When loaded and subject to plastic deformation, the surface transforms to a different position as shown, such that the original middle point has been transformed by  $|x|$ . Thus, the stresses relative to the new centre of the yield surface should be checked for yield. Usually, the formula for yield surface with kinematic hardening is written as [22]:

$$f(\sigma - x) - \sigma_y = 0 \quad 2.4$$

where  $x$  is the back stress tensor and determines the position of the centre of the yield surface.

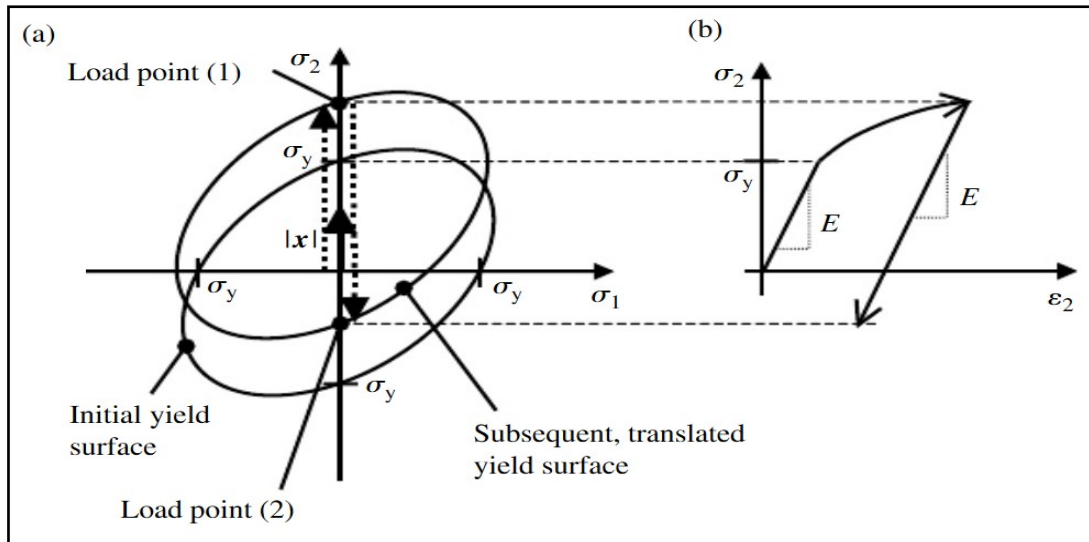


Figure 2-12 Shows (a) the transformation of yield surface under kinematic hardening, and (b) stress-strain curve with shifted yield stress in compression [24]

## 2.4 Springback phenomenon in metal sheet forming

Springback is known as an elastically driven variation of a final part, which happens with the removal of external forces. It is a complicated physical phenomenon, which is principally determined by the stresses within the part during the final step of the forming process. There are several categories of springback according to the final product shape and type of deformation: bending, twisting, membrane and combined bending and membrane [25]. Springback in the case of pure bending can be detected after bending a part in plane strain. Twisting springback can be observed while forming parts with large variances in sectional measurements [27]. In the unloading stage of a material, in-plane tension or compression can be detected as membrane springback. Combined bending and membrane elastic recovery is often found in manufacturing. The shape of the final product is typically very complex because the raw material is formed out-of-plane and at the same time stretched or compressed in-plane [28].

To accurately model springback in metal forming, requires a good understanding of the phenomenon. Simple experiments and complex tests have been carried out to explore the sensitivity of elastic recovery to numerous factors and to gain a good understanding of material behaviour in the forming process. Several approaches exist to predict springback. In the case of simple shape forming, the analytical solutions are considering an effective way to describe this phenomenon, while for more complex products FEA is used to predict elastic recovery and the final shape. When adopting the FE approach, it is essential to remember that the accuracy of the results obtained is controlled by the many parameters that are responsible for the accuracy of the simulation of the forming stage [28].

#### **2.4.1 Analytical methods to predict springback in metal forming**

Analytical solutions for springback in the metal forming process are derived from the modelling of a simple two-dimension problem, for example, plane strain bending, stretch bending, drawing and plane strain cyclic bending. As shown in Figure 2.13, the radius of curvature is  $\rho$ ,  $\theta$  is the angle of bend,  $M$  is the moment per unit width and  $T$  is the tension applied at the middle surface of the sheet (force per unit width) [9].

Consider the bending process of a sheet along a straight line in Figure 2.14 a. A plane strain form is assumed to exist in the plane vertical to the bending line and the cross-section remains plane and normal to the mid-surface after unloading [28]. The two-dimensional case is shown in Figure 2.14.

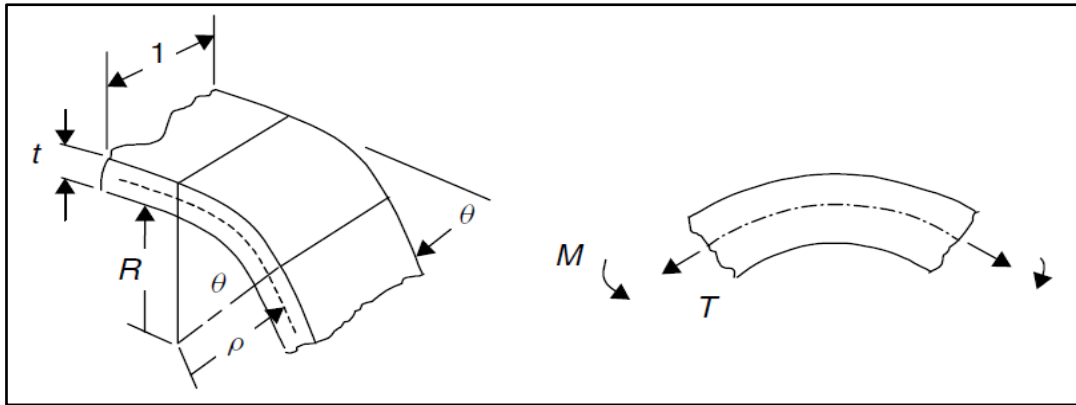


Figure 2-13 Sheet bending along a line [29]

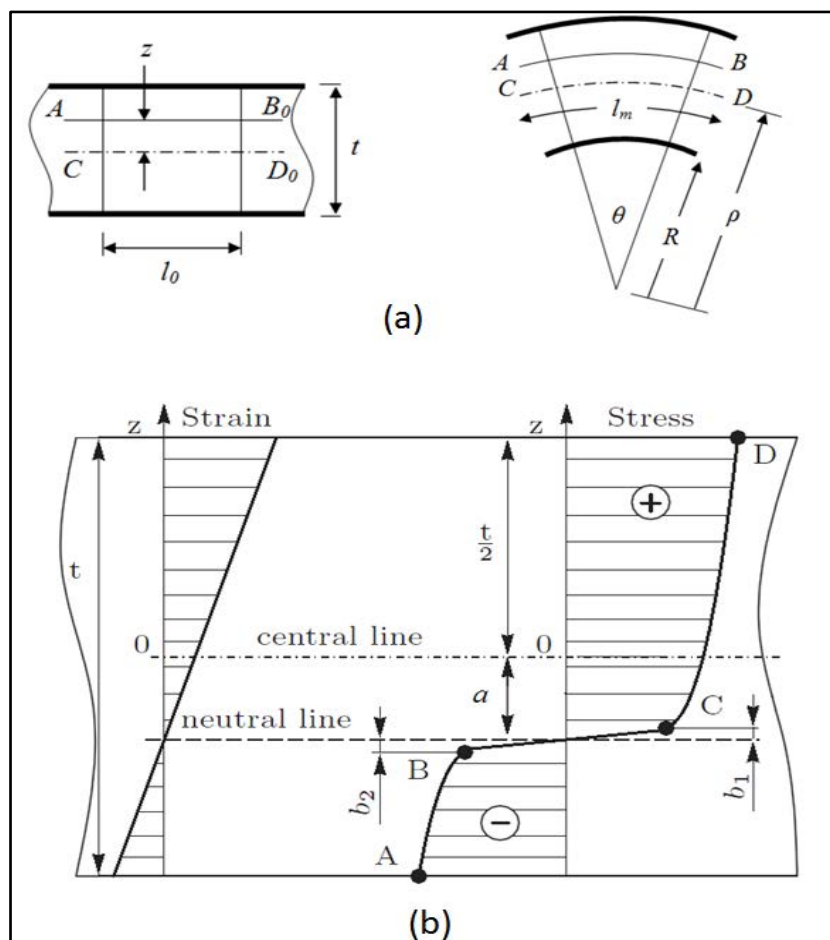


Figure 2-14 Plane strain bending: (a) parameter explanation; (b) Equilibrium diagram of stress distribution [29]

The initial length of the segment is  $l_0$  ( $AB_0$ ) located at a distance  $z$  beyond the mid-surface ( $CD_0$ ). After bending through an angle  $\theta$  the radius of curvature will be  $\rho$  and the length of the segment will be  $l$  ( $AB$ ). The radius of curvature of the bend is  $\rho = R + 0.5 t$ , where  $t$  is sheet thickness and  $R$  is the internal radius. The slice length  $l$  can be written in terms of the length of the fibre at the mid-surface  $l_m = (\rho\theta)$ , the radius of bend curve and the distance  $z$ :

$$l = (\rho + z) \theta = l_m \left( 1 + \frac{z}{\rho} \right) \quad 2.5$$

The circumferential true strain is known [28]

$$\varepsilon_\theta = \ln (l/l_0) = \ln \left[ \frac{l_m}{l_0} \left( 1 + \frac{z}{\rho} \right) \right] \quad 2.6$$

This can be divided into components, the true strain in the mid-plane:

$$\varepsilon_a = \ln \left( \frac{l_m}{l_0} \right) \quad 2.7$$

Plus bending true strain:

$$\varepsilon_b = \ln \left( 1 + \frac{z}{\rho} \right) \quad 2.8$$

If the inner radius of curvature  $R$  is large, we could ignore the difference between the engineering strain value and the true strain value, and the engineering strain is simpler to deal with.

The membrane and bending engineering strain can be expressed as:

$$e_m = \Delta l_m / l_0 \quad 2.9$$

$$e_b = \frac{z}{\rho} \quad 2.10$$

The membrane strain has a value of:

$$\varepsilon_m = \frac{a}{\rho} \quad 2.11$$

where the location of a neutral line is  $a$ , as shown in Figure 2.13b. The whole engineering circumferential strain can be written as:

$$e_\theta = \frac{z + a}{\rho} \quad 2.12$$

Assuming isotropic material behaviour, for the plane strain condition, in a state of the Von Mises yield situation, the main stress can be obtained from [29]:

$$\sigma_1 = \frac{2}{\sqrt{3}} \sigma_f = S_0 \quad 2.13$$

where  $\rho_f$  is the uni-axial flow stress and  $S_0$  is the plane strain flow stress.

Normally, metal shows elastic-plastic behaviour with strain-hardening performance. In the elastic region, the circumferential stress is obtained from Hook's law for plane strain:

$$\sigma_\theta = \frac{E}{1-\nu^2} \varepsilon_\theta = E' \varepsilon_\theta \quad 2.14$$

where  $E$  is Young's modulus and  $\nu$  is Poisson's ratio. A power law estimates the plastic-hardening behaviour [28]:

$$\sigma_\theta = \bar{C} (\varepsilon_0 + \varepsilon_\theta^p)^n \quad 2.15$$

Where  $\bar{C}$  and  $n$  are hardening factors.  $\varepsilon_0$  being a pre-strain it can be estimated from the earlier condition:

$$\sigma_{f(0)} = C \varepsilon_\theta^n \quad 2.16$$

where  $\rho_{f(0)}$  is the primary uni-axial yield stress and  $C$  is the coefficient of strength of the material in the uni-axial case. The relationship between the plane strain and uniaxial magnitude of this constraint can then be estimated by [28]:

$$C' \approx C \left( \frac{2}{\sqrt{3}} \right)^{n+1} \quad 2.17$$

#### 2.4.1.1 Loading stage

The stresses that act on the part being formed during the deformation process are represented by the next derived equation. Let the location of the yield points in the region where the part is in compression or tension be determined by variables  $b_1$  and  $b_2$  where these parameters are defined relative to the neutral line as shown in Figure 2.14(b).

In areas of tension or compression stresses, the coordinates of the yield points are [10]:

$$z_1 = -a + b_1 \quad (2.18)$$

$$z_2 = -a - b_2 \quad (2.19)$$

Substitute Eqs. (2.16) and (2.17) into Eq. (2.12) to yield the strain value in

the tension area as:

$$\varepsilon_{\theta t}^y = \frac{z_1 + a}{\rho} = \frac{b_1}{\rho} \quad (2.20)$$

and in the compression area as:

$$\varepsilon_{\theta c}^y = \frac{z_2 + a}{\rho} = -\frac{b_2}{\rho} \quad (2.21)$$

The boundaries of the elastic section are defined by the variables  $b_1$  and  $b_2$  and can be found by applying Hooke's law:

$$b_1 = b_2 = \rho \varepsilon_{\theta t}^y = \frac{\rho}{E'} S_0 \quad (2.22)$$

The value of  $E'$  is obtained from Eq. (2.14) and  $S_0$  is the primary plane strain flow stress, Eq. (2.13).

The entire circumferential strain ( $\varepsilon_\theta$ ) can be defined in plastic deformation area as the total constant strain at yield ( $\varepsilon_\theta^y$ ) and the strain due to the material work hardening ( $\varepsilon_\theta^{wh}$ ):

$$\varepsilon_\theta = \varepsilon_\theta^y + (\varepsilon_\theta^{wh}) \quad (2.23)$$

The above equation can be re-written in term of material work-hardening in the regions subject to tension and compression:

Tension region 
$$\varepsilon_{\theta t}^{wh} = \varepsilon_{\theta t} - \varepsilon_{\theta t}^y = \frac{z+a}{\rho} - \frac{S_0}{E'} \quad (2.24)$$

Compression region 
$$\varepsilon_{\theta c}^{wh} = \varepsilon_{\theta c} - \varepsilon_{\theta c}^y = \frac{z+a}{\rho} + \frac{S_0}{E'} \quad (2.25)$$

Eq. (2.15) determines the circumferential stress in the plastic deformation area. To obtain the stress, the plastic strain needs to be identified. The plastic strain is calculated by adding the plastic strain to the strain due to work-hardening. However, the plastic strain  $\varepsilon_\theta^p = \varepsilon_\theta - \varepsilon_\theta^e$  is less than the strain due to work-hardening  $\varepsilon_\theta^{wh} = \varepsilon_\theta - \varepsilon_\theta^y$  and, thus the circumferential stress is overestimated.

In conclusion, the circumferential stress in the plastic region of the part being formed can be written as:

that due to tension 
$$\sigma_{\theta t}^p = C' \left( \varepsilon_0 + \frac{z+a}{\rho} - \frac{S_0}{E'} \right)^n \quad (2.26)$$

that due to compression 
$$\sigma_\theta^p = - C' \left( \varepsilon_0 + \left| \frac{z+a}{\rho} + \frac{S_0}{E'} \right| \right)^n \quad (2.27)$$

In the area being compressed, the plastic strain is negative; thus, its absolute magnitude is used in the power law to obtain the circumferential stress. The force and bending moments acting on per unit length of the part can be calculated from:

$$T = \int_{-t/2}^{t/2} \sigma_\theta dz \quad (2.28)$$

$$M = \int_{-t/2}^{t/2} \sigma_{\theta} dz \quad (2.29)$$

The tensile force can be divided into three component parts:

$$T = T^e + T_T^p + T_C^p \quad (2.30)$$

Where  $T^e$  present the force produced by the elastic stresses,  $T_T^p$  is the tensile force produced by the plastic stresses and  $T_C^p$  is the compressive forces produced by the plastic stresses. The contributions of the elastic and the plastic stresses to the total tension will be:

$$T^e = \int_{z2}^{z1} E' \frac{z+a}{\rho} dz \quad (2.31)$$

$$T_T^p = \int_{z1}^{t/2} C' \left( \varepsilon_0 + \frac{z+a}{\rho} - \frac{S_0}{E'} \right)^n dz \quad (2.32)$$

$$T_C^p = - \int_{-t/2}^{z2} C' \left( \varepsilon_0 \left| \frac{z+a}{\rho} + \frac{S_0}{E'} \right| \right)^n dz \quad (2.33)$$

The sum of Eqs. (2.31), (2.32) and (2.33) gives the total moment per unit width acting about the mid-plane:

$$M = M^e + M_T^p + M_C^p \quad (2.34)$$

Where  $M^e$  is the elastic bending moment,  $M_T^p$  is the plastic part of the total bending moment in the tension area and  $M_C^p$  is the plastic part of the total bending moment in the compression area:

$$M^e = \int_{z2}^{z1} E' \frac{z+a}{\rho} z dz \quad (2.35)$$

$$M_T^p = \int_{z1}^{t/2} C' \left( \varepsilon_0 + \frac{z+a}{\rho} - \frac{S_0}{E'} \right)^n z dz \quad (2.36)$$

$$M_C^p = - \int_{-t/2}^{z2} C' \left( \varepsilon_0 \left| \frac{z+a}{\rho} + \frac{S_0}{E'} \right| \right)^n z dz \quad (2.37)$$

### 2.4.1.2 Unloading stage – (springback)

In this stage, the applied forces on the sheet are removed and the formed blank will release the bending moments. This springback (i.e. change in curvature of the formed parts) will change the final shape from that of the target shape. The total difference between design shape and the formed will be a function of the applied forces. The variation in internal stresses due to elastic unloading will be:

$$\Delta\sigma_{\theta} = E'\Delta\varepsilon_{\theta} \quad (2.38)$$

where

$$\Delta\varepsilon_{\theta} = \frac{z}{\rho} - \frac{z}{\rho'} = \Delta\left(\frac{1}{\rho}\right)z \quad (2.39)$$

After unloading,  $\rho'$  presents the radius of curvature of the formed part.

The change in bending moment  $\Delta M$  due to the difference in internal stresses can be calculated from [10]:

$$\Delta M = \int_{-t/2}^{t/2} \Delta\rho_{\theta} z dz = \int_{-t/2}^{t/2} E' \Delta\left(\frac{1}{\rho}\right) z^2 dz \quad (2.40)$$

$$\Delta M = \frac{E' t^3}{12} \Delta\left(\frac{1}{\rho}\right) = \frac{t^3}{12} \frac{\Delta\rho_{\theta}}{z} \quad (2.41)$$

while  $\Delta M = -M$  as a result of removal of the applied forces. Then, the difference in forming curvature due to the applied bending moment is:

$$\frac{E' t^3}{12} \Delta\left(\frac{1}{\rho}\right) = -M \quad (2.42)$$

Re-arranging gives

$$\Delta\left(\frac{1}{\rho}\right) = -\frac{12M}{E' t^3} \quad (2.43)$$

The bending angle,  $\theta$ , will change with change in bending curvature. This can be calculated from the length of bending arc  $l$  which remains constant after springback.

$$l = \theta \rho \quad \text{so} \quad \theta = l \frac{1}{\rho} \quad (2.44)$$

Differentiating, Eq. (2.44) with respect to bending curvature gives an expression for change in bending angle (springback),  $\Delta\theta$ :

$$\frac{d\theta}{d\left(\frac{1}{\rho}\right)} = l = \rho\theta \quad (2.45)$$

which may be written: 
$$\Delta\theta = \Delta\left(\frac{1}{\rho}\right) \rho\theta = -\frac{12M}{E't^3} \rho\theta \quad (2.46)$$

From Eq. (2.46), it is possible to define the relationship between springback and some of the parameters that affect it. For example,  $\Delta\theta$  (springback) is proportional to the angle of bending  $\theta$ ; also, it is proportional to the ratio  $\frac{\rho}{t^3}$ . The presence of  $t^3$  in the denominator means the thickness of metal sheet has a very strong (inverse) effect on the magnitude of the springback.

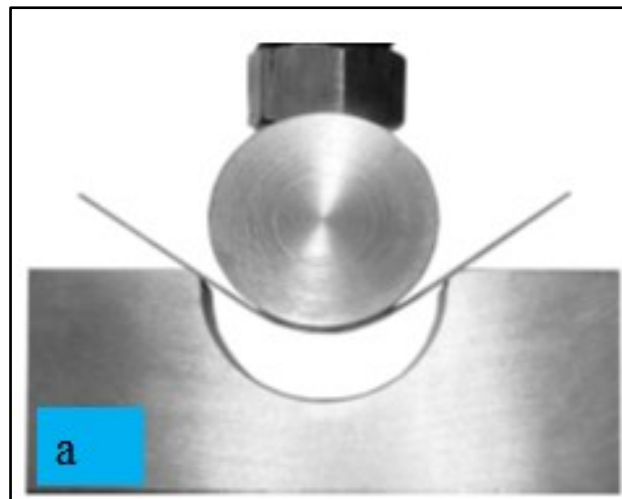
#### 2.4.2 Numerical approach to predict springback in metal forming

To predict formed part quality in sheet metal forming, many trials are necessary to reach a suitable die design to produce defect-free parts. Finite element simulations are used to improve the quality of the final shape by predicting the outcome of the deformation process by taking into account such factors as material properties, contact status, stress-strain distribution, history of the forming force and force release method, etc. The most significant parameters that affect the springback reported in the literature are part geometry, the material selected, element type and final part quality.

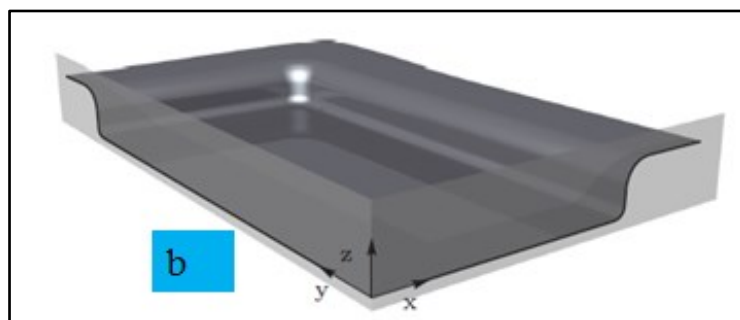
Springback depends on the shape of the formed object and three simple shaped components have been used in studies to study the influence of modelling parameters on springback [28] as shown in Figure 2.15; (a) unclamped cylinder bending, (b) the scaled-down car roof and (c) the top-hat section. Description of material behaviour during the initial yielding and

plastic deformation are critical parameters in the FEA of metal sheet forming [28, 30]. It is essential to use reliable data in order to obtain a precise forecast of material behaviour during the stamping process.

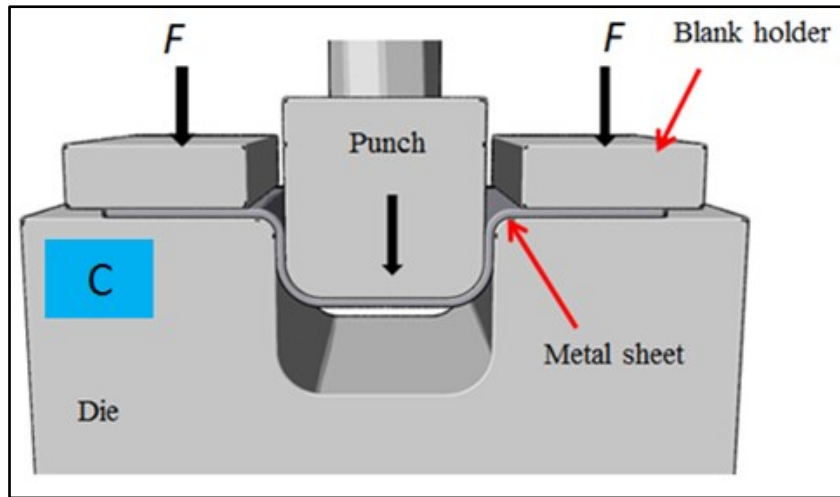
Springback simulation also is affected by the contact condition between the formed sheet and the tools [30]. Two main methods are used equally in FE simulations to describe the friction between the forming tools and the metal sheet; (1) the penalty method and (2) the Lagrange multiplier method [31]. For accurate FE analysis of springback, there are different element types based on final geometry and forming procedure that can be used to describe the sheet.



Unclamped cylinder bending (cont.)



Scaled-down car roof (cont.)



Top-hat section

Figure 2-15 Three parts a,b and c known as sensitive to springback [28]

Some very simple forming processes can be simulated as two-dimensional and axisymmetric, but in most cases, a three-dimensional model is needed [32]. In recent years, new forming methods have been invented to reduce production costs, such as multi-point forming, rubber forming and hydroforming. These new techniques have created secondary problems such as how to simulate hyper-elastic materials [28].

Today, several commercial codes such as MARC, COSMOS or ABAQUS [32] are available to represent the mechanical behaviour of diverse materials and in this research, ABAQUS was chosen as the simulation tool for modelling and analysing flexible metal forming processes [33, 34]. Two main methods have been used to solve the dynamic equilibrium equations at every time step in the forming process. The first is the explicit method which takes the conditions at time  $t$  to find an expected solution at time  $t+\Delta t$ , without iterating to check the convergence of the solution. This requires a relatively small time step to obtain accurate results. The second method is the implicit approach which obtains a solution at time  $t+\Delta t$  using the solution obtained at time  $t$  but with an iteration procedure to give the required

level of accuracy [35]. Sun *et al.*, [34] investigated fast and slow linear contacts for a range of simple dynamic problems and monitored the difference in results obtained by implicit and explicit integration approaches. They concluded that the explicit method is much less computationally expensive than the implicit for fast contact problem. In contrast, the implicit method is more suitable for slow contact problems.

Narasimhan and Lovell [36] applied the explicit technique for the loading step analysis and the implicit method for the unloading step (springback). The springback predictions obtained showed good agreement with the experimental results. Li *et al.*, [37] reported that the contact behaviour in the metal sheet forming process is very complicated during the loading step, especially in MPF. That the use of an implicit algorithm to solve this type of problem will need a huge memory and a lot of processing time, and includes the possibility of a failure to converge to a solution. Use of the explicit method is more suitable for contact problems such as metal forming (quasi-static problems) in terms of improving solution efficiency. The unloading of the formed part was a simpler process due to there being no contact issues, and the implicit algorithm provided good results with less calculation time.

### **2.4.3 Experimental approach to predict springback in metal forming**

To study and characterise springback in sheet metal forming experimentally, several techniques have been utilised, the most common one is air bending V-bending [38], U bending [39] and straight flanging [40]. These approaches are attractive as the springback magnitude is large and easy to measure, see Figures 2.16-2.18. These methods are usually chosen to investigate the effect of basic parameters, such as mechanical properties of the sheet, tool radius and sheet thickness on springback.

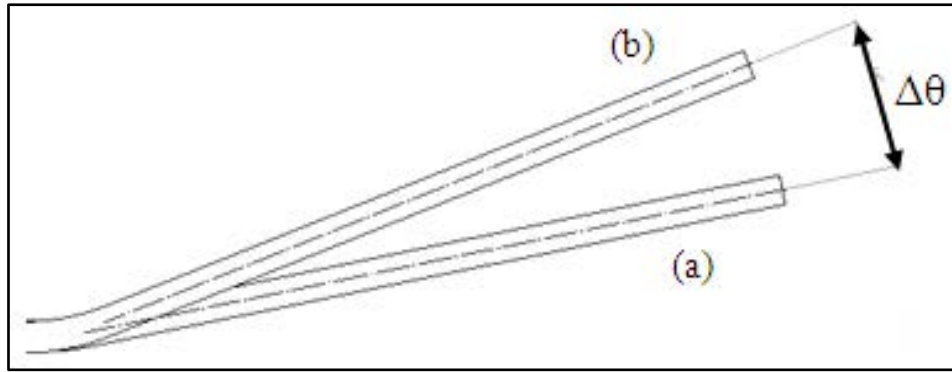


Figure 2-16 Springback ( $\Delta\theta$ ) for V-bending (a) loading (b) unloading step

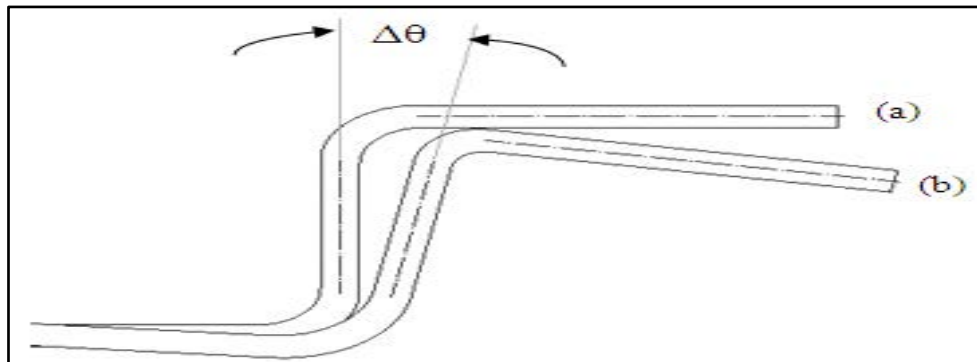


Figure 2-17 Springback ( $\Delta\theta$ ) for U-bending (a) loading (b) unloading step

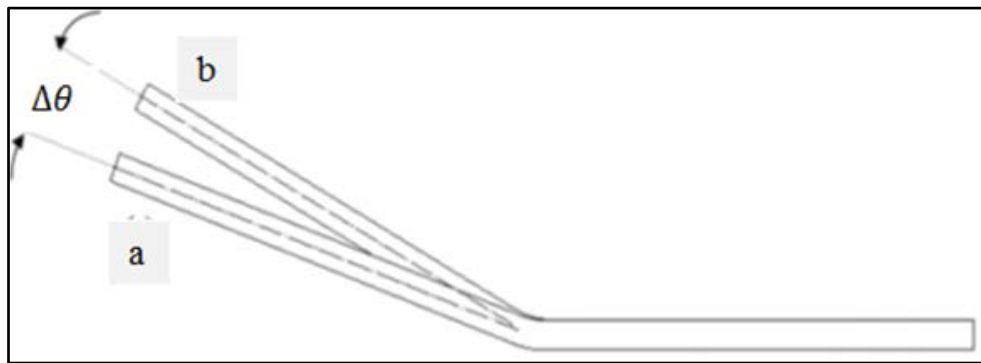


Figure 2-18 Springback ( $\Delta\theta$ ) of straight flanging part (a) loading (b) unloading step

The use of tension as a technique to control or minimise springback has been studied using the stretch bending test [41] to study the influence of in-plane tension on springback as shown in Figure 2.19.

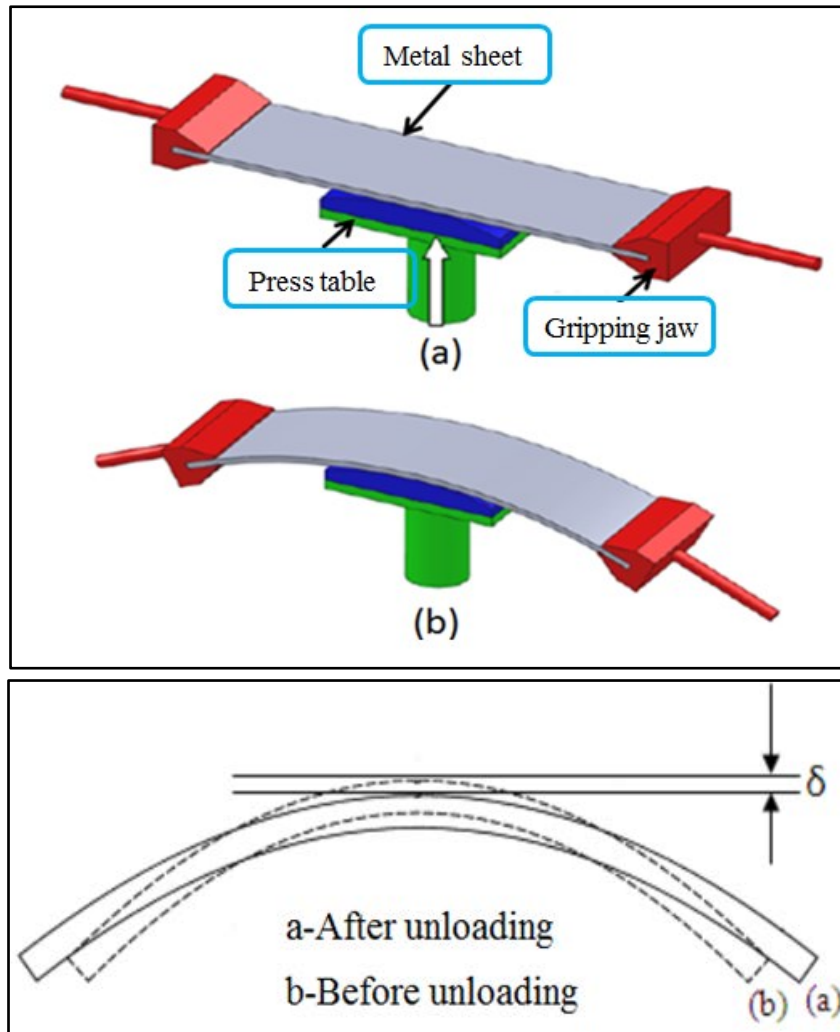


Figure 2-19 Definition of springback in the stretch bending [41]

An experiment called the draw-bend test, proposed by Carden *et al.*, [42], can be used to investigate the level of springback in sheet metals under forming conditions similar to those found in industry, see Figure 2.20.

The system contains two actuators oriented at  $90^\circ$  to one another. The tooling radius is that of a cylinder located at the intersection line of the upper and the lower actuators. A constant horizontal restraining force,  $F_b$ , is provided by the upper actuator, whereas the lower actuator draws the blank downwards at a constant speed  $v$ .

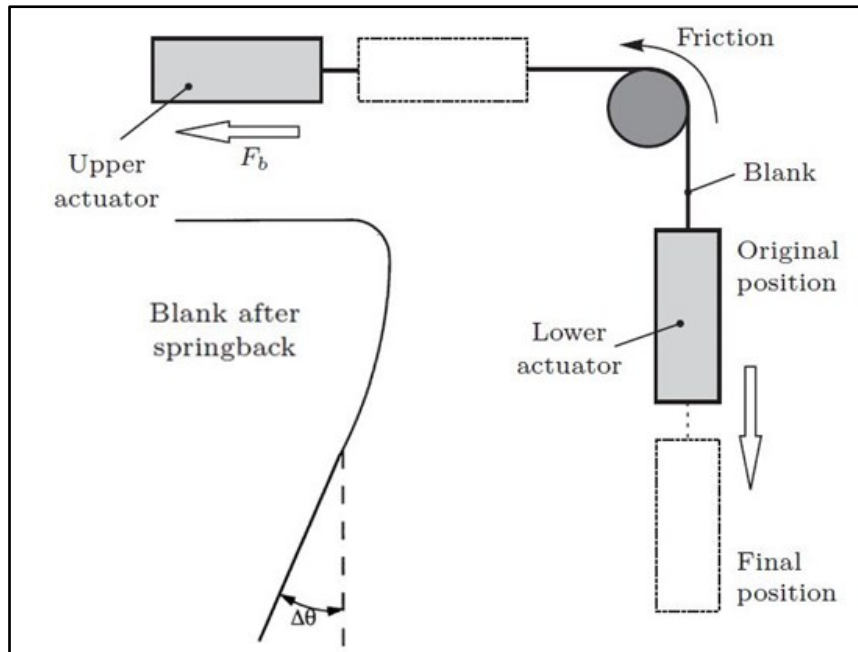


Figure 2-20 Schematic of draw-bend test [42]

Once drawn in excess of the tool radius, the blank experiences tensile loading, bending and unbending. As a result of these actions, a reversal loading in the material occurs. Finally the test sample is allowed to springback by removal the loads and  $\Delta\theta$  is measured. This method is considered as a well-characterized case of a forming process that matches actual process settings and has the advantage of simplicity [43].

## 2.5 Design of experiments and optimisation approach in metal sheet forming

To study the relationship between process parameters and quality of the formed part in sheet metal forming, Design of Experiments (DOE) procedures has been used by many researchers as effective tools for optimising the forming process parameters [44]. The optimisation method is a process used to find an optimal solution under certain specified conditions and to obtain an objective function that can be used to maximise or minimise a set of response parameters [45]. The time to complete the optimisation process can be very long for complicated

shapes [23], but the response surface method (RSM) is considered a reliable technique to reduce this time [46].

The RSM assesses an objective function at a number of points in the design space to achieve a good estimation of objective function [47]. RSM has been used in modelling of several prediction factors influencing springback in the metal sheet forming process. Srinivasan *et al.*, [48] used RSM to predict springback in air bending of steel sheets, the model's result obtained were in good agreement with the experimental results. Naceur *et al.*, [49] optimised tool geometry by using RSM to minimise springback in sheet metal forming. Chou and Hung [39] have used response surface method to optimise process parameters such as punch radius and die gap values to reduce springback in channel wall bending.

## **2.6 Review of research into springback errors**

Springback in sheet metal forming can be controlled or minimised by two strategies [50]. The first is based on mechanical reduction of springback such as applying an optimal blank holder force to minimise the springback. Liu *et al.*, [51] stated that by applying a variable blank holder force during the forming process improved dimension accuracy. Multi-step sheet forming is another example of a mechanical way to reduce the springback and was introduced by Li *et al.*, [52]. Numerical simulation and analysis predicted that springback would be reduced when multi-step MPF was used, and this result has been validated. The advantage of these approaches is that they are an effective way to control springback and, importantly, the tool's shape is not required to be modified [53].

The second way to eliminate springback is geometry-based springback compensation. These methods are based on making an accurate prediction of springback by using FE simulation and then applying appropriate allowances on the tools so the final formed shape will closely

approximate that of the target. Examples of this approach are Displacement Adjustment (DA) [53] and Spring Forward (SF) methods [54].

## **2.7 Summary**

In this chapter, a review has been provided of sheet metal forming techniques such as flexible sheet metal forming and MPF. Springback, as an unavoidable error in sheet metal forming, has been explained, and the most common techniques used to control or eliminate it have been introduced.

According to the literature reviewed, the ABAQUS software (with explicit and implicit approaches) has been used to successfully simulate the loading and unloading steps of the forming process. The DOE and optimisation analysis has been shown by some researchers to be an appropriate procedure to identify the optimum process parameters to minimise springback and improve formed part quality.

In this study, the MPF pin's size was a fixed parameter as MPF tools were designed by [2] and manufacturing by Loadpoint Ltd [55], most MPF process parameters that influence springback were investigated using suitable ranges. Statistical approaches such as DOE and Analysis of Variance (ANOVA), which can be applied to identify the most critical working factors that influence the final product quality and the optimal working parameter combinations, are seldom used in MPF in practice.

On the basis of the literature review, an intensive investigation is proposed to provide a better understanding of the relationship between springback and thickness distributions of the formed part. Also, a new method to measure the local forming force on individual pins of MPF tools will be introduced and the effect of these measured forces on springback investigated.

From the literature review, rubber forming has largely been limited to solid tools used for sheet metal forming. In this project a low-cost tool will be investigated with the aim of combining a rubber cushion with a multi-point tool to gain the advantages of both processes; to reduce cost and setup time while improving the quality of the final part in terms of wrinkling and springback.

## **CHAPTER 3:**

# **MULTI-POINT FORMING TOOLS AND MEASUREMENT APPARATUS**

This chapter provides a description of the mechanical tests conducted to extract relevant mechanical properties of the different material used. These are essential for accurate FE simulation of the forming processes. A brief description is given of existing MPF tool components [2]. The specification of the apparatus used to measure the total and individual forming forces, punch movements and to compare the shape of the final formed part to desired design shape are listed and described.

### **3.1 Mechanical tests for material properties**

The most common procedure to derive basic mechanical properties of materials is the tensile test because it is simple and easy to use. Mechanical properties of the material such as yield strength, percent elongation, ultimate tensile strength, anisotropy parameters and plastic flow can be determined via the tensile test. Although the tensile test has the benefits of simplicity and low cost, only limited strain values can be obtained due to the fact that the process is applied under uniaxial stress conditions.

#### **3.1.1 Uniaxial tensile test to failure**

The properties of a metal blank of aluminium alloy 5251-O were derived from uniaxial tensile tests, performed using a Zwick / Roell uniaxial tension/compression machine in the School of Metallurgy and Materials at the University of Birmingham (UOB), see Figure 3.1. The load capacity of the machine is 200 kN with changeable speed from 0.005 to 200 mm/min, a wide range which allows choice of a strain rate suitable for the relevant forming process. The test was performed using a displacement control with a crosshead speed of 0.5

mm/s [23, 56]. The tensile test was applied on a standard specimen as shown in Figure 3.2, formed by a wire cutting machine at different angles to the direction of rolling:  $0^{\circ}$ ,  $45^{\circ}$  and  $90^{\circ}$  as in Figure 3.3. For each of these directions, two specimens were prepared. Six samples were cleaned and measured prior to the tests using a micrometre to give accurate width, gauge length and thickness measurements.

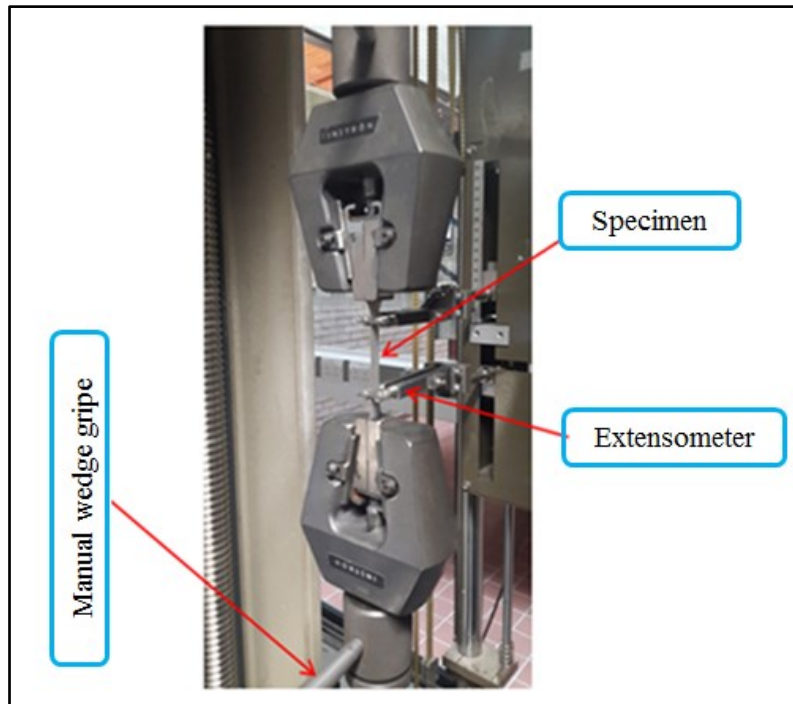


Figure 3-1 Uniaxial tensile machine

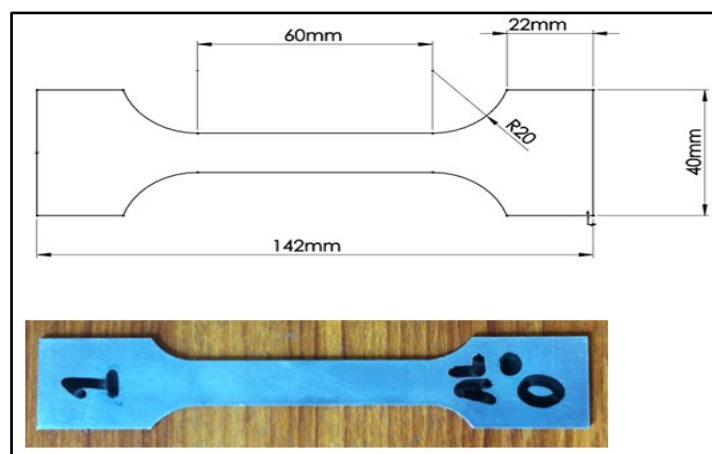


Figure 3-2 Standard specimen for mechanical tests

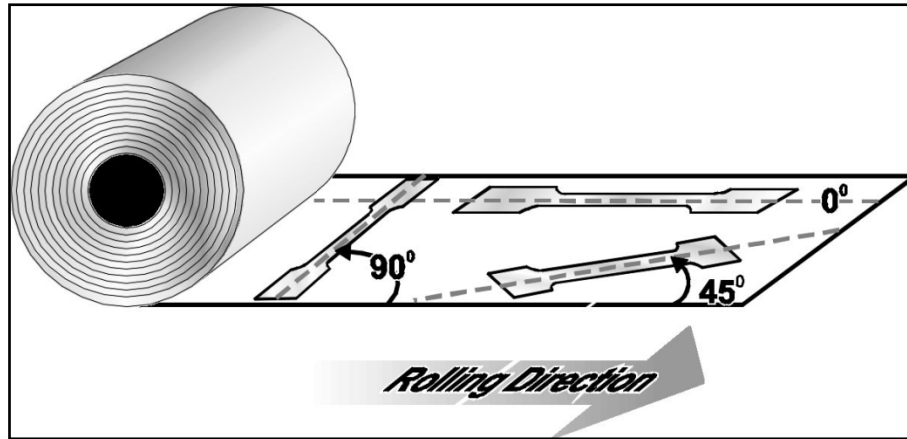


Figure 3-3 Tensile test specimens (different angles to the rolling direction)

The test results determined the engineering stress and strain using Eqs (3.1) and (3.2).

$$\sigma_{eng} = \frac{P}{A_0} \quad (3.1)$$

$$\varepsilon_{eng} = \frac{\Delta L}{L_0} \quad (3.2)$$

Where  $P$  is the tension load applied to the specimen,  $A_0$ ,  $L_0$  and  $\Delta L$  refer to the original area, gauge length and displacement of the specimen respectively. Under the assumption of constant volume, the true stress and true strain were computed from Eqs (3.3) and (3.4):

$$\sigma_T = \sigma_{eng} (1 + \varepsilon_{eng}) \quad (3.3)$$

$$\varepsilon_T = \ln (1 + \varepsilon_{eng}) \quad (3.4)$$

The data imported by the PC connected to the Zwick / Roell tensile machine, and the above equations, were used to plot the stress-strain curve for the aluminium alloy 5251-O in three directions (see appendix 1). The modulus of elasticity was calculated as the slope of stress-strain in the elastic region, according to ASTM E-8, Standard Methods for Tension Testing of

Metallic Materials [57], the yield stress was taken from the stress-strain curves by drawing a horizontal line from yield point act to vertical axis which is force (N).

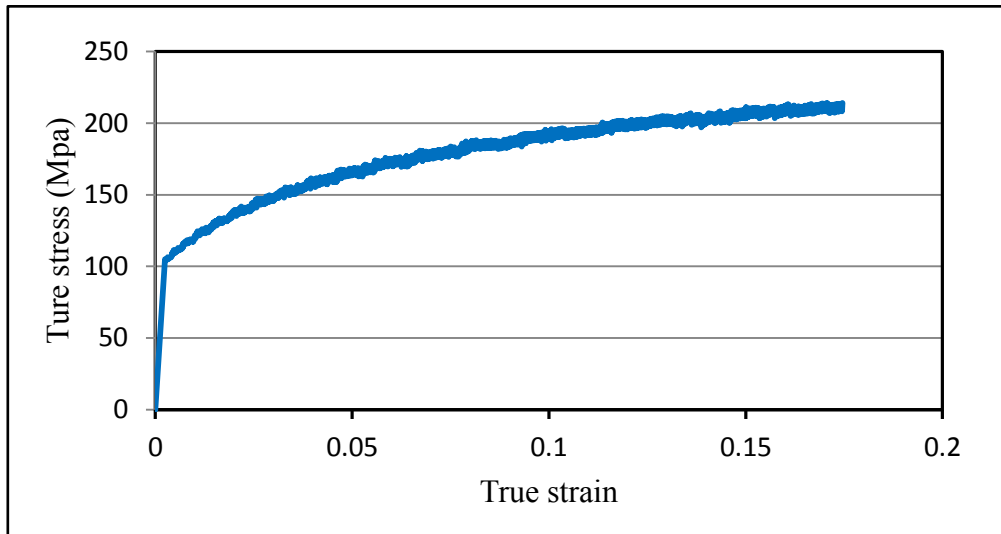


Figure 3-4 Stress-strain curve for Aluminium alloy 5251-O

Figure 3-4 shows the unstable stress-strain curve for the specimens of Al alloy 5251-O obtained for different direction relative to the rolling direction, the slight differences observed are due to the Portevin-Le Chatelier (PLC) effect found in Aluminium and Magnesium alloys [58, 59]. This is due to the interaction between solute atoms and mobile dislocations known as dynamic strain ageing and consequent inhomogeneous deformation with a number of localisation bands [60]. This progression starts at a so-called critical strain, which is the lowest strain required for the beginning of the serrations in the stress-strain curve. The critical strain is both temperature and strain rate dependent [61].

Figure 3.5 displays the mechanical properties of the Al 5251-O metal sheets namely, yield stress (Y) and ultimate stress (U) for different orientations relative to rolling. It is clear from Figure 3.5 that as the orientation angle increases there is a small monotonic increase in the stress value (maximum stresses value at 90° to the rolling direction) [62].

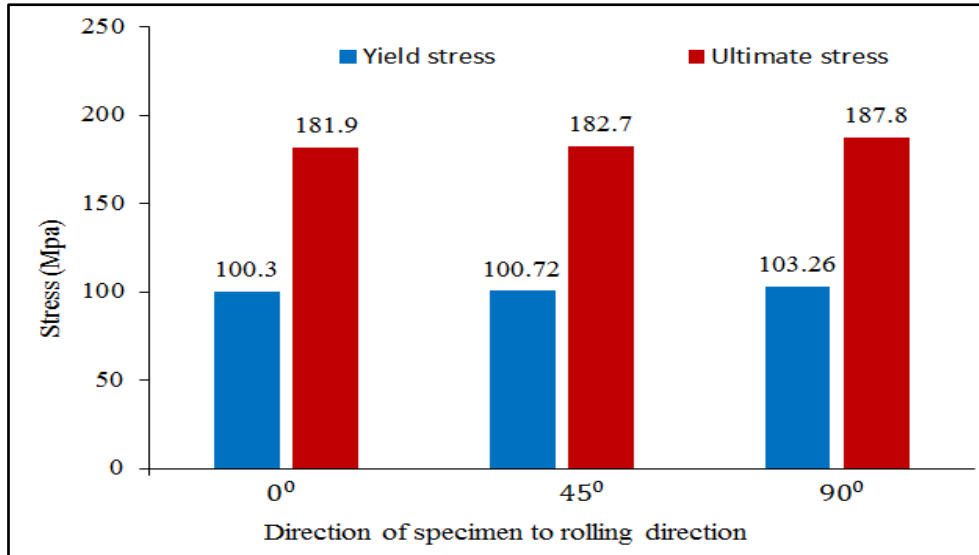


Figure 3-5 Yield and ultimate stress for Al 5251-O

### 3.1.2 Anisotropy test

Sheet metal properties are not same in all directions (orientation dependency). This property of metallic materials, related to the direction of rolling, is named anisotropy. Generally, the state of anisotropy is identified by the R-value, defined as the relation of width strain to thickness strain.

In the plastic deformation region, the metal is exposed to plastic anisotropy, which may vary depending on the angle relative to rolling (rolling, transverse and diagonal directions) so the properties of the blank are non-homogeneous [23].

Plastic anisotropy is given by the anisotropy constant:

$$r_a = \frac{\varepsilon_2}{\varepsilon_3} = \frac{\varepsilon_w}{\varepsilon_t} = - \frac{\varepsilon_w}{(\varepsilon_w + \varepsilon_t)} \quad (3.5)$$

where,  $\varepsilon_2$  is the width strain of the specimen and  $\varepsilon_3$  is the thickness strain of specimen. The summation of width strain ( $\varepsilon_w$ ) and length strain ( $\varepsilon_l$ ) of the specimen is equal to the strain in the direction of the specimen thickness ( $\varepsilon_t$ ). An indication of the type of strain can be

obtained from Eq. (3.5), if the value of  $r_a$  is greater than unity the sheet is formed in the width direction to a greater extent than in the direction of sheet thickness, which is known as ‘thinning resistance’. If the value of  $r_a$  is less than unity, the sheet will be thinner and this leads to the real possibility of sheet failure during the forming process. The main purpose of this test is to determine the degree of anisotropy of the blank, which may affect the metal sheet forming process, particularly the springback.

Using same specimen as in Figure (3.2) to determine plastic strain ratio, the r-value was calculated from the width and the gauge length after the tensile test, after the specimen had been subjected to 20% length strain [63]. With the machine stopped the final length and width were measured three times in different locations and the average used in Eq. (3.5). The normal R-value is calculated as [64]:

$$R_a = \frac{r_0 + 2r_{45} + r_{90}}{4} \quad (3.6)$$

The resulting R-values for the aluminium alloy at  $0^\circ$ ,  $45^\circ$  and  $90^\circ$  to rolling orientation are listed in Table 3.1. as expected, the value of  $r_a$  at orientation  $90^\circ$  is the highest and  $45^\circ$  is the lowest [65].

Table 3-1 Ra for aluminium alloy 5251-O

Rolling direction	No of samples	$r_a$	Average value	$R_a$
$0^\circ$	1	0.605	0.591	0.5807
	2	0.574		
	3	0.593		
$45^\circ$	1	0.522	0.529	
	2	0.535		
	3	0.531		
$90^\circ$	1	0.604	0.622	
	2	0.638		
	3	0.625		

### **3.1.3 Uniaxial Compression Test for Polyurethane properties**

Polyurethane materials are utilised in MPF because they have a combination of the durability and toughness of metals and the elasticity of rubber [33]. In FE analysis, polyurethane is described as hyper-elastic materials: when subjected to very large strains they undergo elastic deformation - i.e. temporary deformation of the material which then returns to its original shape when the applied force is released. Generally, a simple elastic deformation describes a linear relationship between stress and strain, as in metals. But in the case of rubber material the elastic deformation with high linearity is applied [33]. As a result, a unique formula is required to describe the stress-strain characteristics. ABAQUS has numerous models such as Arruda-Boyce, Ogden, van der Waals, Marlow, neo-Hookean and Mooney-Rivlin to describe strain energy potentials and model elastic cushion material.

Experimental data for polyurethane (90 shore A hardness [66]) material was obtained using the uniaxial compression test, as shown in Figure 3.6, because it is considered more relevant to the deformation occurring during the MPF process.

According to the standard ASTM D575 [33], the polyurethane specimen should be circular with diameter  $28.6 \pm 0.1$  mm and thickness  $12.5 \pm 0.5$  mm, see Figure 3.6. The final test pieces were obtained by cutting them from long rods of polyurethane of the required diameter; three specimens were tested and the results averaged to reduce any errors arising when cutting the specimens from the rod. The testing technique followed by the uniaxial compression test was to determine the deflection corresponding to 70% of the maximum compression ratio used in this research, and then the force was applied to produce a compression rate of 10 mm/min. To avoid lateral slippage between the test machine and the polyurethane specimen during the test, a sheet of sandpaper (400 grit waterproof sandpaper

was found satisfactory) was located between the test tool surface and rubber polyurethane surface as recommended in ASTM D575-91 (2012). Figure 3.7 shows the load-compression curves gained from the compression test.



Figure 3-6 Compression test for A90 Polyurethane specimen

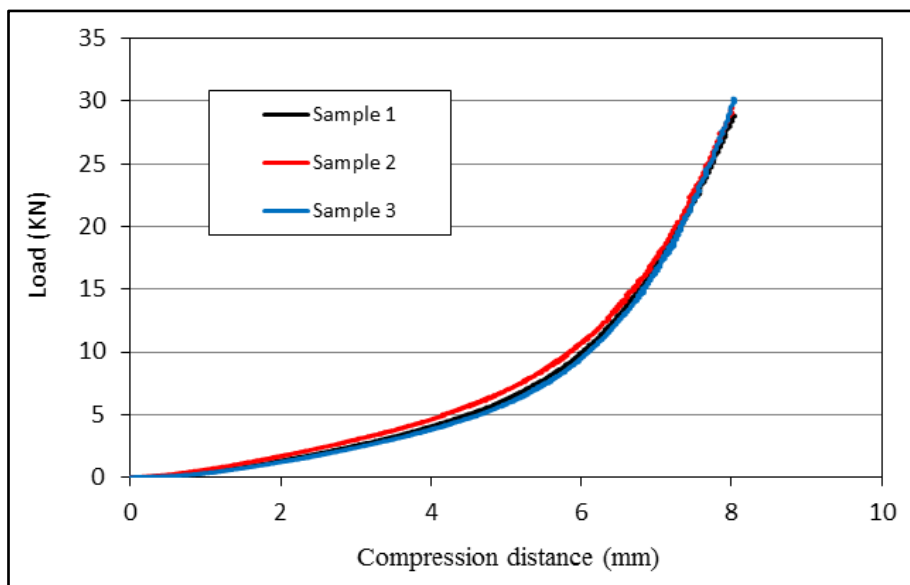


Figure 3-7 Load-displacement relations obtained for 90 Shore A Polyurethane

### 3.2 Conventional MPF experimental setup

This section outlines the specification of the MPF tools shown in Figure 3.8 used to produce double curved metal sheets. The pin size, as shown in Figure 3.9, is fixed in this rig, though a number of process parameters affecting springback and mentioned in the literature review have been taken into the account in the rig design. These parameters are the radius of curvature of the design shape, elastic cushion thickness and the force holding the blank in place.

The test rig was assembled on a MACKAY BOWLEY press, located in the School of Engineering at the University of Birmingham (see Figure 3.10). This is a 4 column downstroke hydraulic press and with 200-tonne clamp and 200-tonne punch (serial number 10994/99) digitally controlled

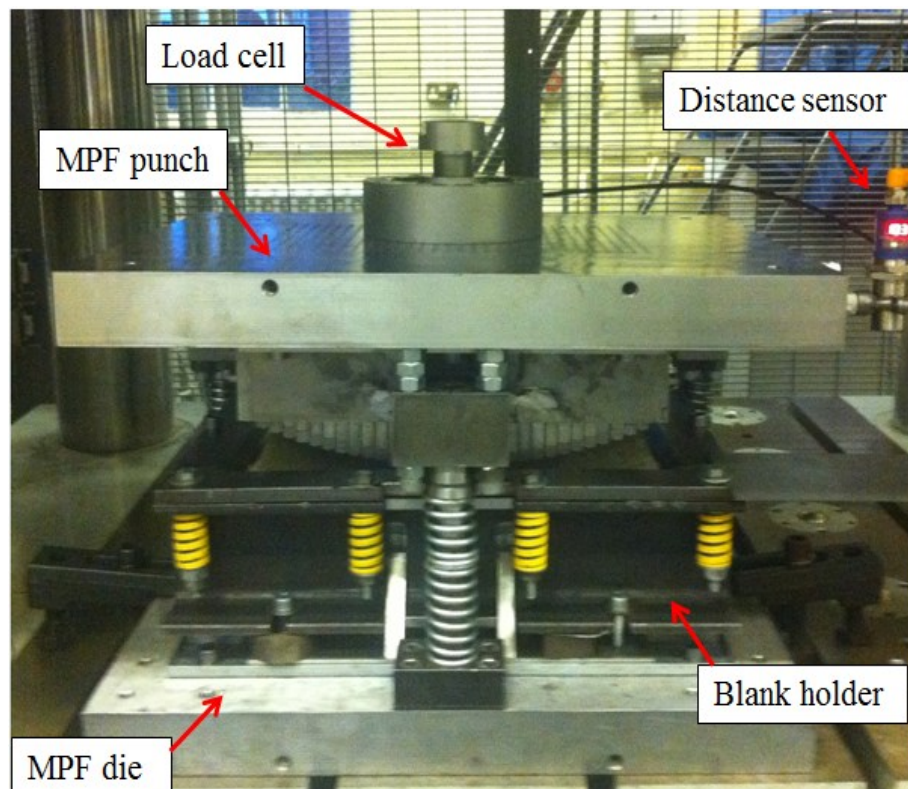


Figure 3-8 MPF test rig

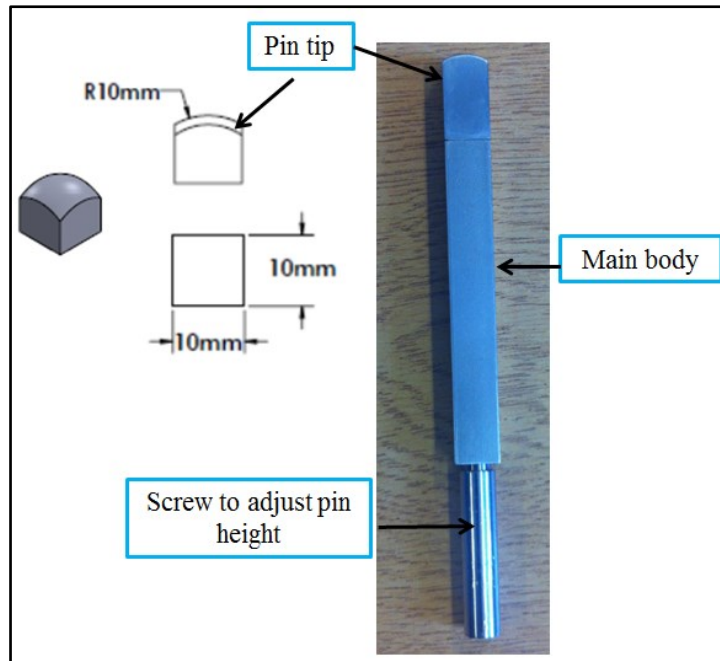


Figure 3-9 Pin dimensions

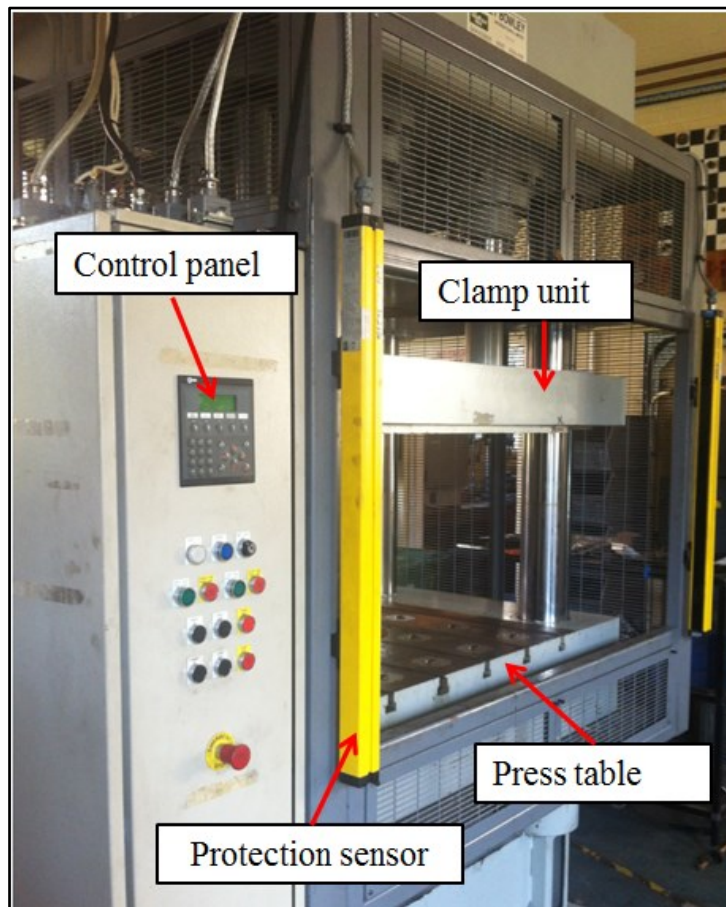


Figure 3-10 Press machine

### 3.2.1 MPF punch and die details

The MPF tools were developed to form double curved parts with different radii of curvature from 400 mm up to 800 mm. The pin is the main factor in constructing re-configurable tools, and should be of an appropriate material to withstand the given external loads during use, with appropriate shape and size. Here the pin cross-section was 10×10 mm with a 10 mm tip radius and with 0.25 mm gap between adjacent pins. The pins were packed uniformly in a matrix of 30×20 pins, as in Figure 3.11, to form a continuous formed surface. An active mechanical method is used to modify the reconfigurable pin tool. i.e. the height of the pins can be adjusted by rotating the lead screw located at the bottom of the pin as shown in Figure 3.9. The MPF punch and the die are each constructed of 30×20 pins with an active blank size 300 mm × 200 mm. A comprehensive discussion of existing MPF tools, with details of the design of tool parts, pin height adjustment and surface control methods are given in [2].

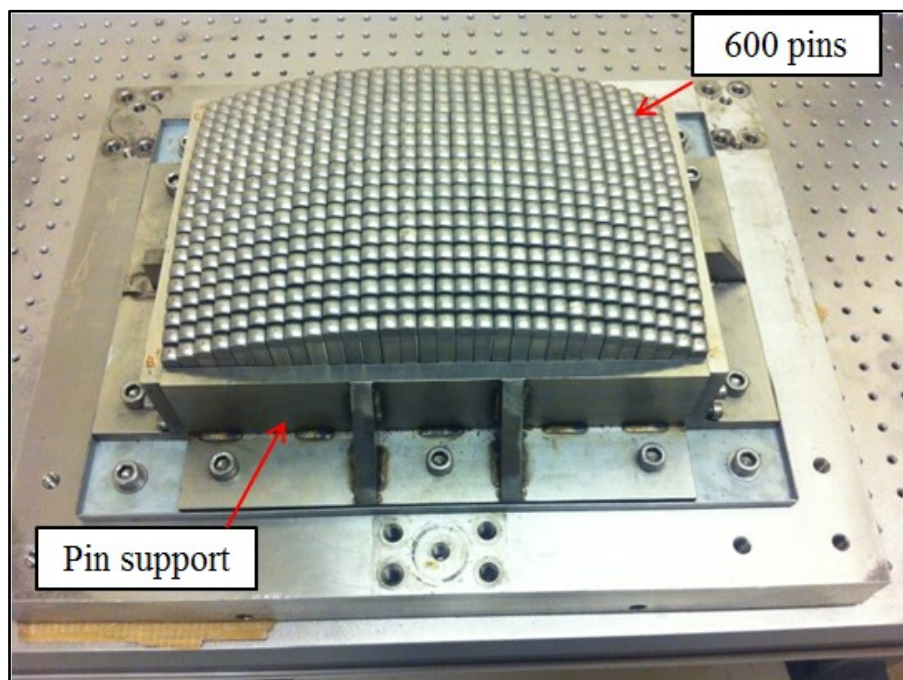


Figure 3-11 MPF punch

### 3.2.2 Blank holder

The influence of blank holder force on the eformed part will be investigated in this research. The blank holder was designed according to the simulation predictions which included the effect of the blank holder on material flow into the die and part quality such as thickness variation, wrinkling and springback. In this work the upper plate of the blank holder is held by bolts fitted with springs of known stiffness. The information supplied by the manufacturer was validated by compression machine and it was confirmed that every 1 mm compression of the springs produced a force of 244 N [2]. This gave the ability to change the value of the force holding the metal sheet during the forming process. The head of bolts were fixed and the rotating the nuts to compress the spring increased the compression force until it reached the required value. For example, to clamp the sheet by 20 kN, every one of the ten springs should be screwed up 8.2 mm. The location of the springs along the blank holder was determined carefully to ensure uniform pressure distribution on the metal sheet while it was clamped during the forming process.

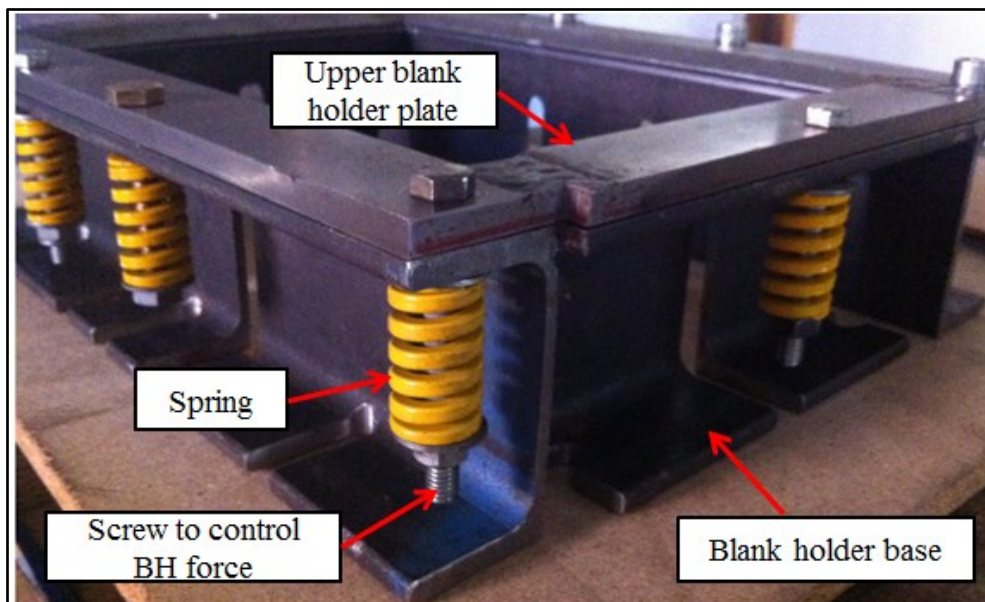


Figure 3-12 Blank holder with springs

### 3.2.3 Load cell (100 Series low profile)

A load cell is a transducer which converts the measured load to an output as a measurable electrical signal. There are many force sensors, with the strain gauge the most commonly used as it is fit for almost all engineering applications. They are chosen for an application according to the way they sense load (tension, compression, bending, shear, etc.).

The selected load cell is a high accuracy compression type with sufficient capacity to suit a wide range of applications; it is manufactured by Richmond Industries, one of the UK's leading load cell manufacturers. This model of load cell (100 Series low profile) has the option to connect directly to a PC/Laptop via a USB port as shown in Figure 3.13. Data can then be viewed and logged on PC or laptop. The logged data can be loaded into Excel and many other spreadsheets to produce graphical reports, etc. [67]

To ensure the reliability of this load cell, it was subjected to known forces and the output reading recorded the same value as the applied force, which gives confidence in future results.

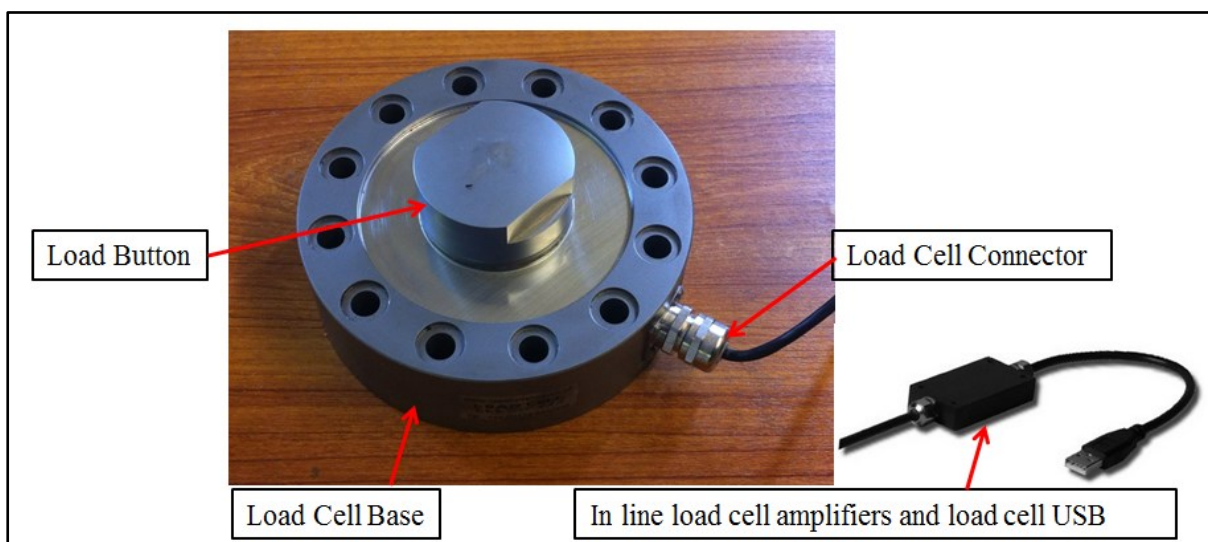


Figure 3-13 Richmond Industries 100 Series low profile load cell

### 3.2.4 Distance sensor

A Microsonic M30 ultrasonic proximity sensor with an operating range of 30 mm to 250 mm was used to sense the position of MP punch movement [68]. The M30 was connected to an Omega data recorder which was connected to a PC/Laptop. Windows-based software enabled the user to analyse and display the data using powerful tools that are part of the package. The software can also be used to display real-time data from the M30 directly onto the PC/Laptop screen [69].

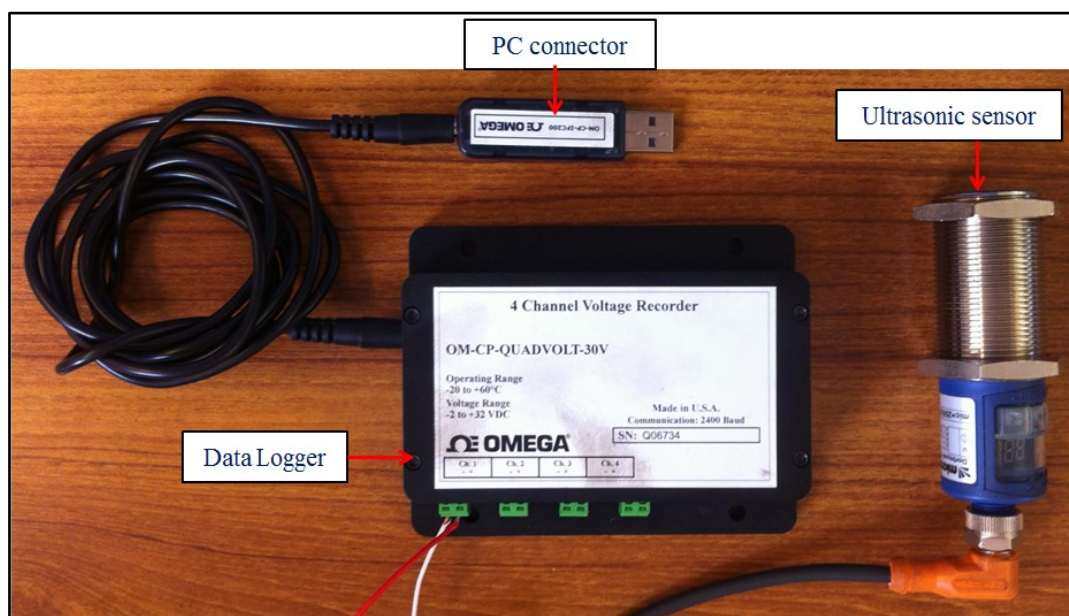


Figure 3-14 Microsonic M30 distance sensor connected to data logger

### 3.2.5 3D Faro arm scanner

The FARO scan arm is an ideal contact/non-contact measurement system, which combines laser line and hard probe and makes this instrument an effective way to inspect complex parts without having to make contact. The formed product is scanned with high resolution and accuracy ( $\pm 25 \mu\text{m}$ ) and the scanner provides rapid cloud point collection (scan rate = 560,000 points/sec) which can be imported to the Geomagic software and compared with

imported CAD files (such as Solidworks) representing the designed part [70]. Comparison between the formed part and designed part will identify wrinkling, springback and thickness variation.

The scanned image can be compared to the image of the designed shape stored in a CAD file to identify wrinkling, springback and thickness variation. A series of steps are required to ensure the images are properly aligned (such as scan registration, etc.), points verified (sample, repair, etc.) before analysis and comparison takes place (compare, measure, etc.).

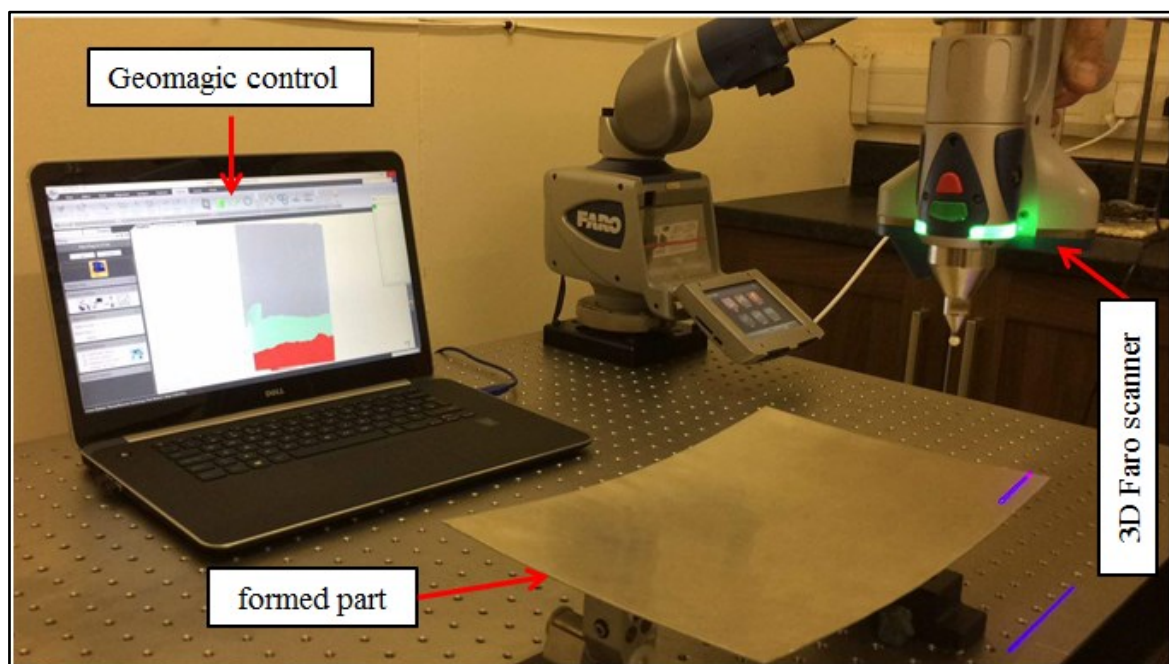


Figure 3-15 Geomagic software connected to Faro arm scanner

### 3.3 Measurement tools for individual pin force

To measure the forming force on the different pins within the narrow working area requires a sensor with high specification. One such sensor considered suitable is the Fibre Bragg Grating (FBG) which is both small and lightweight.

### **3.3.1 Fibre Bragg Grating sensor**

Fibre Bragg Grating (FBG) sensing technology is now commonly used in manufacturing and industry [71]. FBG sensors have a number of exclusive advantages over traditional sensors (electrical and piezoelectric). For example, they are small (inner core of 4 to 9  $\mu\text{m}$  diameter and with outer cladding 125  $\mu\text{m}$  diameter) [72], lightweight and immune to electromagnetic interference. FBG sensors are also sensitive to both temperature and strain [73].

### **3.3.2 Working principle of FBG sensors**

A FBG sensor is a strain measuring device that consists of periodic variations in the refractive index of a short length of optical fibre, usually in the form of a grating. Figure 3-16 shows how, when incident light ( $P_i$ ) travels through the grating a specific wavelength ( $P_r$ ) - the Bragg wavelength - is reflected, while the remainder of the spectrum ( $P_o$ ) passes through the grating unaffected. If the fibre is subject to axial strain, the grating is stretched and causes a shift in the wavelength of the reflected light proportional to the strain. Once the instrument is calibrated, it is possible to measure strain (and other parameters) dynamically.

Figure 3.17 shows the structure of the real-time system for measuring the strain in MPF tools. The system is in four parts: parameter to be measured (strain on pins), FBG sensors, FBG interrogator and computer [16].

### **3.3.3 A FBG sensing system**

Figure 3.18 shows how the tools that when connected together make the sensing system to collect measurement data and analysis them. These tools include the optical fibre, FBG interrogator (SmartScan), Ethernet cable and PC with SmartSoft software.

One or more optical fibres (SmartScan can accommodate up to 4 channels) with dozens of FBG sensors, each having a slightly different wavelength so as not to interfere with one another are installed on the individual pins of the MPF tool. These sensors are connected to the SmartScan dynamic interrogator. This arrangement provides the local forming force information by recording elastic strain. The SmartScan interrogator unit sends light down the optical fibres and records the wavelengths returned from the various sensors. The reflected wavelength is transmitted through the Ethernet cable to the processing unit (computer) to analyse and convert to local forming force information corresponding to the stage of the forming process.

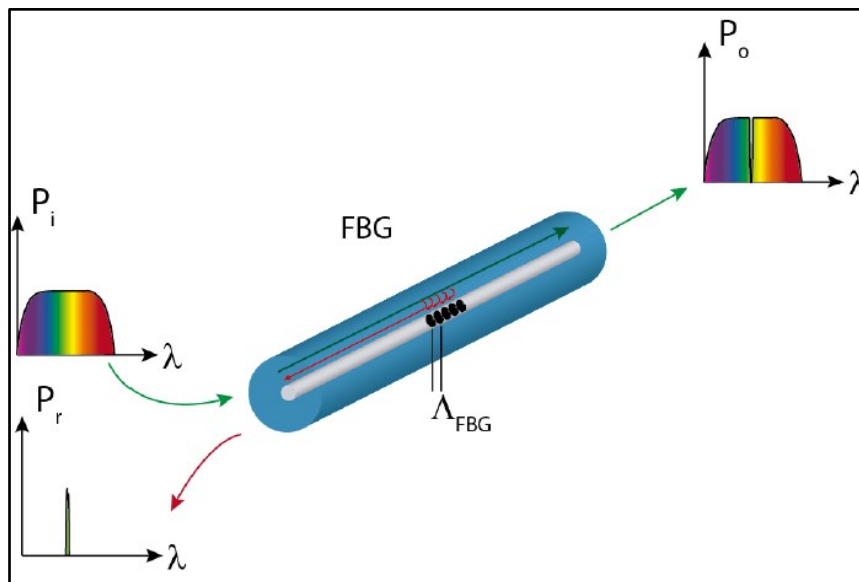


Figure 3-16 Concept and working principle of FBG sensor [71]

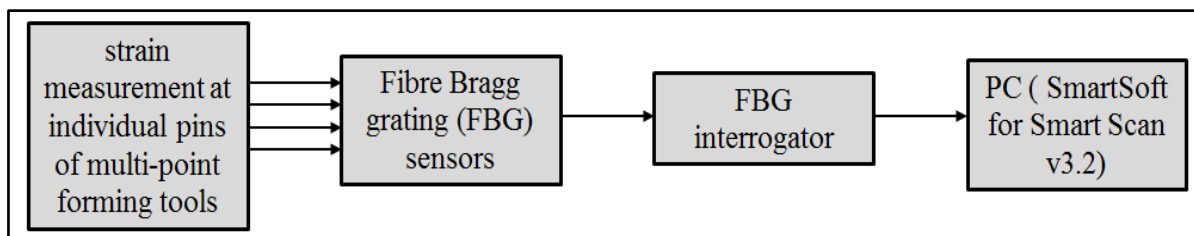


Figure 3-17 Block diagram of strain measurement system

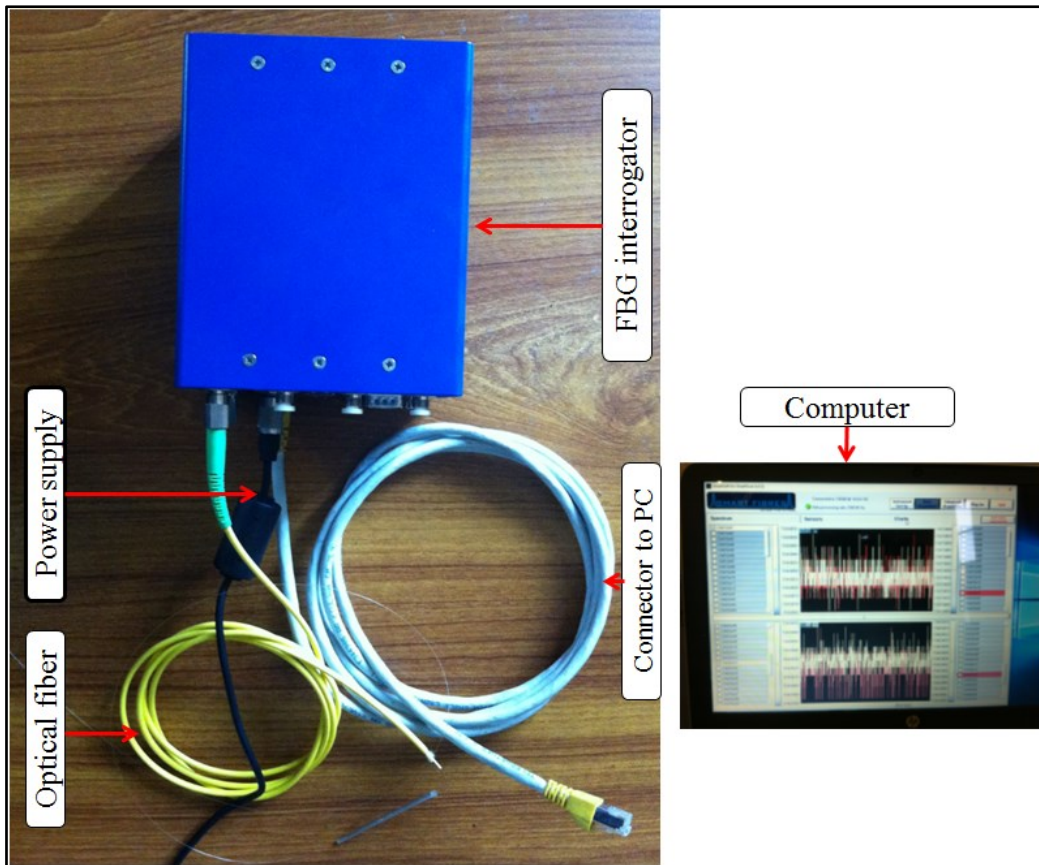


Figure 3-18 Tools to sense, measure and analyse local forming force

### 3.4 Summary

This chapter reports the experimental work facilities to obtain the mechanical properties that are necessary to model the behaviour of the material samples using FEA. The stress-strain curves for all tested specimens were for drawn aluminium 5251-O alloy and polyurethane A90. The aluminium alloys experienced a serrated stress-strain curve due to the so-called PLC effect [23, 58].

A brief description has been given of the MPF tools with associated apparatus used to complete the validation of simulation results (such as MPF tools, load cell, distance sensor and 3D Faro arm scanner for final measurements of formed parts).

A sensing system to measure the local force on selected pins in the MPF tool for the first time is presented, and includes optical fibre sensors, interrogator unit, Ethernet cable, and the processing unit to convert reflected wavelengths to measures of strain

## **CHAPTER 4:**

### **DEVELOPMENT OF FINITE ELEMENT MODELS FOR MPF**

#### **4.1 Finite element modelling of MPF process**

The FE approach enables an investigation to be made of the effect of forming parameters on product quality and determine optimal conditions for forming tools to achieve the best target shape before moving forward to the prototype stage. As modern numerical tools become both more readily available and better able to simulate metal forming processes, it is now possible to accurately simulate nonlinear problems for a full three-dimensional model much quicker than experimentally.

FE simulation is, of course, sensitive to the parameters input to the simulation; these will include both the physical properties involved such as frictional forces and computational factors such as mesh size and element type. In this section, the FE model for MPF is used to explore the impact of significant parameters in the forming process (forming curvature, blank holder force and elastic cushion hardness and thickness) on the quality of the produced part in terms of springback. The system was assumed to be symmetric, including the boundary conditions, so that only one quarter was modelled to reduce computation time considerably.

ABAQUS was used to produce the simulation as it had previously been used to solve several of engineering problems with reliable results [33]. It provides a varied range of elements that can be utilized to simulate the properties and behaviour of virtual shape features using materials such as rubber, polymers, metals and concrete. ABAQUS offers the ability to simulate linear and nonlinear problems and to simulate every part in isolation in the case of multi-components [2, 74, 75].

Usually, a full analysis by ABAQUS involves three main steps: pre-processing, simulation and post-processing as shown in Figure 4.1

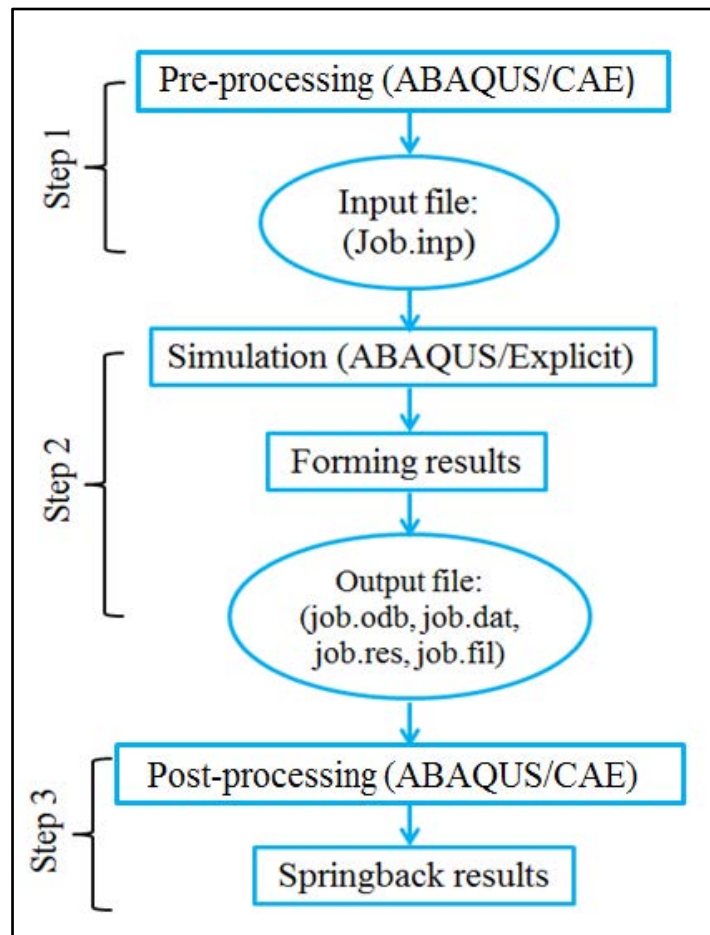


Figure 4-1 The procedure of ABAQUS simulation [76]

In the first step, a model of the real problem must be built, material properties is defined, contacts rules are chosen, process boundary conditions is applied and the mesh element type is selected. Then the input file created by ABAQUS. Then, in the second step, the numerical simulation using ABAQUS/Explicit or ABAQUS/Standard approaches attempts to solve the problem that is defined in the model. The evaluation of the results in the last step after the simulation has been finished uses the visualization module, which offers various options for

displaying the results, these include animations, X-Y data to draw stress-strain distributions, forces, displacement, profiles etc. [33].

ABAQUS/Explicit and ABAQUS/Standard are capable of solving a wide variety of problems, through an understanding of the characteristics of implicit and explicit techniques does help to determine which technique is more appropriate for a particular problem. ABAQUS/Explicit was selected to conduct numerical simulation of MPF processes, and has proved valuable in metal forming simulations. Unique advantage of the explicit approach over the implicit is the solving of complex interaction problems. Moreover, when the model becomes large, the implicit method requires the resources of a much large computer system than the explicit method [77].

To solve dynamic problems including deformation of objects; an explicit approach has been applied, as a result the solution at the time  $(t+\Delta t)$  is found from information related to time  $(t)$ . For every incremental step, the initial kinematic states are applied to compute the state for the following increment. The node acceleration ( $\ddot{u}$ ) can be estimated at the start of the increment depending on dynamic stability using Equation 4.1 [78].

$$\ddot{u}^{(i)} = M^{-1} ( P^{(i)} - I^{(i)} ) \quad (4.1)$$

Where  $M$  is the mass matrix,  $P$  is the vector of applied load,  $I$  is the vector of internal forces and the superscript  $(i)$  refers to the increment number of an explicit dynamic step.

By applying time integration, and using fixed time increment  $\Delta t$ , it is possible to compute the velocity and the displacement as shown in Equations 4.2 and 4.3 [79]:

$$\dot{u}^{(i+\frac{1}{2})} = \dot{u}^{(i-\frac{1}{2})} + \frac{\Delta t^{(i+1)} + \Delta t^{(i)}}{2} \ddot{u}^{(i)} \quad (4.2)$$

$$\mathbf{u}^{(i+1)} = \mathbf{u}^{(i)} + \Delta t^{(i+1)} \dot{\mathbf{u}}^{(i+\frac{1}{2})} \quad (4.3)$$

The central-difference integration operator is explicit in the sense that the kinematic state is advanced using known values of  $\dot{\mathbf{u}}^{(i-\frac{1}{2})}$  and  $\ddot{\mathbf{u}}^{(i)}$  from the prior increment.

To reduce simulation time one small time increment is used to get a solution and load rate scaling and mass scaling techniques are introduced. A significant reduction in computational time is produced but the simulation still provides acceptable results [26].

#### 4.1.1 Model development

A FE model was generated and used to investigate the MPF technique. The model simulates two groups of pins creating the die and the punch respectively, the metal sheet, two elastic cushion layers and the blank holder frame. Figure 4.2 illustrates the apparatuses of the model and their dimensions.

The model was arranged to produce double curved panels with various radii of forming curvature. Pins with a tip radius of 10 mm and  $10 \times 10$  mm cross section area were used as suggested by Abosaf [2]. The active sheet dimensions (area covered by the pins) were 300 mm  $\times$  200 mm (the whole model). The MPF punch and die were each constructed with 600 pins ( $30 \times 20$  pins). C3D8R type is deformable solid elements were applied to model the metal sheet and the layers of elastic cushion in ABAQUS software during simulation. The metal sheet were divided to five layers of elements as suggested by Wang *et al.*, [77]. Also, three layers of elements were used through thickness for the elastic cushion. So, the total numbers of elements in the models were 1,084,180 and 47,201 for the metal sheet and the elastic cushion layers respectively. (It is a reminder, only a quarter of the sheet and elastic

cushion layers were modelled, element size for sheet is  $0.4 \times 0.4 \times 0.24$  mm and for elastic cushion is  $1 \times 1 \times 1$  mm).

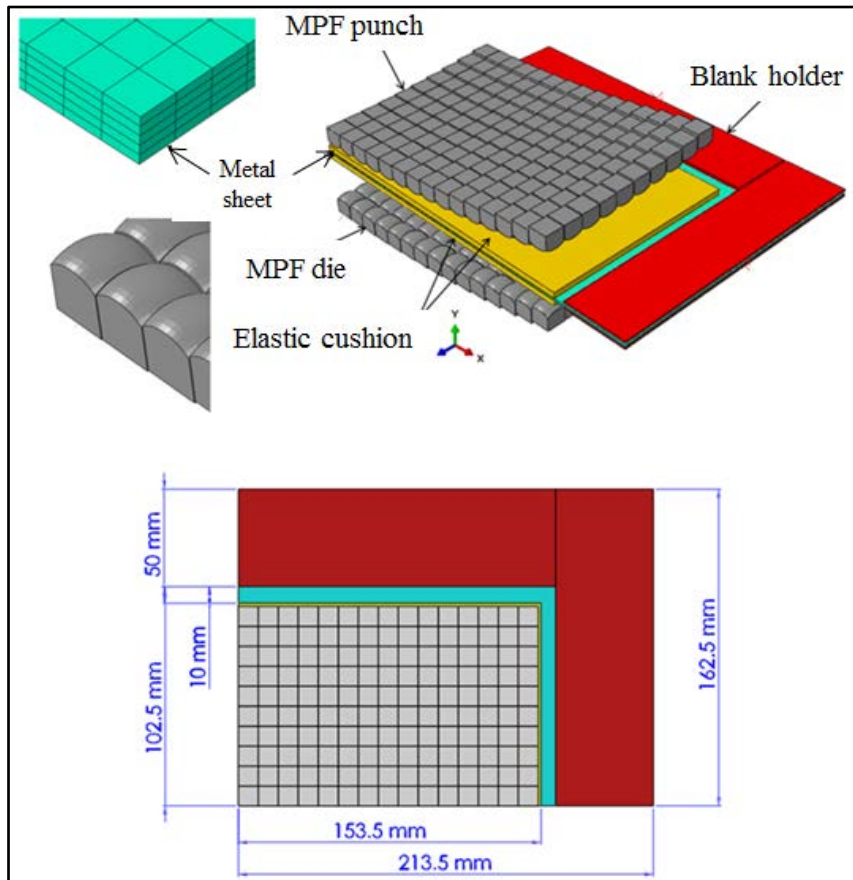


Figure 4-2 Finite element model and model dimensions [80]

The pins were organized to form a doubly curved surface (a saddle) with 400 mm radii of forming curvature. A discrete rigid body was used for modelling both the punch and die, with R3D4 element type as suggested by Zareh-Desari *et al.*, [81]. As a final point, the blank holder frame was modelled as an analytical rigid body, as this was computationally less expensive than a discrete rigid part [82].

#### 4.1.2 Boundary condition and material properties

As the final part is symmetry, a quarter of FE model was used to simulate the forming process. Thus, symmetrical boundary conditions were applied to the metal sheet and elastic cushion layers. The lower part of the blank holder and the die were obstructed from movement in the all directions X, Y and Z but the upper part of the blank holder and the punch were fixed in two directions X and Z only and allowed to travel along the vertical direction (Y). Forces of different values were applied to hold the metal sheet in the Y-direction depending on the required force. Figure 4.3 shows the FEM with applied boundary conditions.

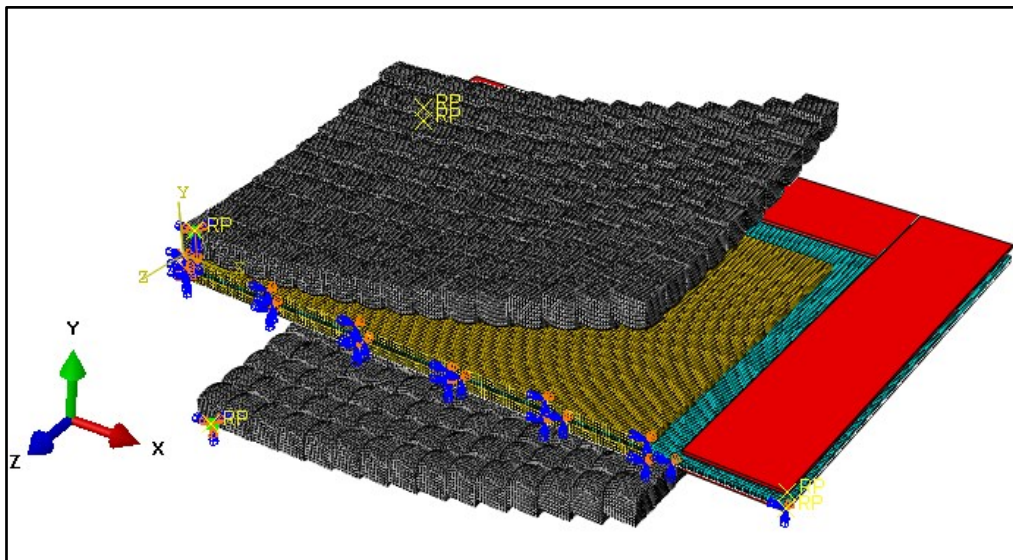


Figure 4-3 Boundary conditions and mesh types of FE model [80]

The metal sheet was aluminium alloy 5251-O, 1.2 mm thick. To know the mechanical properties of the metal sheet, tensile tests were carried out using a Zwick / Roll test machine on specimens prepared at  $0^\circ$ ,  $45^\circ$ ,  $90^\circ$  with respect to the rolling direction as described in Chapter 3. Table 4-1 shows the measured properties of tested material.

Table 4-1 Measured mechanical properties of tested material

Property	Value
Modulus of elasticity (E)	65 GPa
Density ( $\rho$ )	2700 kg/m <sup>3</sup>
Yield stress ( $\sigma_0$ )	100.2 MPa
Poisson's ratio ( $\nu$ )	0.33
Strength coefficient (k)	270 MPa

An isotropic model was selected to define the yield behaviour of the material in simulation by ABAQUS. The elastic behaviour was defined by the young modulus and Poisson's ratio. While the behaviour of the material in plastic region was modelled using Ludwig's equation [83]

$$\sigma = \sigma_0 + K \cdot \varepsilon^n \quad (4.4)$$

where  $\sigma$  presents true stress,  $\sigma_0$  the yield stress,  $\varepsilon$  true strain, K the hardening coefficient, and n the hardening exponent. Figure 4.4 shows the true stress-true strain curve for the aluminium alloy material.

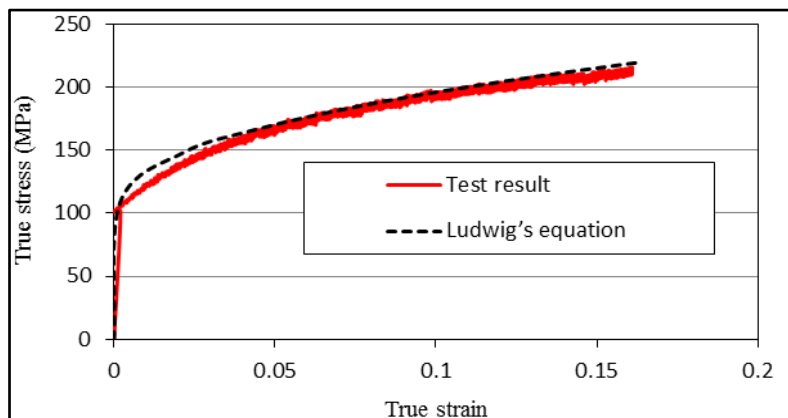


Figure 4-4 Stress-strain curve for aluminium alloy 5251-O [80]

In this research, the behaviour of elastic cushion layers made from polyurethane with a Shore hardness of A 90 was modelled with nonlinear hyper-elastic [84, 85]. FEA was applied to

identify the constitutive model to simulate the behaviour of the elastic cushion layers. ABAQUS offers the evaluation function to test experimental data of hyperelastic material against different forms for the strain energy potentials [86], three models were chosen for this test; Neo Hook, Yeoh, and Mooney-Rivlin, see Figure 4.5. In terms of stability of the model during simulation at high strain rate and best fit with the experimental data (root-mean-square error (RMSE)), it can be realised that the Mooney–Rivlin hyper-elastic material model provided these criteria. So, this relation was chosen to describe the behaviour of the elastic cushion layers. In this constitutive model, the strain energy per unit volume can be

$$U = C_{10} (\bar{I}_1 - 3) + C_{01} (\bar{I}_2 - 3) + \frac{1}{D_1} (J_{el} - 1)^2 \quad (4.5)$$

where  $U$  is the strain energy per unit of reference volume,  $C_{10}$  and  $C_{01}$  and  $D_1$  are material constants.  $C_{10}$ ,  $C_{01}$  presented deviatoric component and  $D_1$  presented compressibility. The experimental data is used to determine the required coefficients of Mooney–Rivlin model for polyurethane material in ABAQUS software [88].  $J_{el}$  is the elastic volume ratio, The values of  $C_{10}$ ,  $C_{01}$  and  $D_1$  are 0.861, 0.354 and 8.69E-02 respectively,  $\bar{I}_1$  and  $\bar{I}_2$  are the first and second strain invariants in the material [81].

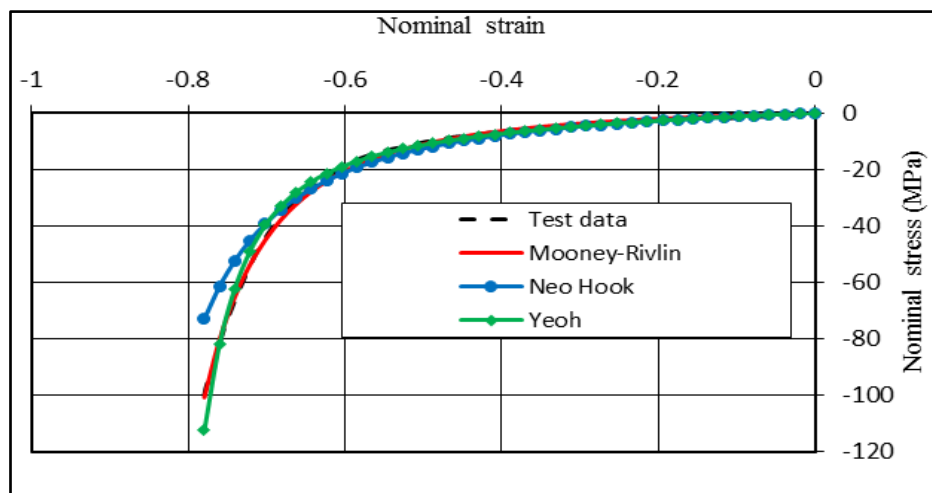


Figure 4-5 Hyperelasticity evaluation for A90 Polyurethane by ABAQUS [80]

## 4.2 Model Validation

A FE model has been developed to simulate the MPF process. This model contains two groups of pins called punch and die, a sheet of material with dimensions of 150 mm × 100 mm × 1.2 mm thick and two sheets of elastic cushion with dimensions of 153.5 mm × 102.25 mm × 3 mm thick for each. As stated above, to reduce the times of computing, since the model is symmetric, only a quarter of the model was used for the simulation, see Figure 4.6.

The analysis of springback required two sequential steps: loading and unloading step. The loading step is when the punch pressed the metal sheet into the die and this is simulated using ABAQUS/ Explicit. Subsequently, the initial state for springback analysis was the unloading step where all the forming forces were released and the implicit procedure was applied to solve the problem (ABAQUS/Standard). The change in the radius of curvature of the formed part (displacement U2) was taken as a reference to evaluate the magnitude of the springback.

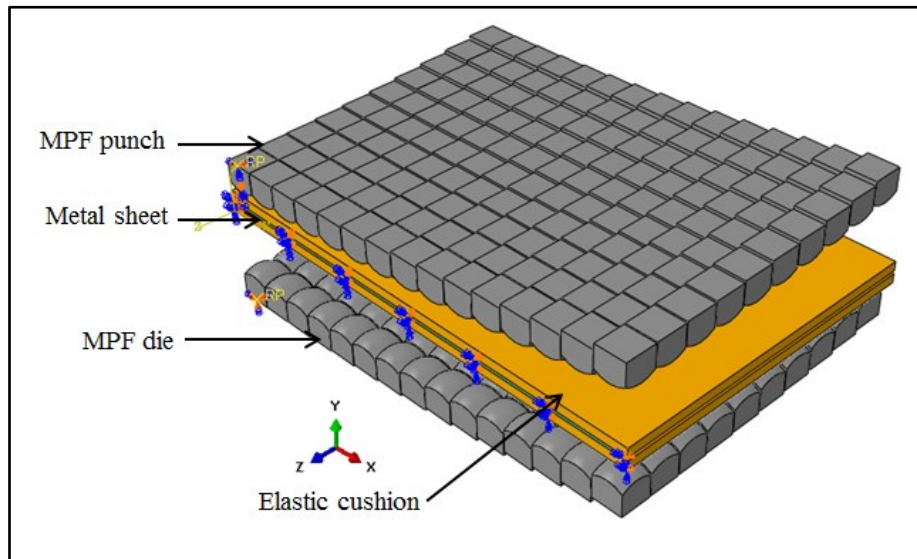


Figure 4-6 Quarter of FEM without blank holder

Two criteria were used to make sure the FE model was stable and ready to use. First, mesh size is an important factor affecting the quality of model's results: a coarse mesh decreases calculation time but provides less accurate outcomes. To get equilibrium state between the precision of the final out comes and the computational time, the size of mesh element was studied for the MPF model to secure accurate simulation results. The second criterion, the model of energy balance can be used to help evaluate whether an ABAQUS/Explicit simulation is resulting a correct response.

#### **4.2.1 Mesh sensitivity analysis**

To simulate springback precisely is so hard, and it is sensitive to many numerical factors; such as element type, the number of elements to describe formed parts, and so on. All these are important factors to be considered when evaluating the quality of the model's results that are produced. A number of studies, such as those by Lee *et al.*, [89], have been conducted to understand the influence of numerical factors on the accuracy of the expected profile after unloading step (springback, U2 in Abaqus). Their results confirmed that the mesh element size has the significant influence on springback prediction accuracy with a smaller element size generally producing more accurate predictions. Alternatively, a fine mesh leads to more computation time. Therefore, the relation between number of elements describing the sheet and springback was studied in order to choose the optimum mesh element size to describe the sheet without adversely affecting the model results. This provided an optimum mesh density to use for all the subsequent investigations of the MPF process. In the FE model, the deformation of MPF tools was ignored as it is very small related to that of the metal sheet and elastic cushion, therefore, all the elements of forming tooling were modelled as rigid bodies.

Figure 4.7 shows the result of increasing the elements number used to represent the metal sheet in the MPF process on springback (radius of forming curvature 800 mm). It can be seen that springback value becomes stable when the number of elements reached 281,250 which represents a  $0.4 \times 0.4 \times 0.4$  mm mesh element size ( $0.064 \text{ mm}^3$ ), as shown in Figure 4.8, and this size was then used for all further simulations. The element dimensions that were studied were,  $1 \times 1 \times 1.2$  mm,  $1 \times 1 \times 0.6$  mm,  $1 \times 1 \times 0.4$  mm,  $0.4 \times 0.4 \times 0.4$  mm and  $0.3 \times 0.3 \times 0.3$  mm

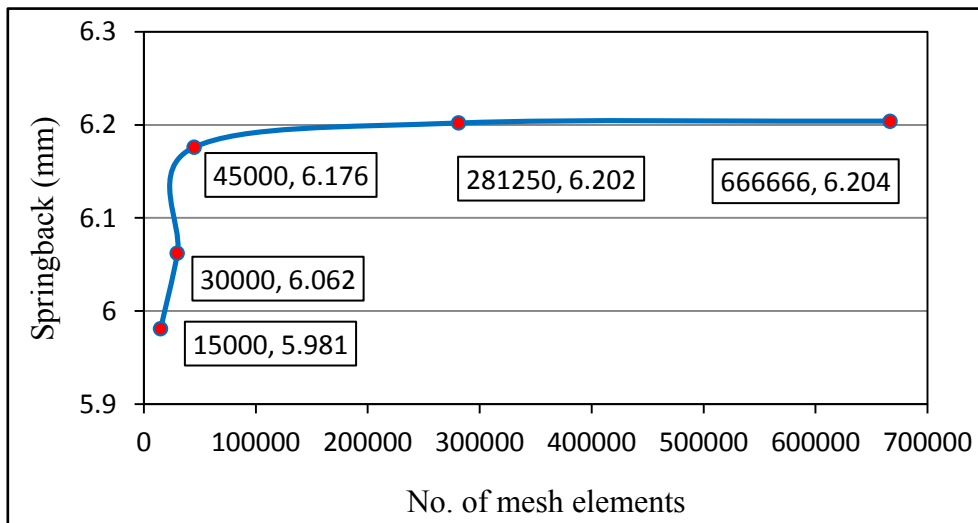


Figure 4-7 Mesh density vs springback

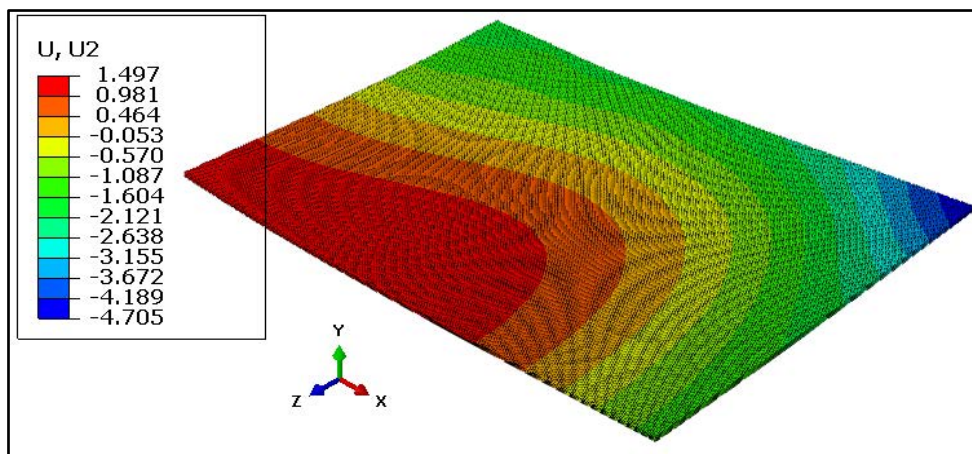


Figure 4-8 Springback for sheet, element size  $0.4 \times 0.4 \times 0.4$  mm

### 4.2.2 Energy balance in quasi-static analysis

Calculation of model energy is a method to make sure the FE model is stable and ready to use. Comparing the history result of kinetic energy and internal energy is a good approach to decide whether an acceptable quasi-static solution has been achieved. In the analysis of metal sheet forming, plastic deformation is considered the source of most internal energy. The kinetic energy (ALLKE) of the deformation sheet should be no large than a few percent (5-10%) of its internal energy ( ALLIE) throughout the most of a quasi-static analysis[74], a small fraction is generally not possible to reach this in beginning stage as the deformable sheet will be moving before it starts any significant deformation. In Figure 4.9, it is clear that the kinetic energy percentage is in agreement with the condition for the FE model in this research..

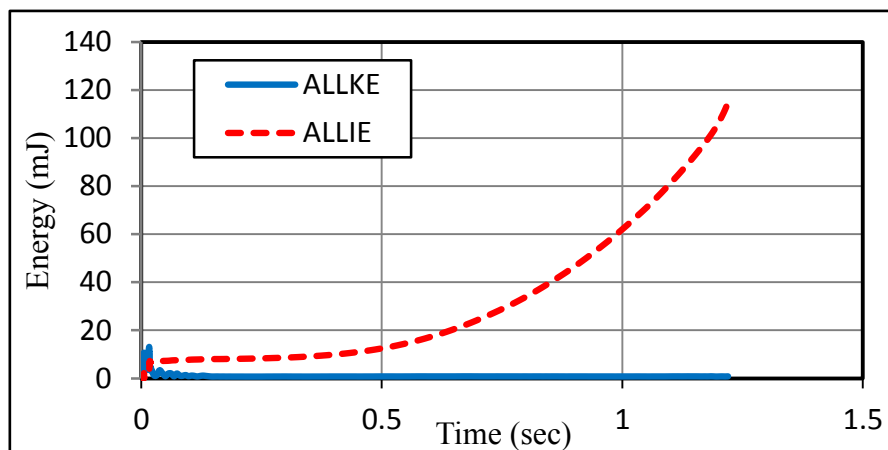


Figure 4-9 Energy balance in quasi-static analyses

### 4.2.3 Experimental validation

The FE model was validated experimentally against the setup as designed by Abosaf [2]. Figure 3.8 ( chapter 3, section 3.2) illustrates the MPF tools for the case with 10 mm pins, and a radius of forming curvature 400 mm, 15 kN blank holder force and elastic cushion 3

mm thick. Tests were carried out to compare the forming force and part profile for both simulation and experimental results. It can be seen in Figure 4.10 that the simulated result of forming force was 60 kN while the experimental force was 63 kN and both exhibited the same trend.

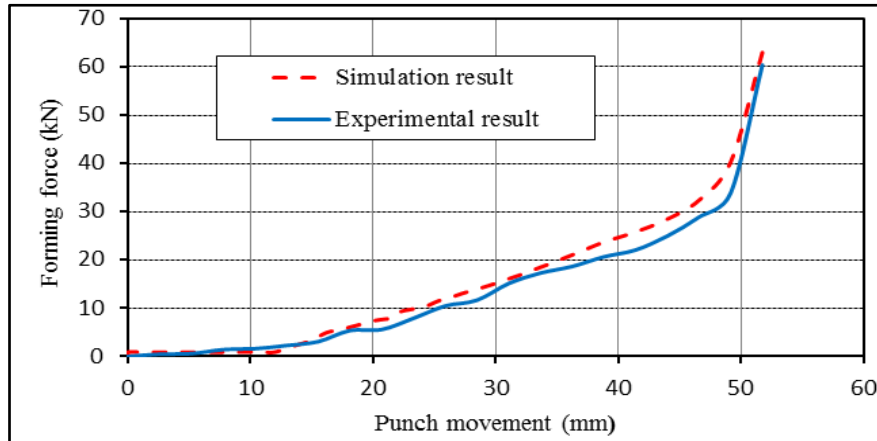


Figure 4-10 Model validation: Forming force [80]

Figure 4.11 shows the comparison between the expected profile of the final product of formed metal sheet using the FE model and the measured profile of the experimental result of the final part by using a FARO Edge Arm 3D scanner [90] along path a-b. There was sufficient agreement between the predicted and experimental results which differed by, at most, 1.94 mm near the centre of the profile.

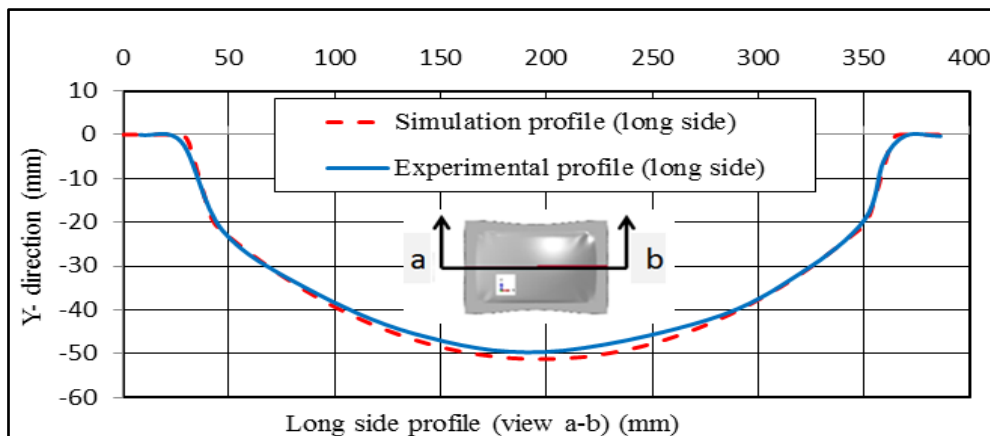


Figure 4-11 Model validation: final profile [80]

### 4.3 Effect of process factors on springback

The most important parameters which, according to the literature review, affected the springback in the formed metal sheets in general were studied in this section, using the validated 3D FE model of MPF with 10 mm pins.

#### 4.3.1 Effect of friction coefficient

The coefficient of friction is one of the process factors affecting metal flow, surface formation, stress distribution and forming force, and the predicted springback in the final product. The deformation behaviour is different if a high or low friction coefficient is applied [30, 91] and its impact on the final part was investigated. It is modelled because its value is different for flat and curved parts and it is hard to measure these values experimentally. Figure 4.12 shows the effect of friction coefficient on the simulated springback. The values of friction coefficient were 0.05, 0.1, 0.15 and 0.2 as dry conditions were assumed for this process [92]. It can be realised that the increase in the coefficient of friction will lead to more tension in the sheet and consequently decreases the springback. Papeleux and Ponthot reported very similar results [93]. Albut [94] concluded that the lubrication of forming tools caused an easier metal flow into the die which leads to increase springback due to a lower friction coefficient.

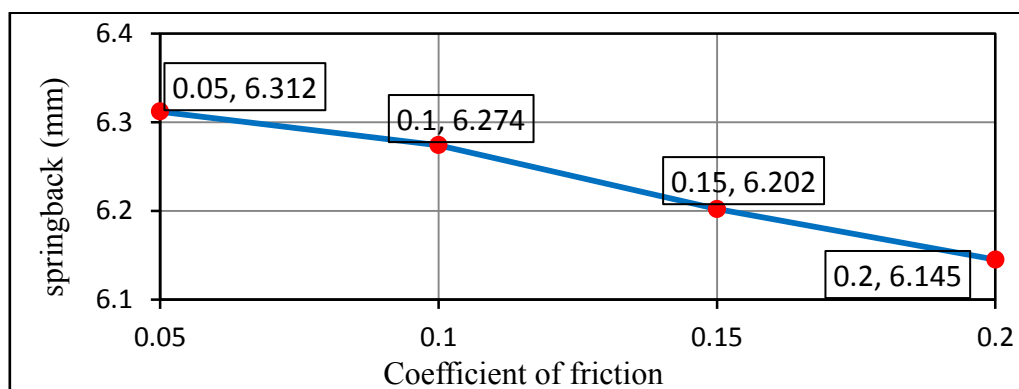


Figure 4-12 The effect of coefficient of friction on simulated springback

Figure 4.13 shows the simulation results of stresses distribution (a) and springback of formed part (b) at friction coefficient 0.2 while all other parameters remain constant.

There were three parameters investigated: radius of forming curvature (A), elastic cushion thickness (B) and blank holder force (C). Only one factor was changed at a time while the other two kept constant, at a value listed in Table 4.2. The displacement in direction Y (U2) between the fully loaded shape at the end of the forming step and the unloaded shape was done using ABAQUS/Standard and used to present springback in the formed part as shown in Figure 4.14 [95]

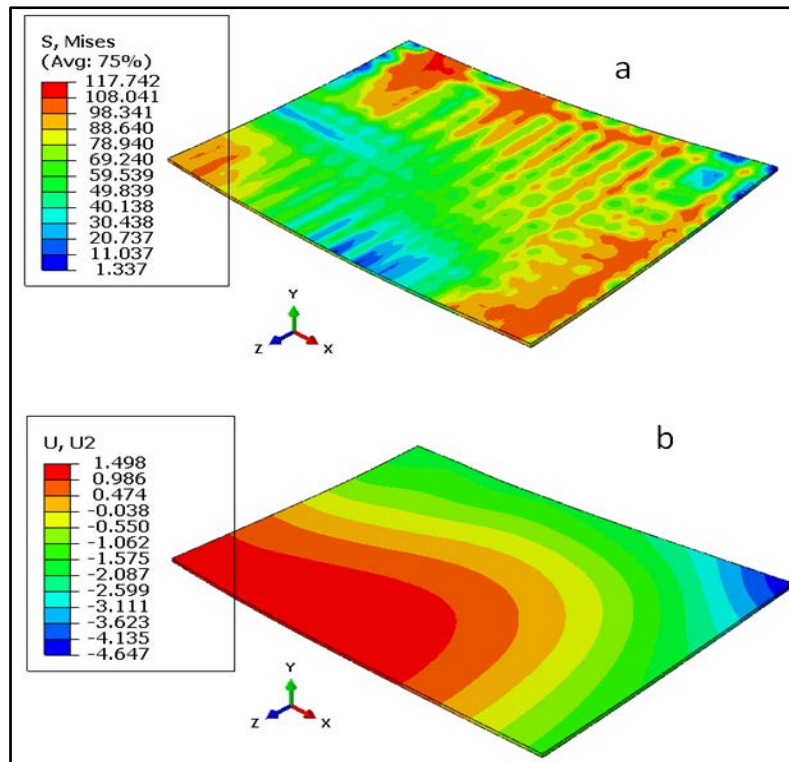


Figure 4-13 Simulated part for coefficients of friction 0.2

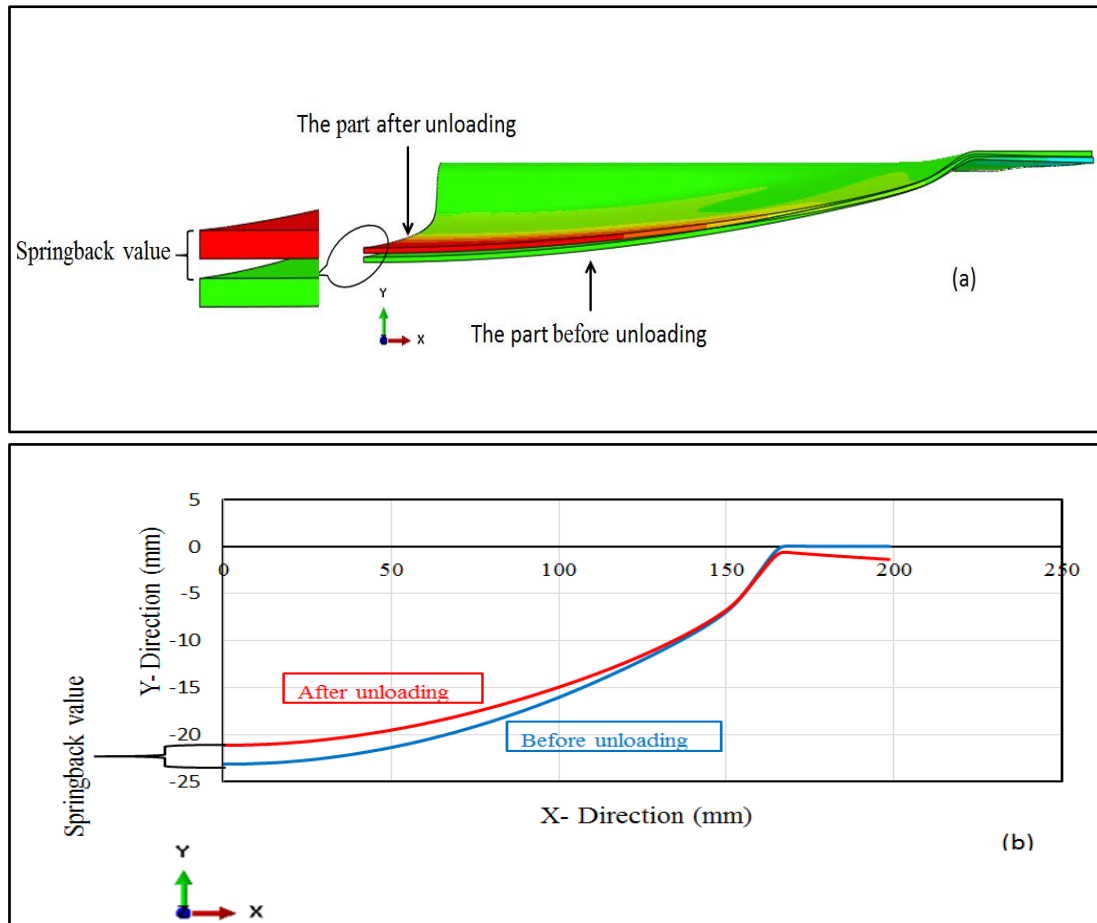


Figure 4-14 3D (a) diagram of formed part, (b) part profile showing how spring back was measured [80]

Table 4-2 Process parameters investigated [80]

Process factors	Units	Levels		
		Low	Intermediate	High
Radius of forming curvature (A)	mm	400×400	600×600	800×800
Blank holder force (B)	kN	5	15	25
Elastic cushion thickness (C)	mm	3	5	7

#### 4.3.2 Effect of radius of forming curvature

The radius of forming curvature had three levels 400, 600 and 800 mm, and each formed part of a sphere. Figure 4.15 shows that the smaller the radius of forming curvature, the lower the

springback that occurs at the final part after unloading step. The springback increases from 2.14 mm to 6.18 mm with increase in radius of forming curvature from 400 to 800 mm. This is because the plastic to elastic deformation ratio is higher for the smaller radius of curvature and more wrinkling takes place at the edges of the formed sheet [84] and it reduces springback value in formed sheet.

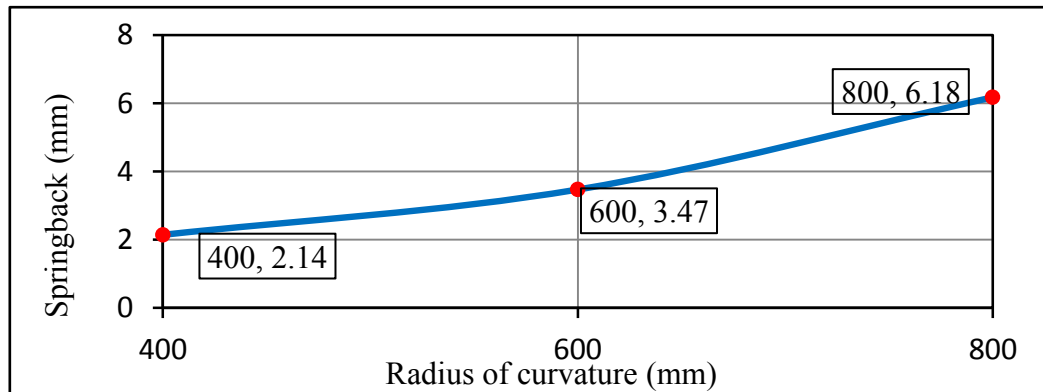
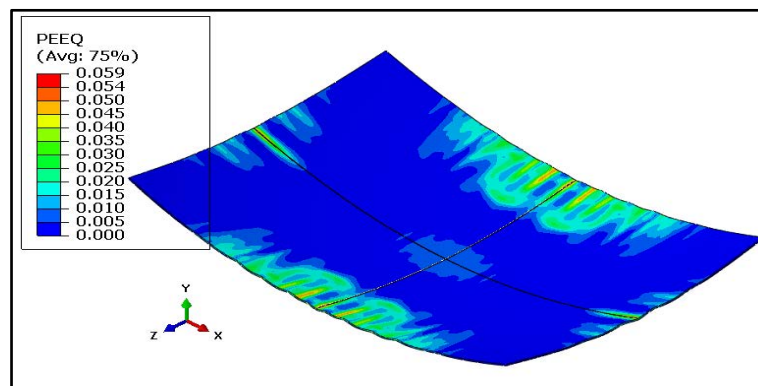
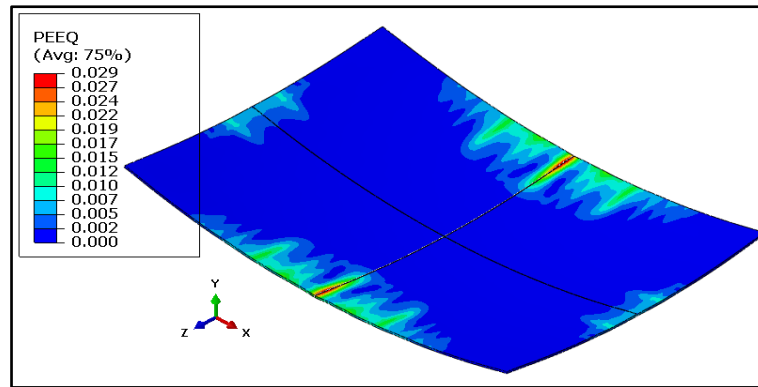


Figure 4-15 The effect of radius of forming curvature on springback

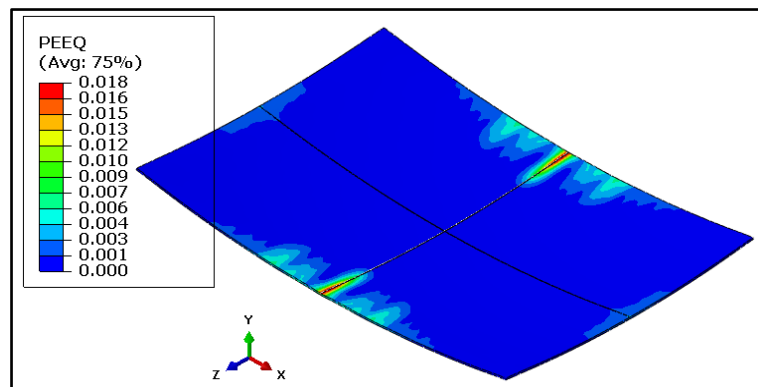
Figure 4.16 (a), (b) and (c) illustrate the equivalent plastic strain distribution of formed sheet for different radius of forming curvature (a) 400 mm, (b) 600 mm and (c) 800 mm. It can be noticed that the maximum value of equivalent plastic strain occurred in the formed sheet with smallest radius of forming curvature (400 mm).



(a) Radius of forming curvature 400 mm (cont.)



(b) Radius of forming curvature 600 mm



(c) Radius of forming curvature 800 mm

Figure 4-16 Equivalent plastic strain distributions for different radii of forming curvature

### 4.3.3 Effect of blank holder force

Three different values of blank holder force were used to hold the sheet during the deformation process; 5, 15, and 25 kN.

Figure 4.17a, b and c show the simulated result obtained for blank holder force of 15 kN. It is clear the largest springback value occurred at the edges of the formed part where the blank holder was located due to less plastic deformation in this area. The effect of the blank holder force on springback was found to be small compared to the other parameters such as the radius of curvature. The general trend for springback was to decrease with increasing blank

holder force but an extreme blank holder force may possibly cause other defects such as tearing of the metal sheet.

Figure 4.18 reveals the relationship between blank holder force and springback in the case of the radius of forming curvature of 800 mm.

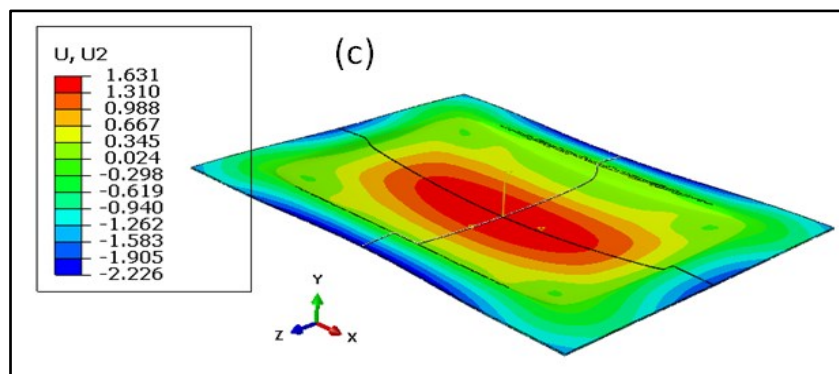
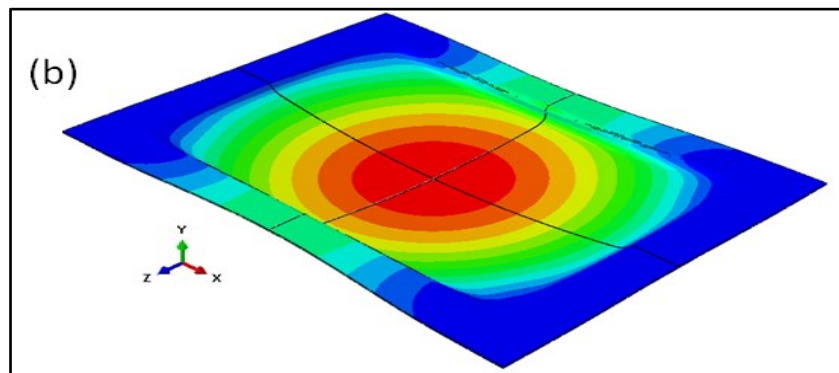
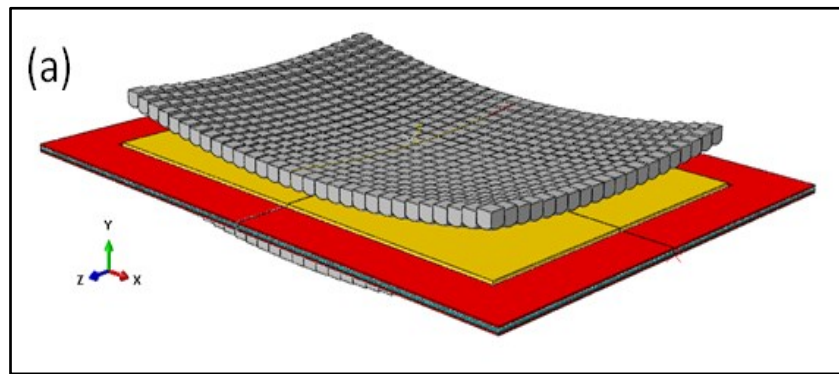


Figure 4-17 Simulated result for springback for blank holder force of 15 kN and radius of forming curvature 800 mm

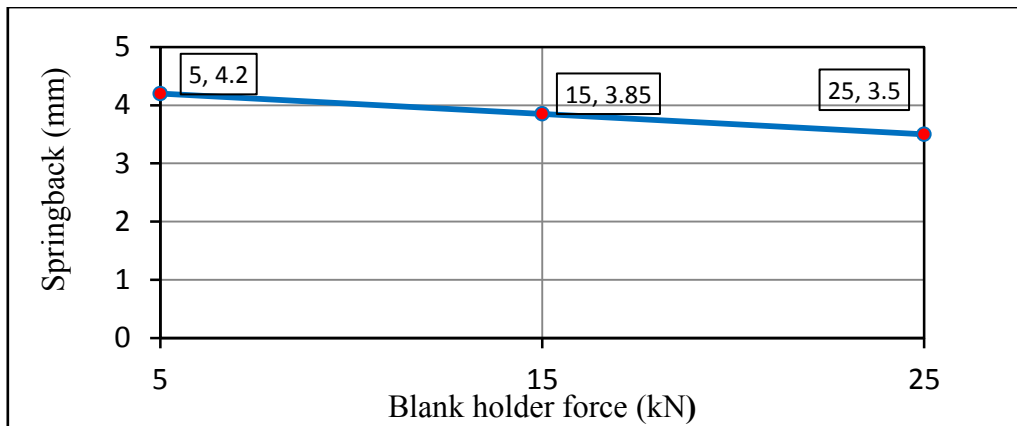


Figure 4-18 The effect of blank holder force on springback, for radius of curvature 800 mm

#### 4.3.4 Effect of elastic cushion type and thickness

The elastic cushion layers are utilised in the MPF process to eliminate dimpling on the formed part. The effect of elastic cushion hardness and thickness on springback is studied in this chapter. Figure 4.19 shows the variation of simulated stresses distribution and springback with respect to elastic cushion for three levels of Shore hardness (a) A50, (b) A65 and (c) A90. The polyurethane sheet with a hardness of Shore A 90 was employed [84] in a simulation study with a radius of forming curvature 800 mm. It can be seen that the springback reduced with increasing elastic cushion hardness as shown in Figure 4.20. This is due to a more uniform stress distribution on the metal sheet. The same finding was reported by Heo *et al.*, [85].

It is shown that the elastic sheet used in the MPF process for metal sheet should be relatively hard (i.e. Shore hardness A90) and that its thickness should be chosen with care.

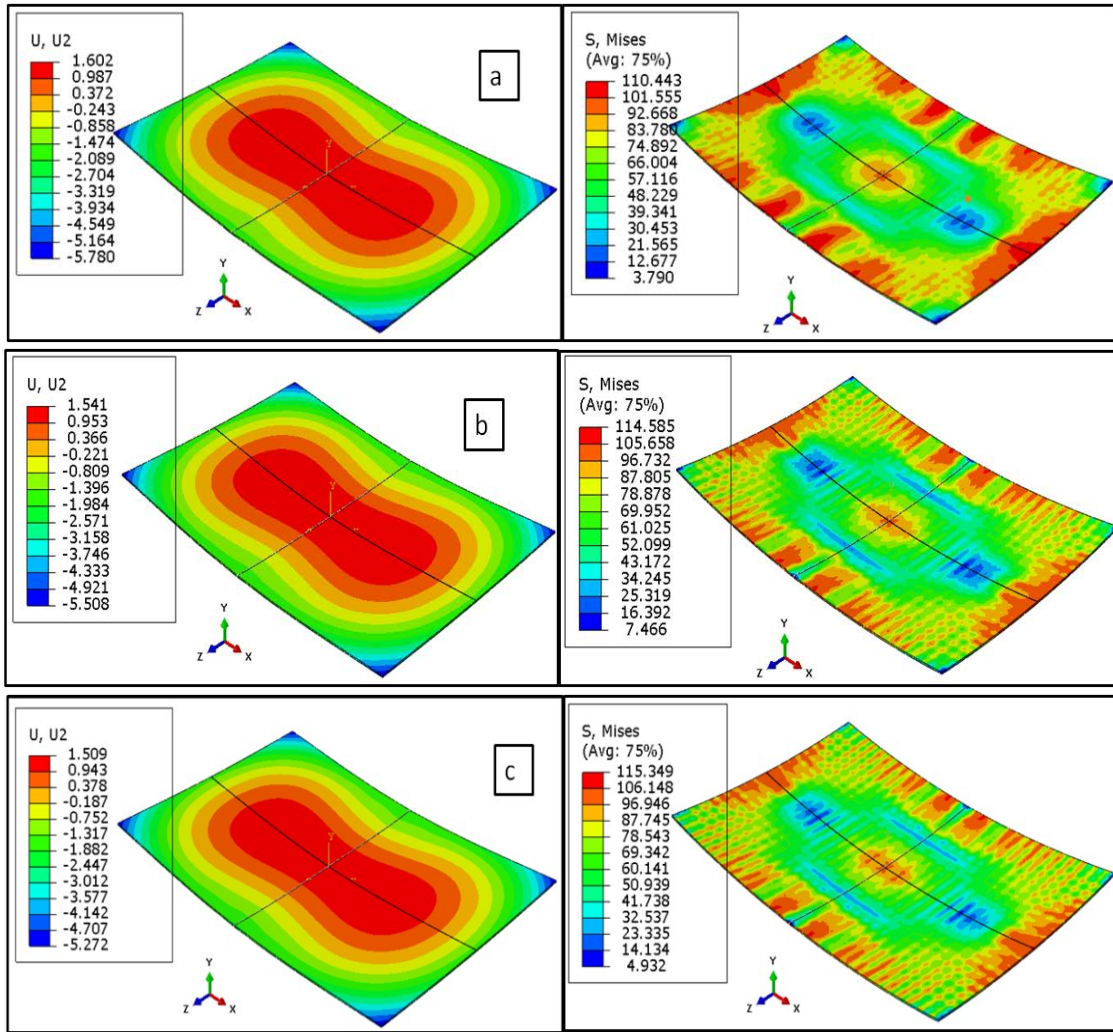


Figure 4-19 Simulated effect of elastic cushion hardness on springback, (a) A50, (b) A65 and (c) A90

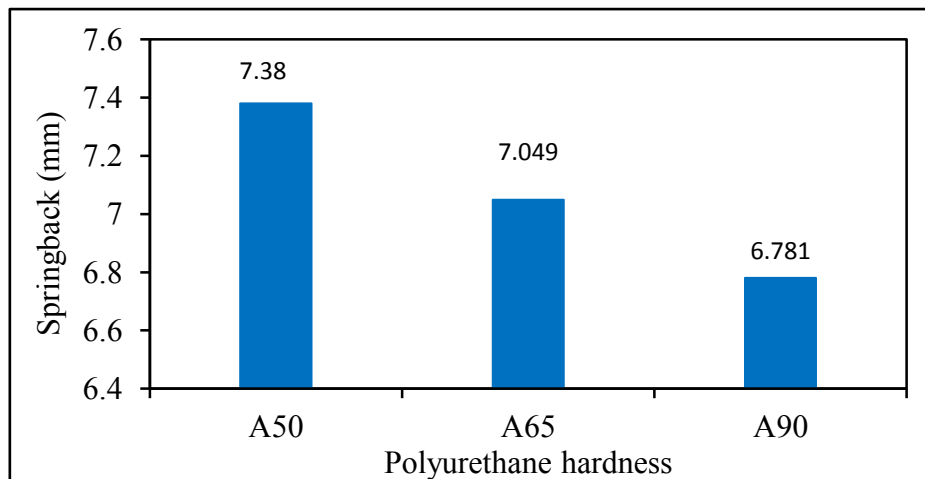


Figure 4-20 The simulated effect of 3 mm thick elastic cushion of different hardness values on springback

Three elastic cushion thicknesses (a) 3, (b) 5 and (c) 7 mm with shore A hardness of 90 and radius of forming curvature 700 mm for simulation investigation, Figure 4.21 reveals the springback simulation results as a function of elastic cushion thickness. It can be seen that the springback decreased appreciably with increasing elastic cushion thickness, as shown in Figure 4.21, and will affect shape accuracy [96].

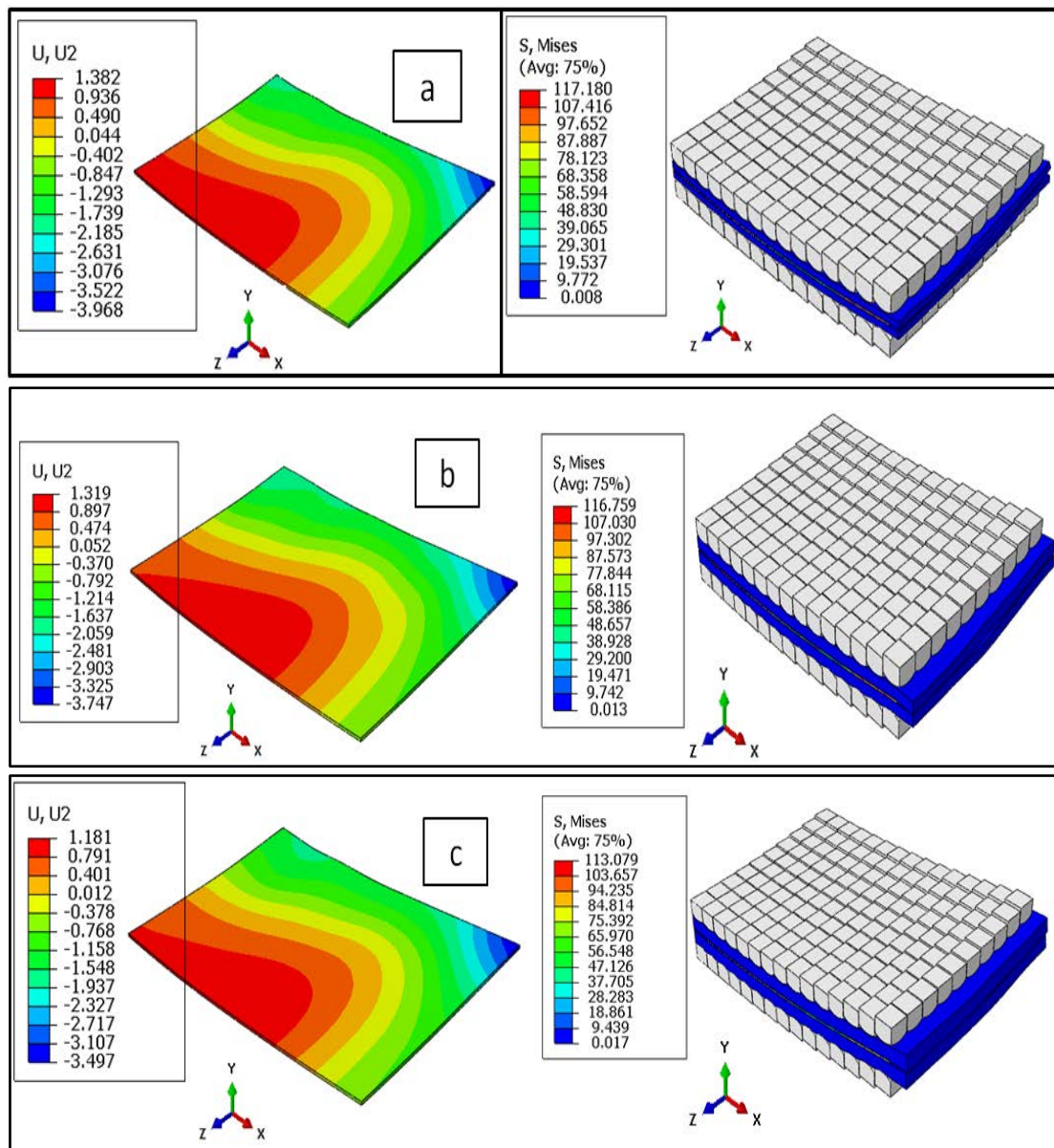


Figure 4-21 Simulation results of effect of Shore A90, elastic cushion thickness on springback, (a) 3 mm, (b) 5 mm and (c) 7 mm. (Radius of curvature 700 mm)

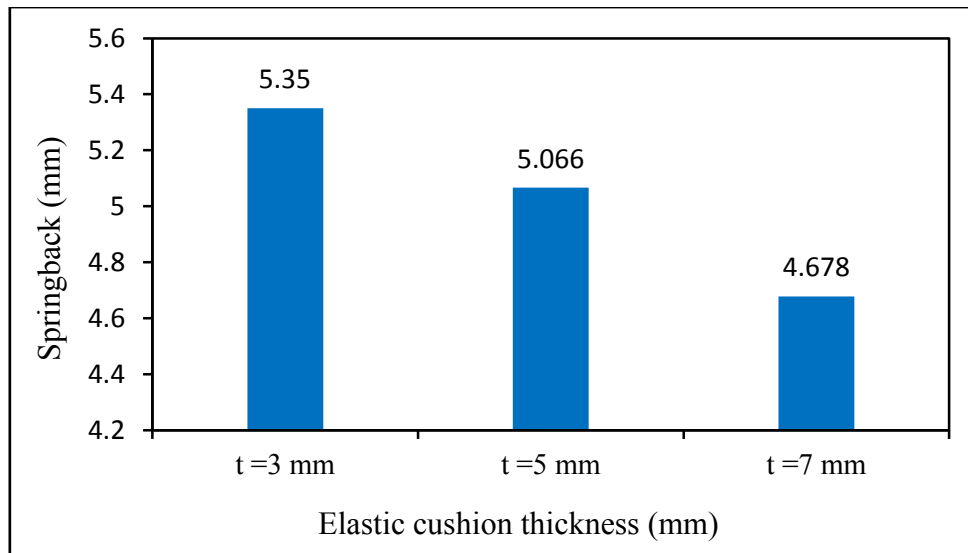


Figure 4-22 The simulated effect of elastic cushion thickness on springback

#### 4.4 Summary

The finite element modeling for the MPF process was developed and explained in detail in this chapter, the material properties of the tested material in this research; both sheet metal and elastic cushion were obtained from the mechanical tests as presented in Chapter 3. The finite element modeling results were validated against experimental work; the forming force versus punch displacement curve showed good agreement between simulated and formed part profile at the end of the forming step.

Effects of friction coefficient, radius of curvature, blank holder force and elastic cushion thickness on springback were explored to highlight the importance of each parameter. It was found that the radius of forming curvature has the most important effect on springback in the MPF process.

## **CHAPTER 5:**

### **FINITE ELEMENT MODEL AND OPTIMISATION OF SPRINGBACK IN MPF**

This chapter presents the details of a numerical method for the simulation and prediction of springback in multi-point forming (MPF). FE models have been developed to simulate the MPF of doubly curved aluminum alloy panels (Al 5251-O). ANOVA and the Response Surface Method (RSM) provided in design-expert software v7 were used to find the most important of the process parameters and to identify what combinations were most relevant to improving the quality of the formed workpiece. The effect these parameters had on the variation of thickness over the formed panel and on the value of springback were explored.

Heo *et al.*, [17] investigated the effect on a formed panel of the dimensions of the punch and of the force holding the clamp in place. They found that a better quality surface of the formed panel was achieved using smaller pin. Abosaf *et al.*, [84] confirmed that the radius of forming curvature of the formed sheet and size of pins used had a significant effect on accuracy of the shape in MPF. Zareh-Desari *et al.*, [81] found that the presence of an elastic cushion was important for accuracy of the formed panel, and was essential for MPDD (multi-point deep drawing). Sun *et al.*, [97] also found that, wrinkling can be eliminated by employing a flexible blank holder in thin metal sheets and enhanced the forming limit. Li *et al.*, [98] confirmed that the use of a thick sheet decreased springback. Davoodi and Zareh-Desari [96] used MPF tools for deep drawing and found that to reduce springback small pins should be used as should a hard, elastic pad with minimum thickness.

Many MPF techniques exist to reduce or compensate for springback. Wenner [99] reported springback of the formed panel could be reduced if the metal sheet was preloaded. Li *et al.*,

[98] proposed over-forming metal sheets to compensate for the expected springback in a given shape.

Woellner *et al.*, [100] explored the influence of the properties of the formed sheet and of the blank holder force (BHF) on springback in deep drawing for which MPF tools were used. They stated that the yield strength of the formed panel had a measurable effect the accuracy of the final shape, with materials such as steel - with high yield strength - showing correspondingly high levels of springback. Also they reported that, in their opinion, to reduce springback it was necessary to clamp the workpiece.

Finite Element (FE) analysis is a cost-effective means of investigating the influence of the different process parameters on geometrical accuracy and to simulate springback [2, 52, 77].. The RSM was used [48, 101, 102] to probe how the different process parameters affected the springback in MPF. Both the variation in thickness across the formed panel and the value of springback were investigated and a relationship between springback and thickness variation was established. An existing MPF tool [2] was used to validate the results of the simulation, thus, the pin size was predetermined. The pins were square with a cross-section of 10 x 10 mm, with a 10 mm radius of the tip.

### **5.1 Design of experiments (DOE)**

DOE and analysis of variance (ANOVA) are established as useful tools for investigating the different effects of the process parameters in sheet metal MPF [2, 101]. In this research the elastic cushion thickness, the force holding the sheet and the radius of curvature of the formed panel were considered to be the most important of the process parameters [2, 17, 45, 85, 95]. To simulate the springback for the entire formed surface, an “approximate response surface (Central Composite design (CCD))” was assumed to exist between the points for

which predicted results were determined. Finding the parameters that gave minimum thickness variation and minimum springback was the final step. These optimal parameters were then applied in a last step analysis to validate the solution as shown in Figure 5.1.

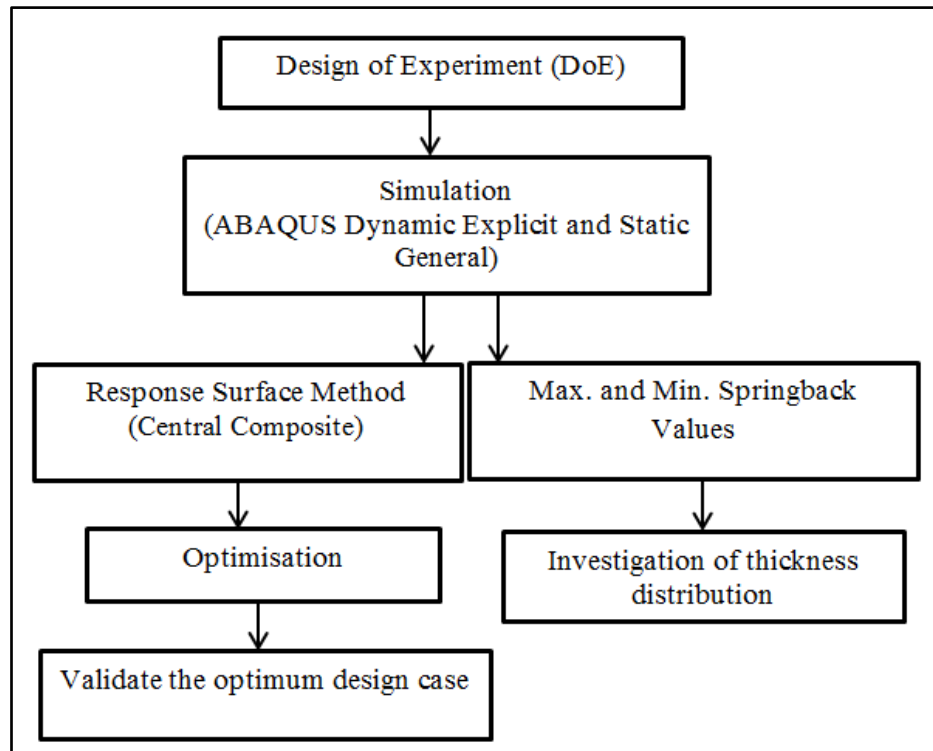


Figure 5-1 Sequences for optimisation and DOE procedures

The RSM generates an equation linking the objective function ( $y$ ) to the inputs of the relevant variables ( $x_i$ ). Usually, the RSM uses a second order general polynomial, as in Equation 5.1, using the results of a series of experiments, see Table 5-2, to develop an empirical model which identifies the most important of the variables. The empirical model coefficients are  $x_1$  to  $x_9$  (see Equations 5.2 and 5.3), and these are found using regression analysis. A Genetic Algorithms (GA) which are a form of optimisation techniques, meaning they are applied to obtain the optimal solution to a specified computational problem that minimise or maximise a particular function. [GA steps 1- assess the fitness of each single in the population, 2- select the best fittest parents from the known population, 3- do crossover action by recombining the

individuals for parents to create new generation, 4- mutate the new generation, 5- if the condition not got, then go back to step 2, else end the action, and return the best individual in the existing population]. In this research they were utilised to determine the settings for the input parameters (process parameters) that best met the mean of objective function.

$$y = a_0 + \sum_{i=1}^n a_i x_i + \sum_{i=1}^n \sum_{j=1}^n a_{ij} x_i x_j + \varepsilon \quad (5-1)$$

where  $a_0$ ,  $a_i$  and  $a_{ij}$  are the model coefficients and  $\varepsilon$  is the noise in the system.

### 5.1.1 Process parameters

In MPF processes the DOE considered selected factors that were known to have an effect on part quality. These were the thickness of the elastic cushion, the force holding the blank and the radius of curvature of the formed panel. Each factor was given a low, a medium and a high value, which covered an adequate range. Table 5-1 presents the selected parameters and their given values.

Table 5-1 Value and level of the selected DOE parameters [80]

Process parameters	Units	Levels		
		Low	Intermediate	High
Radius of curvature of the formed panel (A)	mm	400×400	600×600	800×800
Blank holder force (B)	kN	5	10	15
Elastic cushion thickness (C)	mm	3	5	7

### 5.1.2 Response parameters

An acceptable measure had to be determined by which to assess the final quality of the formed workpiece. This could be a single measure, or a combination of measures, be used as a reference for final part quality. Here, uniformity of thickness and value of springback were chosen to assess the quality of the final part. Springback in the final formed workpiece was

the movement (displacement U2) of the part in the direction of the thickness (Y) as computed by ABAQUS after the last unloading step [52]. In addition, equation (5.2) was used to calculate the variation in thickness of the final parts.

$$\text{Thickness variation} = \sqrt{\frac{1}{N} \sum_{i=1}^N (x_i - \bar{x})^2} \quad (5-2)$$

In Equation (5.2) which has the usual form for measuring an RMS value, N is the number of thickness measurement points,  $x_i$  is the part thickness at point i, and  $\bar{x}$  = mean thickness value for the measured points.

Here the larger the springback, and the greater variation in thickness, the lower the quality of the produced part.

### 5.1.3 Results, analysis and discussion

Table 5-2 lays out the seventeen sets of experimental conditions. It also shows the resulting measurements of thickness variation and springback. Design Expert 7.0 was used to statistically analyse the results of the simulation. by using response surface method with central composite face-centred (CCF) which are first-order ( $2^N$ ) designs augmented by additional 3 centred points and 2N axial points (where N is number of factors) to allow estimation of the tuning parameters of a second-order model [84, 103]. ANOVA was used to identify the more important process parameters. Here, the null hypothesis -  $H_0$ , that there was no relationship between the two measured phenomena; process parameters and condition of the formed panel - was assigned a 5% significance level [84]. From Table 5-3 we see that BHF and radius of curvature of the formed panel have a significant effect on the springback, but that the thickness of the cushion does not. We also see that BHF and radius of curvature of the formed sheet both have a significant effect on thickness variation. However, we also

see that the interaction between cushion thickness and BHF have a significant effect on thickness variation.

Table 5-2 Experimental plan and simulation results [80]

Exp. #	Factor 1	Factor 2	Factor 3	Response 1	Response 2
	A: Radius of forming curvature (mm)	B: Blank holder force (kN)	C: cushion thickness (mm)	Springback (mm)	Thickness variation ( $\mu\text{m}$ )
1	600	10	7	1.2	4.8
2	400	15	3	0.80	6.3
3	800	10	5	1.9	4.1
4	600	10	3	1.5	4.8
5	800	15	3	1.95	4.5
6	600	5	5	1.4	4.8
7	400	5	3	1.32	5.1
8	400	15	7	1.05	5.8
9	400	5	7	1.1	5.5
10	600	10	5	1.35	5.1
11	800	15	7	1.74	4.6
12	400	10	5	1.2	5.7
13	600	15	5	1.35	5.6
14	800	5	7	1.83	3.8
15	600	10	5	1.35	5.1
16	600	10	5	1.35	5.1
17	800	5	3	2.2	3.5

Table 5-3 Factor-response interactions with P-values [80]

Response factors	Springback	Thickness variation
Significant factors		
Radius of curvature of forming panel (A)	0.0001	0.0001
Blank holder force (B)	0.0165	0.0001
Elastic cushion thickness (C)	0.139	0.3147
Parameter interactions	(AB)=0.3911 (AC)=0.0502 (BC)=0.0549	(AB)=0.3338 (AC)=0.1273 (BC) 0.0067

### 5.1.3.1 Springback

In MPF, there are two types of geometrical errors: the first type is wrinkling and dimpling, which take place before the unloading process; the second type is springback which, by definition occurs after unloading [16]. Figure 5.2 shows springback as a function of BHF and Radius of curvature of forming panel for constant elastic cushion thickness. We see that a smaller radius of curvature of the formed workpiece results in a lower springback, Li *et al.*, [52] have reported a similar result. However, we also see that springback is reduced by using a larger BHF. Woellner *et al.*, [100] have presented very similar results. Apparently, there is more plastic deformation if the radius of curvature is smaller or the BHF is larger. That is the plastic to elastic deformation ratio is higher. It follows that if the sheet to be formed is clamped, the elastic recovery becomes insignificant, generating less springback. Figure 5.2 indicates that minimum springback will be achieved with large BHF and small forming radius.

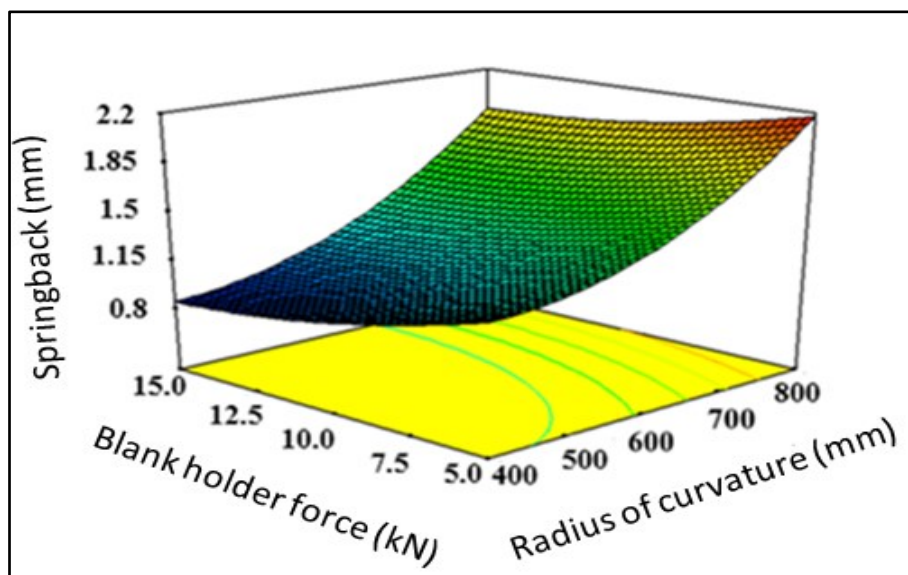


Figure 5-2 Springback as a function of blank holder force and radius of curvature for constant elastic cushion thickness[80]

### 5.1.3.2 Sheet thickness variation

For the sheet metal used, the average initial thicknesses was 1.20 mm with no significant variation, so any changes in thickness was taken to be due to the forming process.

Figure 5.3 shows variation in sheet thickness as a function of BHF and radius of curvature for constant elastic cushion thickness. We see that a larger radius of curvature of the formed panel results in less variation in sheet thickness. However, we also see that variation in thickness of the formed workpiece is increased by using a larger BHF, due to increased deformation due to stretching of the workpiece [84]. Again, Woellner *et al.*, [100] have presented similar results. There is less plastic deformation if the radius of curvature is larger or the BHF is smaller.

When the radius of curvature is large (here the maximum was 800 mm), a larger number of pins act to constrain the workpiece at the start of deformation, which leads to more uniform stress which reduces variation in thickness [84]. Figure 5.3 indicates that minimum thickness variation will be achieved with small BHF and large forming radius. Similar

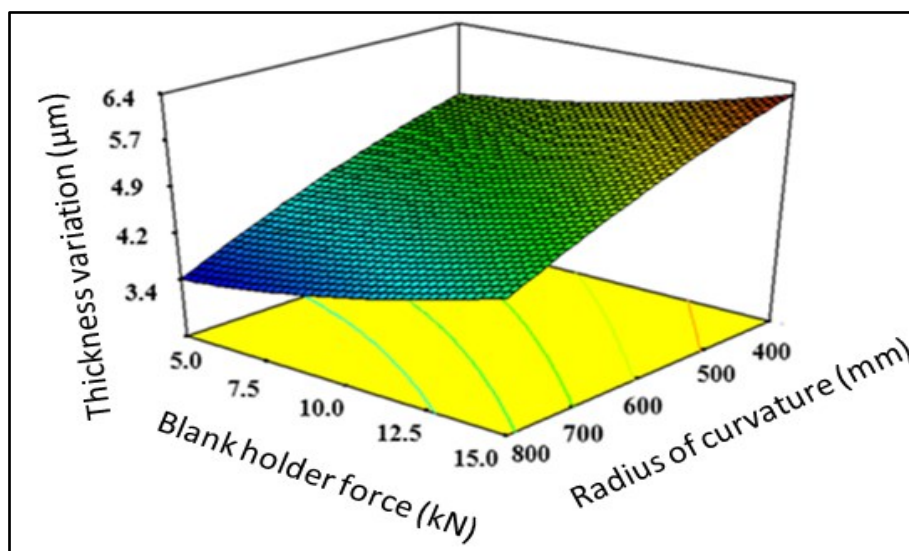


Figure 5-3 Variation in sheet thickness as a function of blank holder force and radius of curvature for constant elastic cushion thickness [80]

Figure 5.4 shows variation in sheet thickness as a function of BHF and elastic cushion thickness. We see that a thicker elastic cushion (7 mm thick) results in less variation in sheet thickness with change in BHF. However, we also see that for the thinner elastic cushion (3 mm thick) variation in thickness of the formed panel with increase in BHF becomes significant.

For the given experiment it appears that the thicker the elastic cushion, the BHF is more evenly distributed over the sheet metal workpiece and stress distribution across the workpiece surface is more uniform, the result is that local deformation is reduced. With the thinner cushion the stress distribution is less uniform because there will be local deformations due to the individual pins. Under such conditiona small changes in BHF will cause local areas of sheet thinning with consequent thickness variation [77].

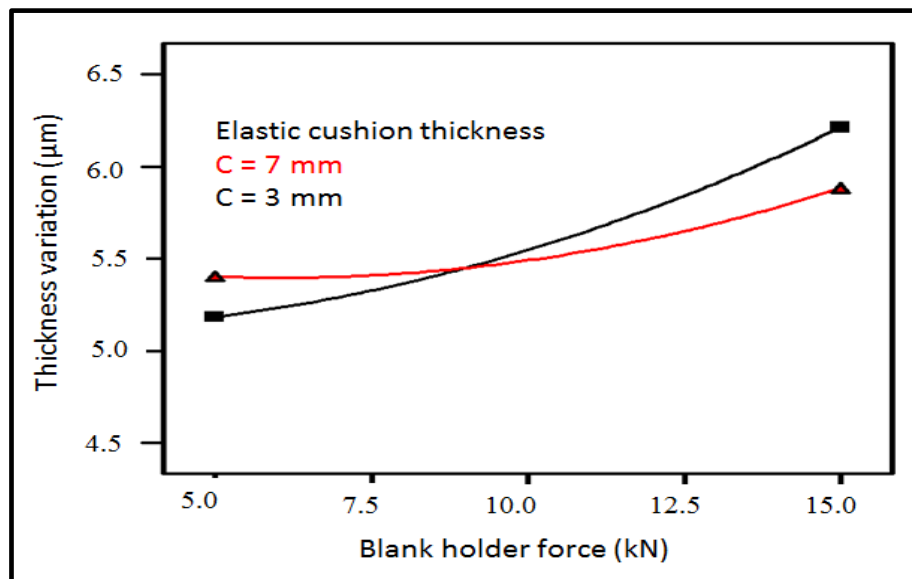


Figure 5-4 Variation in sheet thickness as a function of blank holder force and elastic cushion thickness [80]

#### 5.1.4 Prediction of response factors

To predict springback and variation in thickness, an empirical second-order polynomial (the “objective function”) was developed (see Equation 5.3). This equation is built on the three “significant factors” in Table 5-2.

$$\text{Response} = X + X_1A + X_2B + X_3C + X_4AB + X_5AC + X_6BC + X_7A^2 + X_8B^2 + X_9C^2 \quad (5-3)$$

where X is a constant which depends on the conditions, A is the radius of curvature of forming panel in mm, B is the BHF in kN, C is the elastic cushion thickness in mm, and  $x_1 - x_9$  are the model coefficients which are listed in Table 5-4.

Equation 5-3 predicts variation in panel thickness and of springback for any combination of the “significant factors”: BHF, curvature of the finished panel and elastic cushion thickness.

Table 5-4 Coefficient values for objective function [80]

Coefficient	Springback (mm)	Thickness variation ( $\mu\text{m}$ )
Constant (X)	1.848	4.706
$x_1$	-4.109E-003	1.265E-003
$x_2$	-0.139	7.473E-003
$x_3$	0.378	0.569
$x_4$	3.000E-005	3.750E-005
$x_5$	-1.938E-004	1.563E-004
$x_6$	8.000E-003	-0.0143
$x_7$	5.715E-006	-3.201E-006
$x_8$	3.144E-003	6.079E-003
$x_9$	-0.0366	-0.051

### 5.1.5 Optimisation of process parameters

The goal was to simultaneously minimise both variation in sheet thickness and springback. The optimal settings of the three process parameters to achieve that goal were found by solving two empirical equation of springback and thickness variation together, using the GA mentioned earlier in section 5.1 until the condition of minimum thickness variation and springback was met. For an MPF die with 10 mm pins and with the three process parameters limited to within the preselected ranges shown in Table 5-1, the optimal simulation settings were found to be: BHF 8 kN; radius of curvature 600 mm; and elastic cushion 3 mm thick, see Table 5-5.

For the experimental validation, a 3-D point cloud image of the final part was obtained using the FARO Edge 3D scanner [2] This image was then compared to the design shape and any deviation in the Y direction was recorded as a measure of the springback, see Figure 5.5. Using a digital micrometre the sheet thickness was measured with a resolution of 0.01 mm at a number of points in the X and Z directions, from the centre of the formed workpiece in directions parallel to the sides, see Figure 5.5. The mean and standard deviation (Sd) of these measures were determined and the Sd was used as a representation of the variation in thickness, see Equation 5.2 above. Table 5-5 presents the experimental results for thickness variation and springback, and shows very good agreement between simulation results and experimental measurements.

Table 5-5 Comparison of numerical simulation results and experimental validation [80]

	Radius of curvature (mm)	Blank holder force (kN)	Elastic Cushion Thickness (mm)	Springback Value (mm)	Thickness Variation( $\mu\text{m}$ )
Optimised solution	600	8	3	1.38	4.10
Experimental result	600	8	3	1.42	3.95

The optimum value of springback is 1.38 mm but minimum value of springback as listed in table 5.2 can be different. The optimum solution will consider all pre-selected parameters and gets balance between them to produce a part meets the objective function which is minimise springback and thickness variation. Thickness distribution “error” =  $\frac{4.10-3.95}{3.95} = 3.8\%$

$$\text{Springback “error”} = \frac{1.42-1.38}{1.38} = 2.9\%$$

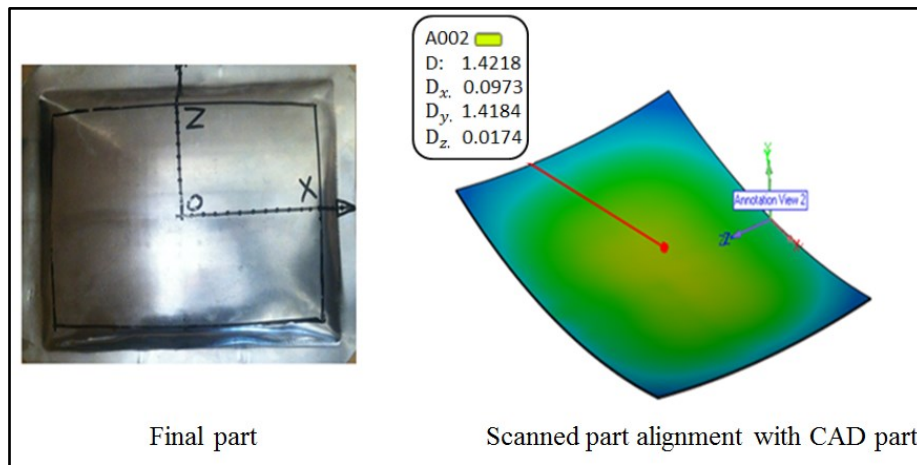


Figure 5-5 Measured springback for final formed surface [80]

## 5.2 Thickness distribution and local strain on formed part

Factors that impact on springback include distribution of strain, type of contact and the resulting local deformations. In the forming of cold metals, the preferred forms of deformation to minimise springback are thinning and stretching [104]. Here thickness distribution was examined for the two cases: high and low springback.

Figures 5.6 and 5.9 show the distribution of thickness across the formed panels for the two cases listed in Table 5-2 as Exps #2 and #17. Figures 5.7 and 5.8 show the sheet thickness across the centre of the plate parallel to the long side (O-X) and parallel to the short side (O-Z) for Exp #17.

The initial thickness of the metal sheet was 1.20 mm. The springback was predicted to be 2.2 mm - the worst case of all the simulations. For O-X, the plot shows thinning right across the sheet with maximum thinning in the sheet occurring at the centre of the sheet (the point of first pin contact [84] ). There was also a small region where the thickness decreased sharply, in the transition zone between the end of the formed area and the blank holder, see Figure 5.7. Here the sheet was highly stretched because it was clamped by the blank holder while immediately adjacent the punch was pressing the sheet into the die.

For O-Z, the short side, see Figure 5.8, the thinning that takes place at the centre, O, is the same as for OX, this thinning is due to localised stresses. As the point of observation moves along the line OZ the thinning of the sheet decreases until a slight thickening occurs just over half way to the transition zone. This thickening is considered to be caused by a compressive stress acting perpendicular to the drawn-in direction [105]. Thinning of the sheet can be seen at the border between the forming zone and transition zone, and is due to this being the area of first contact between the sheet and the punch [84]. However, once in the transition zone thickening of the sheet occurs. Under the action of the punch there is a movement of material from the centre of the sheet to the edges. . Also, that side of the sheet was not long enough and the height of the part (800 mm) not enough to accommodate the material flow from the centre. Consequently, there was thickening of the formed sheet.

From the figures it can be seen that maximum thickening of the sheet occurred beneath the blank holder. This is due to the holding force which impedes the flow of the metal, by different amounts, depending on the magnitude of the clamping force.

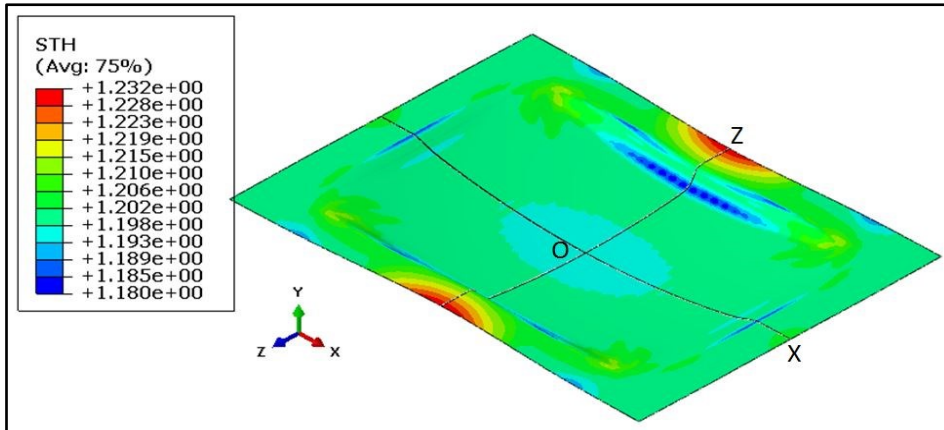


Figure 5-6 Simulated distribution of sheet thickness for BHF = 5 kN and R=800 mm

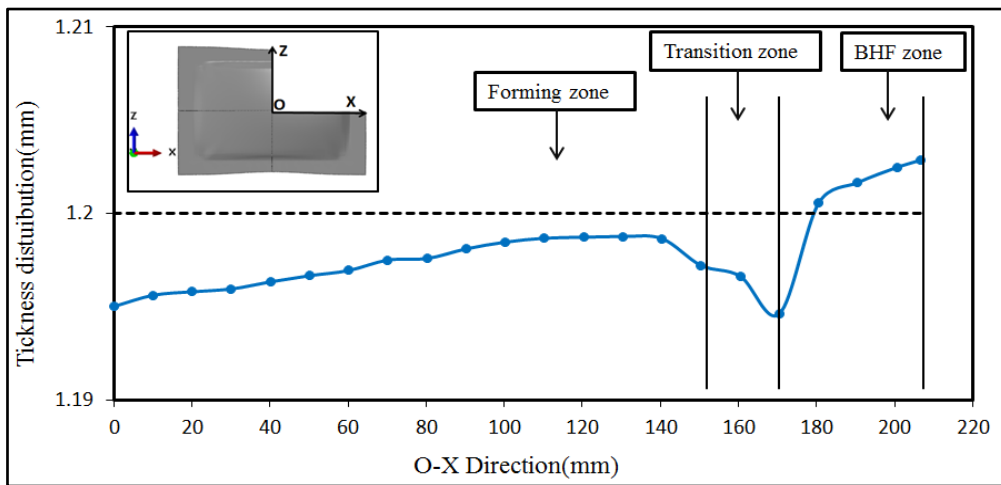


Figure 5-7 Simulated thickness distribution along O-X (Exp #17) (The vertical axis is sheet thickness and the O-X direction is as shown in the panel.) [80]

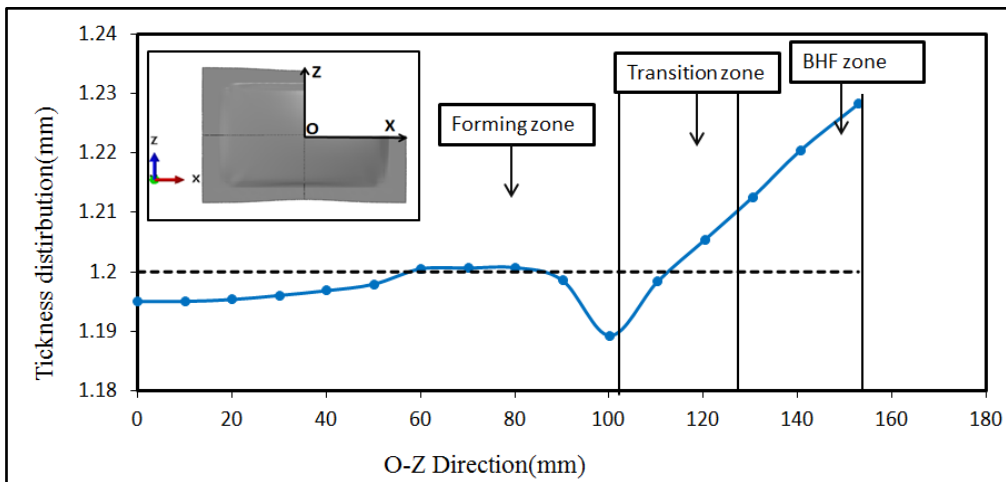


Figure 5-8 Simulated thickness distribution along O-Z (Exp #17) (The vertical axis is sheet thickness and the O-Z direction is as shown in the panel.) [80]

Figure 5.9 shows the simulated distribution of sheet thickness for BHF = 15 kN and R=400 mm. Figures 5.10 and 5.11 show the sheet thickness across the centre of the plate parallel to the long side (O-X) and parallel to the short side (O-Z) for Exp #2. Here, the BHF was 15 kN and the radius of curvature of the formed workpiece was 400 mm. The predicted value of the springback was 0.8 mm which was the minimum of all the simulations.

The depth of deformation at the centre (O) was substantially greater than for Exp #17 so there was enhanced sheet thinning because there was more stretching of the sheet. The distribution of forces meant no sheet thickening took place in the formed area, though there was thickening below the blank holder.

The low level of springback in the formed workpieces is due to the greater deformation due to the smaller radius of forming curvature (R = 400 mm) [98] jointly with a large clamping force (BHF = 15 kN) [37].

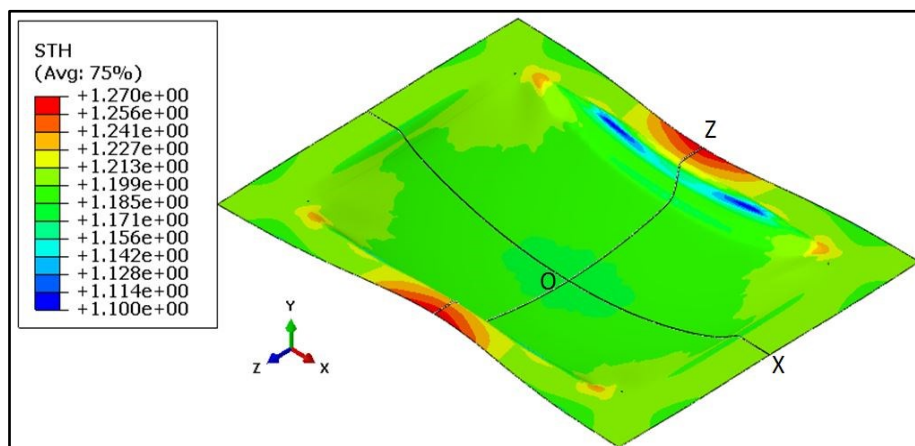


Figure 5-9 Simulated distribution of sheet thickness for BHF = 15 kN and R=400 mm

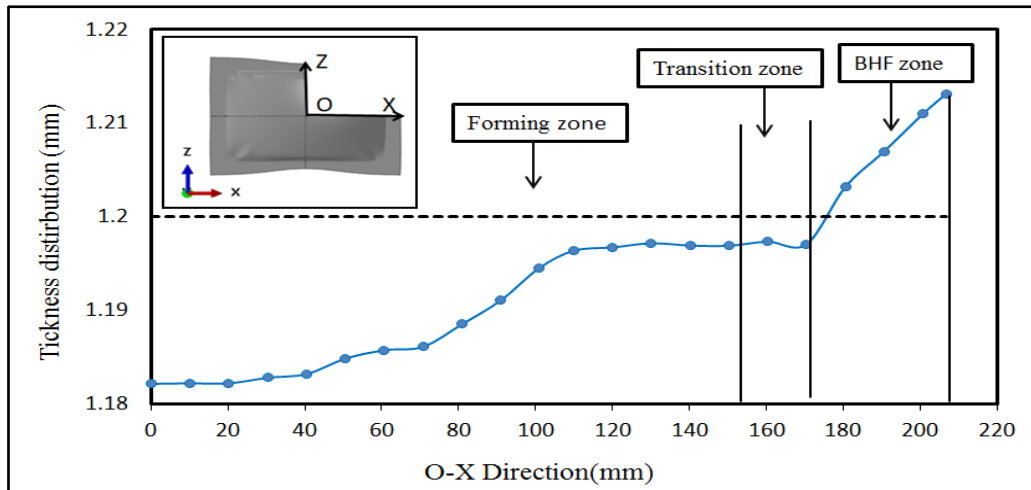


Figure 5-10 Simulated thickness distribution along O-X (Exp #2) (The vertical axis is sheet thickness and the O-X direction is as shown in the panel.) [80]

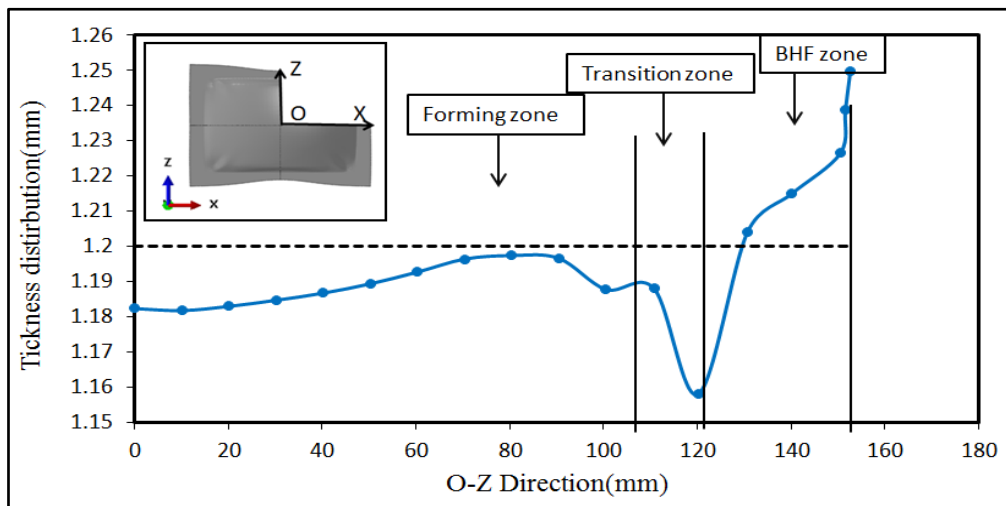


Figure 5-11 Simulated thickness distribution along O-Z (Exp #2) (The vertical axis is sheet thickness and the O-Z direction is as shown in the panel.) [80]

To analyse the distribution of the local strain and resulting deformation along paths O-X and O-Z on the formed workpieces for the two cases: BHF = 5 kN and R=800 mm; and BHF = 15 kN and R=400 mm, it is required to evaluate the final local deformations at the end of the loading process.

1. The metal sheet was partitioned into 5 longitudinal layers and modelled using the eight-node brick finite element: C3D8R
2. ABAQUS provided  $\boldsymbol{\varepsilon}$ , the strain tensor, directly after the FE simulation at each integrating point in the global coordinate system  $(x, y, z)$ , see Figure 5.12.
3. The strain  $\boldsymbol{\varepsilon}'$  in local coordinate system  $(x', y', z')$  was then derived from:

$$\boldsymbol{\varepsilon}' = \boldsymbol{\beta}\boldsymbol{\varepsilon}\boldsymbol{\beta}^T \quad (5-4)$$

The two coordinate systems are related by the matrix equation,  $\begin{Bmatrix} x' \\ y' \\ z' \end{Bmatrix} = \boldsymbol{\beta} \begin{Bmatrix} x \\ y \\ z \end{Bmatrix}$ , where  $x'$  is the

direction along the tangent and  $y'$  is the direction normal to the surface, see Figure 5.13

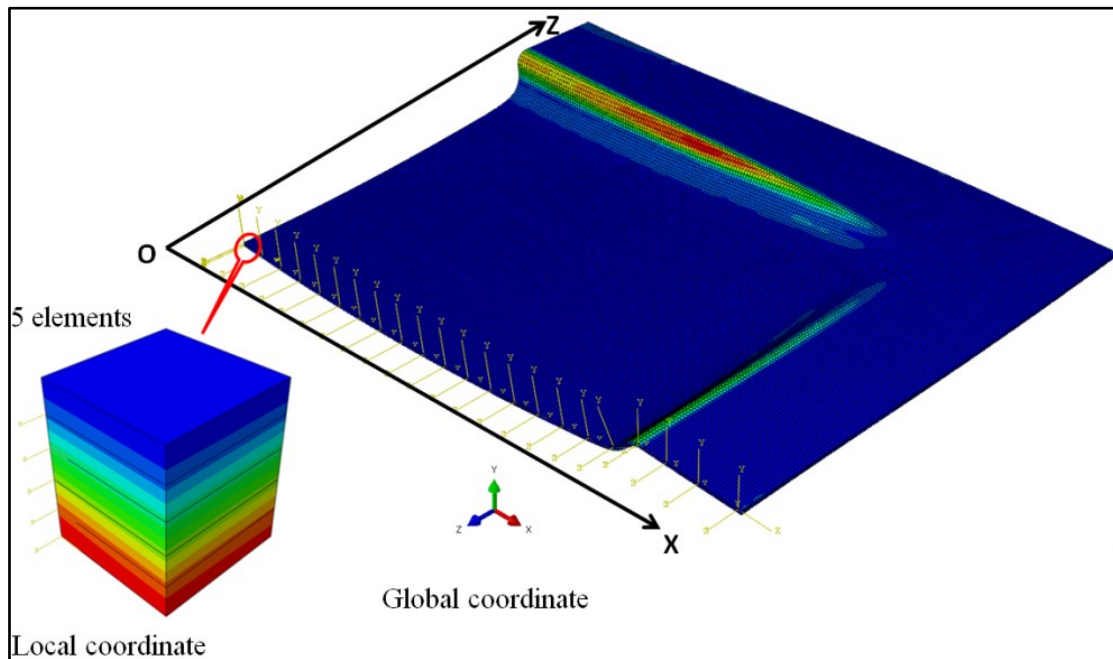


Figure 5-12 Local and global coordinate: ABAQUS

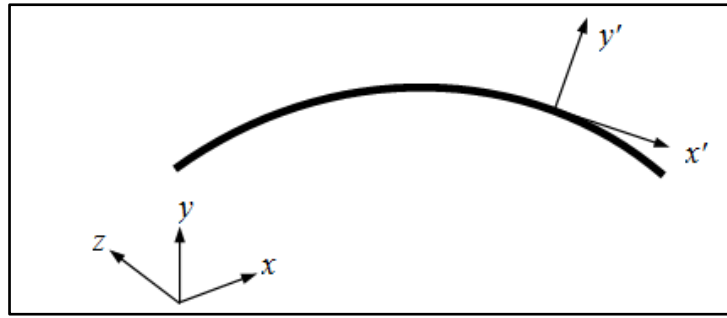


Figure 5-13 Inter-relation of local and global coordinate systems

Figures 5.14(a), (b) and (c) show the local strain (logarithmic strain LE in three direction LE11, LE22 and LE33) for selected elements along the path O-X (see Figure 5.12) in the formed part with an 800 mm radius of forming curvature and blank holder force 5 kN before unloading step. As shown in Figure 5.14(a), the positive value of LE11 (which is the strain in X-direction) means stretching in all layers in the O-X direction accept the first layer (black line) at transition zone shows negative value for LE11 due to compressive stresses. For the same measured element, a negative value of LE22 (which is strain in y-direction Figure 5.14(b)) means a compression in the thickness. However, the thickness strains shown in LE22 are mostly negative in all 5 layers, which indicates that thinning occurred along his path for the metal sheet during the MPF process in this case [77].

In the Z direction as shown in Figure 5.14(c) for same element along O-X path, there is stretching (positive values of LE33 as in Figure 5.14(c)) in the centre of the formed sheet (at point O) which changes to compression (negative values of LE33) at about  $X > 150$  mm. At this point and beyond the LE33 becomes negative value, which indicates a thickening take place on the formed sheet at this zone (under blank holder).

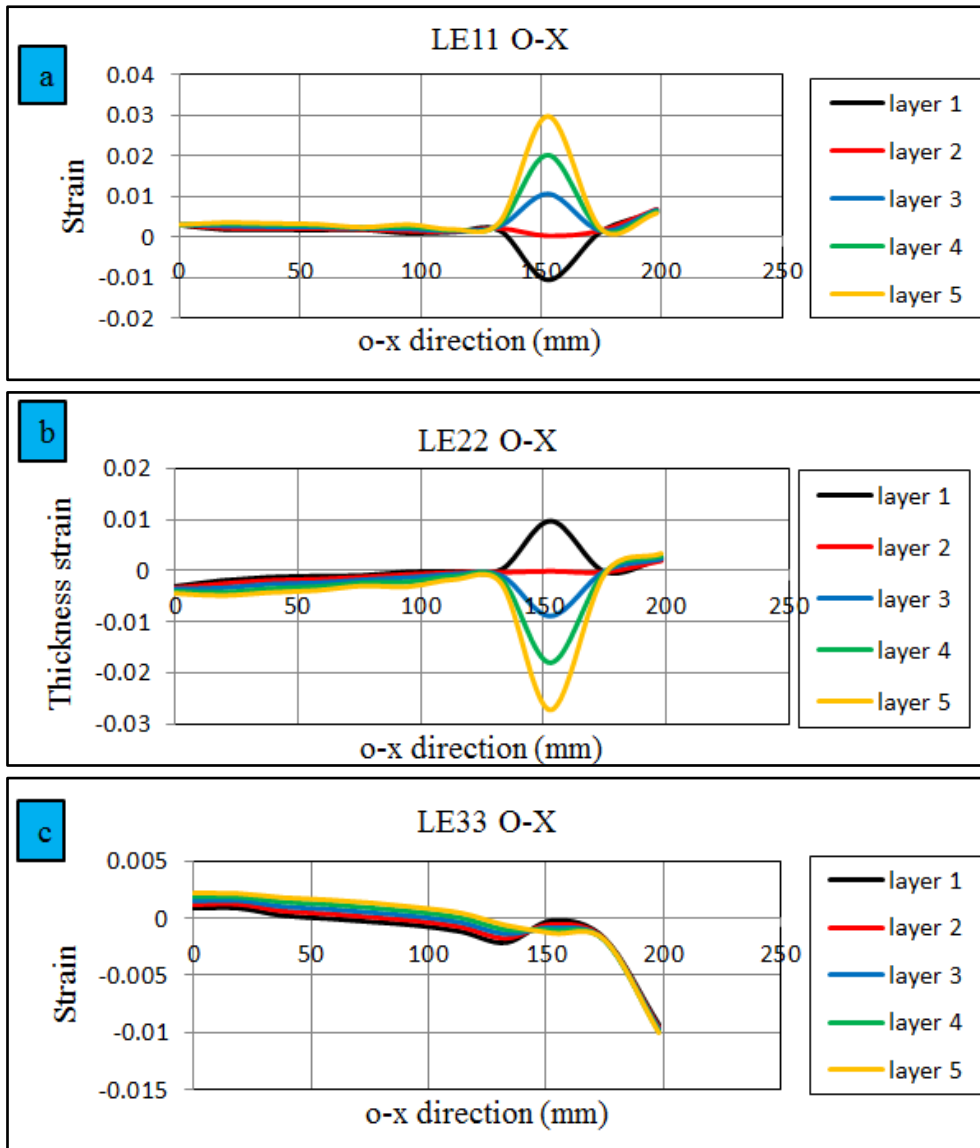


Figure 5-14 Local deformation along path O-X for 800 mm radius of forming curvature and blank holder force 5 kN

Figures 5.15 (a), (b) and (c) present the strain values along path O-Z (see Figure 5.12) for the same selected elements. The positive strain values in figure 15(a) of LE11 in X-direction of the element at point O. Which is stretching on metal sheet, and then the strain slowly decreased until it becomes a compression at transition zone as a result of compressive stresses.

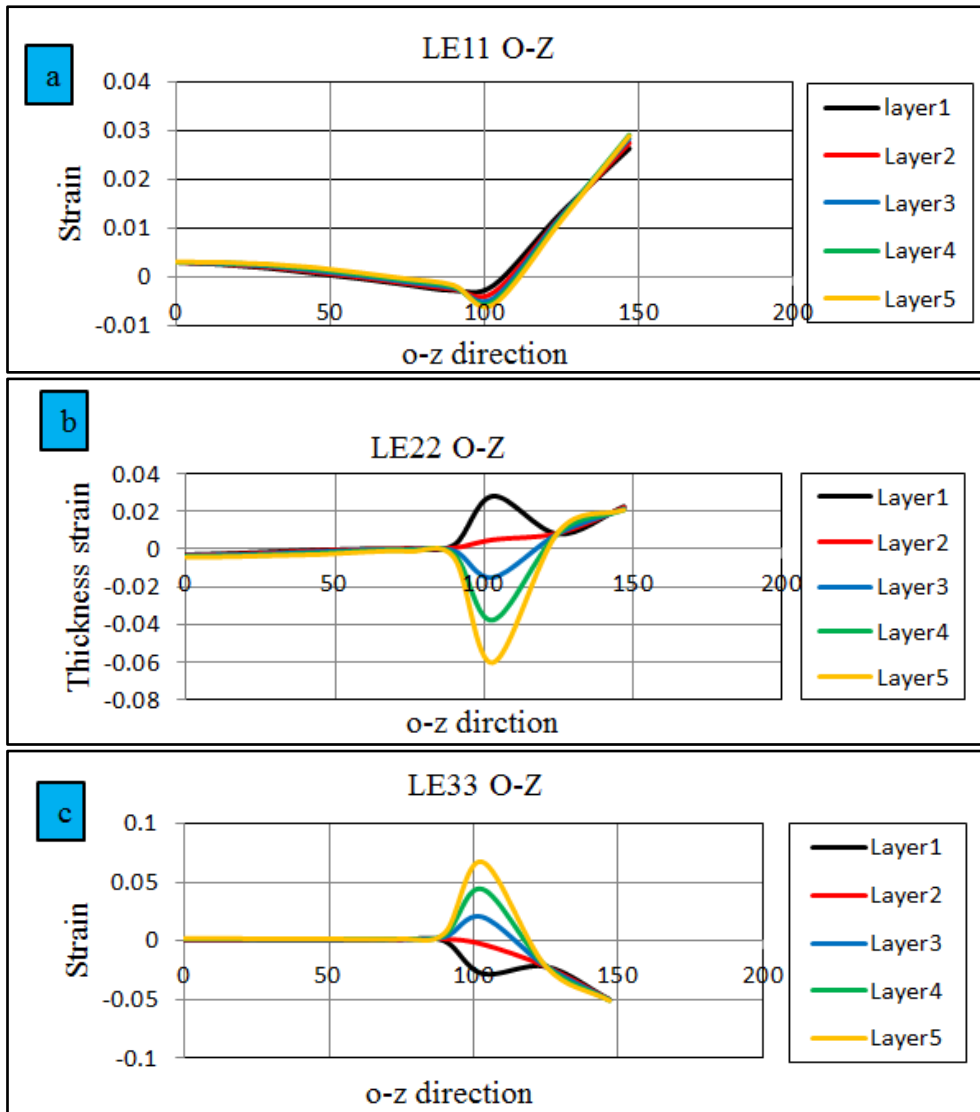


Figure 5-15 Local deformation along path O-Z for 800 mm radius of forming curvature and blank holder force 5 kN

The material in the transition zone was subjected to a tensile stress in the lower layer and compressive stress in the upper layer. This was due to the reverse bending effect, a similar effect was also found by Wang *et al.*, [106]. In addition the strain values of LE22 and LE33 along the path O-Z which illustrated in Figures 5.15 (b) and 5.15 (c) presented same trends along the path O-X.

Figures 5.16(a), (b) and (c) show the local strain along the path O-X, and Figures 5.17(a), (b) and (c) along the path O-Z, for formed part with 400 mm radius of forming curvature and blank holder force 15 kN. It can be seen that Figures 5.16 and 5.17 show the same general trends as in Figures 5.14 and 5.15. However, so the smaller radius of curvature it can be seen that greater deformation occurred in all three directions LE11, LE22 and LE33. A smaller radius of curvature of the formed surface represents larger deformation during the metal forming [95].

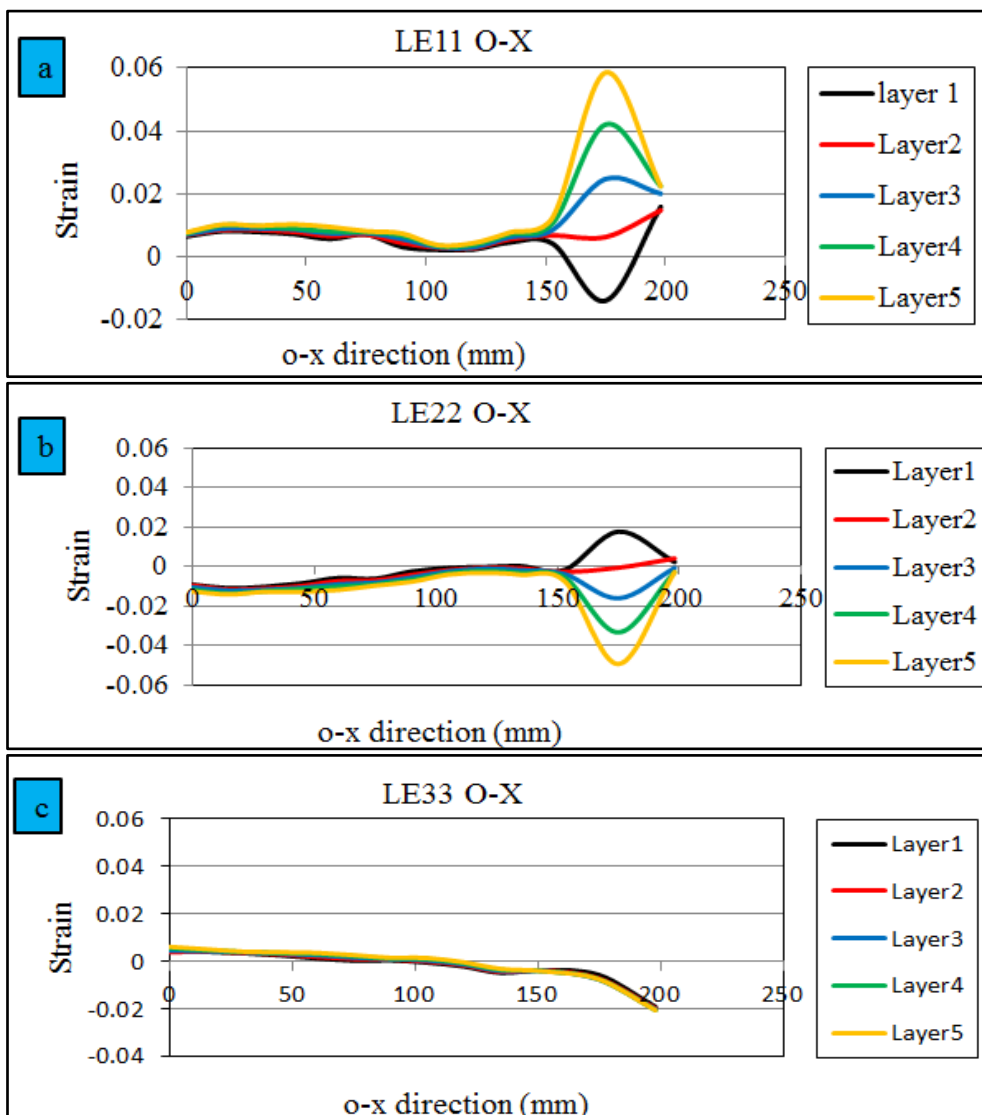


Figure 5-16 Local deformation along path O-X for 400 mm radius of forming curvature and blank holder force 15 kN

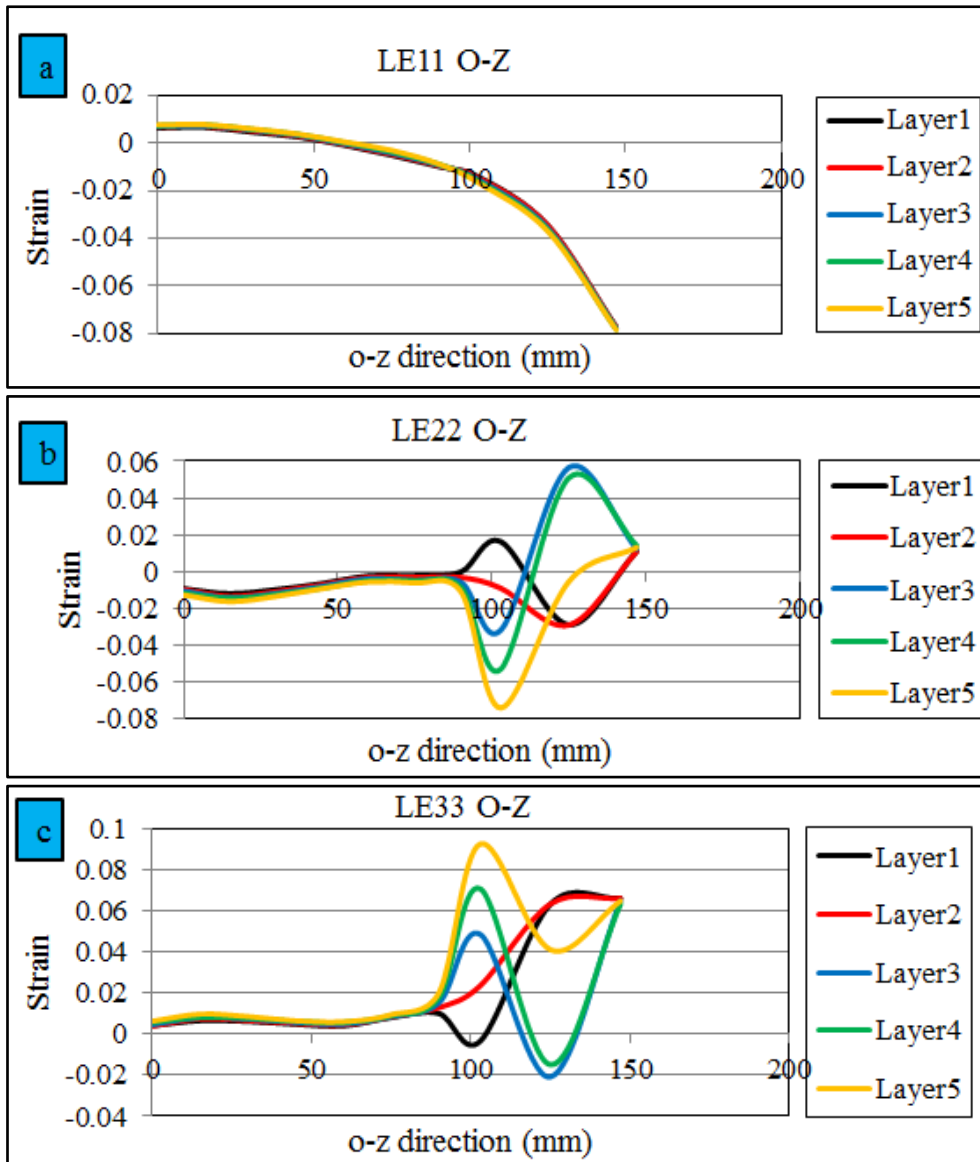


Figure 5-17 Local deformation along path O-Z for 400 mm radius of forming curvature and blank holder force 15 kN

### 5.3 Summary

In this investigation, MPF of doubly curved sheets of aluminium alloy 5151-O was numerically simulated using FE analysis. RSM and ANOVA were used to identify the parameters most affecting springback and thickness variation. Also the local deformation on final formed parts was investigated for the two cases of maximum and minimum springback.

The following conclusions can be drawn from this study:

1. Springback is significantly affected by the radius of the forming curvature of the part and blank holder force.
2. Thickness variation is significantly affected by radius of curvature, blank holder force and the interaction between blank holder force and elastic cushion thickness.
3. As the radius of forming curvature increases, springback increases and thickness variation decreases.
4. As blank holder force increases, springback decreases and thickness variation increases.
5. The optimum condition to achieve minimum springback and thickness variation in this investigation was found to be 600 mm for the radius of forming curvature, 8 kN for blank holder force and 3 mm for elastic cushion thickness (all working parameters were constrained within their preselected range of values).
6. Having a large plastic deformation through sheet stretching and thinning while avoiding sheet thickening is the key factor in minimising springback. This can be achieved by using small radius of forming curvature and high blank holder forces.

## **CHAPTER 6:**

# **EXPERIMENTAL INVESTIGATION OF FORCE MEASUREMENT FOR MPF TOOLS**

In this chapter a relationship is developed between springback in the formed part after the final unloading and the forming force as measured on selected individual pins under different compression ratios (30%, 40%, 50% and 60%) of the elastic cushion using Fibre Bragg Sensors (FBGS) to determine the strain in pins as a “smart way” [107, 108]. As described in the previous chapter, FBG sensors have a series of unique advantages over conventional electrical and piezoelectric sensors, including high precision, small volume, lightweight and ease of installation [109].

### **6.1 Sensing principle of fibre Bragg grating**

A FBG is a kind of distributed Bragg reflector (Bragg grating) built into a short length of a single optical fibre. It contains a core which is enclosed by a coating. When light from a broadband source is incident on one side of the reflector, the inscribed Bragg gratings act as a mirror reflecting certain wavelengths while passing the rest with virtually no loss, as shown in Figure 6.1 [110]. These reflected wavelengths can be used to measure a number of parameters including strain. FBG sensors can measure very high strain ( $> 10,000 \mu\text{m/m}$ ) and are therefore very well suited to highly strained composite structures. Also it is not distance dependent and connecting lengths of up to 50 km are possible [109]. FBG sensors were added to the surface of certain pins to obtain real-time information of strain on those individual pins.

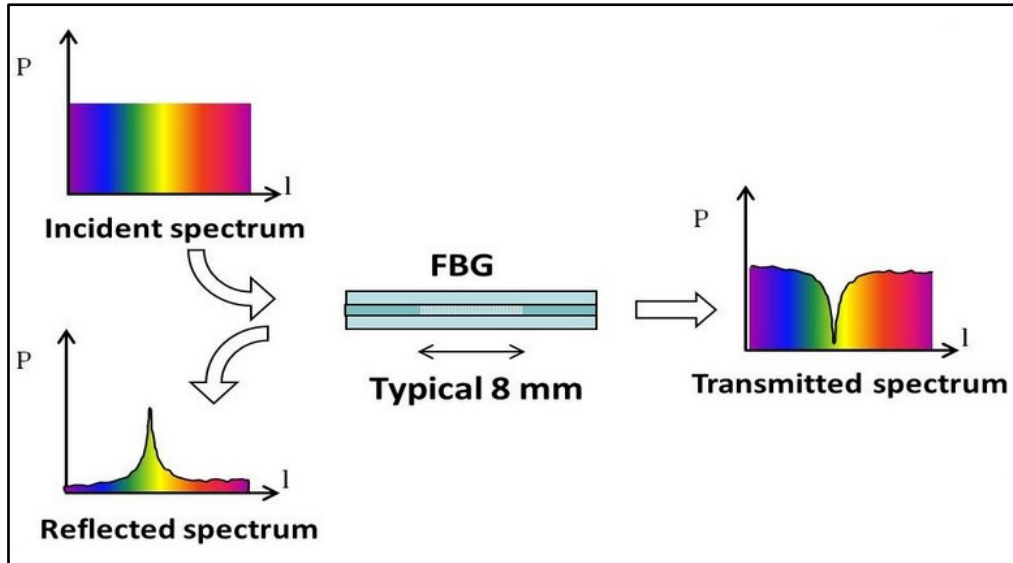


Figure 6-1 Working principle of a Fibre Bragg grating [111]

### 6.1.1 Strain sensitivity of FBG

As stated above a FBG reflects only certain wavelengths of light ( $\lambda_B$ ) allowing the remaining wavelengths in a broadband spectra to pass through, see Figure 6.1. FBGs can deliver very sensitive strain measurements for different materials and assemblies [112]. Bertholds *et al.*, in 1988, was the first attempt to use FBGs for strain measurements [113]. The effect of the strain was to stretch the FBG which elongated of the optical fibre and changed the grating spacing which, because of the photoelastic effect, changed the refractive index [114, 115].

The Bragg wavelength reflected by the grating,  $\lambda_B$ , depends mainly on the fibre grating periodicity,  $\Lambda$ , and the effective refractive index  $n_{eff}$ . It is calculated using the following equation [116]:

$$\lambda_B = 2 n_{eff} \Lambda \quad (6.1)$$

Both strain and temperature affect the Bragg wavelength, as both change the grating periodicity, the latter due to the thermal expansion/contraction through the thermo-optic and

thermal expansion coefficients. Figure 6.2 shows the response of FBG sensor to strain action in details.

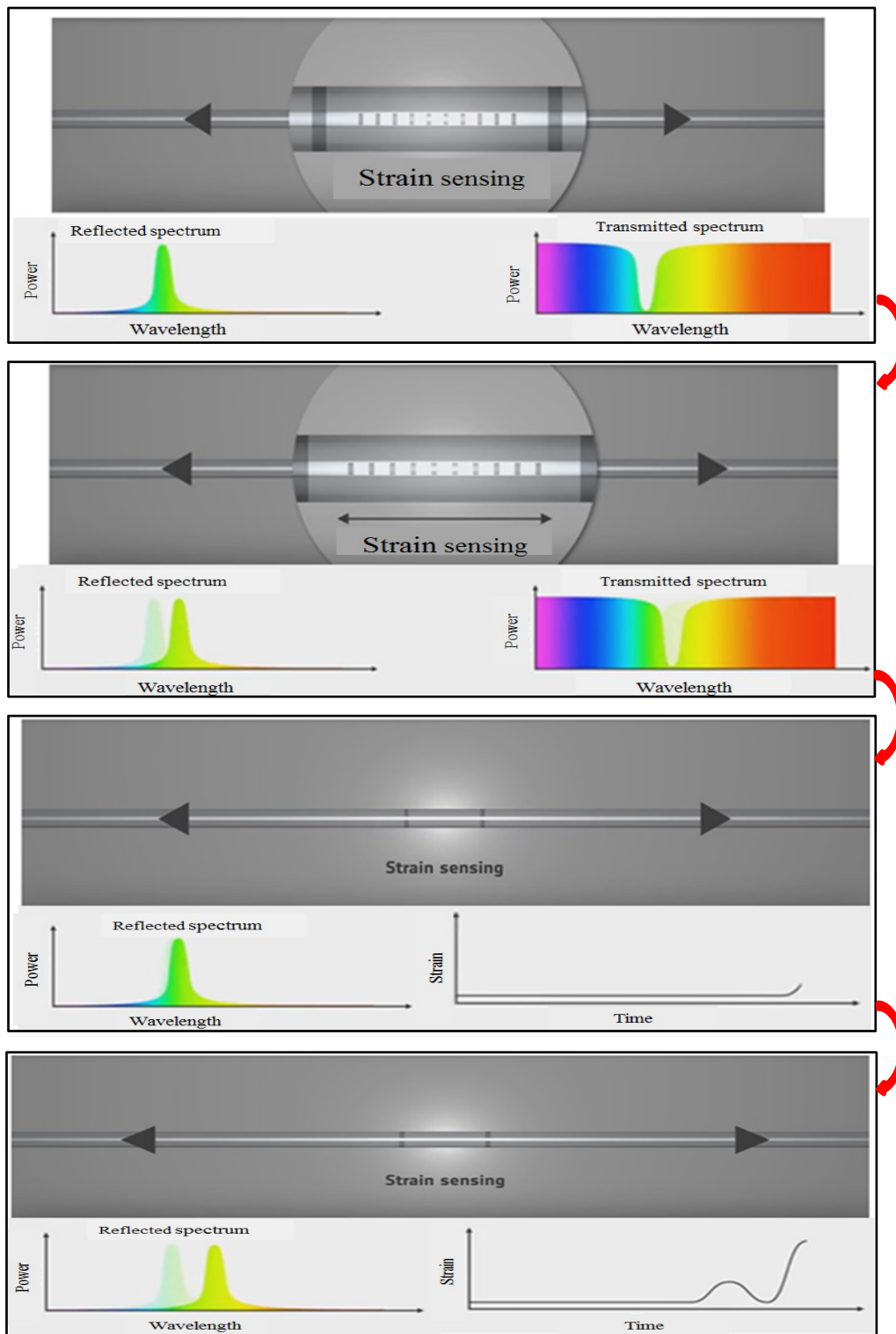


Figure 6-2 Principle of strain sensitivity using FBGs [111]

Thus any change in the refractive index of the fibre grating and/or fibre grating periodicity will cause a change in the wavelength of the reflected light from  $\lambda_{B0}$  to  $\lambda_B$ . where the subscript “0” refers to the original condition. Thus the reflected wavelength can be considered as a function of strain  $\varepsilon$  and temperature T, and its change can be written as follows [116]:

$$\Delta\lambda_B = \lambda_B (\varepsilon, T) - \lambda_{B0} (\varepsilon_0, T_0) \quad (6.2)$$

Expanding Equation (6.2) as a Taylor series and taking the first order approximation, then for a fibre with a coefficient of thermal expansion,  $\alpha_t$ , thermo-optic coefficient,  $\alpha_n$ , and photo-elasticity coefficient,  $p_e$ , then wavelength shift can be expressed as [117]:

$$\Delta\lambda_B = \lambda_B [(1 - p_e) \Delta\varepsilon + (\alpha_t + \alpha_n) \Delta T] \quad (6.3)$$

Where  $\Delta\varepsilon$  is the change in strain of the optical fibre, and  $\Delta T$  is the temperature change. Generally, the temperature of the environment remains more or less constant and temperature effects are negligible. Thus any shift in the Bragg wavelength ( $\Delta\lambda_B$ ) will be caused by applied strain - extending or compressing the grating - and the photo-elastic effect as given in Equation (6.3) [117].

### **6.1.2 Operation principle of forming force measurement**

The basic operation of forming force measurements as carried out on four individual pins is shown on a quarter of the 3D FE model in Figure 6.3. A “smart” sensory individual forming force tool is constructed by gluing a single fibre containing one FBG sensor axially along the pin by using 1×60 adhesive made by HBM Company, which is suitable for strain gauges and very easy to use. Each FBG attached to each pin reflects with a different wavelength allowing real-time information of total change in strain to be obtained for that chosen pin.

The schematic diagram in Figure 6.3 shows the system used to measure the forming force for the MPF tool (punch and die), FBG sensors installed on the pins' longitudinal surfaces, the data acquisition system and analysis devices. A multi-channel FBG interrogator was used to acquire the elastic strain change signals from the FBGs. The collected data for elastic strain was analysed and evaluated by a computer for the forming processes.

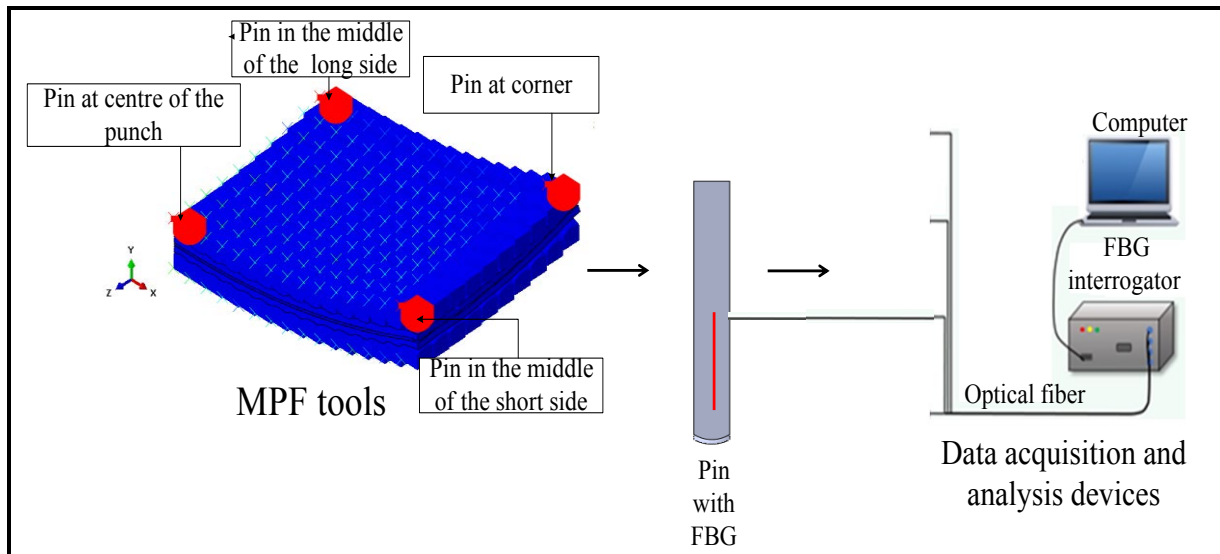


Figure 6-3 Measurement system for forming force on individual pins (quarter MPF tool)

Figure 6.3 shows the location of the four pins on the MPF tool with FBG sensors attached to monitor the elastic strain during sheet forming process, which was proportional to the value of the forming force.

In the first part of the Equation (6.3)  $\Delta\varepsilon$  represents the strain effect that occurred due to the applied force ( $\varepsilon_m$ ), assuming that the temperature effect was negligible as the surrounding environment temperature was stable ( $\Delta T = 0$ ), Equation (6.3) can be re-written as:

$$\frac{\Delta\lambda_B}{\lambda_{B0}} = k \Delta\varepsilon \quad (6.4)$$

where  $k = (1 - p_e)$  and  $p_e$  = photo-elastic coefficient = 0.22, then  $k = 0.78 \times 10^{-6} \mu\epsilon^{-1}$  (strain gauge factor) [118].

Substituting these values into Equation 6.4, we obtain:

$$\frac{\Delta\lambda_B}{\Delta\epsilon} = 0.78 \times 10^{-6} \mu\epsilon^{-1} \times \lambda_B \quad (6.5)$$

Note that the reflective wavelengths of typical FBG sensors are around 1550 nm [119].

From Equation (6.5), it can be calculated that when the FBG is strained by  $1 \mu\epsilon$  the reflected Bragg wavelength increase by  $1.21 \text{ pm}$  (picometer) if the centre wavelength of the selected FBG is 1550 nm [119]. The difference in wavelength of FBG sensor due to an external force can be detected experimentally. The initial wavelength of the sensor is known, and  $k$  is constant. From Equation (6.5) it is possible to calculate the change in elastic strain ( $\Delta\epsilon$ ) using Equation (6.6), to obtain the value of the forming force on the four pins:

$$\epsilon = \frac{\sigma}{E} = \frac{F}{A * E} \quad (6.6)$$

Where  $F$  is the force on the pin,  $A$  is the cross-section area of the pin and  $E$  is Young's modulus of the pin's material.

As shown in Figure 6.4 the forming force is not vertical on every pin but depends on the pin's position and shape. The forming force is vertical on the pins that are at the centre of the MPF tool, but it will gradually incline away from the horizontal depending on the radius of forming curvature until at the edges of the MPF tool it reaches the maximum degree of inclination. The pin matrix supported by a thick plate to prevent pins from bending was described in Section 3.2.1 and shown in Figure 3.11, see also Abosaf [2]. The simple Equation (6.6) was used to calculate the local force on the pin.

For small values of the radius of forming curvature ( $R=400$  mm), the vertical distance between the pins is bigger. . In this case, forming force distribution will be different from that for a big radius of forming curvature ( $R=800$  mm) because the difference between pins' heights is smaller as shown in Figure 6.5.

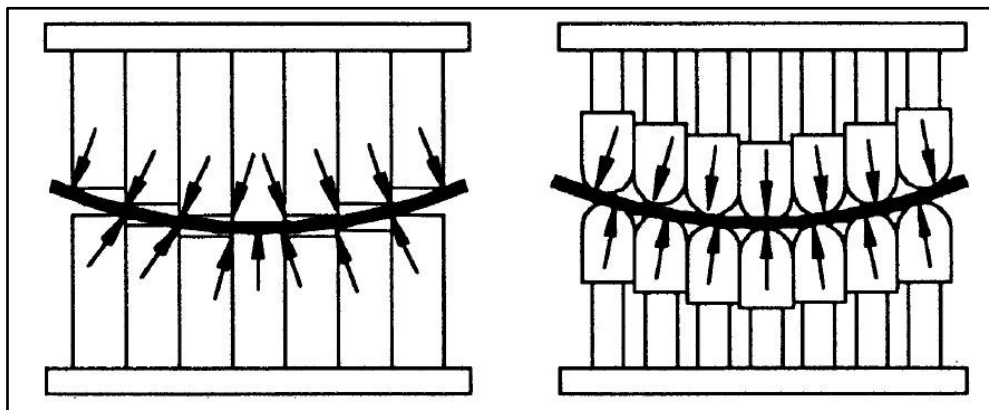


Figure 6-4 Different pins shape and different force distributions [120]

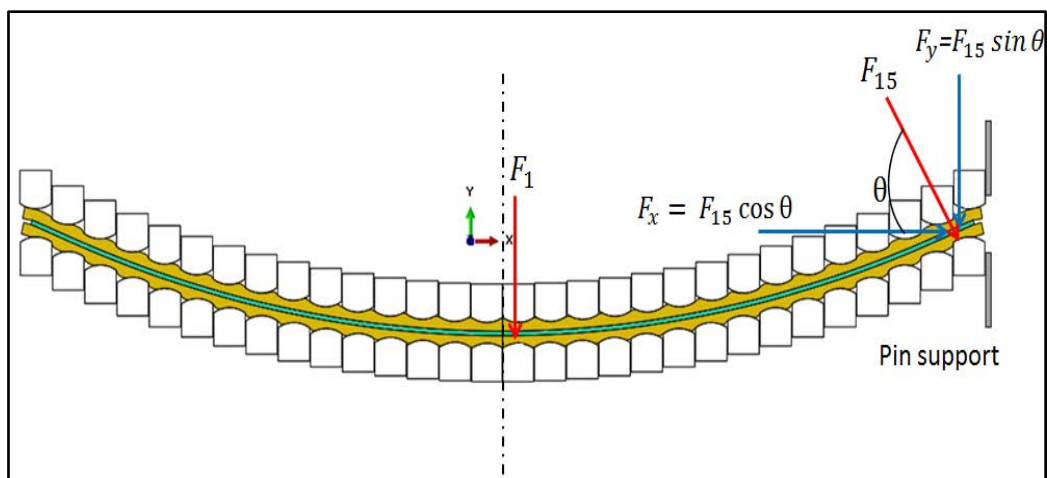


Figure 6-5 Force distributions on different pins ( $R=800$ mm)

As a consequence, at the end of loading step, the value of the force on the same pin at the same position in the two cases will be different, as shown in Figure 6.6 (a) and (b) which is

the result of a simulation result for a 40% compression ratio for same pin at centre of the punch with 800 mm and 400 mm radii of forming curvature.

Figure 6.7 shows the simulated force results on selected pins at different position in two cases. As the radius of forming curvature becomes bigger, the force distributions become uniform due to small differences between pins heights.

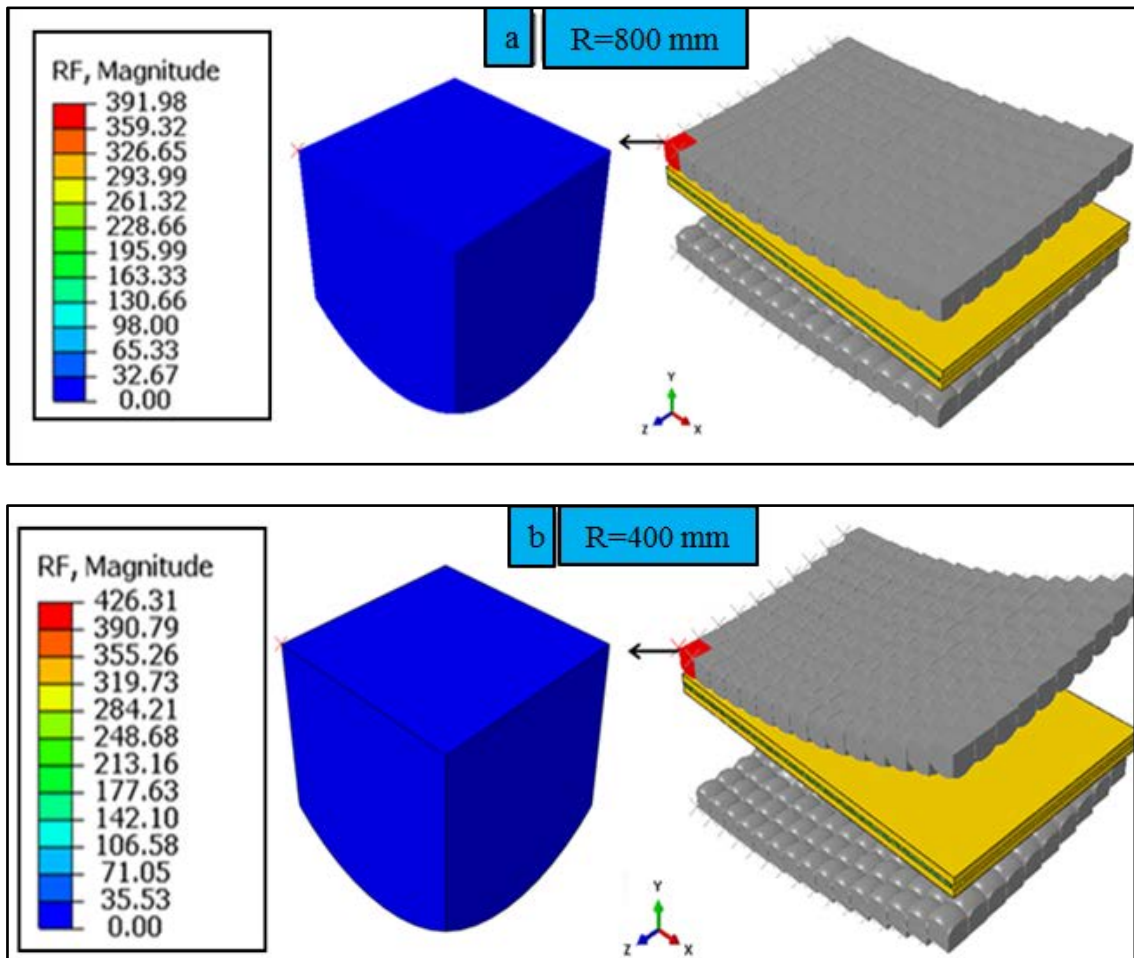


Figure 6-6 Forming force on pin at centre of the punch for different forming radii

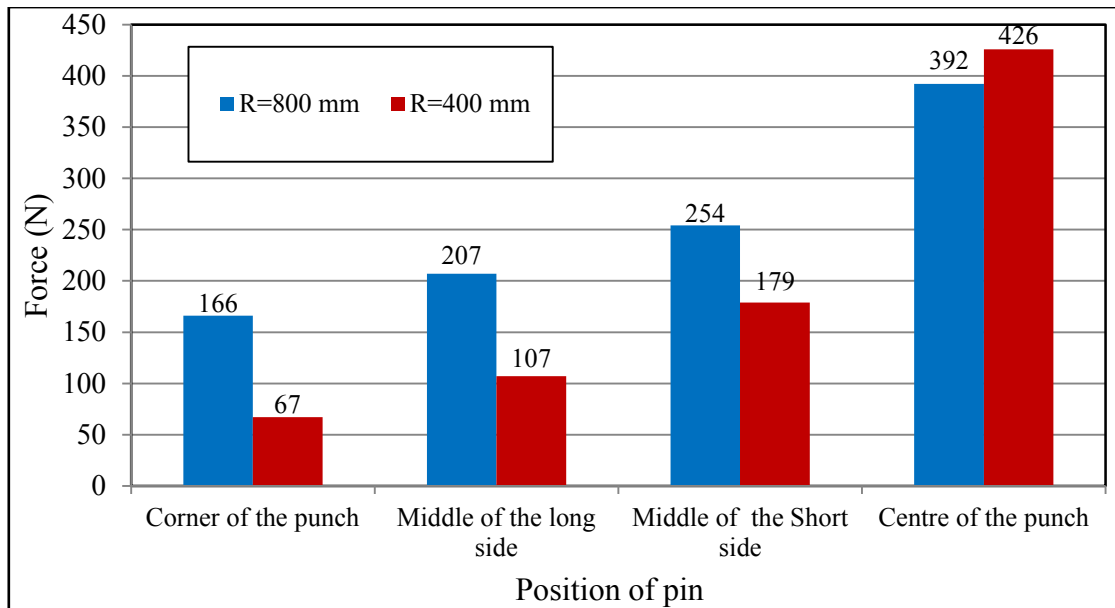


Figure 6-7 Forces on individual pins for different radii of forming curvature

## 6.2 Numerical simulation of the FBG system

To verify the proposed operating principle of individual forming force measurement on selected pins, a FEA of the MPF tool was carried out using ABAQUS software.

Figure 6.8 (a) shows the position of selected pins for the force measurement. Pin number 1 at the corner of the MPF tool where maximum springback occurs. Pins 2 and 4 were situated at the middle of the long and short sides respectively of the MPF tool where the springback was less. Pin number 4 was situated in the middle of the tool, minimum springback. The simulated results for springback at the end of the unloading step in the MPF process with 800 mm as radius of forming curvature are shown in Figure 6.8 (b).

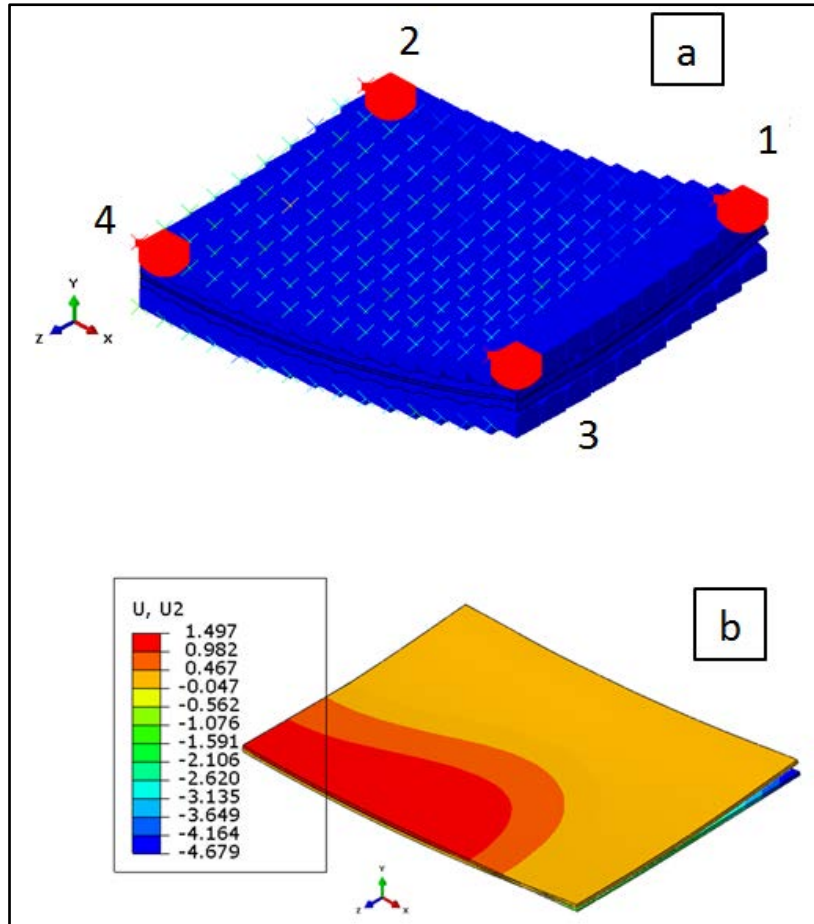


Figure 6-8 (a) Positions of selected pins and (b) simulated springback value after unloading for 40% compression ratio of elastic cushion

Figure 6.9 shows the elastic cushion subject to different compression ratios of its original thickness (3 mm). For example 40% compression ratio of elastic cushion means  $3 \text{ mm} \times 0.4 = 1.2 \text{ mm}$ , when the punch reaches end of forming distance, then it will moves downward 1.2 mm and so on.

The simulated forming forces on individual pins at different compression ratios of the elastic cushion are shown in Figure 6.10. It is clear that the force on the selected pins increased as the punch moves down and increases the compression ratio of the elastic cushion (30%, 40%, 50% and 60%) and without causing dimpling of the formed sheet.

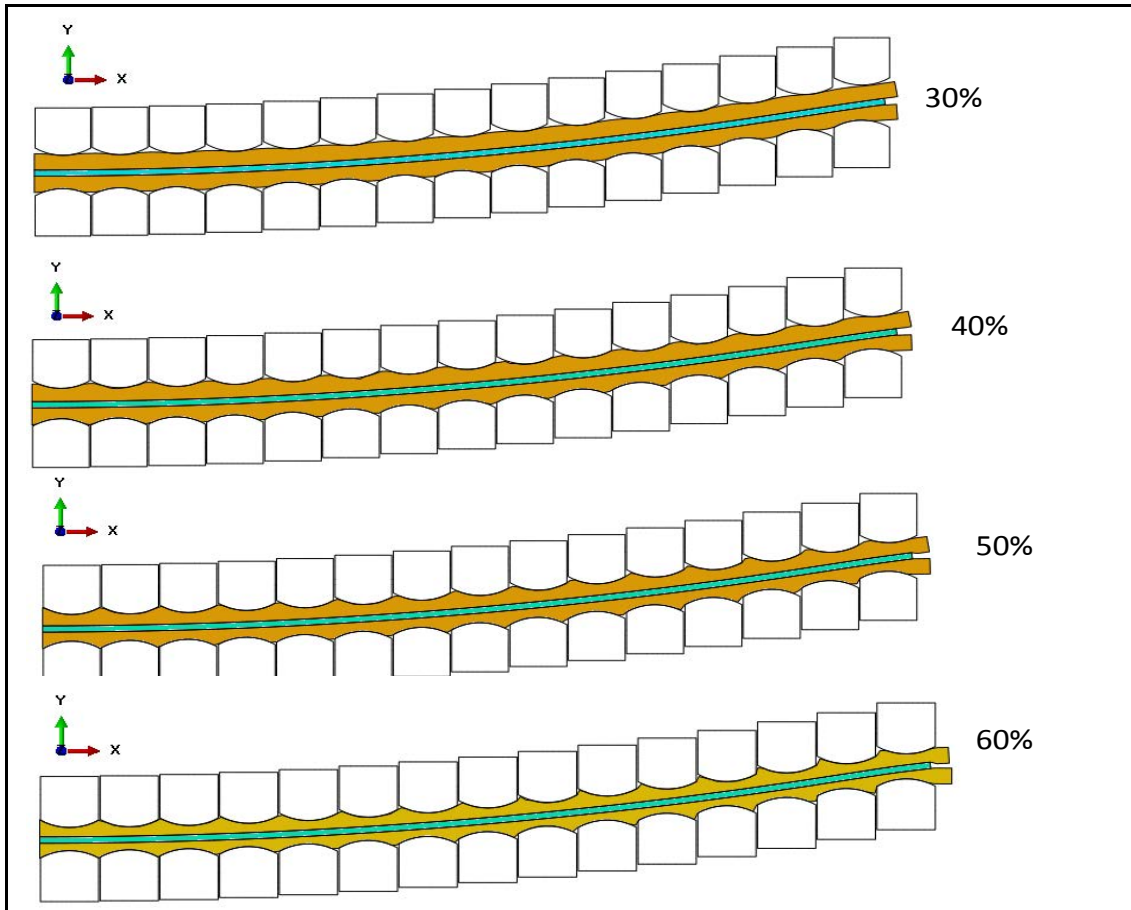


Figure 6-9 simulation results of different elastic cushion compression ratios

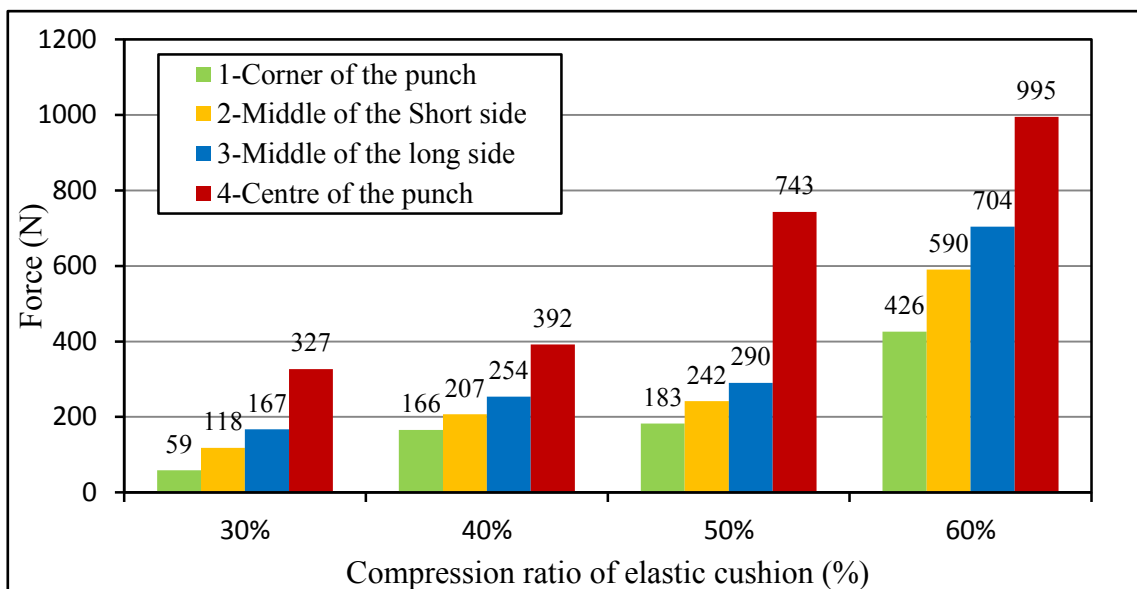


Figure 6-10 Forming force on individual pins

Figure 6.11 shows the relationship between springback of the final formed part (R=800mm) at the end of the loading step for different compression ratios of the elastic layer and the values of the forming force on the selected pins. For example, at 30% compression ratio of elastic layer, the forming force on the pin at centre of MP punch was over 300 N and springback more than 6.5 mm, while at 60% compression ratio was nearly 1000 N and about 5.0 mm springback.

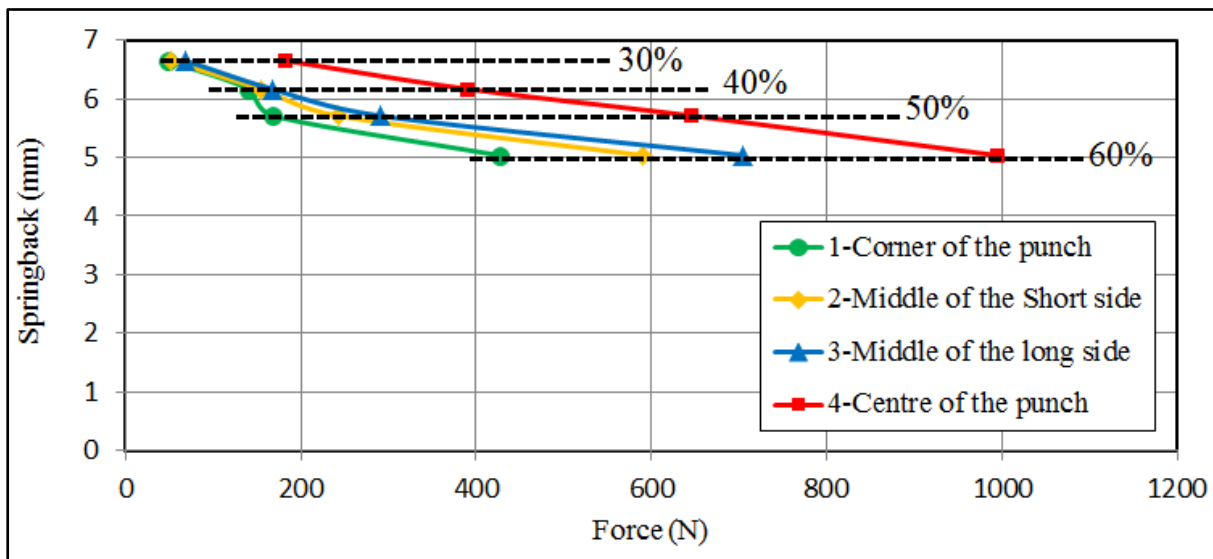


Figure 6-11 Springback vs force on different pins for different compression ratios

There was a sharp increase in predicted force on the pin as the space between the pin tips filled with elastic material due to the increased compression ratio, see Figure 6.9. This caused more resistance to movement of the MP punch, as result the local force increased and springback decreased.

### 6.3 Experimental validation setup and discussion

Experimental work to validate the simulated results was carried out to test the proposed “smart” way of measuring the forming force on the single pins shown in Figure 6.3. Figure

6.12 shows the MPF tools installed on the press machine, and Figure 6.13 the selected pins with FBGs attached.

The essential components that have been used to measure the forming force on individual pins are listed here and discussed in chapter 3 section 3.2.

- 1- FBG sensor.
- 2- Optical fibre.
- 3- FBG interrogator from Smart Fibres Ltd.
- 4- Computer with SmartSoft for SmartScan (v3.2).
- 5- MPF tool.

Figure 6.13 shows photos of the selected pins in situ with, inset, a photo of one pin with the FBG attached. Each candidate pin used to measure the forming force was bonded with a single FBG sensor (each unstrained FBG reflected a different wavelength of light, see appendix 2) connected to the FBG interrogator.

Before the bonding of the FBG sensors to the pins, it was important to prepare the pin's surface to avoid introducing any measurements error such as strain transfer between compressed pin and FBG sensor. To prepare the pin surface for installing the FBG sensors, a soft abrasive paper was used to clean the selected pin's surface which was then further cleaned with methanol.

To record the change in FBG wavelength ( $\Delta\lambda_B$ ) from each sensor when the grating is being compressed due to the action of the MP tool, an FBG interrogator from Smart Fibres Ltd was used to record the change of FBG sensor signal. This had with a resolution of 1 pm and maximum data acquisition rate of 2.5 kHz per channel for each of four channels.

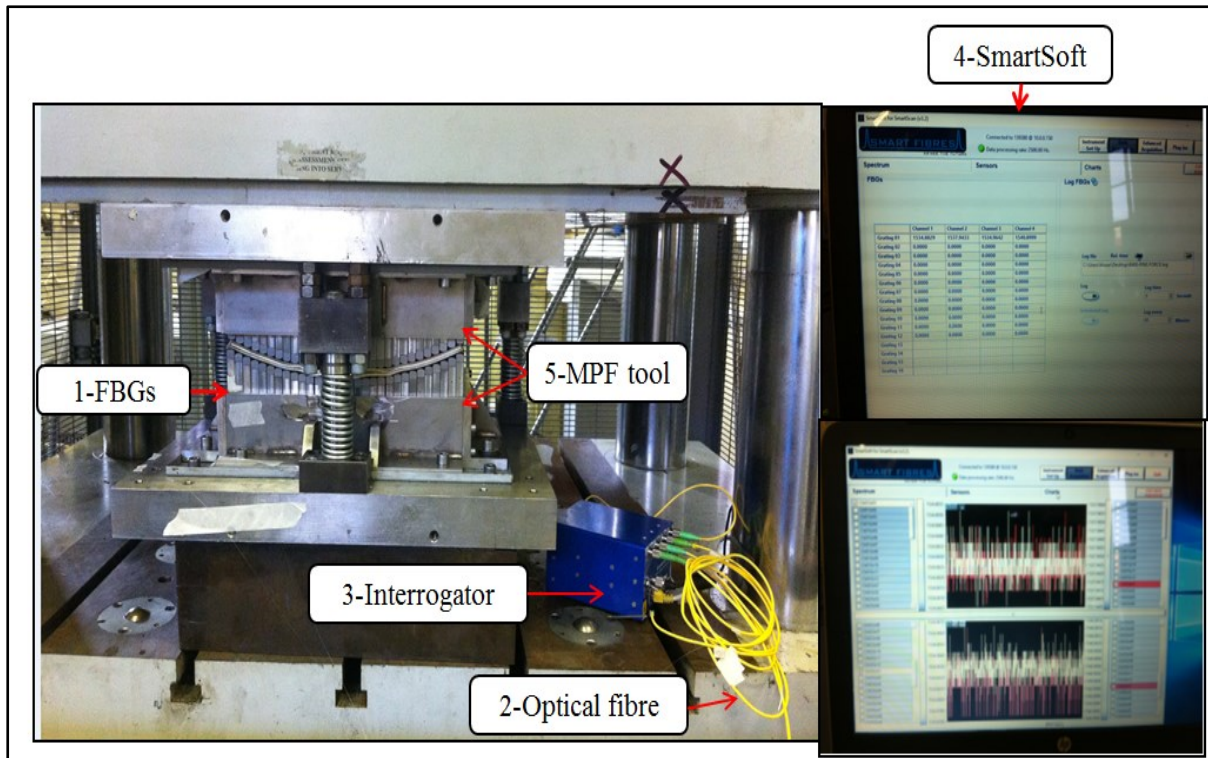
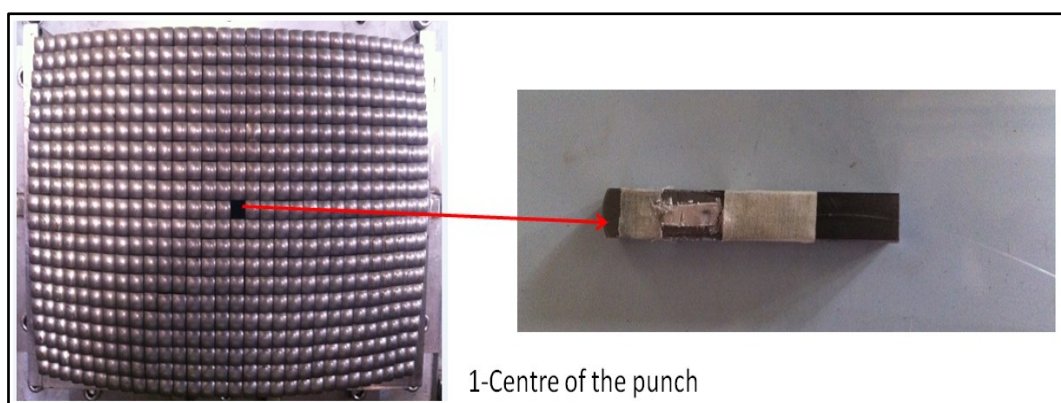


Figure 6-12 Experimental setup

A press machine was adapted for loading the MPF tool to form the sheet of 1.2 mm thick, aluminium alloy O-5251, with a radius of forming curvature 800 mm. For this operation springback on the final formed part was large, see Section 4.3.2.



Continue Figure 6-13

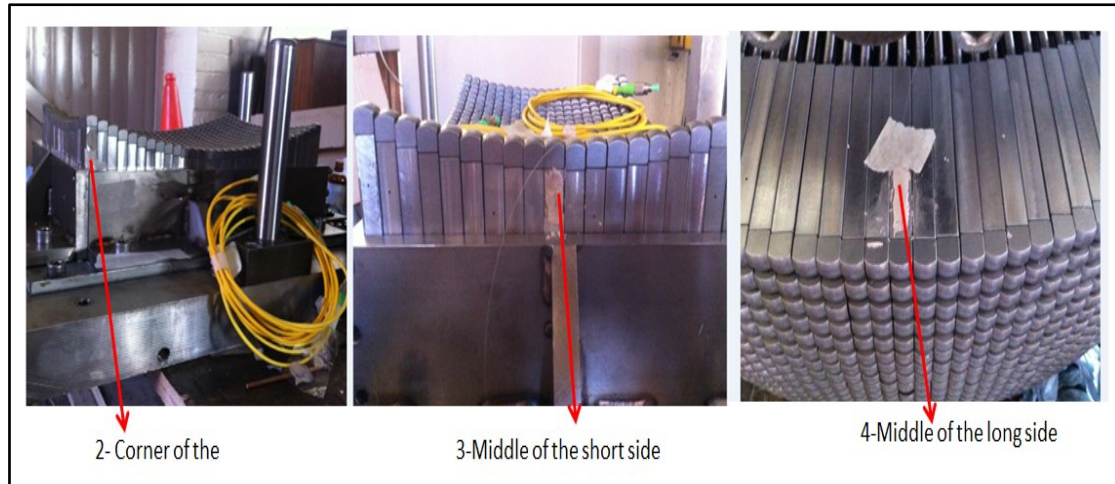


Figure 6-13 Locations of selected pins on MPF tool

The wavelength changes and forming time histories were recorded for all four pins during the forming process using SmartSoft, and displayed on the computer. As an example, data collected for the FBG wavelength shift for the single pin at the centre of the punch is shown in Figure 6.14.

A FBG sensor with central wavelength just less than 1535 nm was installed on the central pin. For the first several seconds the movement of the punch is taking up the slack in the system and no change in wavelength is observed. As the punch continues to move down it starts to compress the elastic cushion covering the aluminium metal sheet and gradually over the period from about 5 seconds to about 17 seconds, the wavelength of FBG changes as the cushion is increasingly compressed (see Figure 6.9).

At about 17s the rate of decrease in FBG wavelength increases significantly as the forming process starts. The sharp fall in wavelength continues until at about 25s the wavelength plateaus at 1534.938 nm due to the compression strain in the pin as a result of the end of the forming process. At about 40s, the load is released.

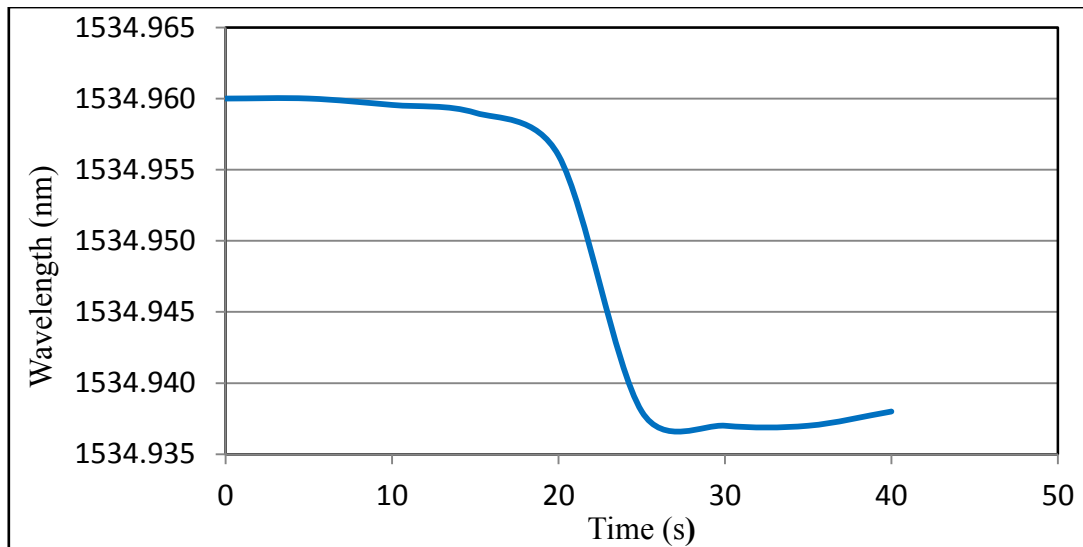


Figure 6-14 Wavelength shift versus forming time for the single pin at the centre of the MPF punch

Table 6-1 Wavelength changes under forming force for the selected pins

Processes steps	Time (s)	Wavelength (nm)							
		FBG1 Corner	$\Delta\lambda_B$	FBG2 Mid Long side	$\Delta\lambda_B$	FBG3 Mid Short side	$\Delta\lambda_B$	FBG4 Centre of punch	$\Delta\lambda_B$
Before loading	0	1534.882		1540.897		1537.942		1534.960	
Forming process	5	1534.882	0.000	1540.896	-0.001	1537.941	-0.001	1534.960	0.000
	10	1534.882	0.000	1540.895	-0.002	1537.940	-0.002	1534.959	-0.001
	15	1534.881	0.001	1540.895	-0.002	1537.938	-0.004	1534.957	-0.003
	20	1534.879	-0.003	1540.893	-0.004	1537.936	-0.006	1534.956	-0.004
	25	1534.873	-0.009	1540.885	-0.012	1537.930	-0.012	1534.938	-0.022
	30	1534.872	-0.010	1540.885	-0.012	1537.926	-0.016	1534.937	-0.023
	35	1534.873	-0.009	1540.889	-0.011	1537.927	-0.015	1534.937	-0.023
Loading release	40	1534.874	-0.008	1540.891	-0.009	1537.931	-0.011	1534.941	-0.019
Min. $\Delta\lambda_B$			-0.010		-0.012		-0.016		-0.023

According to Equation (6.5), the ratio between wavelength shift and axial strain of a FBG equal the sensitivity of the FBG sensor which is typically  $1.2 \text{ pm}/\mu\epsilon$  ( $1 \text{ pm} = 10^{-3} \text{ nm}$ ). From the literature [2], it is known that Young's modulus of MPF tools is about 200 GPa, the cross section area of the pin is  $10 \text{ mm} \times 10 \text{ mm}$  and value of  $\Delta\lambda_B$  can be taken from Table 6.1. By using Equation (6.6) the force on each pin can be found as:

$$F = \epsilon \times A \times E \quad (6.7)$$

$$\text{Force on the pin at corner} = [(-0.01 / (0.78 * 1534.882))] \times (0.01 * 0.01) \times 209 \times 10^9 = 167 \text{ N}$$

$$\text{Force on the pin at mid-point of long side} = [(-0.012 / (0.78 * 1540.897))] \times (0.01 * 0.01) \times 200 \times 10^9 = 199.7 \text{ N}$$

$$\text{Force on the pin at mid-point of short side} = [(-0.016 / (0.78 * 1537.942))] \times (0.01 * 0.01) \times 209 \times 10^9 = 266.8 \text{ N}$$

$$\text{Force on the pin at centre of punch} = [(-0.023 / (0.78 * 1534.960))] \times (0.01 * 0.01) \times 200 \times 10^9 = 384.2 \text{ N}$$

In order to evaluate the accuracy of the simulations of the elastic strain on the pins, a comparison between the simulated and measured forces for each pin is shown in Figure 6.15, where

$$\text{Numerical error} = \frac{\text{Experimental result} - \text{Simulation result}}{\text{Simulation result}} \times 100 \quad (6.8)$$

$$\text{Numerical Error for the pin at corner} = [(167 - 166) / 166] \times 100 = 0.6\%$$

$$\text{Numerical Error for the pin at middle of long side} = [(199.7 - 207) / 207] \times 100 = -3.5\%$$

$$\text{Numerical Error for the pin at middle of short side} = [(266.8 - 254) / 254] \times 100 = 5.1\%$$

$$\text{Numerical Error for the pin at centre of punch} = [(384.2 - 392) / 392] \times 100 = -1.99\%$$

The negative values for the Numerical Error mean that the experimental results were smaller than the simulated.

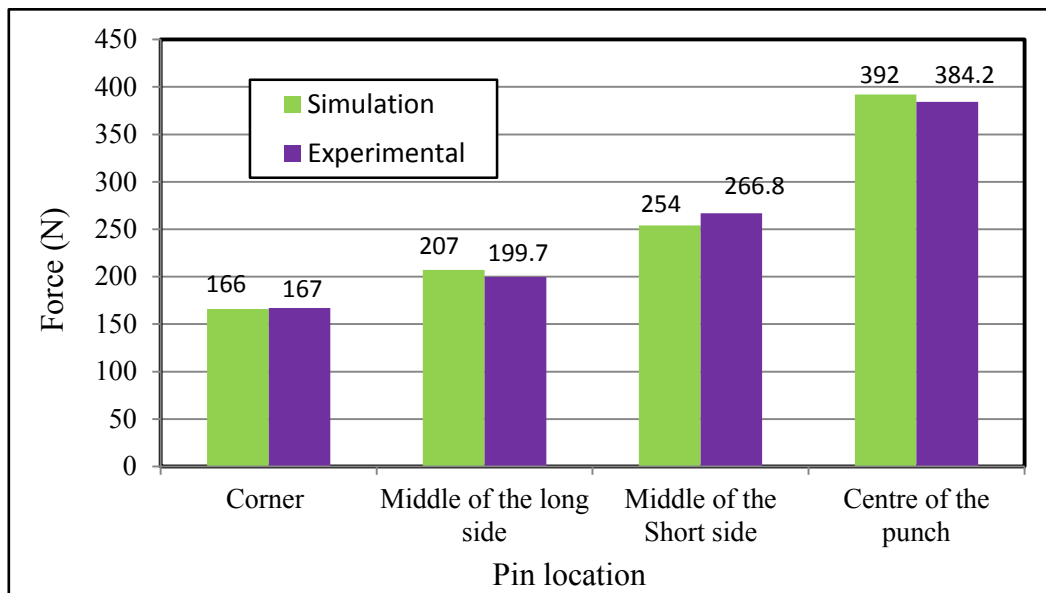


Figure 6-15 Validation of simulated forming force for radius of forming curvature 800 mm

#### 6.4 Summary

A “smart system” has been introduced for the first time for the purpose of measuring the forming force on individual pins in a MPF tool by using single fibre Bragg Sensors to monitor changes in strain in the pins. Here the effect of radius of forming curvature and of the forming force on selected pins on springback had been determined experimentally and used to validate simulated results.

## **CHAPTER 7:**

### **PROCESS DEVELOPMENT TO REDUCE GEOMETRICAL DEFECTS IN MULTI-POINT FORMING**

#### **7.1 Elastic punch with flexible MPF dies for metal forming (EP-MPF)**

The improvement of producing double curved part will be discussed in this chapter; a flexible forming setup has been developed by replacing the upper pin matrix by a thick elastic block to form an aluminium alloy sheet into doubly curved panels. The effect of the elastic punch on the quality of the formed part in terms of wrinkling, spring back and forming force were investigated.

Experimental work has been carried out to validate the concept of the proposed approach and to compare the new setup results with results obtained from conventional MPF, then an optimisation method has been used to investigate the influence of the elastic block dimensions, compression ration of the elastic block and radius of forming curvature on final part and process quality in terms of wrinkling, springback and forming force values.

The key of successful forming processes on the excellence of the formed sheet panels rely on tool structure of the punch and the die, the force of sheet forming and the blank. Failure to design appropriate tool will lead to dimension problem. To eliminate or reduce these limitations and achieve acceptable shape dimensions, several tool techniques have been used.

Elastic pads such as rubber and polyurethane contained in a rigid box recently has been applied in forming tools industries. This process is commonly used to form short runs of light metal parts in aerospace applications. Many advantages can be offered by using this flexible forming technique, while it also has certain disadvantages.

Using an elastic punch to form metal sheet improves the surface finish of final product Thiruvarudchelvan [121], also reducing the tooling cost, the forming tool can be easily changed to a new shape without alignment or mismatch issue. Material thinning is reduced by using elastic punch for metal forming [87]. It can be use the same tool setup to form a different material with different thicknesses [122]. In additions to these advantages, Polyurethane has the elasticity of rubber materials and the toughness and durability of metals [33]. However, using an elastic punch to form sheet metal has certain disadvantages. It has limited lifetime depending on process parameters, lack of sufficient to produce sharp features in the final part and suitable for low production or prototype specimen [123].

A history of using the flexible tools to form sheet metal is listed in study done by Thiruvarudchelvan [121]. Brown and Battikha [124] investigated the capability of flexible die to produce a defect-free part. In addition, they optimised the process parameters to get the optimum case. Lee *et al.*, [125] have presented the flexible forming process of aluminium tube with an experimental investigation of bending parameters such as bent radius, the influence of rubber property and roller radius. They found that, rubber hardness was the important parameter affects the radius of bent. Quadrini *et al.*, [126] studied the forming of a thin sheet of aluminium alloy utilising various flexible die shapes and materials, they reported that the rubber with highest hardness leads to best forming result. Chen *et al.*, [127] investigated the influence of process parameters such as forming speed and compression ratio of rubber in formed part quality. They reported that springback of flanging at rubber forming process was less than that of conventional stamping. Kut, S. and Niedziałek, B. [66] reported that, selected an appropriate hardness of the elastic punch (A90) leads to eliminate the defects from final parts. A theoretical model for static and kinematic friction in elastic pad forming

method applied by Ramezani *et al.*, [88], they have got a better match between simulation and experimental results.

## 7.2 Concept of elastic-punch multi-point forming (EP-MPF)

Elastic-punch multi-point forming is a metal sheet forming process in which a combination of rubber-pad forming and multi-point forming to gain the advantages of both processes. To prove the value of EP-MPF processes, an experimental model has been developed.

The basic components of the EP-MPF approach to form a doubly curved panel are shown in Figure 7.1. The thick blue element is the elastic punch which has replaced the upper MPF pin matrix (the punch) and gives some initial flexibility to the process. The lower matrix of pins is used as the die to form the desired three-dimensional shape. The metal sheet is inserted between the elastic punch and an elastic cushion to prevent dimpling on the surface of the formed part due to the discrete pins forming the matrix. The experimental setup based on this concept was installed on a press as shown in Figure 7.2.

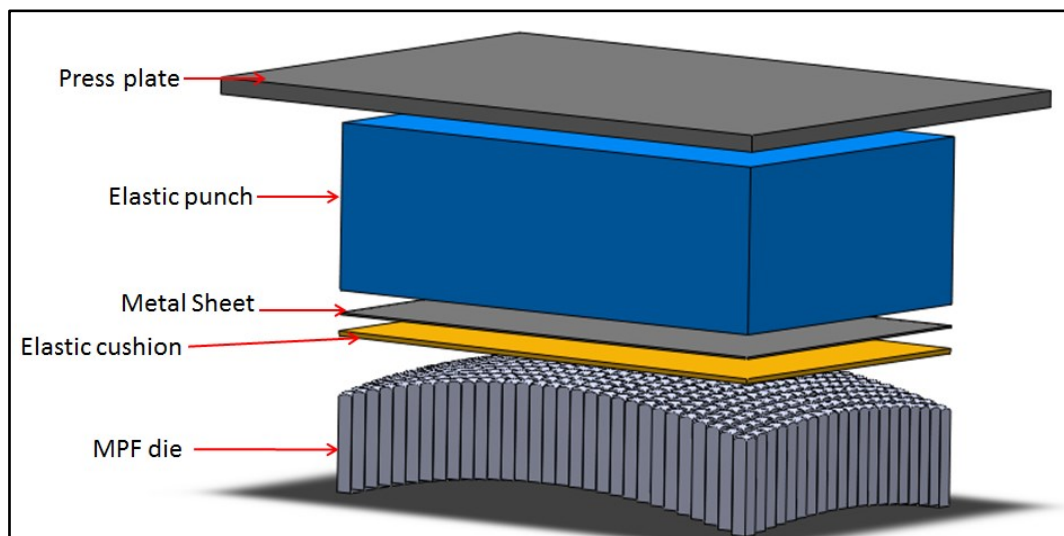


Figure 7-1 Schematic diagram of EP-MPF tool

The set up time of the tools required to form the design shape was less than half of time for traditional MPF. In addition, the alignment process required in traditional MPF using tool guides is not needed in this approach. A load cell with adequate capacity was used in conjunction with a distance sensor fixed on the press plate to measure punch movement as shown in Figure 7.2.

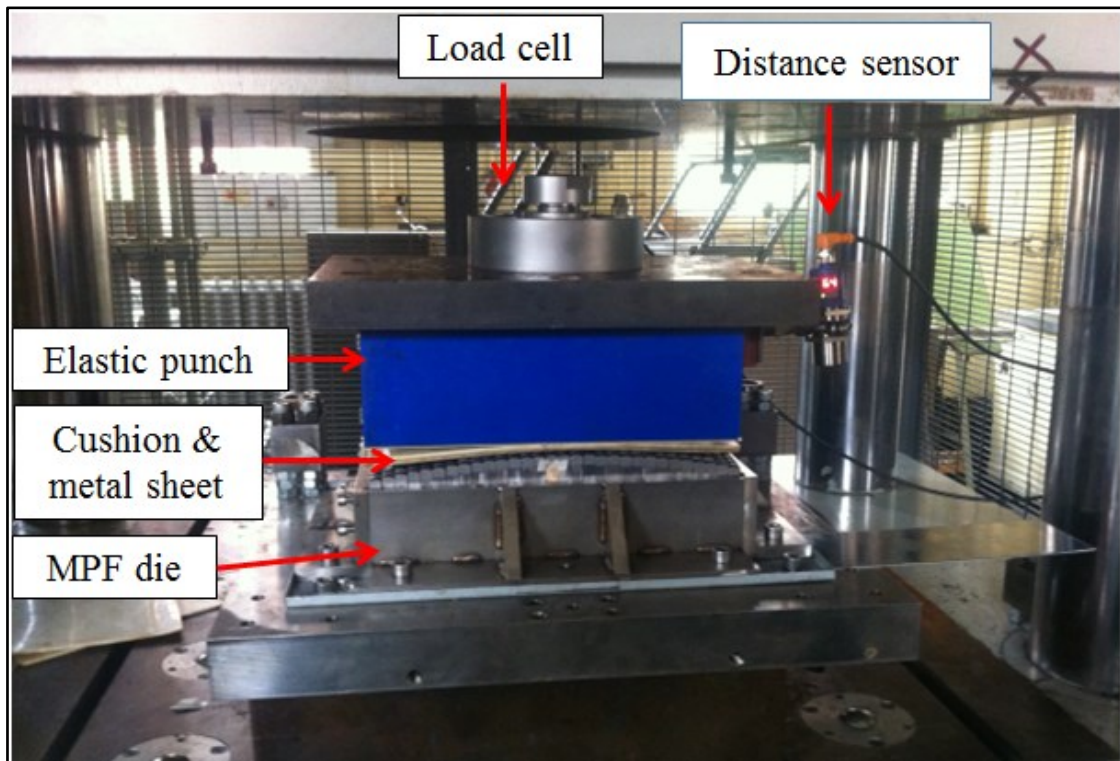


Figure 7-2 Experimental setup of EP-MPF

### 7.3 FE modelling of EP-MPF

This section reports on the FE model developed to simulate the concept of EP-MPF and investigate the formed part quality in terms of wrinkling and springback.

The equipment for the techniques was designed to produce doubly curved panels in aluminium alloy 5251-O. The FE model for EP-MPF technique combines the MPF die, metal sheet, elastic cushion, elastic block without container due to high hardness of polyurethane

A90, and press plate, as shown in Figure 7.3. In order to reduce the computation time, only a quarter of all components were modelled due to the symmetry of the model.

The MPF die to create doubly curved panels with different radii of curvature was a compound of  $30 \times 20$  pins with 0.25 mm spaced, with every pin having a cross-section  $10 \times 10$  mm and tip radius 10 mm. The polyurethane (A90) is defined as a hyper-elastic material for both elastic block and elastic cushion in the simulation analysis. The Mooney- Rivlin material model was chosen among three common models (Mooney- Rivlin, Yeoh and Neo Hook) to describe the relation between stress-strain of rubber material [2, 80].

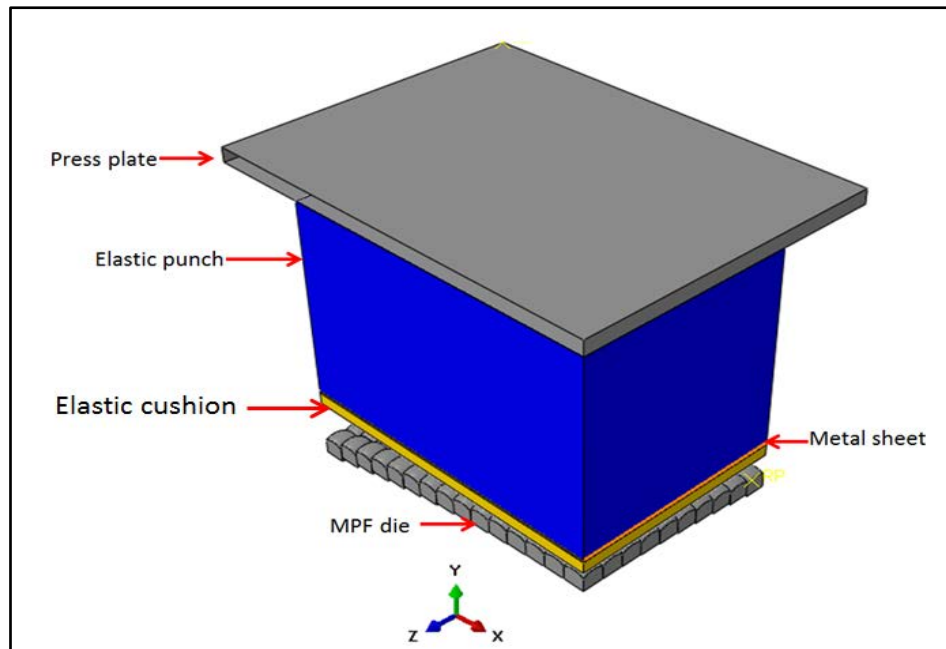


Figure 7-3 FE models of EP-MPF techniques

The dimensions of the sheet in the FE models were  $153 \times 102 \times 1.2$  mm thick. The elastic cushion dimensions were  $153.5 \times 102.5 \times 6$  mm thick, and the elastic punch was  $153 \times 102 \times 100$  mm thick. The three components were modelled using deformable solid elements. As the assembly was constructed assuming symmetry, the symmetric boundary conditions were

applied to the metal sheet, elastic cushion and elastic block. The MPF die node at the symmetry end was fixed in the X, Y and Z directions. As mentioned previously, the elastic punch was not placed within a rigid container. Therefore, the forming force was applied as a given movement to the press plate node in the Y-direction, as shown in Figure 7.4.

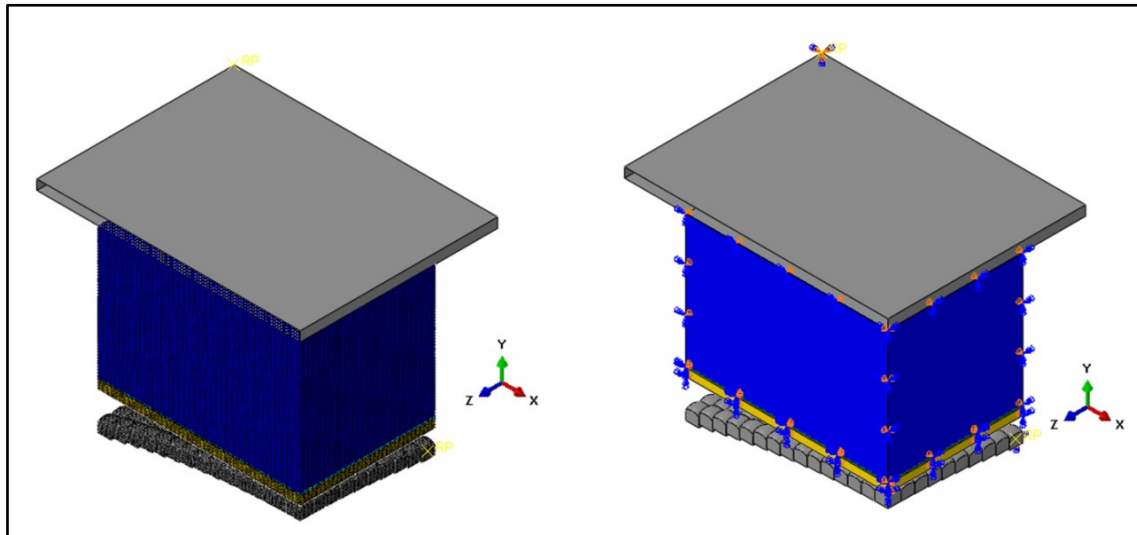


Figure 7-4 Mesh elements and boundary conditions in FE model

#### 7.4 Experimental results and discussion

Figure 7.2 shows the experiment setup of the EP-MPF tools for two mutually perpendicular radii of forming curvature, 400 mm and 800 mm to investigate the results produced by EP-MPF technique. The experimental results for the parts formed by EP-MPF approach compared with the same parts produced by the MPF process in a previous study done by Abosaf *et al.*, [84] are shown in Figure 7.5.

Wrinkling was considered as the distance between the formed and target shapes at every wrinkling wave as shown in Figure 7.6.

The root mean square error (RMSE), see Equation 1, was used to determine the numerical value of wrinkling

$$RMSE = \sqrt{\frac{1}{n} \sum_{i=1}^n x_i^2} \quad (1)$$

where  $n$  is the number of wrinkling waves, and  $x_i$  is the difference between the magnitude of the wrinkle and the target curve at the  $i^{\text{th}}$  peak.

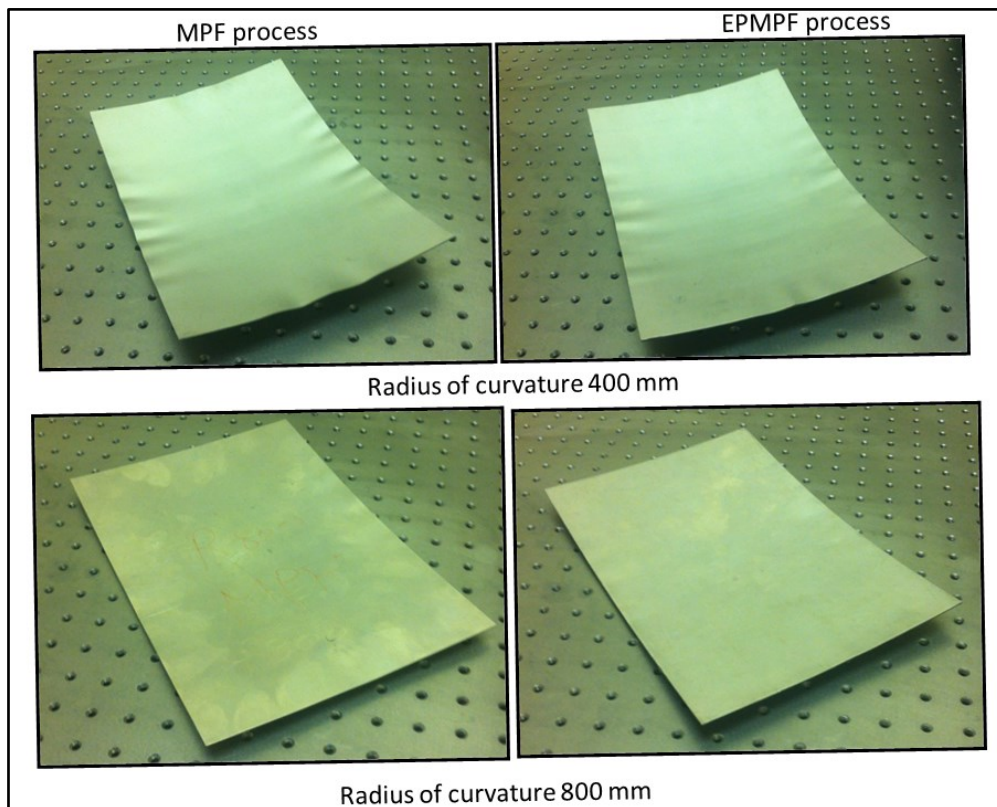


Figure 7-5 Samples of parts fabricated by each technique

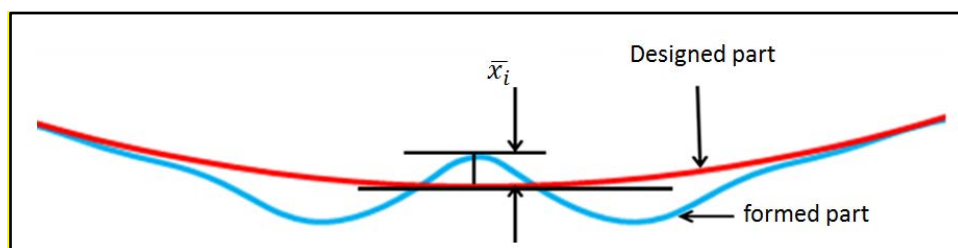
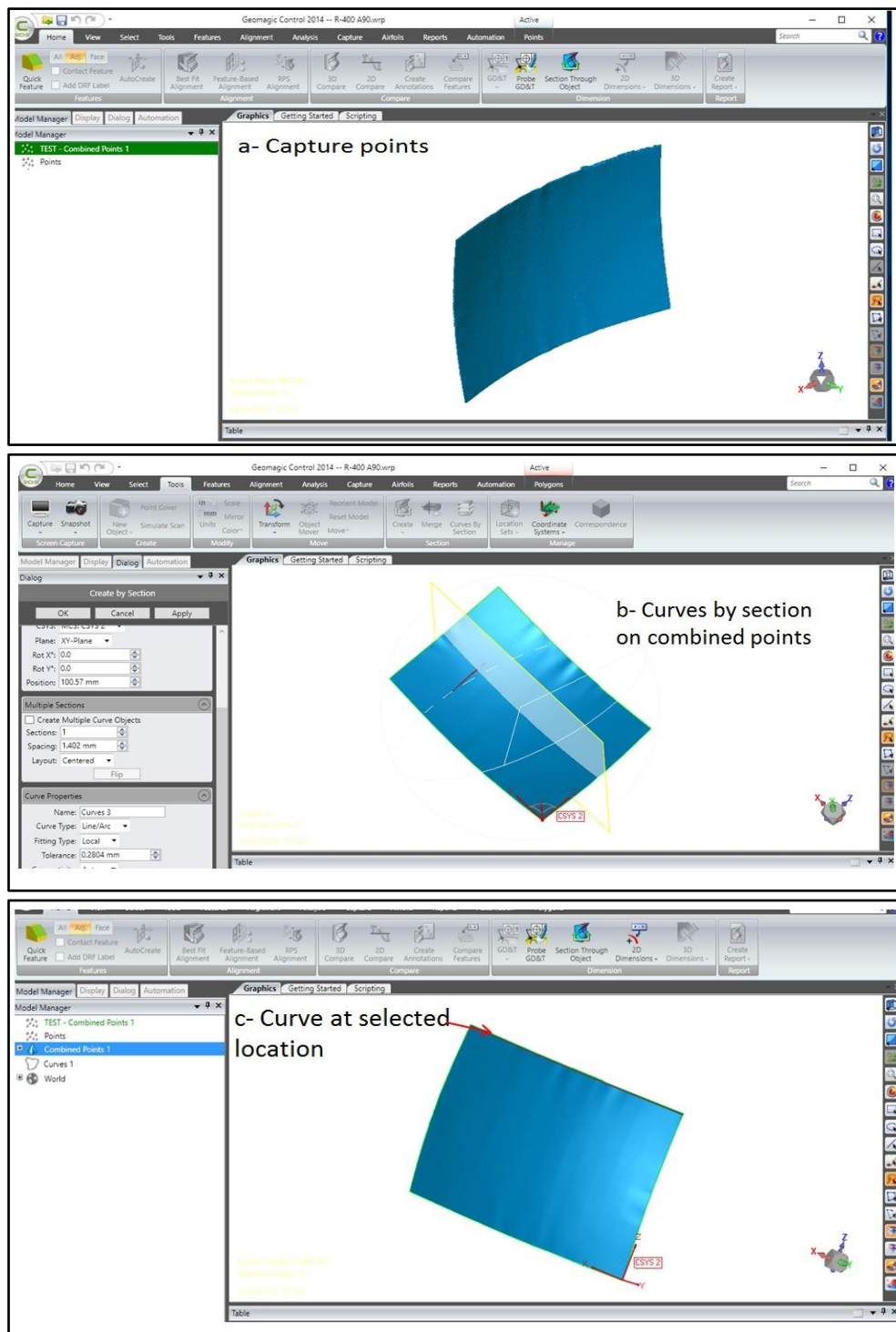


Figure 7-6 Wrinkling measured method [83]

A FARO Edge Arm 3D scanner with Geomagic control was used to capture the shape of the final product as shown in Figure 7.7(a) to (f) in steps to compare it with designed part to measure shape variation [70].



Continue Figure 7-7

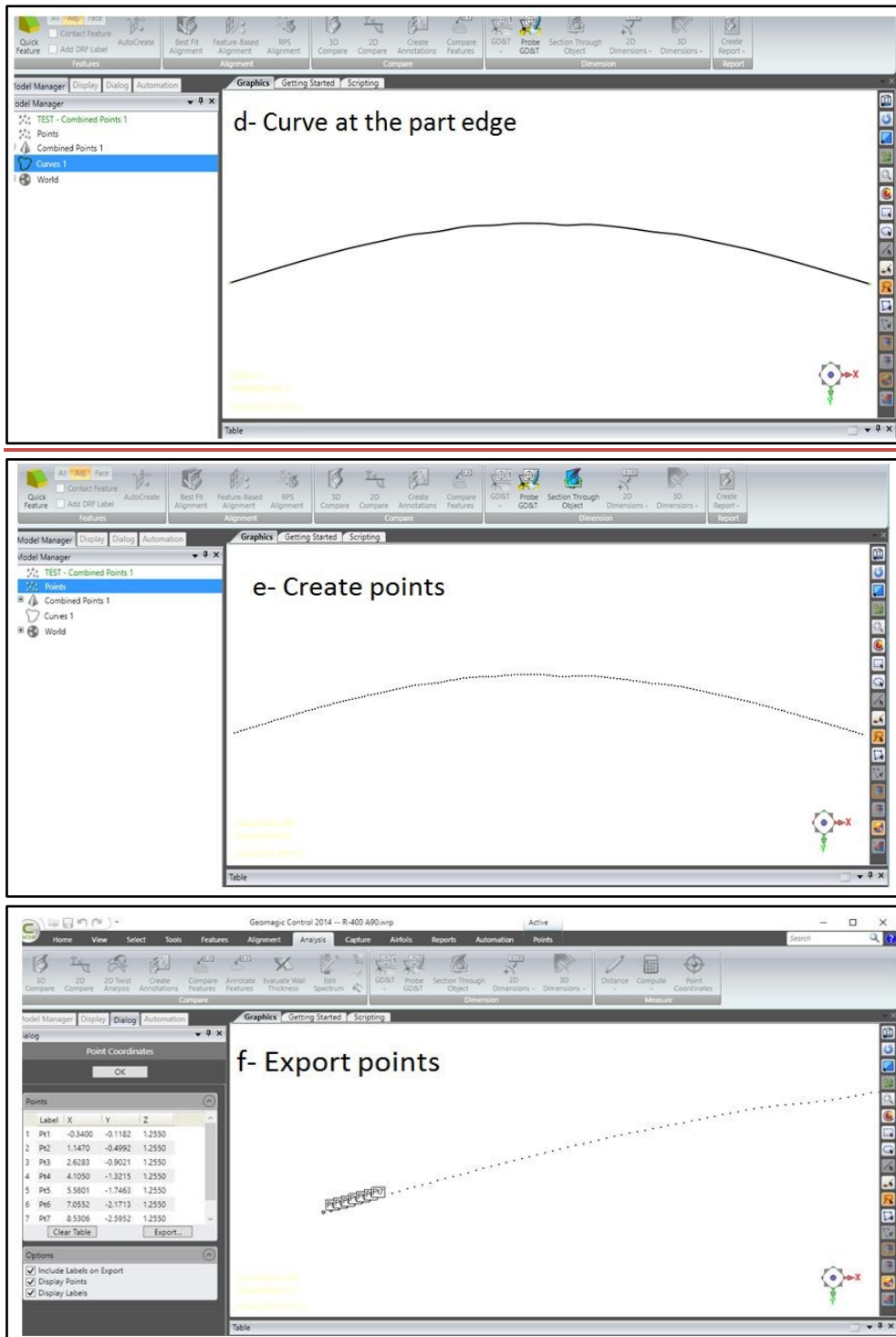


Figure 7-7 Scan steps to capture formed part

For the part formed with radius of forming curvature 400 mm, wrinkling was taken as the normal distance between the target and formed shape at every wrinkling amplitude along path

O-C as shown in Figure 7.8, and the root mean square error (RMSE) was used to calculate a numerical value for wrinkling [2].

In the case of the formed part with 800 mm radius of forming curvature, the captured points ( steps a to f ) were compared to the ideal shape and the deviation in thickness direction along path O-B was used to represent the springback [80] as shown in Figure 7.9.

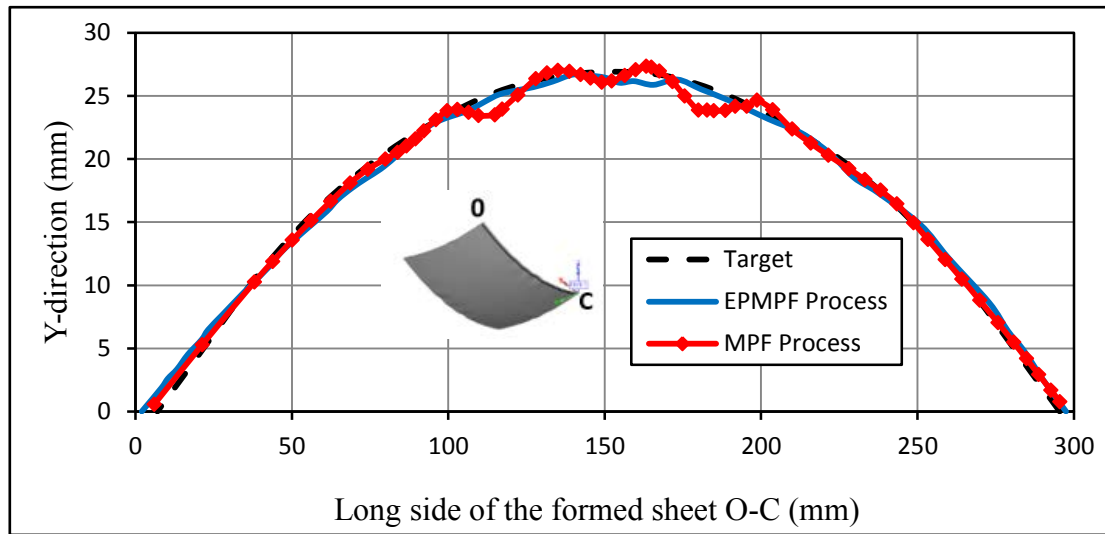


Figure 7-8 Wrinkling at edge of formed part (R = 400 mm)

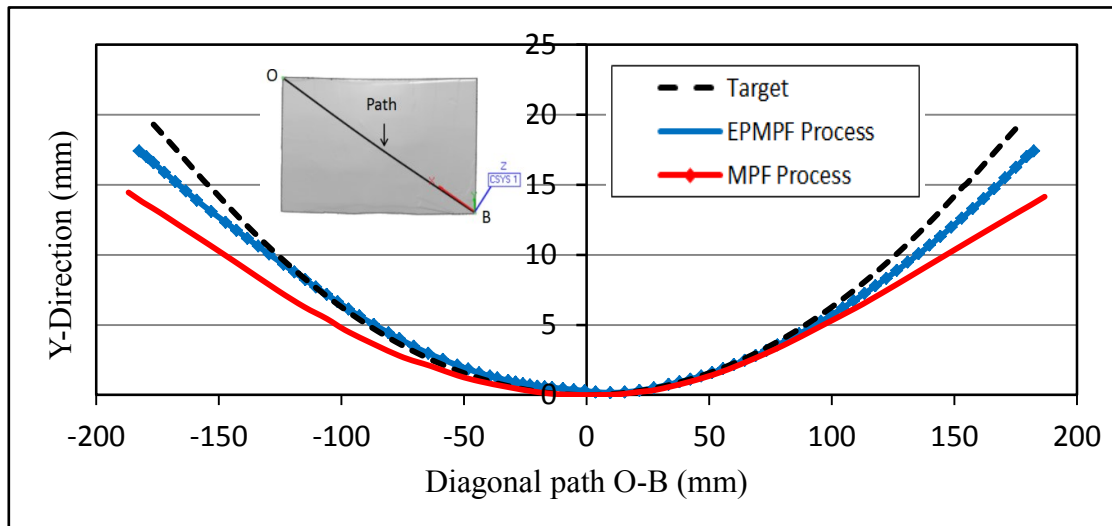


Figure 7-9 Springback of formed part along path O-B (R = 800 mm)

## 7.5 Simulation results and discussion

The forming process using an elastic punch can be divided into three steps. The first step is self-deformation of the elastic punch; the second step is sheet deformation under the forming force of the elastic punch until the sheet is shaped into the MPF die cavity and, the third and final step is the unloading stage (i.e. load release).

Under the process conditions explained above, FEA simulation was carried out for two radii of forming curvature 400 mm and 800 mm.

### 7.5.1 Comparison of simulated forming forces for EP-MPF and MPF

Figures 7.10 and 7.11 show the forming force- versus time curves using EP-MPF and MPF techniques to form doubly curved panels with radii of forming curvature 400 mm and 800 mm. The forming force of MPF had been measured experimentally in previous work, Elghawail, *et al.*, [80]. As can be seen in the two figures, there are significant differences between the values and trends of the forming force to produce the same part from a 1.2 mm thick sheet of aluminium alloy 5251-O.

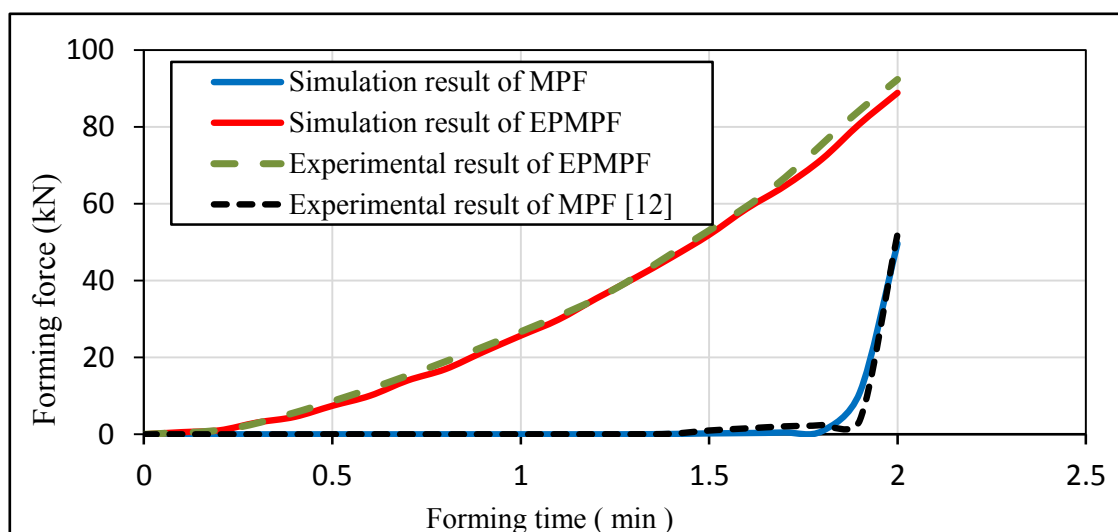


Figure 7-10 Forming force-versus time curve for 800 mm radius of forming curvature

The forming force required in the EP-MPF technique rose to 90 KN to produce the part with 800 mm radius of forming curvature. However, when using the MPF punch, it only reached 50 KN [128]. The forming forces have very different trends. In the case of using the elastic punch, the forming force can be divided into three stages. In the initial 15 seconds, when the elastic punch first contacts the sheet, the forming force is very small. Then the force gradually increases due to self-deformation of the elastic punch, also the sheet is bending as the punch moving forward into the die; this process extends from about 15 seconds approximately 1 minute. Finally, the forming force continues to increase due to plastic deformation of the sheet as it moves to copy the shape of die cavity and more pressure is applied on the punch to make sure the die is fully covered [129], this occupies the last 2 minutes of the process.

In the case of the MPF punch, the forming force remains very small until close to the end of the process when it suddenly increases as the sheet starts to deform. The same explanations apply to the part with 400 mm radius of forming curvature.

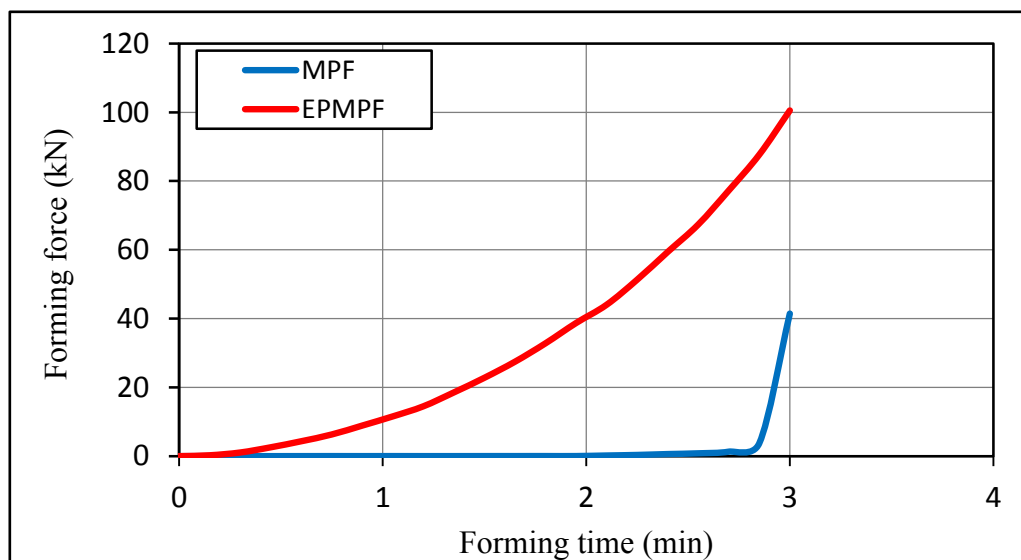


Figure 7-11 Forming force-versus time curve for 400 mm radius of forming curvature

It can be seen that in the case of the MPF punch, the total forming force increases with increase in radius of forming curvature. This result is due to more pins coming into contact with the sheet at the beginning of the forming process [2]. With the elastic punch, there is an increase in the forming force with a decrease in radius of forming curvature. This is because more force is needed to push the rubber forward to cover the entire MPF die.

### **7.5.2 Stress distribution on top and bottom surfaces of the formed sheet**

FE models were developed for doubly curved panels with 400 mm and 800 mm as radii of forming curvature, and then analysed using ABAQUS. The calculated pressure distributions on the top and bottom surfaces of the sheet at the end of the forming process are shown in Figures 7.12 and 7.13

Figure 7.12 shows pressure distributions on the formed part with 400 mm radius of forming curvature using MPF and EP-MPF forming techniques. Large bending deformations are required in this case [2] and, as can be seen, the stress pressure in the part formed with the EP-MPF technique are well distributed compared with stress pressure produced by the MPF punch.

This is because the elastic punch formed together with the sheet metal during the loading step, which means the relative motion between the punch and the sheet is very small and the influence of frictional forces is, therefore, negligible. However, the MPF punch is rigid, so the relative motion at the interface is much larger and the presence of friction makes it more difficult for the blank material to flow, especially in those conditions where the friction coefficient increases [52]. This led to stress instability and wrinkling [2, 130]. In both cases, in the middle of the long side edge, it is clear that the stresses fluctuated between maximum and minimum values, which are what causes wrinkling [2, 130].

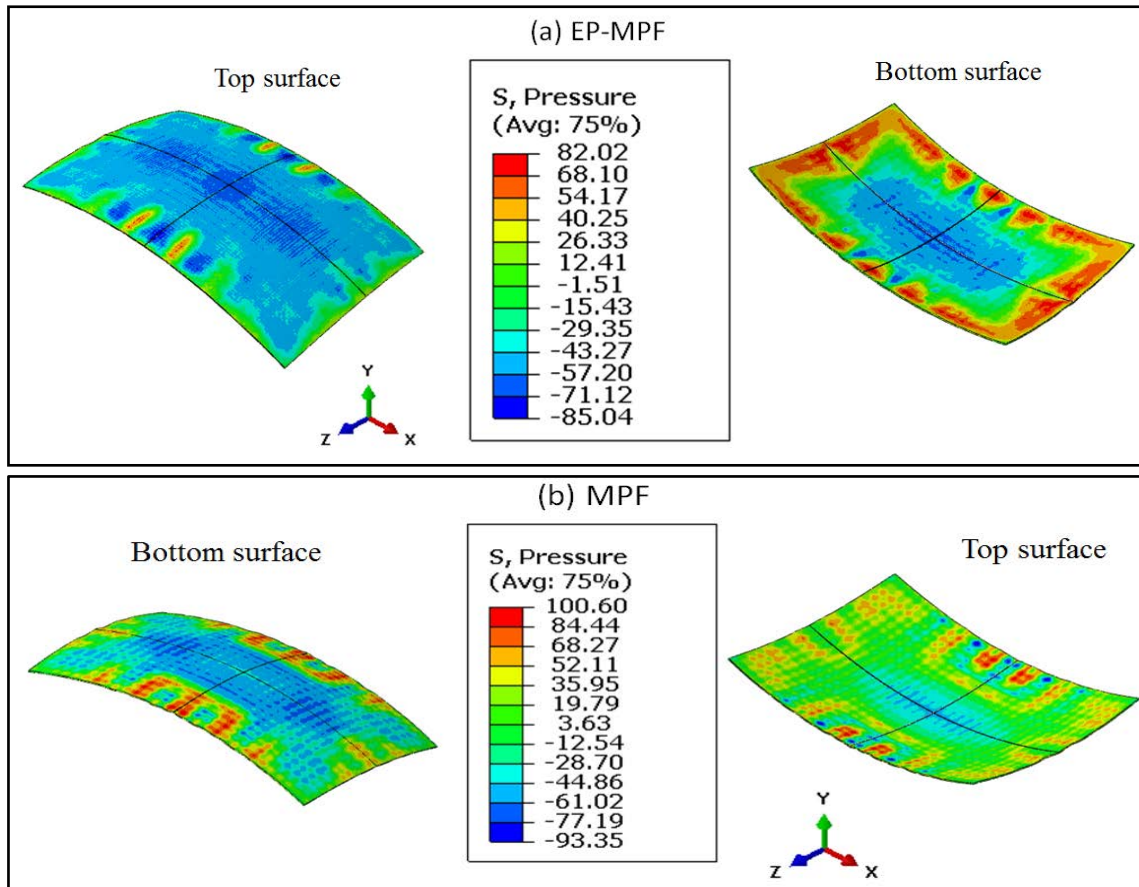


Figure 7-12 Pressure distributions on top and bottom surface of formed part pre-springback (R=400 mm)

However, the wrinkling amplitudes are smaller in case of the elastic punch than with the MPF punch.

For the part with the larger radius of forming curvature 800 mm which required less bending deformation, the results are shown in Figure 7.13. Here, the pressure distributions is more uniform ( which is the key to control springback) on the top and the bottom surfaces of the part formed by EP-MPF than the part produced by the MPF punch. This leads to stress stability, the disappearance of wrinkling waves and reduction in springback value in the formed part compared to the formed part produced by the MPF punch.

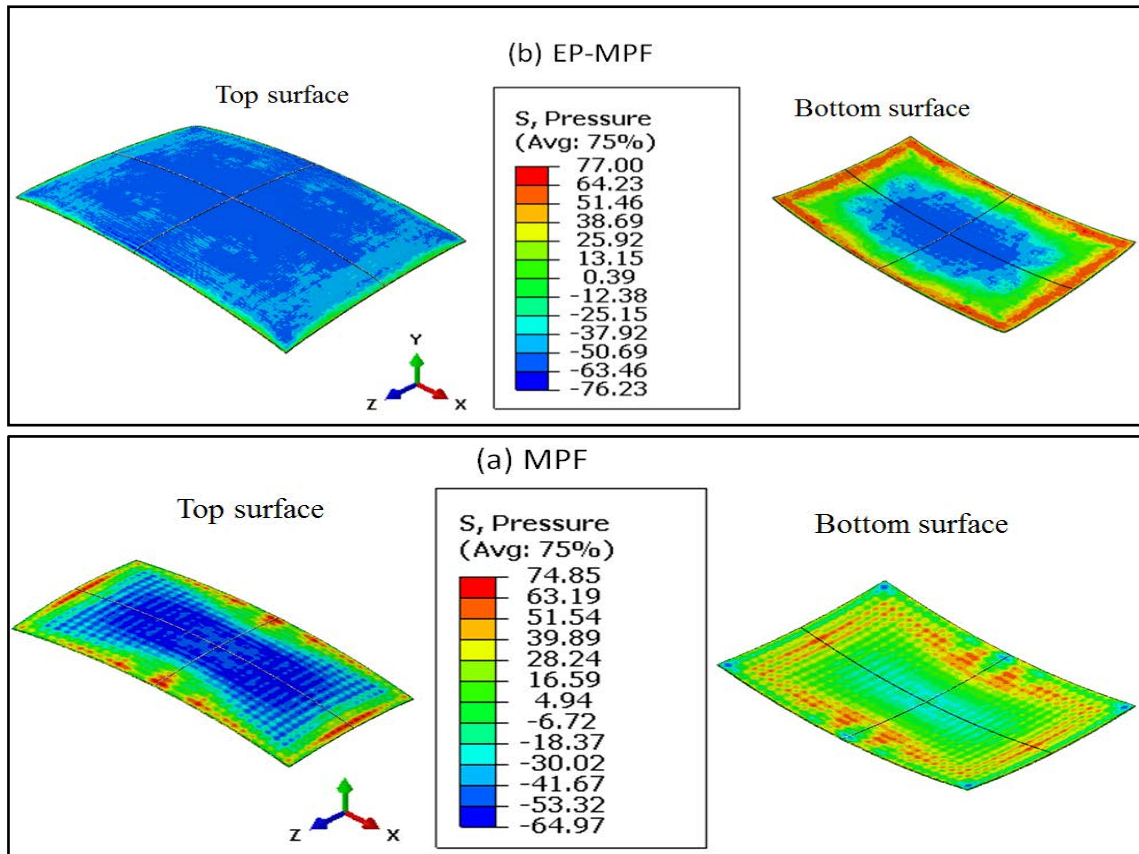


Figure 7-13 Pressure distribution on top and bottom surface of formed part pre-springback (R=800 mm)

### 7.5.3 Wrinkling

The simulation results of the formed parts with 400 mm radius of forming curvature produced by MPF and EP-MPF show that wrinkling can be significantly reduced by using an elastic punch with Shore hardness A 90 [66], as is shown in Figure 7.14 along path O-C.

The RMSE value for wrinkling using MPF punch was 1.30 mm, and 0.534 mm when using the elastic punch, with is considered a significant reduction.

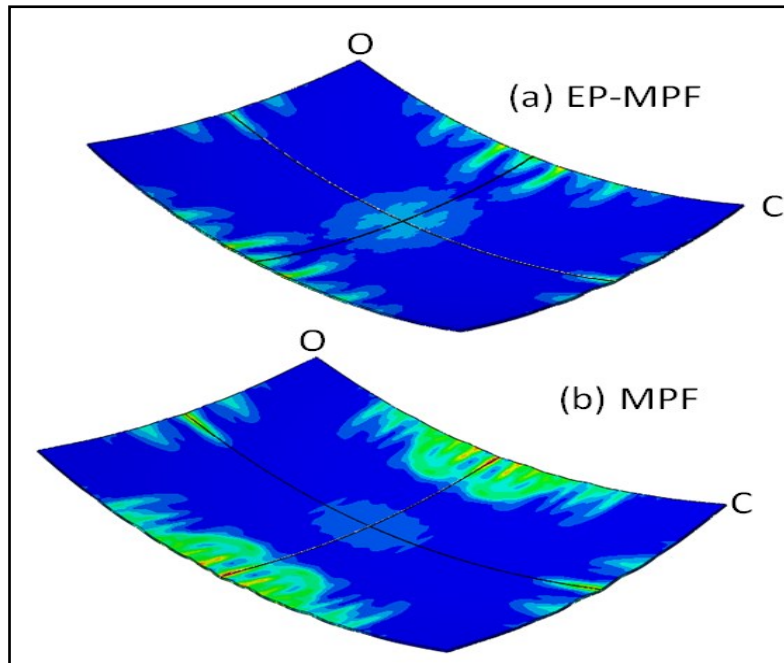


Figure 7-14 Wrinkling simulation at formed part using two different techniques ( $R = 400$  mm)

#### 7.5.4 Springback

In this section, the effect of EP-MPF technique on the springback (SB) of the formed part with 800 mm radius of forming curvature was compared with the results obtained using the MPF punch. In order to study the effect of elastic punch on springback, a comparison between the post-springback part and the final part was used.

Figures 7.15(a) and (b) show the simulation results for springback in the formed part with radius of forming curvature 800 mm produced by the two techniques. From Figure 7.15 (a) shows the part as simulated by MPF tools had a total springback of 6.21 mm. Figure 7.15 (b) shows the part as simulated by elastic punch (EP-MPF), the springback was 3.66 mm. Thus, springback for the elastic punch was significantly smaller. These results are also related to uniformity of stress distribution and friction on the final formed part, which is considered of major importance in determining springback phenomena. The more uniform the stress and

friction conditions, the less the springback variation [127, 131]. In the case of friction, for the elastic punch, the relative motion and the friction force between the punch and the top surface of the formed sheet are less than in the case of the MPF punch, where relative motion and friction are concentrated on the tip of the pins and are affected by the properties and thickness of the elastic cushion.

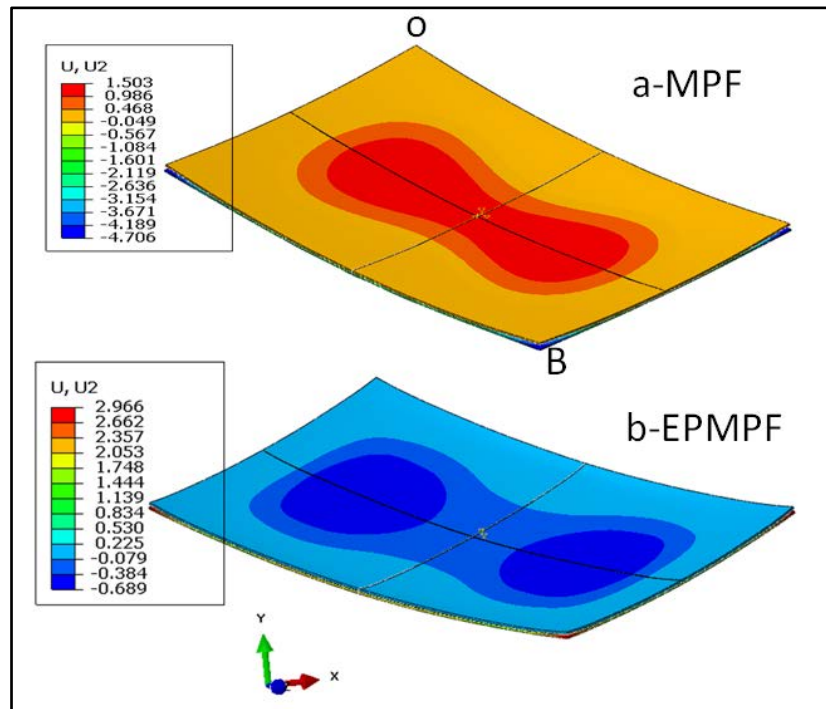


Figure 7-15 Springback simulation results for workpiece formed by MPF and EP-MPF

Figures 7.16 and 7.17 show the target shape, the simulated shape at the end of the application of the forming force before springback and the simulated shape post-springback for the two forming techniques.

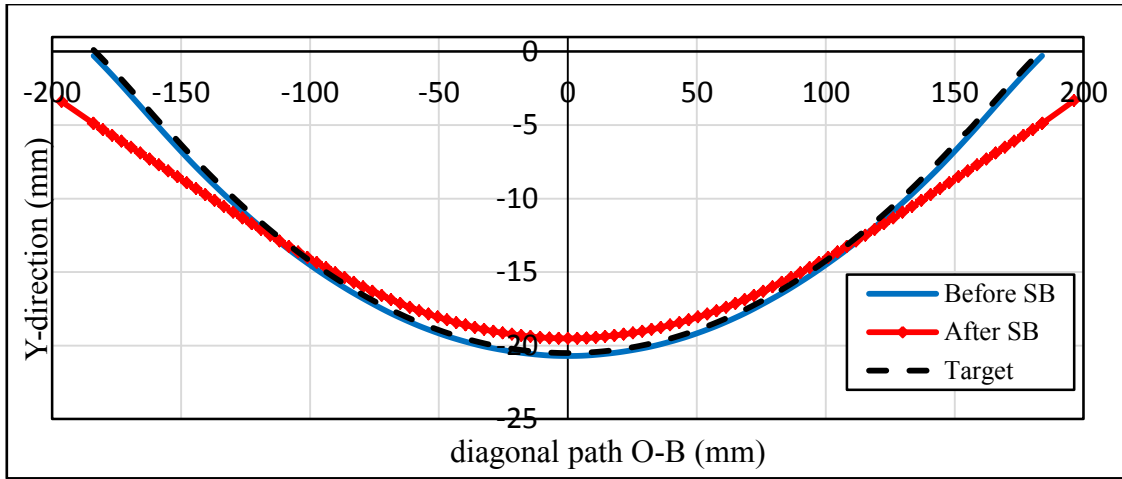


Figure 7-16 Springback of part formed by MPF (R = 800 mm)

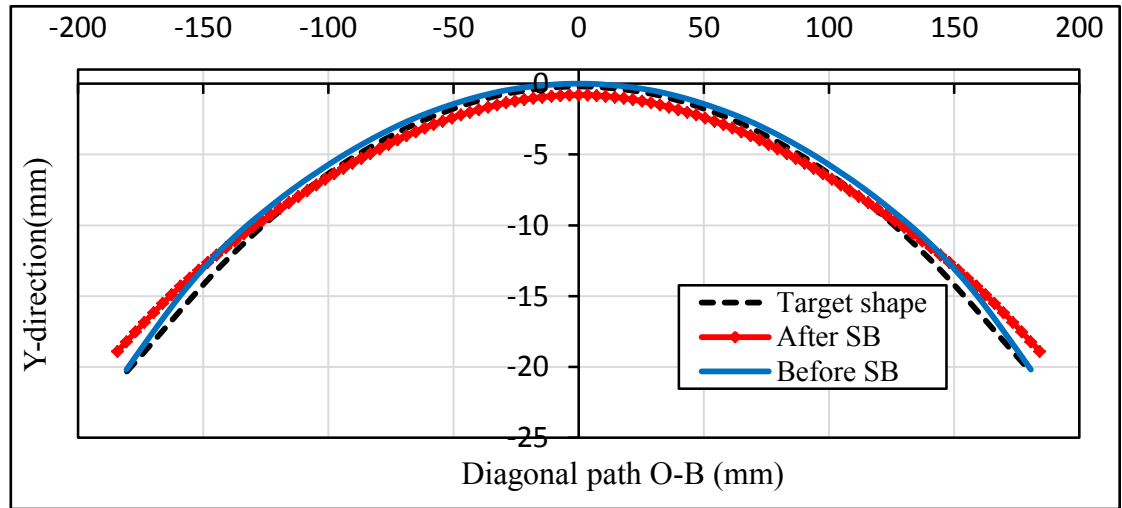


Figure 7-17 Springback of part formed by EP-MPF (R = 800 mm)

## 7.6 Optimisation of EP-MPF process parameters

This section reports an investigation of the effects of significant EP-MPF process parameters on the quality of the formed part. The input factors (independent variables) are radius of forming curvature, punch thickness (elastic block) and punch compression ratio (as the punch an elastic block, the compression ratio is  $\frac{t_0 - t_f}{t_0} \times 100$  which  $t_0$  is the original punch thickness and  $t_f$  is the punch thickness at the end of loading step ) and each factor was given three

values, as shows in Table 7.1. The response criteria (minimise) (dependent variables) determining the quality of the formed part were wrinkling amplitude, springback and forming force. Examples of results are given in Section 7.5.

Table 7-1 Level and value of the DOE parameters

Process factors	Units	Parameter Magnitude		
		Low	Intermediate	High
Radius of forming curvature (A)	mm	400×400	600×600	800×800
Punch thickness (B) and in other tables.)	mm	100	125	150
Punch compression ratio (C)	%	50	60	70

The simulation results in Table 7.2 were statistically analysed using Design Expert 7.0 which contains several experimental design techniques such as Response Surface Method, factorial and Taguchi. The RSM with central composite faced (CCF) was applied in this study to generate the experimental plane as shown in Table 7.2 (see section 5.1.3) [132, 133]. Additionally, ANOVA was implemented to identify the most significant process parameters and their effect on the final product.

### 7.7 Results and discussion

The numerical simulation results to three response parameters (wrinkling, springback, and forming force) are listed in Table 7.2 for an experimental plan in accord with RSM (CCF).

ANOVA was used to evaluate the effect of every independent variable and their interactions related to the response factors. The null hypothesis was that the variable had no effect on the formed part. Thus a probability *P*-value below 5% indicates that the independent variable has a significant effect on the formed shape [134]. For the wrinkling defect, only A (radius of curvature) was significant, whereas for springback all three variables and their interactions

were significant factors and, finally, the value of forming force was significantly affected by A and C (punch compression ratio).

Table 7-2 Experimental plan and simulation results

Exp.#	Factor 1	Factor 2	Factor 3	Response 1	Response 2	Response 3
	A: Radius of forming Curvature (mm)	B: Punch thickness (mm)	C: Compression Ratio (%)	Wrinkling (mm)	Springback (mm)	Forming force (KN)
1	800	150	50	0.00	2.76	109.6
2	600	125	60	0.10	2.53	111.3
3	800	100	50	0.00	4.00	123.2
4	400	100	50	1.26	2.32	53.2
5	600	125	60	0.10	2.53	111.3
6	600	100	60	0.00	2.89	121.7
7	600	125	50	0.15	2.99	82.8
8	800	100	70	0.00	1.68	213.6
9	400	150	50	1.10	2.32	68.3
10	400	150	70	0.89	2.30	129.3
11	400	125	60	0.26	1.98	98.7
12	600	125	60	0.10	2.53	111.3
13	800	150	70	0.00	1.75	229.3
14	800	125	60	0.00	2.14	170.0
15	400	100	70	0.52	1.91	141.5
16	600	150	60	0.00	2.42	122.0
17	600	125	70	0.00	2.26	175.1

Table 7-3 Process parameters and corresponding P-values

Response factors Significant factors	Wrinkling	springback	Forming force
Radius of forming curvature (A)	0.0005	0.0186	<0.0001
Punch thickness (B)	0.7574	0.0386	0.9070
Punch compression ratio ( C )	0.1363	<0.0010	<0.0001
Significant interaction	-	AB=0.0094 AC=0.0003 BC=0.0027	-

### 7.7.1 Wrinkling

According to the ANOVA analysis results presented in Table 7.3, the only process factor significantly affecting wrinkling is the radius of forming curvature, and the influence trend is shown in Figure 7.18. The trend is the same as in the traditional MPF process, increasing the radius of forming curvature leads to reduction in wrinkling, even its elimination. A small radius of forming curvature will generate high bending deformation leading to wrinkling appearing at the edges of the formed part [135]. As the elastic punch was flat initially it maintains surface contact with the sheet facing into a convex MPF die. As the punch travel increases, it will generate high pressure on the middle and the edges of the metal sheet where the wrinkling starts to appear. Under this condition, wrinkling will be suppressed and be less than the wrinkling that appears in case of conventional MPF (see Section 7.5.3).

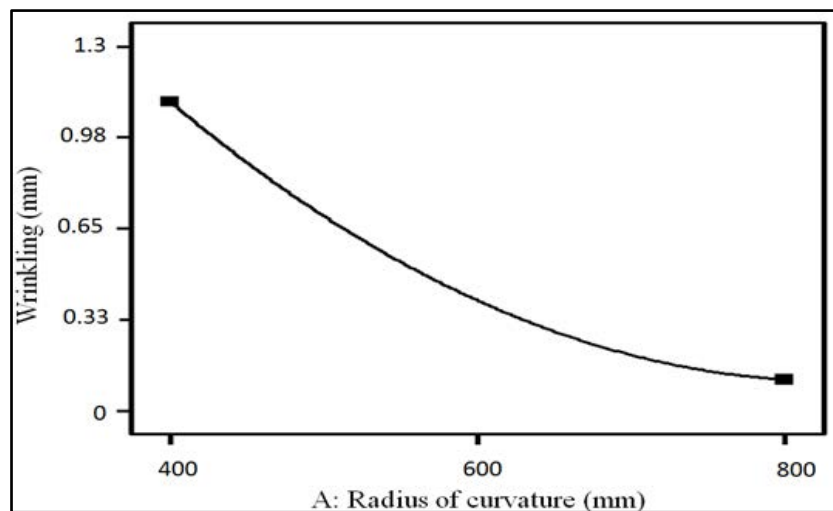


Figure 7-18 Effect of radius of curvature on wrinkling

### 7.7.2 Forming force

Figures 7.19 and 7.20 show the impact of two significant working parameters, radius of forming curvature and compression ratio of the punch, on the value of the forming force. It is clear that from Figure 7.19 that by increasing the radius of forming curvature, the required

force for forming process also increases. The number of pins that will be in contact with the elastic punch for large radius of forming curvature under high pressure (outer edges) is more than for case of small radius of forming curvature; i.e. the height difference between pins is smaller when generating the 800 mm radius. As consequence the forming force will increase. In addition, the punch (A90) will need additional force for its own self-deformation [128].

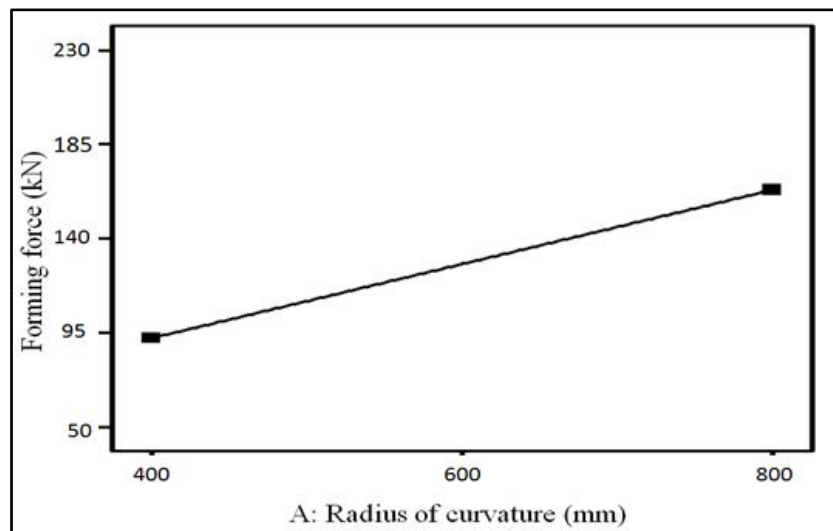


Figure 7-19 Effect of radius of forming curvature on forming force

The influence of the punch compression ratio on forming force is shown in Figure 7.20. In this study the minimum ratio of punch compression was 50% of punch thickness to push the metal sheet completely against the MPF die (punch thickness 100 mm and radius of curvature 400 mm). To reduce defects such as springback on the final formed part by increasing the punch compression ratio (which makes the stress distribution more uniform) will require more force, as shown in Figure 7.2. For example, for the situation of A=600 mm and B= 125 mm, the forming force at 50% is equal to 82.8 kN while at 70% equals 175 kN.

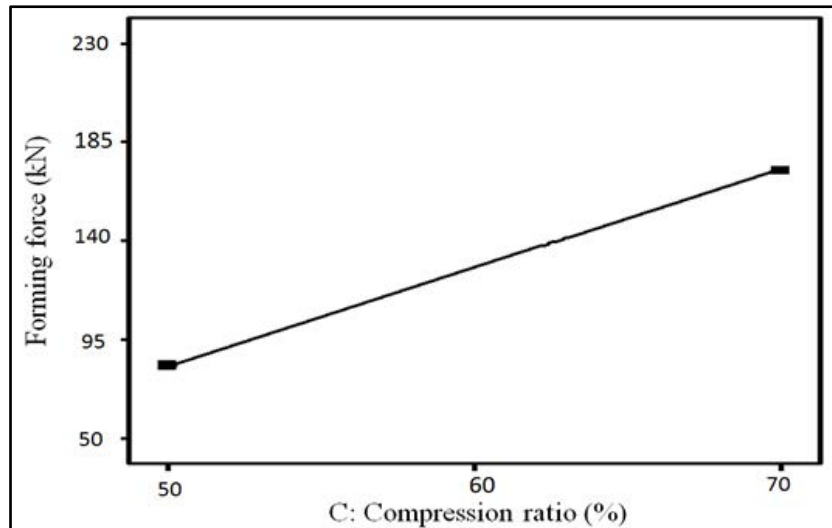


Figure 7-20 Effect of punch compression ratio on springback

### 7.7.3 Springback

Figure 7.21 shows how the springback value is affected by radius of forming curvature and punch thickness. It is clear from the figure that the combination of largest radius of forming curvature ( $A=800$  mm) and smallest thickness of the punch ( $B=100$  mm) leads to maximum springback in the formed part. Either increasing the thickness of the punch or decreasing the radius of forming curvature (see Section 5.1.3.1) will decrease the springback value but may cause other defects to appear on the final part such as wrinkling (see Section 7.7.1). It should also be noted that the process will not be linear as the surface of the 3D plane representing the interactions is not flat but more saddle-shaped.

Figure 7.22 shows the effect of radius of forming curvature and punch compression ratio on springback. Generally, as the radius of forming curvature increase the ratio of punch compression will create more uniform stresses distribution on the sheet which leads to reduction in springback value but it will need a large external force to finish the loading stage.

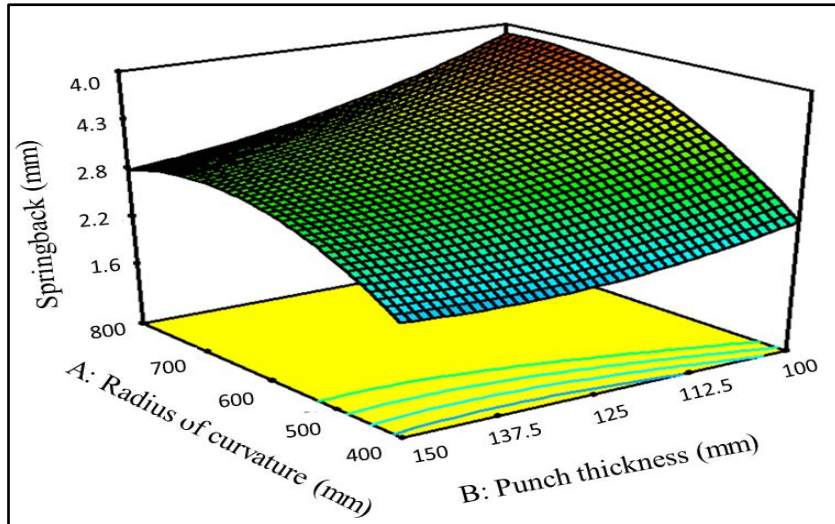


Figure 7-21 Effect of radius of forming curvature and punch thickness on springback

As mentioned in Section 7.7.2. Once again the process is not linear because, again, the surface of the 3D plane representing the interactions is not flat but more saddle-shaped.

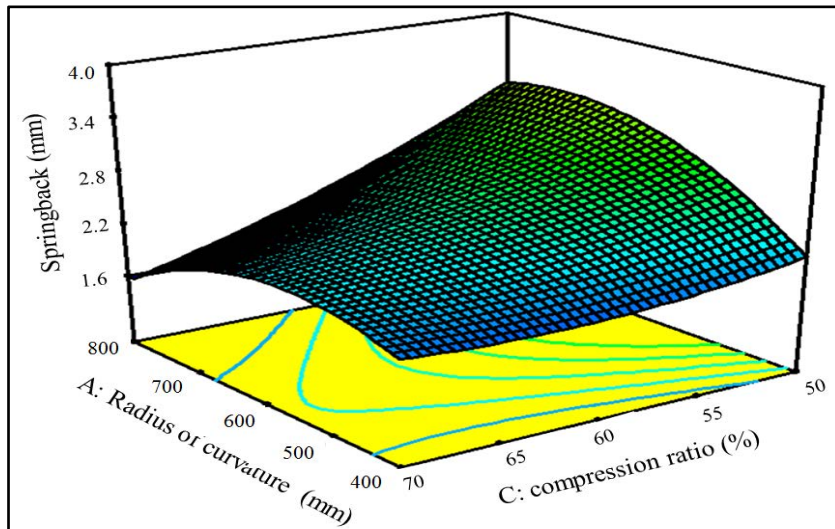


Figure 7-22 Effect of radius of curvature and compression ratio on springback

Figure 7.23 shows the effect of punch thickness and punch compression ratio on springback. As punch compression ratio increase ( $C=70\%$ ), the springback value decreased to a minimum value at a punch thickness of about 120 mm due to the stability and uniformity of

the stresses generated in the metal sheet, but the value of the force required to complete the loading step will be high.

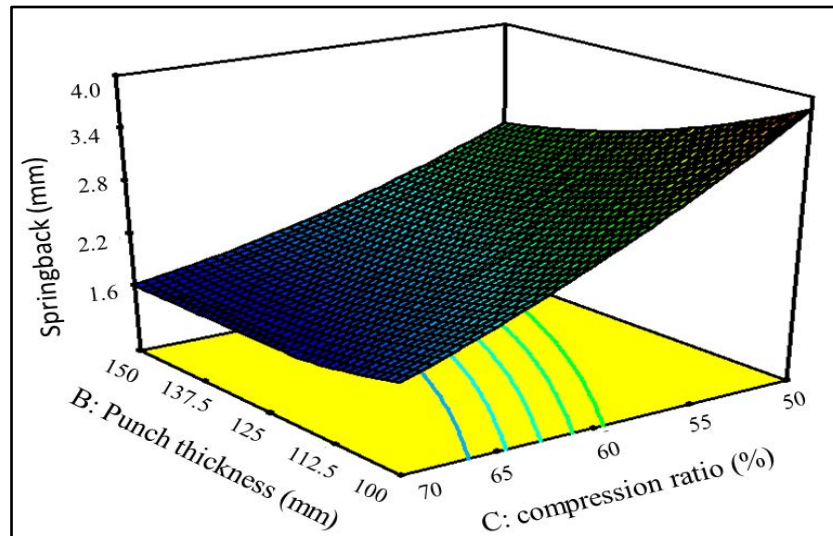


Figure 7-23 Effect of punch thickness and punch compression ratio on springback

### 7.8 Prediction of response factors

As described in Section 5.1.4 Prediction of response factors, the three independent process variables can be used to generate an empirical model as a general second order quadratic polynomial, Equation 7-1, to estimate the quality of the final formed part for any combination of process parameters at any of the prescribed values shown in Table 7.1.

Following Equation (5.3) the response surface is presented as:

$$\text{Response} = X_0 + x_1 A + x_2 B + x_3 C + x_4 AB + x_5 AC + x_6 BC + x_7 A^2 + x_8 B^2 + x_9 C^2 \quad (7.1)$$

Where A, B and C are independent variables; A is the radius of forming curvature, B is the punch thickness and C is the compression ratio of the elastic punch, and  $x_i$  ( $i = 0, 1, \dots, 9$ ) are unknown coefficients obtained by using regression analysis, see Table 7.4,

Table 7-4 Coefficients of objective function

Coefficient	Wrinkling	Springback	Forming force
Constant (X)	15.23	7.377	-270.9
$x_1$	-0.011	0.029	0.185
$x_2$	-0.045	-0.098	-0.020
$x_3$	-0.270	-0.204	4.750
$x_4$	-5.25E-6	-3.90E-5	0.0
$x_5$	5.94E-5	-1.81E-4	0.0
$x_6$	2.65E-4	8.50E-4	0.0
$x_7$	5.35E-6	-1.08E-5	0.0
$x_8$	1.34E-4	2.63E-4	0.0
$x_9$	1.59E-3	1.34E-3	0.0

### 7.9 Optimal parameters for working process

To form a doubly curved part of high quality, the optimal values of the working parameters should be known. In this investigation the main target is to produce a part with minimum wrinkling and springback by using, if possible, a low forming force. The independent variables were selected to be within the ranges specified in Table 7.1. The response parameters (independent variables) were set to meet the objective function and minimize wrinkling, springback and forming force (see appendix 3).

The optimum solution to meet the objective function in this study was obtained after it had been applied to the objective criteria (“IN RANGE” for working factors and “MINIMIZE” for response parameters) and the empirical equation solved for the three factors working together till they produced the solution that best met the objective function, see Table 7.5

Table 7-5 Optimum values of process parameters to jointly minimise wrinkling, springback and forming force

	Radius of forming curvature (mm)	Punch thickness (mm)	Compression ratio (%)
Optimum parameters setting	600	100	63

The previous 3D FE model, see Section 7.3, was used to test the optimal process parameters in Table 7.5, and the simulation results are shown in Figure 7.24. Next, experimental work was carried out to validate the predicted results. The measurements steps described in Section 7.4 were repeated. Figure 7.24 show plots of wrinkling along the long side and Figure 7.25 shows the scanned formed part with optimum process parameters, where wrinkling was measure along path O-A and springback was measure along path O-B. However, Figure 7.26 presented the final comparison between target shape (R=600 mm), simulation and experimental results. It can be seen that there is no wrinkling on two results, simulation and experimental formed part.

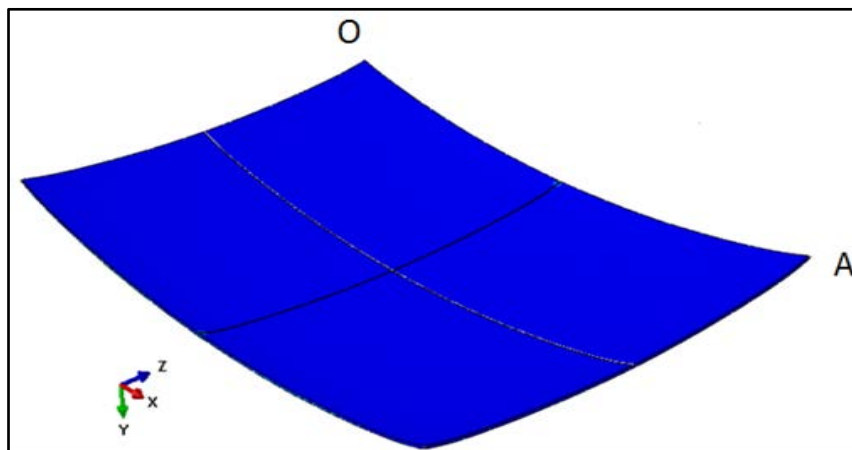


Figure 7-24 Simulation result of wrinkling for optimum values of process parameters

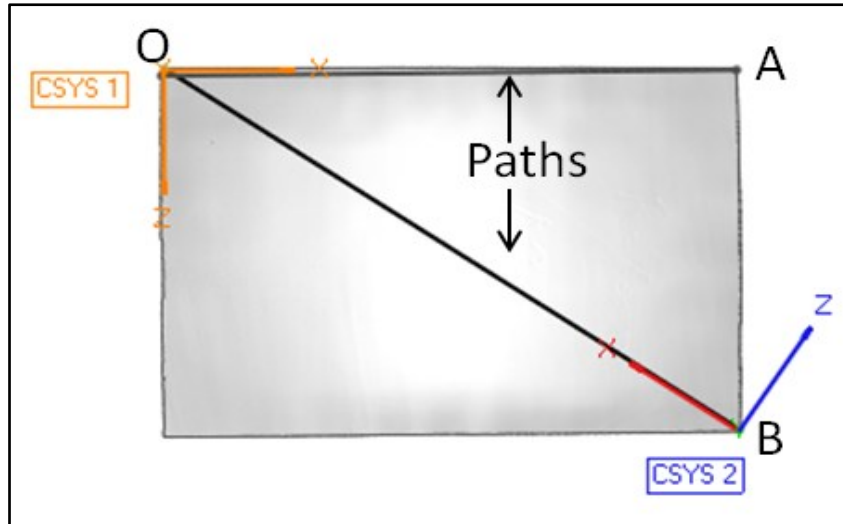


Figure 7-25 scanned formed part (optimum process parameters)

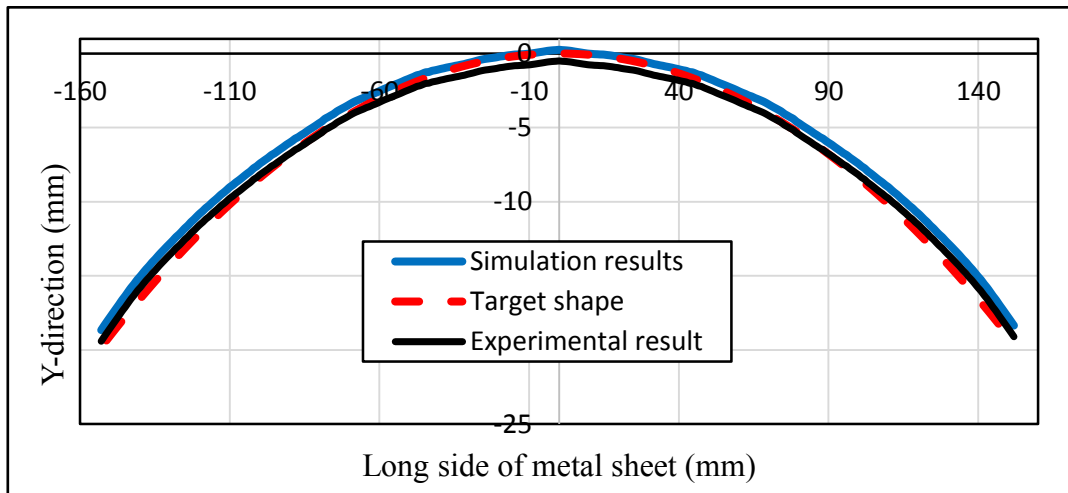


Figure 7-26 Comparison between simulation, experimental results and target shape for optimum values of process parameters

Figure 7.27 shows simulated result of springback across the diameter of the metal sheet after forming process had ended. The total value of springback occurred on the formed part is 2.58 mm.

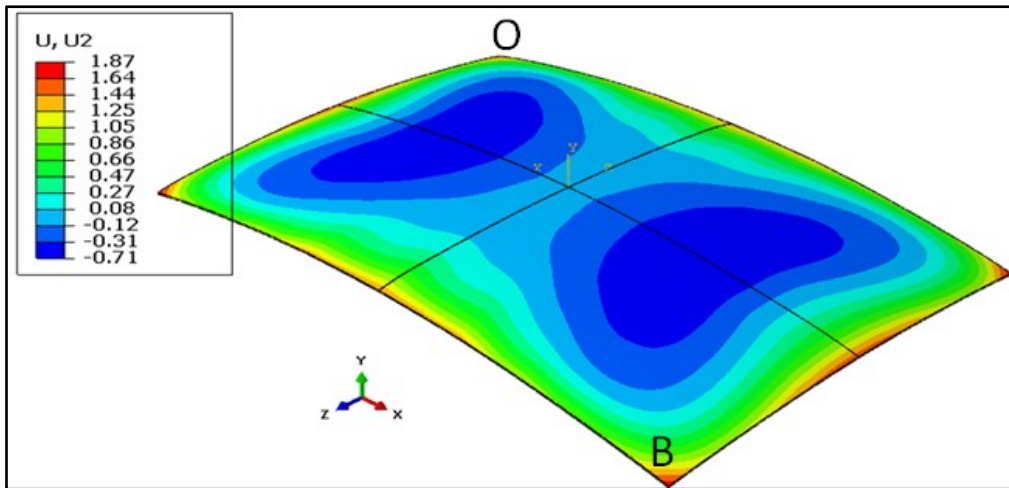


Figure 7-27 Simulation result of springback for optimum values of process parameters

The simulation, experimental results and target shape of the final part with optimum values of process parameters were compared in Figure 7.28. It was good agreement between final results.

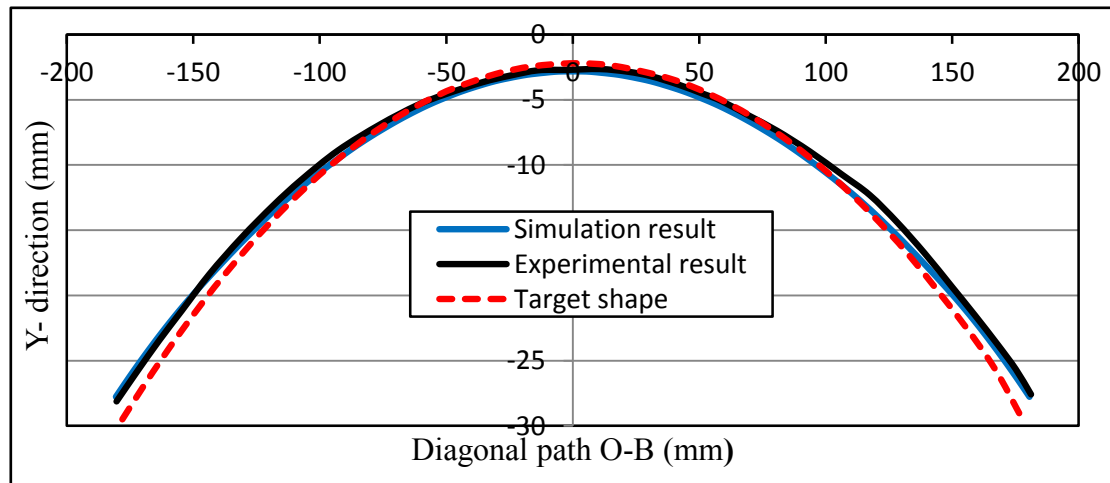


Figure 7-28 Springback along diagonal of formed part O-B (mm) for optimum values of process parameters

Table 7.6 gives the predicted and experimental results value of the three selected process parameters.

Table 7-6 Predicted and experimental results at optimum process parameters

	Wrinkling (mm)	Springback (mm)	Forming force (kN)
Predicted	0.00	2.58	132.3
Experimental	0.00	2.69	131.0

To evaluate the accuracy of the simulations of the process parameters, a numerical error between the simulated and measured results is calculated as

$$\text{Numerical error} = \frac{\text{Experimental result} - \text{Simulation result}}{\text{Simulation result}} \times 100$$

Numerical error for wrinkling = 0.0

Numerical error for springback =  $[(2.69 - 2.58) / 2.58] \times 100 = 4.26 \%$

Numerical error for forming force =  $[(131 - 132.3) / 132.3] \times 100 = -0.98 \%$

The negative values for the Numerical Error mean that the experimental results were smaller than the simulated.

### 7.10 Summary

Doubly curved panels with different radii of curvature were successfully produced experimentally using an elastic punch and compared with panels produced by conventional MPF. Numerical simulation using FEA with optimisation was used to investigate the influence of process parameters such as radius of forming curvature, punch thickness and punch compression ratio on springback, wrinkling and forming force.

To compare the quality of final parts, wrinkling, springback and forming force values were taken as response parameters. Based on the final experimental and simulated results, the optimal process parameters were found and the following conclusions can be drawn from this study:-

- 1- Replacing a MPF pin punch by an elastic punch, can reduce tooling costs by 50% and dramatically decrease the setup time required to adjust the pins for a new design shape.
- 2- The same tooling can be used to form metallic sheets with different properties and thicknesses.
- 3- Wrinkling of the final part can be reduced significantly with a 400 mm radius of forming curvature without the use of a blank holder compared to the part produced by conventional MPF punch.
- 4- Springback on the final part can be reduced significantly by correct choice of process parameters such as compression ratio of the elastic punch.
- 5- Radius of forming curvature and compression ratio of the punch were the variables that most influenced part quality, while punch thickness had less importance in this research. The effects of the three process interactions AB, AC and BC were investigated; the interactions were only significant on springback value.
- 6- An empirical model has been generated for the objective function which enables prediction of the quality of the formed part for any combination of working parameters within pre-selected ranges.

## **CHAPTER 8: CONCLUSION**

### **8.1 Conclusions**

In this thesis the multi-point forming process has been investigated in terms of full MPF and elastic punch multi-point forming (EP-MPF) in order to minimise defects in the formed parts and improve the quality of the final part. To evaluate geometrical defects such as wrinkling and springback caused by elastic recovery after the final unloading, FEA was used to simulate the sheet metal forming process as used in the manufacturing sector. It was essential to understand the fundamentals of the springback phenomenon, and to have knowledge of the material and process factors that affect springback, in order to provide accurate and reliable inputs to the FEA.

A combination of statistical approaches with FEA was employed to assess the process of metal sheet forming and to successfully detect and determine the most significant modelling and working factors that defined the optimal arrangement of the studied parameters to achieve the highest quality product.

A validated 3-D numerical model of the MPF process was used to investigate the effect of the radius of forming curvature, elastic cushion thickness and blank holder force on formed part quality in terms of springback and thickness variation. A second series of experiments was with a “flexible” forming process using an elastic punch which investigated the effects of radius of forming curvature, elastic punch thickness and compression ratio of the elastic punch on forming process quality in terms of wrinkling and springback, also forming force.

The Response Surface Method was adopted to study 17 runs of the three dependent variables and three independent variables in both types of forming process. Finally, an empirical model was derived and used to estimate the quality of the final formed part for any combination of process parameters.

For aluminium alloy 5251-O sheets, 1.2 mm, thick formed by two flexible forming techniques into a spherical shape, it can be concluding that:

- The statistical method with FEA was successfully applied to determine effects of the most significant working parameters on the quality of the formed part and the trends of those effects.
- The radius of forming curvature was the most significant process parameter among those studied, following by blank holder force in the case of conventional MPF, while the elastic punch compression ratio was in second place in the case of EP-MPF.
- As the radius of forming curvature increased the wrinkling decreased until it disappeared along the sheet edges, and the thickness variation all over the formed sheet became smaller.
- The springback and forming force increased as the radius of forming curvature increased.
- Replacing the MPF punch with an elastic punch substantially improved the forming process by reducing tools cost by at least by 50%, wrinkling was reduced by 50% and springback reduced by 40%.
- The optimisation approach was able to identify the optimal set of forming process parameters to produce a doubly curved part with minimum defects in both flexible forming techniques.

- A “smart” system (FBGs) to measure the forming force on individual pins in a MPF matrix for first time was successfully implemented and it was demonstrated that the springback in the formed part was related to the force measured in selected pins.

## **8.2 Contributions**

The main contributions of this research could be summarised as follows:

- 1) Understand the effect of most significant process parameters on quality of final part by simulation analysis and experimental works for multi-point forming.
- 2) Economic flexible tools were presented (EP-MPF) to produce various shapes with different metals and thicknesses by using same tools. The cost reduction of the tools and production more than 50% compared to traditional MPF.
- 3) On individual pin by using a smart sensor which is Fibre Bragg Grating (FBG) for the first time in metal forming research.

## **8.3 Future Work**

- The forming process using elastic cushions as the punch needs to be investigated further. The work of this thesis, should be extended to consider the likely life span of the elastic punch made from polyurethane A90, this would provide information on formed part quality as a function of time.
- The results obtained, see Table 5.3, show a significant interaction between elastic cushion thickness and blank holder on thickness variation of the formed sheet. A method for investigating this interaction needs to be developed and the effects of the interaction investigated.
- Digital control of MPF tool adjustment could be developed to ensure more accurate positioning of pin heights, to save time when forming different shapes, and this could

also allow for automatic compensation for springback as the MPF tools used in this research are small with a closed arrangement.

- As the springback compensation method depends on material properties, it needs to measure the force on selected pins caused by formed part relaxation (springback) at the end of formed process (release forces) and convert these forces to distance in order to adjust pins height to compensate for springback without being affected by metal sheet properties.

## References:-

1. <http://www.autoform.com/en/glossary/sheet-metal-forming/>, accessed on 04/06/2017.
2. Abosaf, M., 2017. , Finite Element Modelling of Multi-Point Forming. PhD thesis, University of Birmingham, doctoral Dissertations.
3. Groover, M.P., 2007, Fundamentals of modern manufacturing: materials processes, and systems., . John Wiley & Sons.
4. Abebe, M., Park, J.W. and Kang, B.S., 2017, Reliability-based robust process optimization of multi-point dieless forming for product defect reduction. *The International Journal of Advanced Manufacturing Technology*, 89(1-4), pp.1223-1234
5. Nakajima, N., 1969, Research on die and electrode by steel wire bind. *Japanese Journal of Mechanical Academy*, 72, pp. 32-40.
6. Ramezani, M.a.R., Z.M., 2012, Rubber-pad forming processes: Technology and applications. Elsevier.
7. Li, M.Z., Cai, Z. Y. Sui, Z. and Yan, Q. G., 2002, Multi-point forming technology for sheet metal. *Journal of Materials Processing Technology*, 129(1): pp. 333-338.
8. Schuler GmbH., 1998. Metal forming handbook. Springer Science & Business Media.
9. Wang, C., 2002. An industrial outlook for springback predictability, measurement reliability and compensation technology. in Proc. Numisheet (pp. 21-25).
10. Dwi Anggono, A., 2014, Combined method for die compensation in sheet metal forming. Universiti Tun Hussein Onn Malaysia: Doctoral dissertation.
11. Hani Aziz Ameen, H.A.A., Zahraa Abdul Kareem Radhi., 2016, Finite Element Analysis of the Dish Multi-Point Forming Process. *International Journal of Engineering Research & Technology (IJERT)*. Vol. 5( Issue 07).
12. Cimolin, F.V., R. and Canuto, C., 2008, Springback compensation in deep drawing applications. *Meccanica*. 43(2): pp. 101-113.

13. Mole, N.C., G. and Štok, B., 2014, A 3D forming tool optimisation method considering springback and thinning compensation. *Journal of Materials Processing Technology*. 214(8): pp. 1673-1685.
14. Liu, C., Li, M. and Fu, W., 2008, Principles and apparatus of multi-point forming for sheet metal. *The International Journal of Advanced Manufacturing Technology*. 35(11-12): pp. 1227-1233.
15. Abebe, M., Lee, K. and Kang, B.S., 2016, Surrogate-based multi-point forming process optimization for dimpling and wrinkling reduction. *The International Journal of Advanced Manufacturing Technology*. 85(1-4): pp. 391-403.
16. Păunoiu, V., Maier, C., Teodor, V. and Găvan, E., 2011, Numerical analysis of multipoint forming process. *International Journal of Modern Manufacturing Technologies*. 3(2): pp. 85-90.
17. Heo, S.C., Seo, Y.H., Ku, T.W., Kim, J. and Kang, B.S., 2009, Study on application of flexible die to sheet metal forming process. *Transactions of Materials Processing*. 18(7): pp. 556-564.
18. Wang, Z., 2010, Rapid manufacturing of vacuum forming components utilising reconfigurable screw pin tooling. University of Nottingham. Doctoral dissertation.
19. Hardt, D.E., Boyce, M.C. and Walczyk, D.F., 1993, A flexible forming system for rapid response production of sheet metal parts. *Proceedings of IBEC'93*: pp. 21-23.
20. Cai, Z.Y., Li, M. Z. and Chen, X.D., 2006, Digitized die forming system for sheet metal and springback minimizing technique. *The International Journal of Advanced Manufacturing Technology*. 28(11): pp. 1089-1096.
21. Li, M.Z., Cai, Z. Y. and Liu, C. G., 2007, Flexible manufacturing of sheet metal parts based on digitized-die. *Robotics and Computer-Integrated Manufacturing*. 23(1): pp. 107-115.
22. Ghaei, A., 2010, Modeling Springback in Stamped Automotive Structures. University of Windsor, doctoral Dissertations.
23. Alghtani, A.H., 2015, Analysis and Optimization of Springback in Sheet Metal Forming. University of Leeds: Doctoral dissertation.

24. Dunne, F.a.P., N., 2005., Introduction to computational plasticity. Oxford University.
25. Wang, C., 2002. An industrial outlook for springback predictability, measurement reliability and compensation technology. in Proc. Numisheet (pp. 21-25).
26. Choi, H.H., Hwang, S.M. Kang, Y.H., Kim, J. and Kang, B.S., 2002, Comparison of implicit and explicit finite-element methods for the hydroforming process of an automobile lower arm. *The International Journal of Advanced Manufacturing Technology*. 20(6): pp. 407-413.
27. Atzema, E.K., H. Konter, AWA. Meijers, SE. Meinders, T., 2005, Sensitivity analysis component 2: Scaled down car roof. Netherlands Institute for Metals Research.
28. Burchitz, I.A., 2008, Improvement of springback prediction in sheet metal forming. University of Twente. Doctoral dissertation.
29. Hu, J., Marciniak, Z. and Duncan, J. eds., 2002, Mechanics of sheet metal forming., Butterworth-Heinemann. Butterworth-Heinemann.
30. Meinders, T., Konter, A.W.A. , Meijers, S.E., Atzema, E.H. and Kappert, H., 2006, A sensitivity analysis on the springback behavior of the unconstrained bending problem. *International Journal of Forming Processes*. 9(3): pp. 365-402.
31. Kloosterman, G., 2002, Contact methods in finite element simulations., University of Twente. University of Twente.
32. Tisza, M., Numerical modelling and simulation in sheet metal forming. *Journal of Materials Processing Technology*. 151(1): pp. 58-62.
33. Irthia, I.K., 2014, Process analysis and design in micro deep drawing utilizing a flexible die. University of Glasgow: Doctoral dissertation.
34. Sun, J.S., Lee, K.H. and Lee, H.P., 2000, Comparison of implicit and explicit finite element methods for dynamic problems. *Journal of Materials Processing Technology*. 105(1): pp. 110-118.
35. Prior, A.M., 1994, Applications of implicit and explicit finite element techniques to metal forming. *Journal of Materials Processing Technology*. 45(1-4): pp. 649-656.

36. Narasimhan, N.a.L., M., 1999, Predicting springback in sheet metal forming: an explicit to implicit sequential solution procedure. *Finite elements in analysis and design*. 33(1): pp. 29-42.
37. Li, L.S., Y.H. Heo, S. C., Kang, B. S. and Kim, J., 2010, Numerical simulations on reducing the unloading springback with multi-step multi-point forming technology. *The International Journal of Advanced Manufacturing Technology*. 48(1): pp. 45-61.
38. Zhang, L.C., Lu, G. and Leong, S.C., 1997, V-shaped sheet forming by deformable punches. *Journal of materials processing technology*. 63(1-3): pp. 134-139.
39. Chou, I.N.a.H., C., 1999, Finite element analysis and optimization on springback reduction. *International Journal of Machine Tools and Manufacture*. 39(3): pp. 517-536.
40. Livatyali, H.a.A., T., 2001, Prediction and elimination of springback in straight flanging using computer aided design methods: Part 1. *Experimental investigations. Journal of Materials Processing Technology*. 117(1): pp. 262-268.
41. Kuwabara, T., Asano Y., Ikeda S, and Hayashi, H., 2004. An evaluation method for springback characteristics of sheet metals based on a stretch bending test. in *IDDRG*.
42. Carden, W.D., Geng, L.M., Matlock, D.K. and Wagoner, R.H., 2002, Measurement of springback. *International Journal of Mechanical Sciences*. 44(1): pp. 79-101.
43. Li, K.P., W.P. Carden, and Wagoner, R.H., 2002, Simulation of springback. *International Journal of Mechanical Sciences*. 44(1): p. 103-122.
44. Essa, K.E.A., 2011, Finite element prediction of deformation mechanics in incremental forming processes. University of Birmingham: Doctoral dissertation.
45. Rao, S.S. and Rao, S.S., 2009, Engineering optimization: theory and practice. John Wiley & sons. John Wiley & Sons.
46. Zheng, Y.a.D., P.K., 2000, Improved response surface method and its application to stiffened plate reliability analysis. *Engineering structures*. 22(5): pp. 544-551.

47. Mkaddem, A.a.B., R., 2007, Experimental and numerical optimisation of the sheet products geometry using response surface methodology. *Journal of materials processing technology*. 189(1): pp. 441-449.
48. Srinivasan, R., Vasudevan, D. and Padmanabhan, P., 2013, Application of response surface methodology for predicting springback in air bending of electro galvanised steel sheets. *International Journal of Materials Engineering Innovation*. 4(1): pp. 35-56.
49. Naceur, H.G., Y.Q. and Ben-Elechi, S., 2006, Response surface methodology for design of sheet forming parameters to control springback effects. *Computers & structures*. 84(26): pp. 1651-1663.
50. Xu, S., Zhao, K., Lanker, T., Zhang, J. and Wang, C.T., 2005. Springback prediction, compensation and correlation for automotive stamping. *in AIP Conference Proceedings*. AIP.
51. Liu, G., Lin, Z. Xu, W. and Bao, Y., 2002, Variable blankholder force in U-shaped part forming for eliminating springback error. *Journal of Materials Processing Technology*. 120(1): pp. 259-264.
52. Peng, L.H., P., Lai, X. and Ni, J., 2010, Fabrication of metallic bipolar plates for proton exchange membrane fuel cell by flexible forming process-numerical simulations and experiments. *Journal of Fuel Cell Science and Technology*. 7(3): p. 031009.
53. Yang, X.A.a.R., F. ,2011, *A die design method for springback compensation based on displacement adjustment*. *International Journal of Mechanical Sciences*. 53(5): pp. 399-406.
54. Lan, F., Chen, J. and Lin, J., 2006, A method of constructing smooth tool surfaces for FE prediction of springback in sheet metal forming. *Journal of Materials Processing Technology*. 177(1): pp. 382-385.
55. <http://www.loadpoint.co.uk/>.

56. Sulaiman, A.S., 2005, Finite element modelling and characterisation of springback and drawability in aluminium-based alloy. University of Birmingham: Doctoral dissertation.
57. Soboyejo, W., 2002, Mechanical properties of engineered materials (Vol. 152). CRC press.
58. Mazière, M.D., H., 2012, Investigations on the Portevin Le Chatelier critical strain in an aluminum alloy. *Computational Materials Science*. 52(1): pp. 68-72.
59. Klose, F.B., Ziegenbein, A., Hagemann, F., Neuhäuser, H., Hähner, P., Abbadi, M., Zeghloul, A., 2004, Analysis of portevin-le chatelier serrations of type bin Al–Mg. *Materials Science and Engineering: A*, 369(1-2): pp. 76-81.
60. Benallal, A., Berstad, T., Børvik, T., Hopperstad, O.S., Koutiri, I., De Codes, R Nogueira., 2008, An experimental and numerical investigation of the behaviour of AA5083 aluminium alloy in presence of the Portevin–Le Chatelier effect. *International Journal of Plasticity*. 24(10): pp. 1916-1945.
61. Abbadi, M., Hähner, P. and Zeghloul, A., 2002, On the characteristics of Portevin–Le Chatelier bands in aluminum alloy 5182 under stress-controlled and strain-controlled tensile testing. *Materials Science and Engineering: A*. 337(1): pp. 194-201.
62. Najib, L.M., Alisibramulisi, A., Amin, N. M., Bakar, I.A.A., and Hasim, S., 2015, The Effect of Rolling Direction to the Tensile Properties of AA5083 Specimen, in CIEC 2014. Springer. pp. 779-787.
63. Danckert, J.a.N., K.B., 1998, Determination of the plastic anisotropy  $r$  in sheet metal using automatic tensile test equipment. *Journal of materials processing technology*. 73(1): pp. 276-280.
64. Standard Test Method for Plastic Strain Ratio  $r$  for Sheet Metal., *ASTM E517*.
65. Wang, T., Zhu, T., Sun, J., Wu, R., and Zhang, M., 2015., Influence of rolling directions on microstructure, mechanical properties and anisotropy of Mg-5Li-1Al-0.5 Y alloy. *Journal of Magnesium and Alloys*. 3(4): pp. 345-351.

66. Kut, S.a.N., B., 2015., Numerical and Experimental Analysis of the Process of Aviation Drawpiece Forming Using Rigid and Rubber Punch With Various Properties. *Archives of Metallurgy and Materials*. 60(3): pp. 1923-1928.
67. <http://www.loadcellshop.co.uk/accessories-null/in-line-conditioning-modules.>, accessed on 02/03/2017.
68. [http://www.automation24.co.uk/position-sensors/ultrasonic-sensor-microsonic-mic25/iu/tc-i7-193-0.htm.](http://www.automation24.co.uk/position-sensors/ultrasonic-sensor-microsonic-mic25/iu/tc-i7-193-0.htm), accessed on 15/011/2016.
69. [http://www.omega.co.uk/pptst/OM-CP-IFC110.html?gclid=CjwKEAjwt6PKBRCAy9-07PeTtGgSJAC1P9xGq9si9I-j5RSEfjXk-nK7Hul8cZUfa2PUuhviADglhoCNmnw\\_wcB.](http://www.omega.co.uk/pptst/OM-CP-IFC110.html?gclid=CjwKEAjwt6PKBRCAy9-07PeTtGgSJAC1P9xGq9si9I-j5RSEfjXk-nK7Hul8cZUfa2PUuhviADglhoCNmnw_wcB.), a.o., accessed on 04/05/2017.
70. <http://www.faro.com/products/metrology/faro-scanarm/overview#main.>, a.o., accessed on 13/01/2017.
71. Jin, W.L., Venuvinod, P.K. and Wang, X., 1995, An optical fibre sensor based cutting force measuring device. *International Journal of Machine Tools and Manufacture*. 35(6): pp. 877-883.
72. Al-Fakih, E., Abu Osman, NA, and Mahamd Adikan, FR., 2012, The use of fiber Bragg grating sensors in biomechanics and rehabilitation applications: the state-of-the-art and ongoing research topics. *Sensors*. 12(10): pp. 12890-12926.
73. Huang, J., Zhou, Z., Liu, M., Zhang, E., Chen, M., Pham, D. T. and Ji, C., 2015, Real-time measurement of temperature field in heavy-duty machine tools using fiber Bragg grating sensors and analysis of thermal shift errors. *Mechatronics*. 31: pp. 16-21.
74. Documentation., 6.13, A., *Abaqus/CAE User's Guide*. .
75. Documentation., A., *ABAQUS/CAE User's Guide*.
76. Asad, M., 2010., Elaboration of concepts and methodologies to study peripheral down-cut milling process from macro-to-micro scales. *Villeurbanne, INSA*.

77. Wang, S., Cai, Z., Li, M., and Lan, Y., 2012, Numerical simulation on the local stress and local deformation in multi-point stretch forming process. *The International Journal of Advanced Manufacturing Technology*. 60(9): pp. 901-911.
78. ABAQUS., *ABAQUS User Manuals, Version 6.7. United State of Amrica*.
79. Schutte, J.H., Dannenberg, J.F., Wijnant, Y.H. and Boer, A., 2010, An implicit and explicit solver for contact problems. In *24th International Conference on Noise and Vibration Engineering, ISMA 2010*. KU Leuven.
80. Elghawail, A., Essa, K., Abosaf, M., Tolipov, A., Su, S., Pham, D., 2007., Prediction of springback in multi-point forming. *Cogent Engineering*. vol. 4, 1400507. DOI: 10.1080/23311916.2017.1400507
81. Zareh-Desari, B., Davoodi, B., Vedaei-Sabegh, A., 2017, Investigation of deep drawing concept of multi-point forming process in terms of prevalent defects. *International Journal of Material Forming*. 10(2): pp. 193-203.
82. Dassault Systems., *Abaqus/CAE User's Manual*.
83. Hosford, W.F.a.C., R.M., 2011, Metal forming: mechanics and metallurgy. *Cambridge University Press*.
84. Abosaf, M., Essa, K., Alghawail, A., Tolipov, A., Su, S., Pham, DT., 2107, Optimisation of multi-point forming process parameters. *The International Journal of Advanced Manufacturing Technology*: 92(5-8), pp.1849-1859
85. Heo, S.C., Seo, Y.H., Noh, H.G., Ku, T.W. and Kang, B.S., 2010, Numerical study on effect of using elastic pads in flexible forming process. *Transactions of the Korean Society of Mechanical Engineers A*. 34(5): pp. 549-556.
86. Yang, X., O. Olatunbosun, and E. Bolarinwa, Materials testing for finite element tire model. *SAE International Journal of Materials and Manufacturing*, 2010. 3(2010-01-0418): pp. 211-220.
87. Sala, G., 2001, A numerical and experimental approach to optimise sheet stamping technologies: part II—aluminium alloys rubber-forming. *Materials & Design*. 22(4): pp. 299-315.

88. Remezani, M., Ripin Z.M., and Ahmed, R., 2009. , Computer aided modelling of friction in rubber-pad forming process *Journal of Materials Processing Technology*. 209(10): pp. 4925-4934.
89. Lee, S.W.a.Y., D.Y., 1998, An assessment of numerical parameters influencing springback in explicit finite element analysis of sheet metal forming process. *Journal of Materials Processing Technology*. 80: pp. 60-67.
90. <http://www.faro.com/en-us/products/metrology/measuring-arm-faro-scanarm/applications#main>., accessed on 19/02/2017.
91. Slota, J., Jurcisin, M. and Lazarescu, L., 2014, Influence of technological parameters on the springback angle of high-strength steels. *Acta Metallurgica Slovaca*. 20(2): pp. 236-243.
92. Altan, T., Oh, S.L. and Gegel, G., 1983, Metal forming fundamentals and applications. *American Society for Metals*.: p. 353.
93. Papeleux, L.a.J.-P.P., 2002, Finite element simulation of springback in sheet metal forming. *Journal of Materials Processing Technology*. 125: pp. 785-791.
94. Albut, A., 2006, Influence of the friction coefficient on springback effect of a u-shaped part manufactured by tailor welded stripes. University" Politehnica" of Bucharest Scientific Bulletin, Series D: *Mechanical Engineering*. 68(3): pp. 27-36.
95. Li, L., Seo, Y.H., Heo, S.C., Kang, B.S. and Kim, J., 2010. , Numerical simulations on reducing the unloading springback with multi-step multi-point forming technology. *The International Journal of Advanced Manufacturing Technology*. 48(1): pp. 45-61.
96. Davoodi, B.a.Z.-D., B., 2014, Assessment of forming parameters influencing springback in multi-point forming process: a comprehensive experimental and numerical study. *Materials & Design*. 59: pp. 103-114.
97. Sun, G., Li, M.Z., Yan, X.P. and Zhong, P.P., 2007, Study of blank-holder technology on multi-point forming of thin sheet metal. *Journal of materials processing technology*. 187: pp. 517-520.

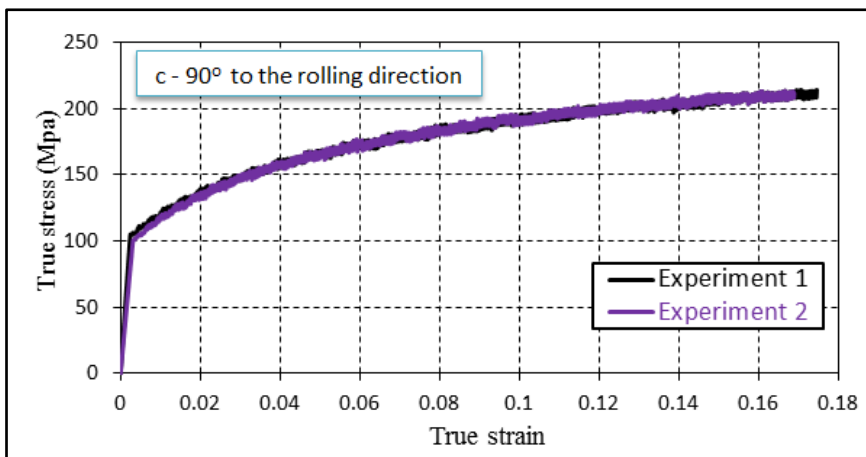
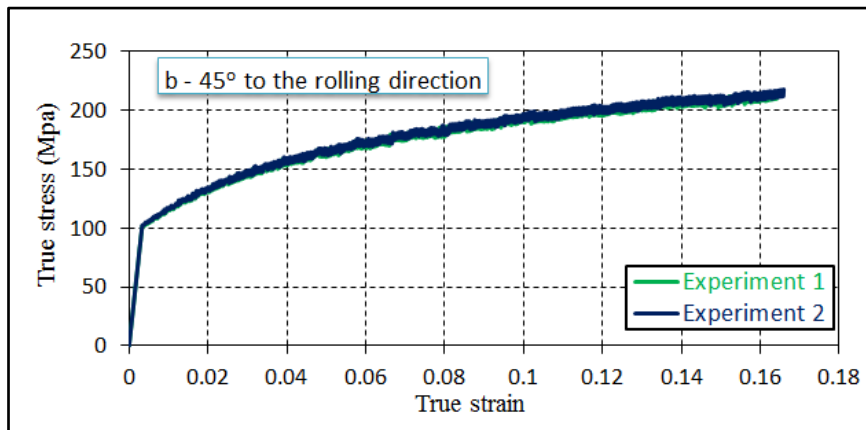
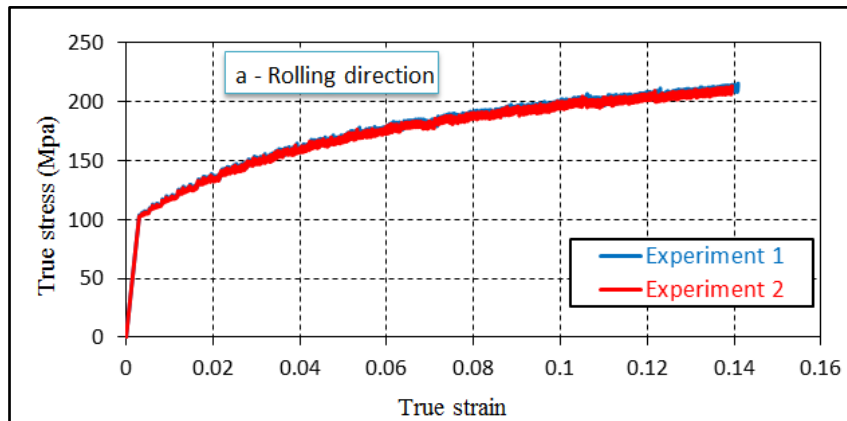
98. Li, M., Yao, J., Cai, Z. and Li, S., 2000. , The research on multi-point alternate forming of sheet metal to minimize springback. *Suxing Gongcheng Xuebao(Journal of Plasticity Engineering)(China)*. 7: pp. 22-25.
99. Wenner, M.L., 1983., On work hardening and springback in plane strain draw forming. *Journal of Applied Metalworking*. 2(4): pp. 277-287.
100. Woellner, N., Lajarin, S.F. and Marcondes, P.V. P., 2013. Blank Holder Force Influence On The Springback Of Advanced High Strength Steels. in *International Congress of Mechanical Engineering, Ribeirão Preto, SP, Brazil*.
101. Essa, K.a.H., P., 2010, Optimization of conventional spinning process parameters by means of numerical simulation and statistical analysis. Proceedings of the Institution of Mechanical Engineers, Part B: *Journal of Engineering Manufacture*. 224(11): pp. 1691-1705.
102. Read, N., Wang, W., Essa, K. and Attallah, M.M., 2015., Selective laser melting of AlSi10Mg alloy: Process optimisation and mechanical properties development. *Materials & Design (1980-2015)*. 65: pp. 417-424.
103. Hassanin, H., Modica, F., El-Sayed, M. A., Liu, J. and Essa, K., 2016, Manufacturing of Ti–6Al–4V Micro-Implantable Parts Using Hybrid Selective Laser Melting and Micro-Electrical Discharge Machining. *Advanced Engineering Materials*. 18(9): pp. 1544-1549.
104. Lee, M.G.K., D., Kim, C., Wenner, M.L. and Chung, K., 2005, Spring-back evaluation of automotive sheets based on isotropic–kinematic hardening laws and non-quadratic anisotropic yield functions, part III: *applications*. *International journal of plasticity*. 21(5): pp. 915-953.
105. Zheng, K., Lee, J., Politis, D. J., Li, N., Lin, J. and Dean, T. A., 2017, An analytical investigation on the wrinkling of aluminium alloys during stamping using macro-scale structural tooling surfaces. *The International Journal of Advanced Manufacturing Technology*: pp. 1-15.
106. Wang, A., Zhong, K., El Fakir, O., Liu, J., Sun, C., Wang, L.L., Lin, J., and Dean, T. A., 2017, Springback analysis of AA5754 after hot stamping: experiments and FE

- modelling. *The International Journal of Advanced Manufacturing Technology*. 89(5-8): pp. 1339-1352.
107. Glaesemann, G.S., Smith, J. A., Clark, D. A. and Johnson, R., 2005., Measuring thermal and mechanical stresses on optical fiber in a DC module using fiber Bragg gratings. *Journal of lightwave technology*. 23(11): p. 3461.
  108. Dong, X., ,Liu, Y., Liu, Z., and Dong, X. 2001., Simultaneous displacement and temperature measurement with cantilever-based fiber Bragg grating sensor. *Optics Communications*. 192(3): pp. 213-217.
  109. Kreuzer, M., 2006, Strain measurement with fiber Bragg grating sensors. *HBM, Darmstadt, S2338-1.0 e*.
  110. <https://www.hbm.com/en/4596/what-is-a-fiber-bragg-grating/>, *White paper Optical Measurement Solutions*. . accessed on 28/09/2017.
  111. <http://www.fbgs.com/technology/fbg-principle/> accessed on 20/11/2017.
  112. Kersey, A.D., Davis, M.A.,Patrick, H. J., LeBlanc, M., Koo, K.P., Askins, C.G., Putnam, M.A. and Friebele, E J., 1997., Fiber grating sensors. *Journal of lightwave technology*. 15(8): pp. 1442-1463.
  113. Bertholds, A.a.D., R., 1988., Determination of the individual strain-optic coefficients in single-mode optical fibres. *Journal of lightwave technology*. 6(1): pp. 17-20.
  114. Ren, L., Chen, J., Li, H.N., Song, G. and Ji, X., 2009., Design and application of a fiber Bragg grating strain sensor with enhanced sensitivity in the small-scale dam model. *Smart Materials and Structures*. 18(3): pp. 035015.
  115. Murukeshan, V.M., Chan, P.Y., Ong, L. S. and Asundi, A., 2001., Intracore fiber Bragg gratings for strain measurement in embedded composite structures. *Applied optics*. 40(1): pp. 145-149.
  116. Liu, M., Zhang, Z., Zhou, Z., Peng, S. and Tan, Y., 2015., A new method based on Fiber Bragg grating sensor for the milling force measurement. *Mechatronics*. 31: pp. 22-29.

117. Prasad, G.A., Anitha, M., Rao, N. K., and Asokan, S., 2011., Measurement of stress-strain response of a rammed earth prism in compression using fiber bragg grating sensors. *International journal on smart sensing and intelligent systems*. 4(3): pp. 376-387.
118. Jiayi, L., Zude, Z., Guoping, D. and Huaqiang, W., 2015., Dynamic Magnetic Field Measurement in the Air Gap of Magnetic Bearings Based on FBG-GMM Sensor. *Journal of the Optical Society of Korea*. 19(6): pp. 575-585.
119. Majumder, M., Gangopadhyay, T. K., Chakraborty, A. K., Dasgupta, K. and Bhattacharya, D.K., 2008., Fibre Bragg gratings in structural health monitoring—Present status and applications. *Sensors and Actuators A: Physical*. 147(1): pp. 150-164.
120. Li, M., Liu, Y., Su, S. and Li, G., 1999., Multi-point forming: a flexible manufacturing method for a 3-d surface sheet. *Journal of Materials Processing Technology*. 87(1): pp. 277-280.
121. Thiruvarudchelvan, S., 1993, Elastomers in metal forming: a review. *Journal of Materials Processing Technology*. 39(1): pp. 55-82.
122. Thiruvarudchelvan, S., 2002, The potential role of flexible tools in metal forming. *Journal of Materials Processing Technology*. 122(2): pp. 293-300.
123. Ramezani, M., Ripin, Z.M. and Ahmad, R., 2010, Sheet metal forming with the aid of flexible punch, numerical approach and experimental validation. *CIRP Journal of Manufacturing Science and Technology*. 3(3): pp. 196-203.
124. Browne, D.J.a.B., E., 1995, Optimisation of aluminium sheet forming using a flexible die. *Journal of materials processing technology*. 55(3-4): pp. 218-223.
125. Lee, J.W., Kwon, H.C., Rhee, M.H. and Im, Y.T., 2003, Determination of forming limit of a structural aluminum tube in rubber pad bending. *Journal of Materials Processing Technology*. 140(1): pp. 487-493.
126. Quadrini, F., Santo, L. and Squeo, E.A., 2010, Flexible forming of thin aluminum alloy sheets. *International Journal of Modern Manufacturing Technologies*. 2(1): pp. 79-84.

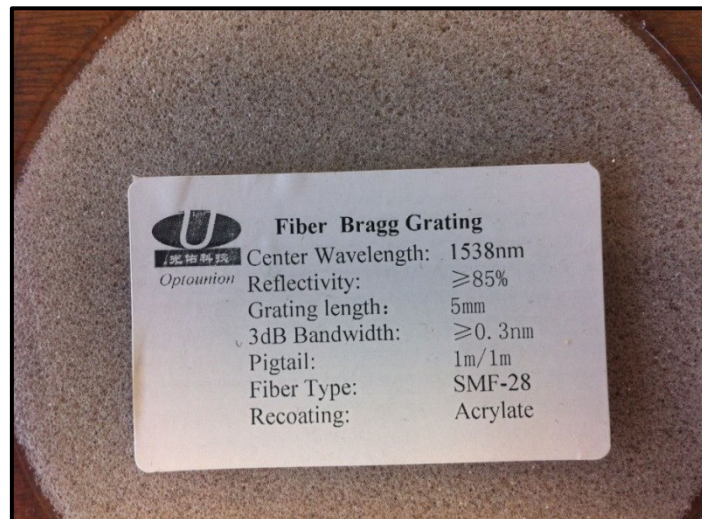
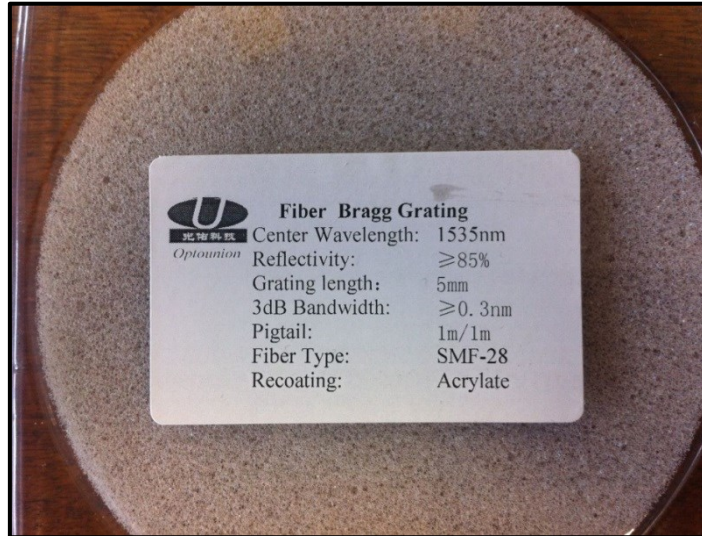
127. Chen, L., Chen, H., Guo, W., Chen, G. AND Wang, Q. 2014, Experimental and simulation studies of springback in rubber forming using aluminium sheet straight flanging process. *Materials & Design (1980-2015)*. 54: pp. 354-360.
128. Belhassen, L., Koubaa, S.,Wali, M. and Dammak, F., 2016, Numerical prediction of springback and ductile damage in rubber-pad forming process of aluminum sheet metal. *International Journal of Mechanical Sciences*. 117: pp. 218-226.
129. Liu, Y., Lin Hua, Jian Lan, and Xi Wei., 2010, Studies of the deformation styles of the rubber-pad forming process used for manufacturing metallic bipolar plates. *Journal of Power Sources*. 195(24): pp. 8177-8184.
130. Cai, Z.Y., Wang, S.H. and Li, M.Z., 2008, Numerical investigation of multi-point forming process for sheet metal: wrinkling, dimpling and springback. *The International Journal of Advanced Manufacturing Technology*. 37(9-10): pp. 927-936.
131. Chen, P.K., M. and Wenner, M.L., 2008, Experimental investigation of springback variation in forming of high strength steels. *Journal of manufacturing science and engineering*. 130(4): p. 041006.
132. Bahloul, R., Ben-Elechi, S. and Potiron, A., 2006, Optimisation of springback predicted by experimental and numerical approach by using response surface methodology. *Journal of Materials Processing Technology*. 173(1): pp. 101-110.
133. Buang, M.S., Abdullah, S. A. and Saedon, J., 2015, Optimization of springback prediction in U-channel process using response surface methodology. *Optimization*. 1: p. 31185.
134. Lind, D.A., Marchal, W.G. and Wathen, M., 2012, Business & Economics. USA, McGraw-Hill/Irwin.
135. Cai, Z.Y., Wang, S.H. and Li, M.Z., 2008, Numerical investigation of multi-point forming process for sheet metal: wrinkling, dimpling and springback. *The International Journal of Advanced Manufacturing Technology*. 37(9): pp. 927-936.

Appendix 1:

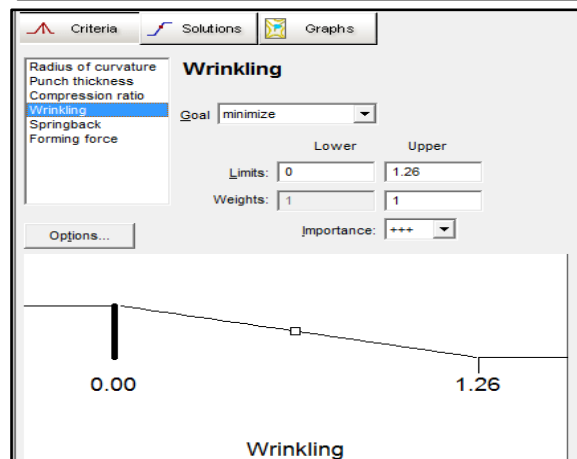
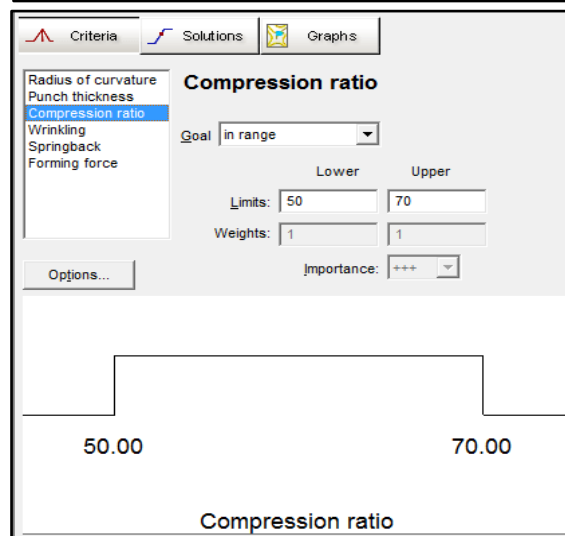
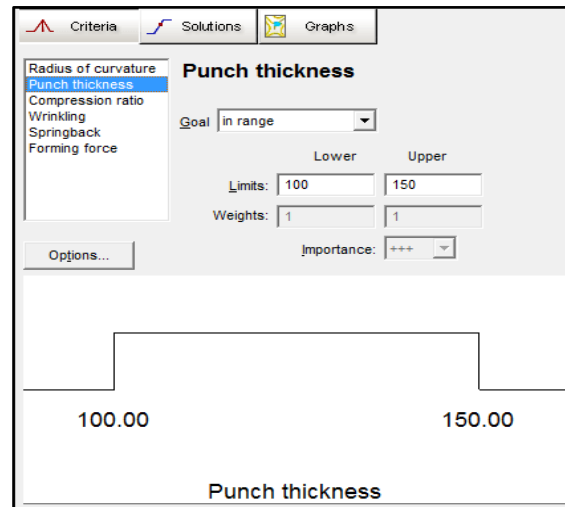


Stress-strain curve for AL5251-O at different rolling direction

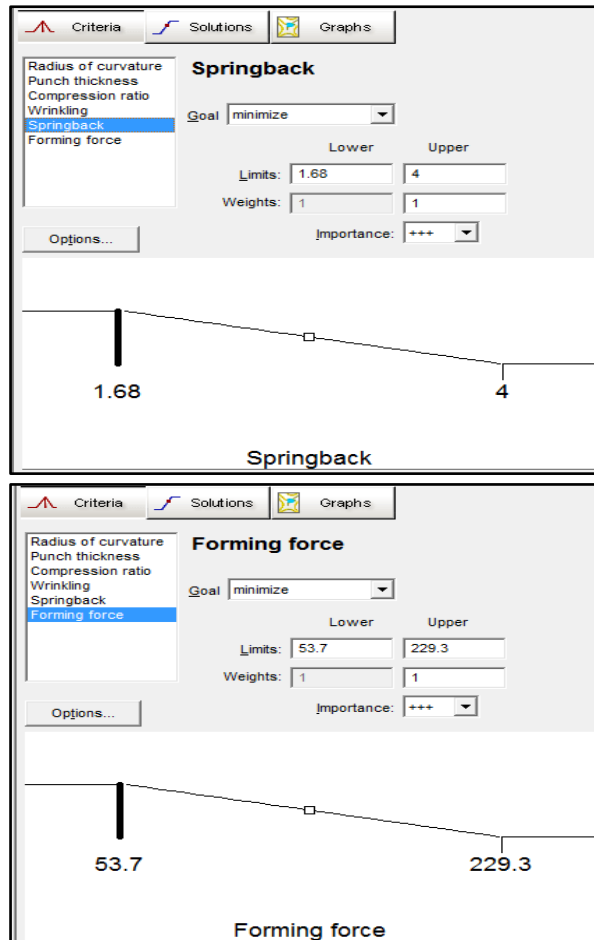
Appendix 2:



Appendix 3:



Cont.



Criteria for independent and dependent variables to get the optimal case



Special glue for FBGs sensors